FIELD SIMULATION OF WASTE IMPOUNDMENT SEEPAGE IN THE VADOSE ZONE:

LATE STAGE INFILTRATION AND DRAINAGE IN A HETEROGENEOUS, PARTIALLY SATURATED SOIL PROFILE

by

Ann M. Stark

Submitted in Partial Fulfillment of

the Requirements for the Degree of

Master of Science in Hydrology

Department of Geoscience

New Mexico Institute of Mining and Technology

Socorro, New Mexico

April, 1992

ABSTRACT

A long-term field (vadose zone) infiltration experiment was conducted near the campus of the New Mexico Institute of Mining and Technology from January 1987 to September 1989. Monitoring of drainage from the experimental plot as well as characterization of the geology and hydrology continued until July 1990.

Two major geologic facies are present beneath the field site. Heterogeneous, stratified alluvial sands, silts and clayey silts with interlayered cobble zones comprise the upper facies. The lower facies consists of primarily well-sorted fine to coarse fluvial sands and clayey sands.

The objective of this research is to produce a conceptual model describing the flow field within a heterogenous, stratified soil profile. This objective parallels the initial objective of the experiment which was to investigate the importance of lateral movement of seepage in the vadose zone.

To improve the visualization of the flow field, a blue dye was applied, prior to site drainage, to the soil via the water irrigation system. Two trenches were excavated in the central region of the field plot. Dye moved as an irregular front in most of the plot, but appeared to be concentrated around poorly packed instrument stations and in nearly saturated soils found near the main water lines. Shallow, erratic dye traces emphasized the nonuniformity of water application while deeper, fingering traces emphasized the effect of texture and layering on dye movement.

Substantial pressure head and moisture content data was collected prior to and during the drainage of the site to further develop the conceptual model of the flow field. Lateral flow from the margins of the plot was prevalent during infiltration. During drainage, essentially unit gradient existed beneath the center of the site. Some lateral flow gradients persisted to the northeast and east due to a pervasive, three-meter deep cobble zone. This layer roughly marked the contact between the two facies.

Moisture content analysis showed that moisture was fairly uniformly distributed in the alluvial facies until impeding layers were encountered. During the drainage period, within the fluvial sediments, moisture content was higher in the western half of the field site than in the eastern due to presence of clay layers, which only slowly drained their moisture. Contacts between layers in the fluvial facies as well as composition of deep cobble layers were difficult to determine, in as much as the geologic logs and drainage profiles did not always coincide.

Characteristic drainage curves were generated using hydrologic field parameters. Good correlation between field drainage data and fitted curves was present. Analysis of calculated hydraulic conductivities emphasized similar drainage behavior among groups of soil layers within individual facies.

TABLE OF CONTENTS

TABLE OF CONTENTS--CONTINUED

LIST OF FIGURES

LIST OF FIGURES--CONTINUED

LIST OF FIGURES--CONTINUED

LIST OF FIGURES--CONTINUED

LIST OF TABLES

ACKNOWLEDGEMENTS

This research was funded by United States Geological Survey award number 14-08-0001-1G to the New Mexico Institute of Mining and Technology. I am the sixth master's student to complete a degree working on this research project.

Much thanks go to Dr. Robert Bowman and Dr. Jan Hendrickx for their guidance and assistance during the project. Very special thanks go to my advisor, Dr. Daniel B. Stephens, for his support, guidance, knowledge and patience during my time at New Mexico Tech and throughout the final stages of my research.

Several graduate and undergraduate students provided a wealth of knowledge, patience, creativity and elbow grease to help me complete my research goals. I am grateful to former graduate students Kevin Flanigan, Dave Grabka, Paula Arnet and Rolf Schmidt-Petersen as well as undergraduate students Meiko Haushalter, Grady Rhodes, Mike Stephens and Mandy Kieft. All of these individuals not only went beyond the call of duty but made field work truly enjoyable, in spite of skunks, snakes, buried probes and clouds of blue dust.

A special thanks goes to Rolf, Roger, Eric, Kathy, Dave, Daphne and, especially, Mike for most of their practical jokes and their great company. Those late night Denny's roundtables, early morning golf games and trips to White Sands definitely made a difference.

I am also very grateful to my employer, CH2M HILL, for providing the resources to allow me to complete my graduate work and begin my professional career.

Lastly, and most importantly, I wish to thank my family for their love, support and that little nudge to always do my best.

Chapter 1. Introduction

1.1 Justification for Study

Southwestern states such as New Mexico are presently being considered as locations for mill tailings and radioactive waste storage. Ground-water recharge to deep water tables in some of these regions is small, making these areas desirable. The study of fluid and solute movement in partially saturated regions of the soils beneath such impoundments therefore becomes increasingly important.

Research and regulation of earthen and manufactured impoundment liners has been an important environmental and engineering topic for many years. A major objective in mine waste disposal research is to minimize or eradicate seepage of any sort through tailings pond liners (Bloomfield, et al., 1981). Persistent seepage has resulted from embankment and liner failures. Examples include failure of a dike around a gypsum tailings pond in Texas, erosion of an embankment containing carbide lime tailings in Louisiana and breakdown of a platinum tailings pond in Bafokeng, South Africa (Lucia, et al., 1981).

Groundwater and surface water resources could be irreparably damaged by leachate seepage from such failures as listed above and from those tailings ponds which are capped and abandoned. To assess the impact of a leaky landfill, tailings pile, etc. on groundwater and surface water,

vertical and lateral seepage from the source must be quantified. Knowledge of unsaturated flow behavior can be used to control subsurface contamination and prevent impoundment design errors.

1.2 Site Design

To simulate and investigate seepage from a tailings pile, a field plot was established to study water and tracer movement through a heterogeneous, unsaturated soil profile. The site is located approximately 120 kilometers south of Albuquerque, near the campus of New Mexico Institute of Mining and Technology (Figure 1-1). Vegetation is sparse due primarily to low precipitation (about 19 cm/year) and a deep water table (19 to 24 meters below ground surface). An irrigated golf course is adjacent to the field site, but, according to Mattson (1989), the experimental site has not been irrigated prior to its development in 1987.

The study site, a 30 m x 30 m plot, occupies a region of an old arroyo. The arroyo parallels the city of Socorro to the west and then follows a north to easterly route, beyond the northern boundary of the city, until it intersects the Rio Grande River. Its flow has been diverted (since 1963) away from the city of Socorro. Small, protective banks were constructed along the site to reduce encroachment from rainfall runoff. A drip irrigation system provided water to the site. Slightly acidified water was pumped through a

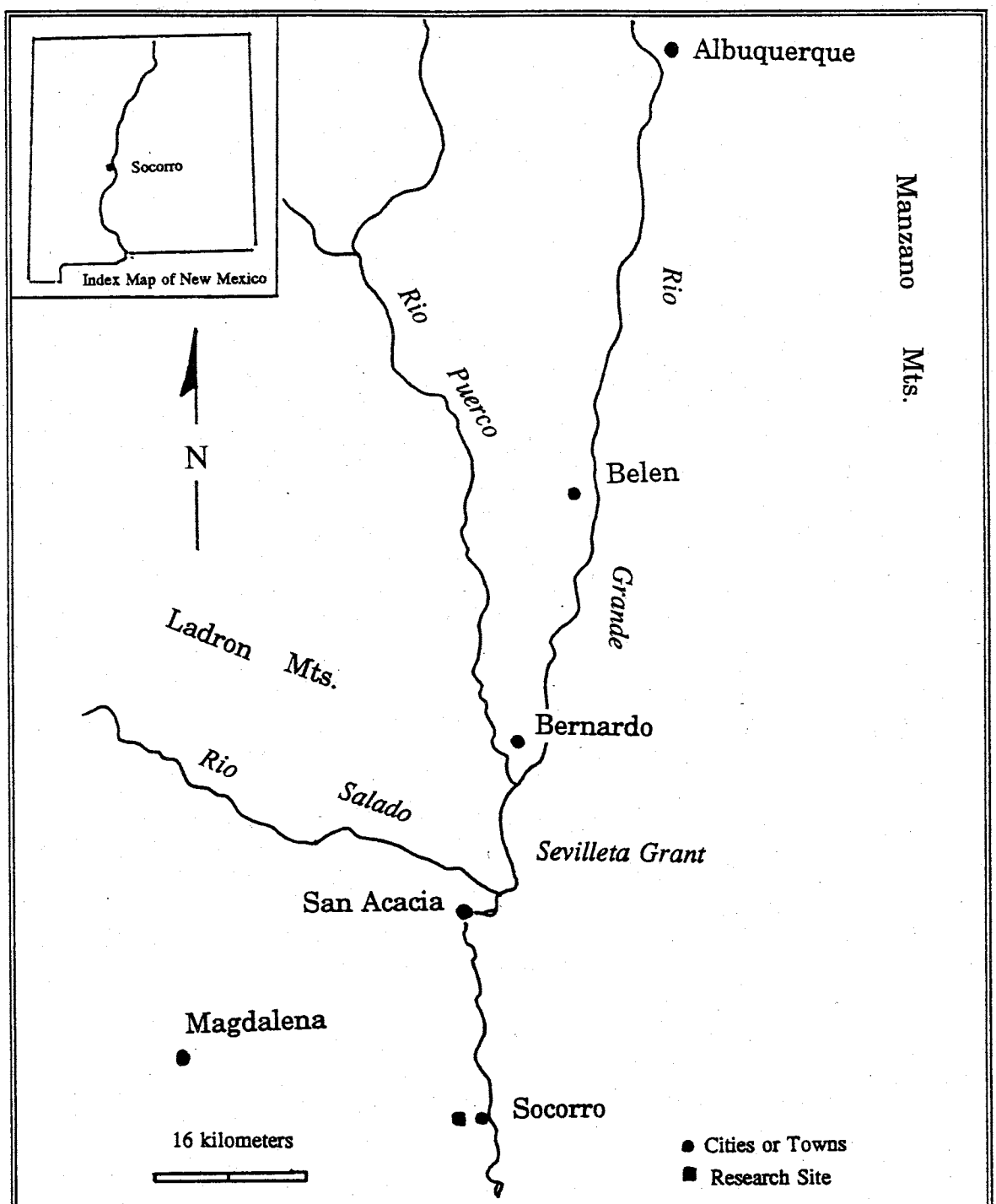

Figure 1-1a. Index Map. (adapted from Mattson, 1989)

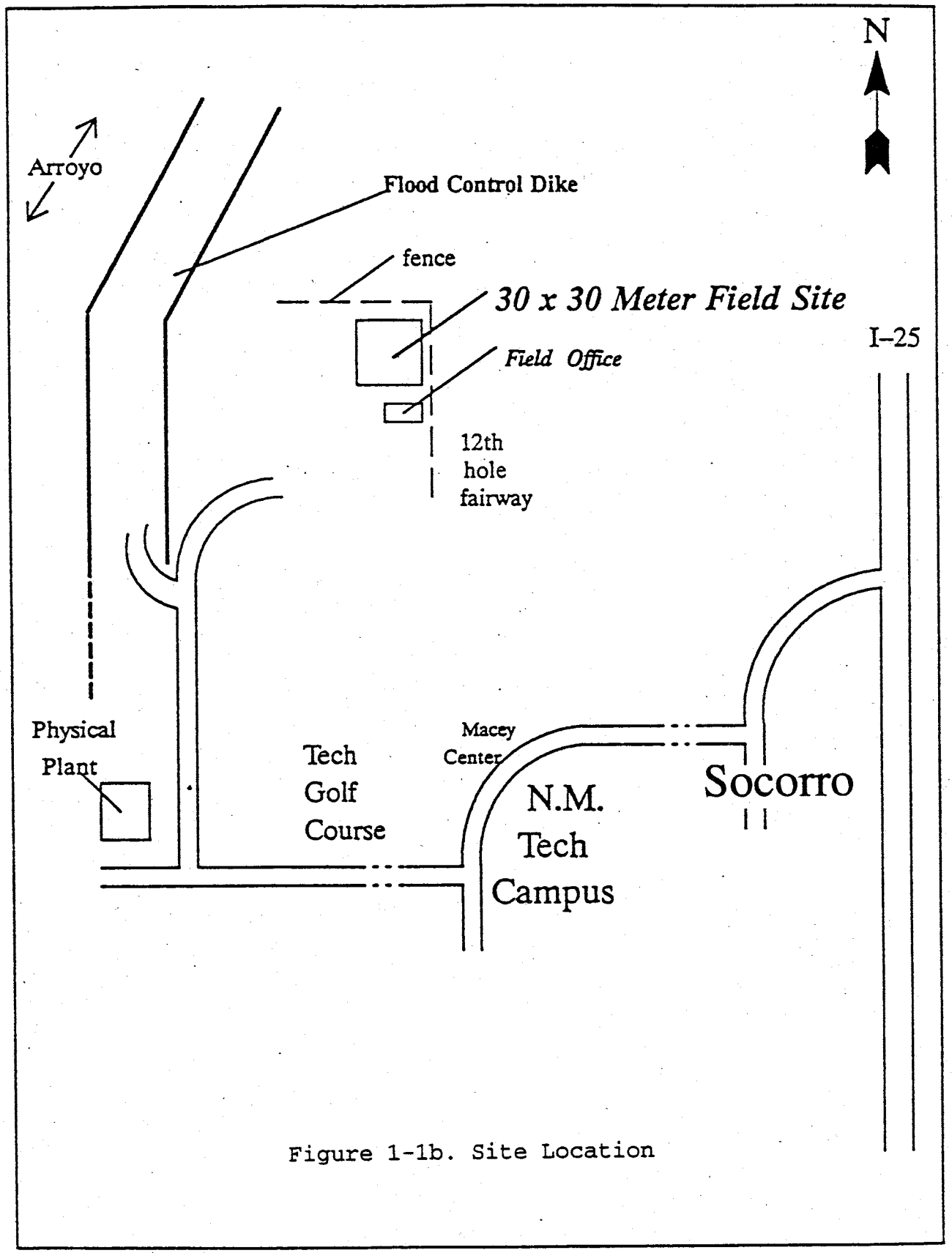

Figure 1-1b. Site Location

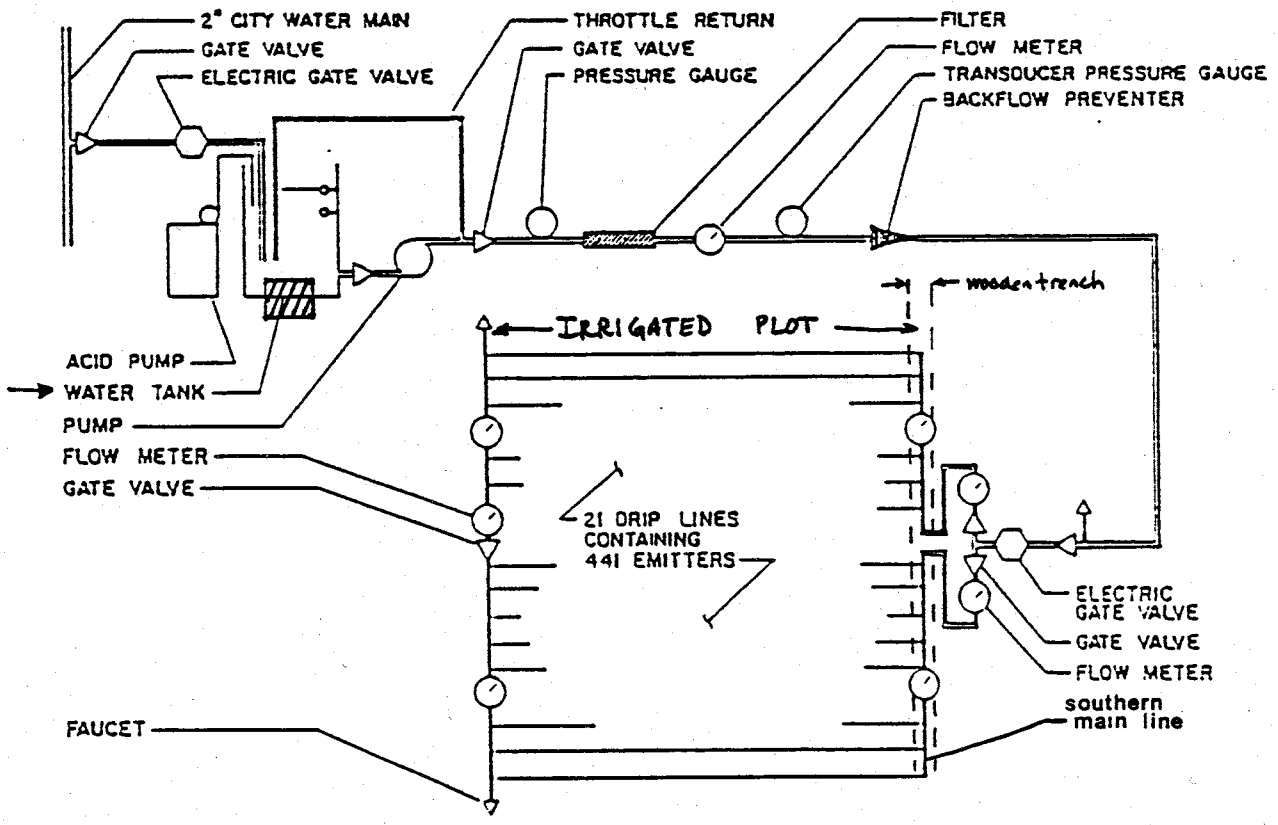

Figure 1-2. Irrigation Network (from Mattson, 1989)

mainline to 21 driplines located in the center 10m x 10m region of the plot (Figure 1-2). Acidification helped prevent clogging of emitters. Each dripline contained 21 emitters spaced approximately 50 cm apart. The emitters were spaced uniformly from dripline to dripline. Evaporation and runoff were minimized by two layers of durable plastic overlying the driplines. Pertinent field site events are described in Table 1. Water was applied at an approximate flux rate of 1.0×10^{-5} cm/sec from the experiment's beginning (Fall, 1986) through May 10, 1989. The flux was then increased to 1.0×10^{-4} cm/s and continued until early September, 1989.

Table 1. Site Chronology

Date	Event
Fall 1986	Site constructed/infiltration begun
January 1987	Data collection begins
May 10, 1989	Order of magnitude increase in flux
June 1989	Multi-tracer transport experiment
August 31, 1989	Dye application begins
September 5, 1989	Infiltration ends/ drainage begins
October 1989	Excavation of trenches begins
March 1989	Shallow (1.5 meter deep) and deep (3.5 meter deep) trenches complete
June 1990	2.3 meter deep trench near station 12-12 completed
July 1990	Drainage test completed

To trace fluid movement in the substrata during

infiltration and drainage events, the plot was heavily instrumented with 21 monitoring stations, each station containing one neutron access tube for moisture content measurements and one or two tensiometer nests (Figure 1-3). Note that the irrigated plot is the center "square" in this diagram. A neutron moisture probe (Model 503DR, CPN Corp., Martinez, CA) was used to determine volumetric moisture content. The probe was calibrated by Mattson (1989). A portable pressure transducer connected to a hypodermic needle (Tensimeter, Soil Moisture Systems, Tucson, AZ) was employed to measure the vacuum above the water in the tensiometer tube. Soil water samplers were installed throughout the field site for the solute transport experiments. Figures 1-4 and 1-5 show locations of these sampler stations which correspond to the geologic logs constructed by Arnet (1991), some of which are included in Appendix A. These are referenced in later sections. For an explanation of site datum, see Figure 1-6.

1.3 Geologic Framework and Previous Site Characterization

The instrumented soil profile consists of two distinct facies: an ancient Rio Grande fluvial facies and a Piedmont Slope fanglomerate facies. The Rio Grande fluvial facies is comprised of layers of fine-medium clean sands with intermittent thin layers of buff-brown clay (Figure 1-7). These layers are found in excess of 3-4 meters below ground surface. Overlying the river sediments is the Piedmont slope

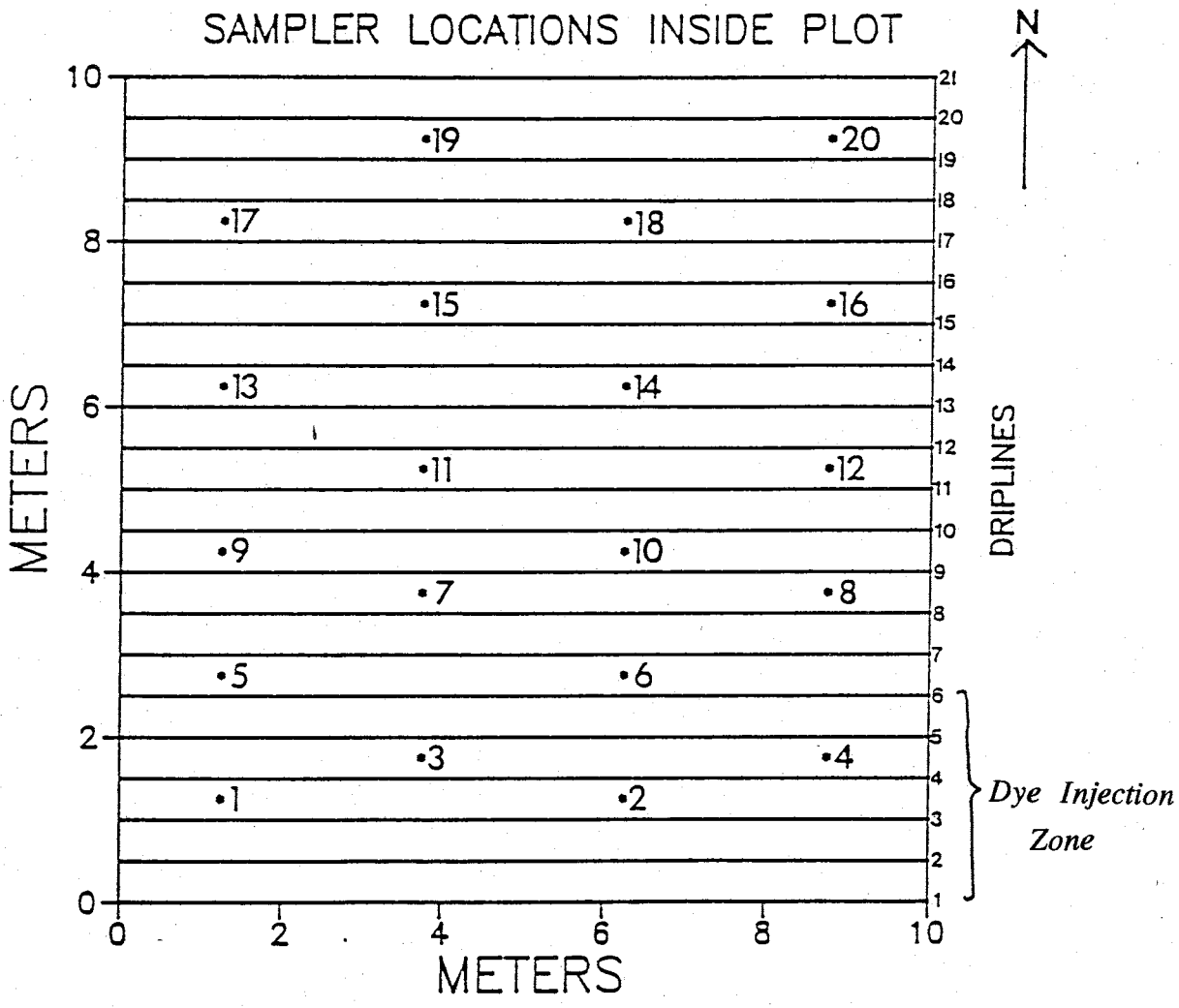

Figure 1-4. Locations of soil water samplers within the dripline system. Boreholes are numbered 1-20 and contained at least two soil water samplers.

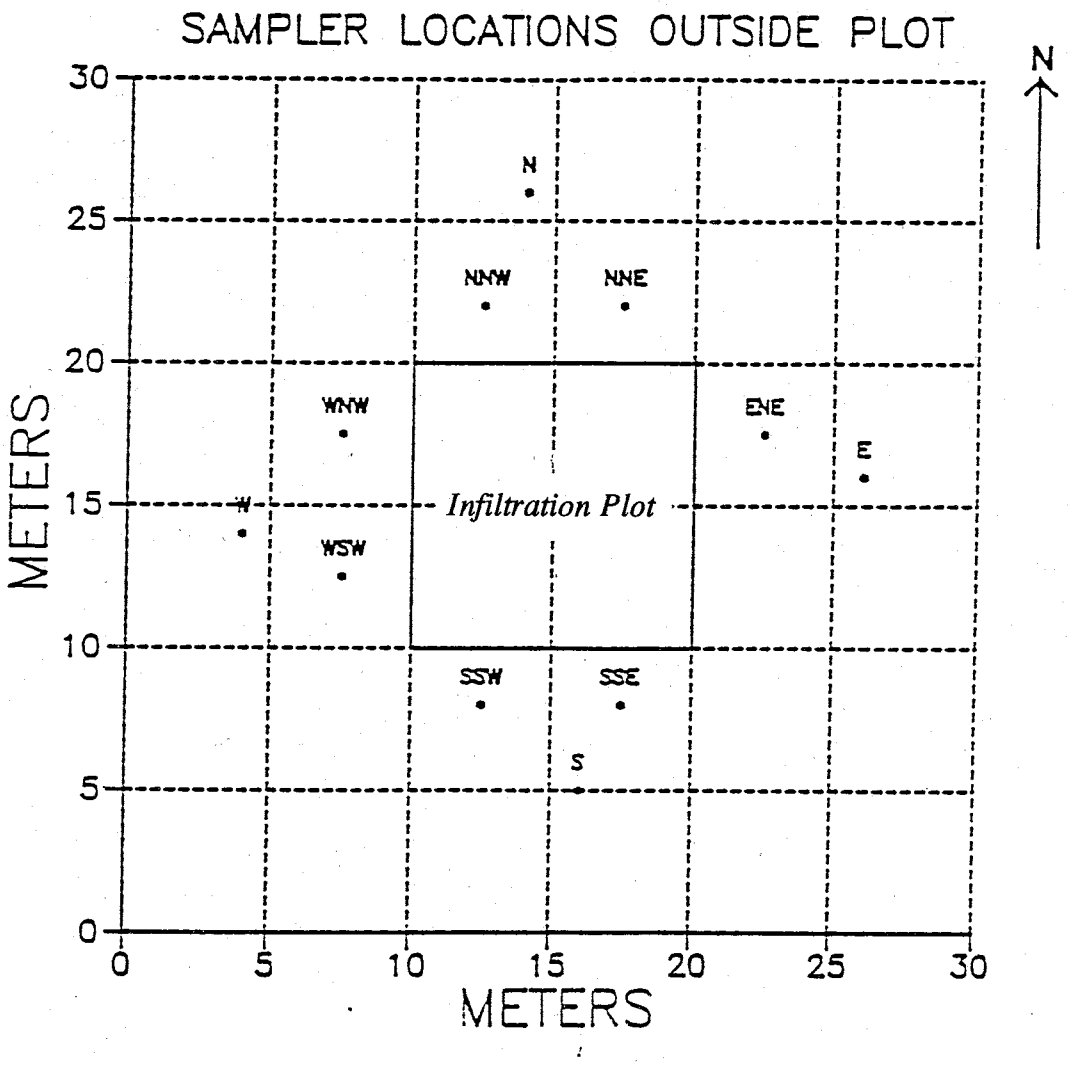

Figure 1-5. Locations of soil water sampler borehole logs outside the dripline system.

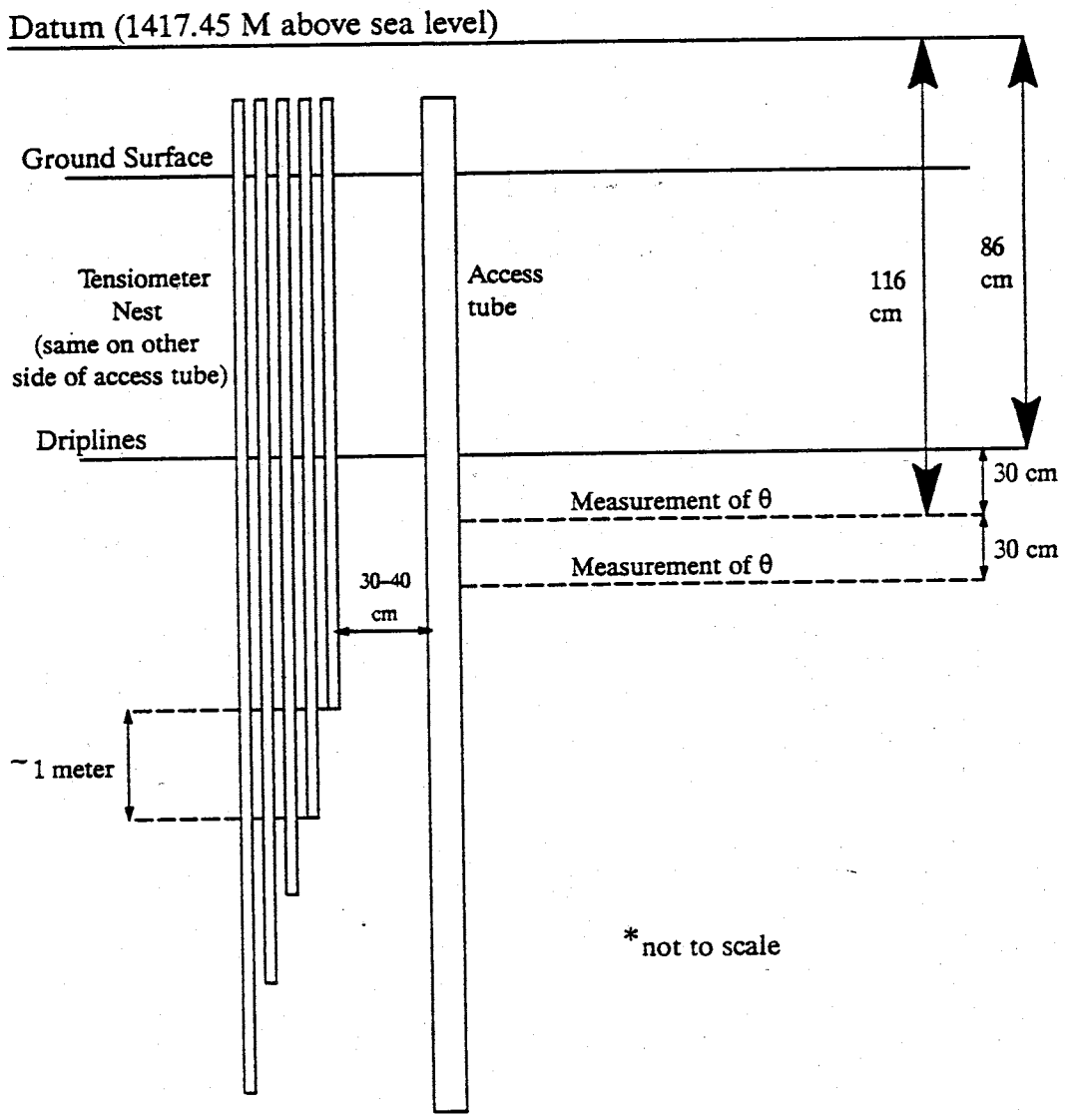

Figure 1-6. Explanation of site datum. (not to scale)

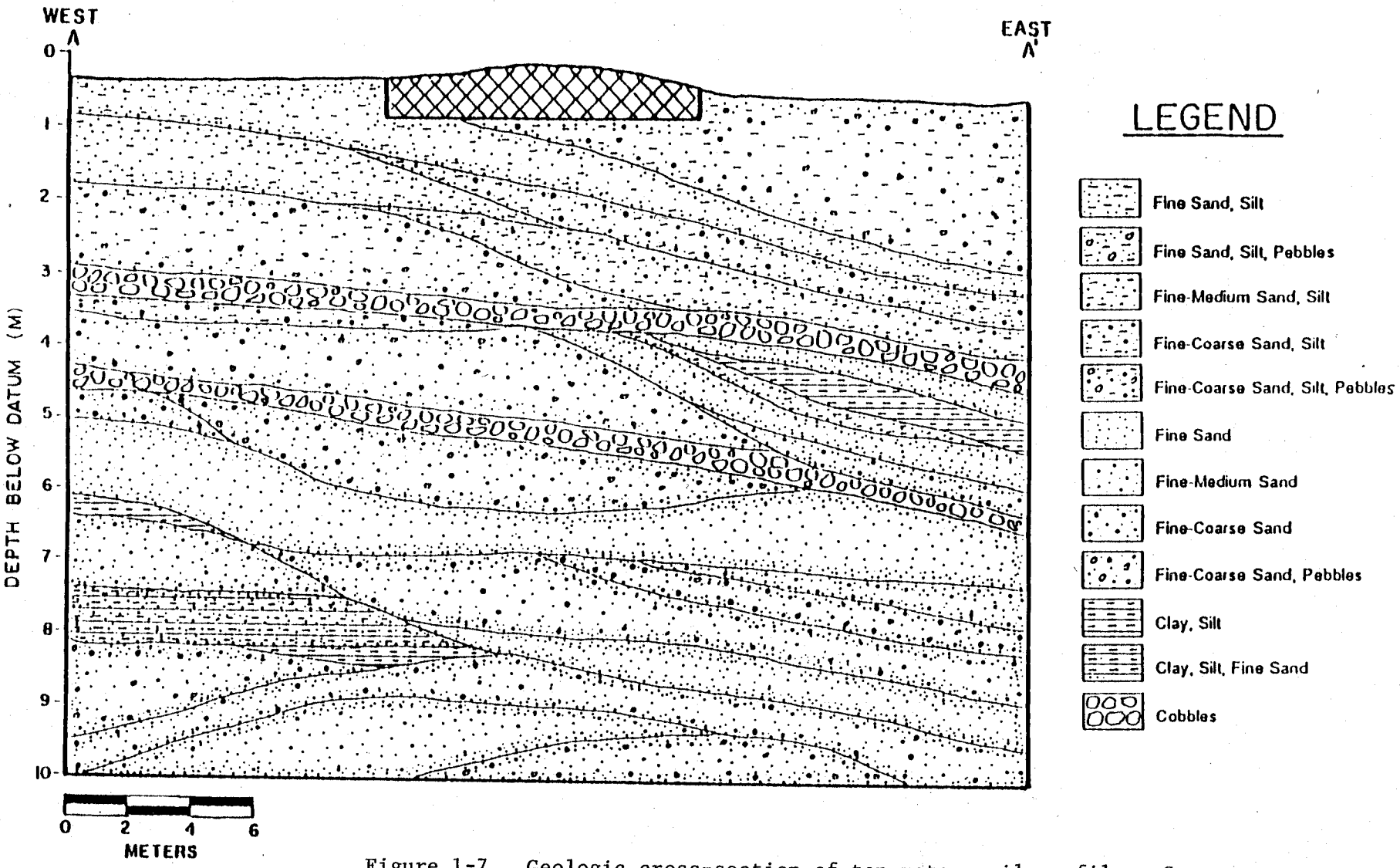

Figure 1-7. Geologic cross-section of ten meter soil profile. Cross-hatched area marks irrigated plot region. (Parsons, 1988)

(or alluvial fan) facies. A variety of interlayered materials including silty clays, red-brown silty sands, gravelly sands and large diameter cobble layers make up this facies. Bedding in the alluvial facies dipped principally east-northeast.

There are two distinct features of the site geology. Several cobble layers are present in the soil profile and play a vital role in transport of fluid, as described in sections below. The subrounded cobbles ranged in size from several centimeters to several tens of centimeters in diameter. Matrix material consisted of silt and/or silty fine sand.

The second feature is the complex texture of individual layers, primarily within the alluvial fan facies. Detailed mapping following trench excavation revealed heterogeneity on a local scale. For example, thin (5 cm) layers of primarily silty sand contained small percentages of fine, subrounded gravel and reddish-brown, thin lenses of clay. On a moderate or regional scale, such variable texture may not be applicable. Analysis of fluid transport at a particular scale must incorporate geologic description at the same or similar scale. A more thorough discussion of site geology and hydraulic properties common to each facies can be found in Parsons (1988) and Arnet (1991).

For information on other phases of this vadose zone experiment, the reader is directed to Parsons (1988) for site geologic and hydraulic parameters; Mattson (1989) for detailed field design and the first infiltration test; Flanigan (1989)

for a discussion of the first bromide tracer and second infiltration tests; Schmidt-Petersen (1991) for geostatistical analysis of hydraulic properties; Grabka (1990) for discussion of the second tracer and infiltration tests and Arnet (1991) for detailed geologic mapping of excavations for assessing parameter variability.

1.4 Research Objectives

The results of the dye trace excavation and the drainage test are the subject of this study. The dye study is important for a number of reasons. Preferential flow along instrumentation can be determined though analysis of dye traces. This can help explain anomalous measurements of moisture content and pressure head from these instruments. Extent of lateral and vertical flow through various soil layers and textures can be visually understood from this study. This type of study thus allows both a qualitative and quantitative estimation of the role soils play in moisture movement.

To analyze flow during the drainage phase, distinction must be made between redistribution and internal drainage. Redistribution refers to water movement in which wetness of successively deeper layers is increased at the expense of previously wetted layers of the soil profile. Internal drainage refers to drainage from an initially saturated profile. Redistribution is more applicable for a draining

field site where the water table is moderately deep, and the profile is not saturated throughout. For this report, the term "drainage" is synonymous with redistribution. The process of redistribution is quite prevalent at the study site especially where moisture has infiltrated and drained laterally (Warrick, et al., 1990).

The actual redistribution process is important for a number of reasons. Root water uptake is highly affected by how much infiltrated water is later redistributed to them. The extent of soil water retention is affected by the apportionment of moisture to different soil regions. These soil moisture distribution details are vital in planning agricultural irrigation scheduling. If suction gradients are small, then redistribution can be gravity driven, provided the wetted depth is considerable and underlying soil is wet. The process slows as moisture content decreases and as hydraulic conductivity (K) subsequently decreases.

The following goals, once achieved, will provide a better understanding of moisture movement during late stage infiltration and drainage from a capped source through a layered soil profile:

1. Describe dyed flow paths based on quantitative information provided by excavated dye traces.

2. Describe the distribution of moisture content and pressure head during drainage.

3. Determine <u>in situ</u> unsaturated hydraulic conductivity of a multi-layered system. The Instantaneous Profile test (Watson, 1966) will be applied to a five meter thick profile for a drainage period of 150 days.

4. Utilize pressure head, moisture content and hydraulic conductivity data to validate one-dimensional analytical models.

Before these goals can be properly fulfilled, a basic theoretical description of moisture movement through soils must be given to provide the introductory groundwork from which a conceptual model of site drainage can be built. Chapter two contains this theoretical foundation and describes some previous work completed in this field of study.

CHAPTER 2. Background

2.1 Theory

When moisture moves through a soil, many factors must be considered to explain how much moisture infiltrates and is drained as well as processes driving or impeding the drainage. These include proximity of vegetation (root effects), location of the water table, climatic factors, antecedent moisture, precipitation patterns, presence of impeding layers and texture of soil layers (Bouma, 1973). Of these factors, the four most important are soil texture, soil structure, porosity (size/ shape and continuity) and soil layering.

Two distinct fluids occupy void spaces in unsaturated materials: air and water. In the unsaturated state, air pressure exceeds water pressure. This difference is referred to as the capillary pressure. However, water adheres more strongly than air to the solid surface, producing a curved air-water interface. Equilibrium is produced in the air-water system when the interfacial forces balance the water displacement forces created by the air (McWhorter and Sunada, 1977). Because the interfaces must become more curved as capillary pressure increases, water can only occupy progressively smaller pores. Thus, volumetric water content (fraction of pores containing water) decreases as capillary pressure increases. Therefore, a finer textured material (such as a clay) which contains primarily small, narrow pores

will hold more moisture at a given capillary pressure (or pressure head or soil water suction) than a sand (Figure 2-1).

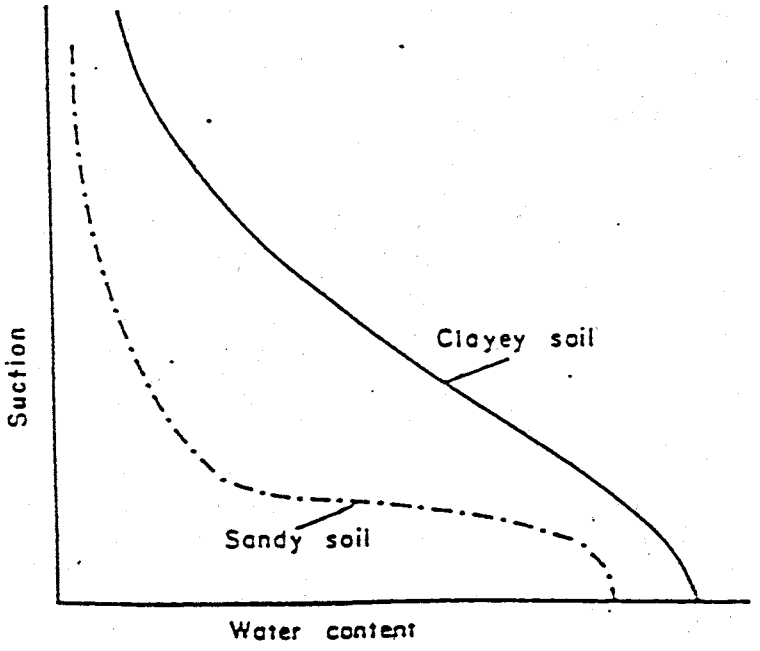

Figure 2-1. Effect of texture on soil-water retention. (from Hillel, 1980b)

A soil begins to drain from saturation once its air entry pressure head has been exceeded. Initially, coarse materials tend to drain quite rapidly while finer materials lose water more gradually. Because finer soils retain more water at higher suctions, they are more conductive during unsaturated flow. Figure 2-2 illustrates this dependence of K on pressure head. Thus, as capillary pressure (or soil water suction) increases, moisture content and hydraulic conductivity decrease, as only the very narrow pores will transmit or bear water.

Bear (1979) also illustrated that the water pressure as well as the air pressure in two bordering soil layers of

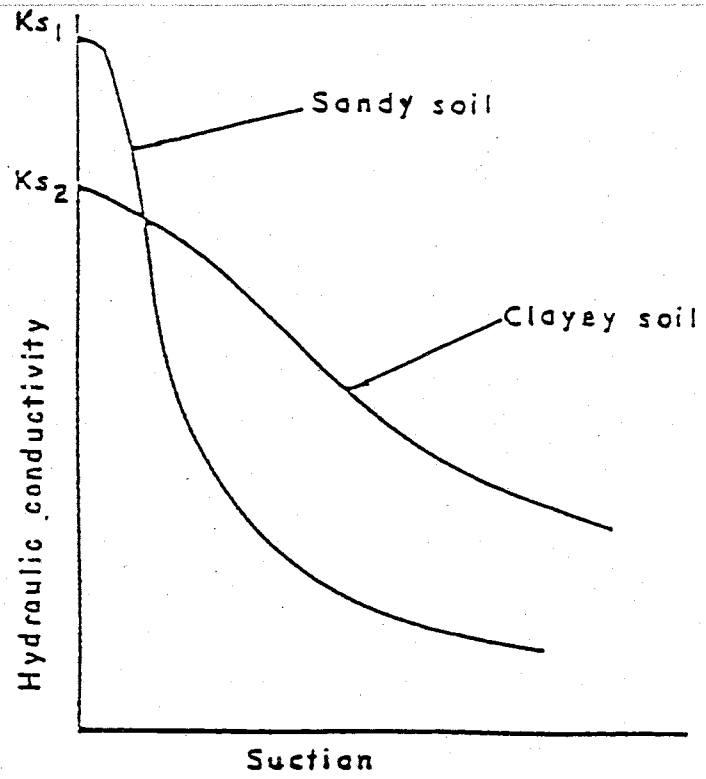

Figure 2-2. Dependence of hydraulic conductivity on suction for two soils. (log-log scale) (from Hillel, 1980b)

different textures must be the same as their boundary is approached. This would require that the capillary pressures be the same. Thus, a discontinuity in moisture content results between layers due to continuity of pressure head across the boundary (Figure 2-3).

For a two-layered soil profile, there are two possible combinations of texture. In the case of a fine textured soil overlying a coarser layer, drainage is gradual through the fine layer until the boundary is encountered. The drying front behaves similarly to the wetting front as it too may be impeded by the coarser layer (Eagleman and Jamison, 1962). Water must accumulate until soil water tension is low enough

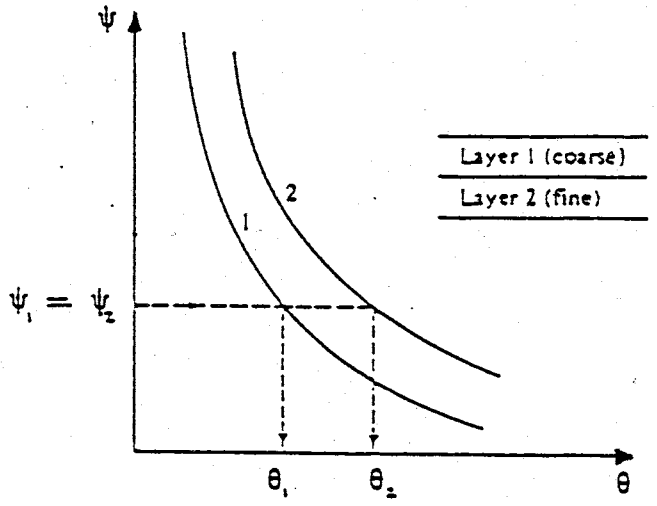

Figure 2-3. Moisture content discontinuity between layers of different retention curves. (adapted from Bear, 1979)

to permit moisture movement into the coarse-textured layer (Miller, et al, 1962) (Figure 2-4). This is commonly referred to as the "capillary barrier" effect. If the tension does not decrease sufficiently, water may move laterally within the fine layer along the contact between the finer and the underlying coarser media. Instabilities in the wetting front during infiltration can also be created at this boundary. Hillel and Baker (1990) demonstrated that flow from a fine layer into a coarser one can become constricted into "fingers" if hydraulic conductivity of the upper layer is much less than the that for the lower.

The other simple texture combination is of a coarse layer overlying a fine-textured one. Once again, the advance of the

(1967) studied water retention hysteresis and found that it could determine which soil layers drain faster than others. Dane and Wierenga (1975) furthered this analysis by incorporating the K-θ relationship. They determined that conductivity values were higher for clay loam than sand during wetting while the reverse was true for the drying phase.

Eagleman and Jamison (1962) used various soil textural pairs to determine effects of soil layering on unsaturated moisture movement. One column contained sand overlying silt loam, while another contained the reverse. Both columns were saturated and vertically drained due to gravity and evaporation gradients. Moisture content and hydraulic gradient were measured, which led to a measure of flow velocity and calculation of hydraulic conductivity.

Table 2 summarizes their results for sand over silt loam and silt loam over sand. "Days since saturation" refers to time following column saturation. Hydraulic gradient was measured across the soil layer boundary, and flow was downward. Hydraulic conductivity was determined for the upper layer in both layering systems. In the case of coarse over fine, as moisture content rapidly decreased, the gradient increased substantially, and the conductivity above the interface, as a function of wetness, sharply decreased, due to the small amount of water remaining at the plane of contact. Conversely, the hydraulic gradients at the contact between silt loam and underlying sand were much smaller. Flow was

restricted by the sand, as little suction was applied to drain the overlying finer pores. At high suctions, little water remains in the pores in coarse media. Thus, conductivity influenced by suction was quite small for moisture movement from silt loam to sand.

For this study, it is relevant to compare these simple layered models to the results from the field experiment. The complex stratigraphy and variable texture of the site soils may or may not permit the application of these models. Also, such application may be useful on a general, site-wide scale, while proving difficult within the region defined by a single monitoring station. These comparisons are made in Chapter four, following the summary of field and analytical methods in chapter three.

Table 2. Summary of moisture movement data for two different layering systems. (from Eagleman and Jamison, 1962)

Layering System	Days since saturation	Moisture[1] %by volume	Hyd.Grad. cm H_2O/cm	Hyd.Cond.[1] cm/day
sand over silt loam	1	14.93	- 2.0	28,600
	5	3.17	- 26.3	219
	10	2.64	- 53.8	3.90
	19	2.20	- 70.5	1.40
	26	2.16	- 107.8	0.11
	33	2.11	- 130.8	0.09
silt loam over sand	1	43.79	- 0.25	0.9520
	7	41.72	- 1.25	0.0671
	14	40.85	1.20	0.0118
	19	40.01	1.0	0.0087
	22	40.35	- 1.0	0.00114
	26	40.23	-1.0	0.00108

[1] Moisture content and hydraulic conductivity measured in top layer

CHAPTER 3. Methodology

3.1 General Approach

To characterize the late infiltration and drainage flow fields in a heterogeneous vadose zone, several stages of site work were undertaken. During the week prior to the drainage data collection (stage 2), a blue dye was injected into the southern quarter of driplines (first stage). Excavation of the dye traces would provide a detailed qualitative estimation of flow paths below the emitters (stage 3 and objective 1).

As described above, a number of tensiometers and neutron probe access tubes were installed in 1987. Tensiometers ranged in depth from 1 to 5.1 meters below datum (MBD) while many access tubes extended to 8.8 MBD. Site datum was 86 cm above dripline level. Approximately 230 tensiometers and all 21 access tubes were used for data collection prior to and during drainage. Precipitation and air temperature values were registered every hour each day via a portable data logger (CR7, Campbell Scientific, Logan, Utah). A Class 2 pan was used to measure evaporation, and four open-ended wells were used to gather water table levels.

Stage four consisted of intense data analysis including mass balance studies and application of a one-dimensional drainage model. Prior knowledge of the geologic fabric coupled with pressure head and moisture content distribution (as shown by data) would reveal the nature of flow behavior

and determine if gradients governing flow lateral or vertical (objective 2).

Found below are descriptions of both the instrumentation and methods of analysis. Results and analysis of data are discussed separately.

3.2 Field Data Collection

3.2.1 Tensiometers (pressure and hydraulic head)

Fluid present in saturated soil is under zero or positive hydrostatic pressure. Moisture in unsaturated media (vadose zone) is characterized by fluid pressure less than atmospheric and hence, negative pressure head or gage pressure. Pressure head, hydraulic head and hydraulic gradient in soil-water systems are measured by the tensiometer. This instrument comes in many forms but generally consists of a porous ceramic cup, connecting tube filled with water, pressure gauge and entryway for water filling (Richards, 1965).

The type of tensiometer employed depends on the data collected and site construction. Richards (1954) devised a multiple cup tensiometer to measure the vertical gradient and hydraulic head in uniform unsaturated soil. Mercury manometers were used to measure suction. Watson (1967) used a coupled tensiometer-pressure transducer to rapidly measure changes in capillary pressure in soil. Advantages in Watson's device included convenient collection of chart records, little or no temperature effects and automated system capabilities.

The attached transducer allowed stability, accurate accountance of hysteresis and adjustment for wide range of temperatures. A complex transducer-tensiometer system was developed by Nyhan, et. al (1989) which interfaced directly with a personal computer (pc) and peripherals. Advantages included rapid collection of pressure changes as well as direct data storage. A Tensimeter (Soil Measurement Systems Las Cruces, NM) was used as a backup for data collection. The device (pressure transducer combined with digital readout) was described in detail by Marthaler et. al (1983). It is a mobile data collector and is relatively inexpensive to obtain.

Cost and maintenance are the objective functions to be considered when devising a tensiometric system. Manometers containing mercury can produce harmful leaks, and they need careful attention. Remotely located field plots may not have the capacity for computerized data collection. Both an automated system and transducers connected to several tens of tensiometers are expensive and require supervision. Therefore, water-filled tensiometers and a mobile pressure transducer satisfied our needs.

Figure 3-1 is a schematic of the tensiometers used at the site. Parts for this design are inexpensive and easy to obtain. Some of the water present in the tube is drawn out though the cup upon initial emplacement in the soil. Once the water in the tube and the soil water equilibrate with one another, a steady pressure head can be determined by a mobile

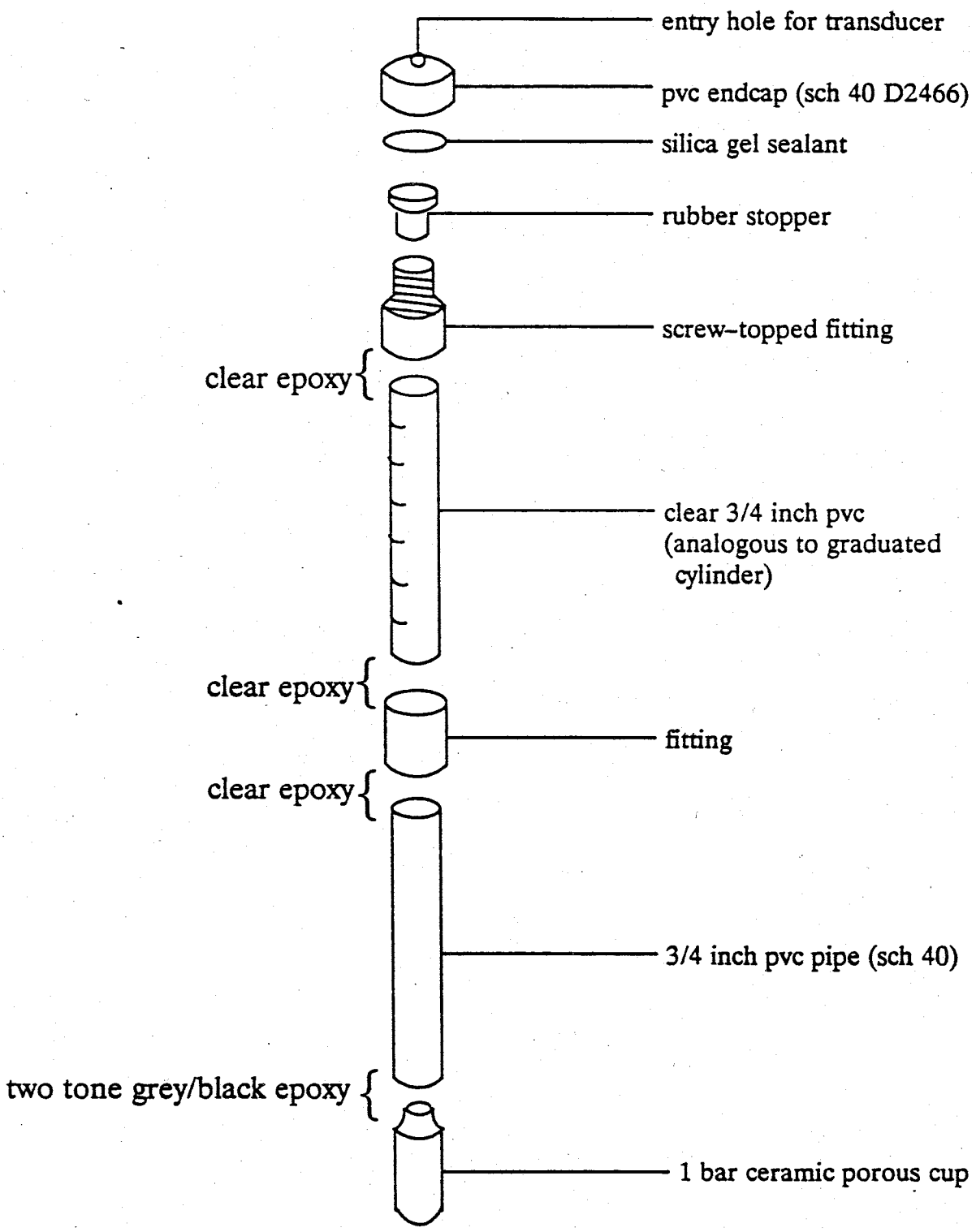

Figure 3-1. Water-filled tensiometer

transducer connected to a Tensimeter (see Figure 3-2) A negative value of gauge pressure is read in millibars. The water level is also recorded relative to the length of the tensiometer. Pressure head is calculated using the equation in Figure 3-2. Hydraulic head is equal to pressure head (negative) plus elevation head (negative). Depths and locations of all the working tensiometers at the site are included in Appendix D.

Some limitations are inherent in the system. The upper limit of soil water suction for reliable pressure head measurements is 0.8 bar. Suctions higher than this promote air entry into the cup which causes the tensiometer to fail as its internal pressure equalizes to atmospheric (Hillel, 1980b). A lag time exists in the instrument during which the water in the tube equilibrates with the soil water. Anomalous readings occur if taken during this period. Lag time is also created when tensiometers are used as soil water samplers (Rudolph, 1990). Temperature and entrapped air can also affect measurements. Deaired water was not used in this experiment as the literature suggested it was not necessary (Marthaler, 1983). Also, readings were conducted early in the morning before sunrise to reduce effects of heat and sunlight on the water column.

Prior to May, 1989, the tensiometers contained a 50-50 mix of antifreeze and water to allow readings to be taken during the day, year round. However, a green-black sludge was

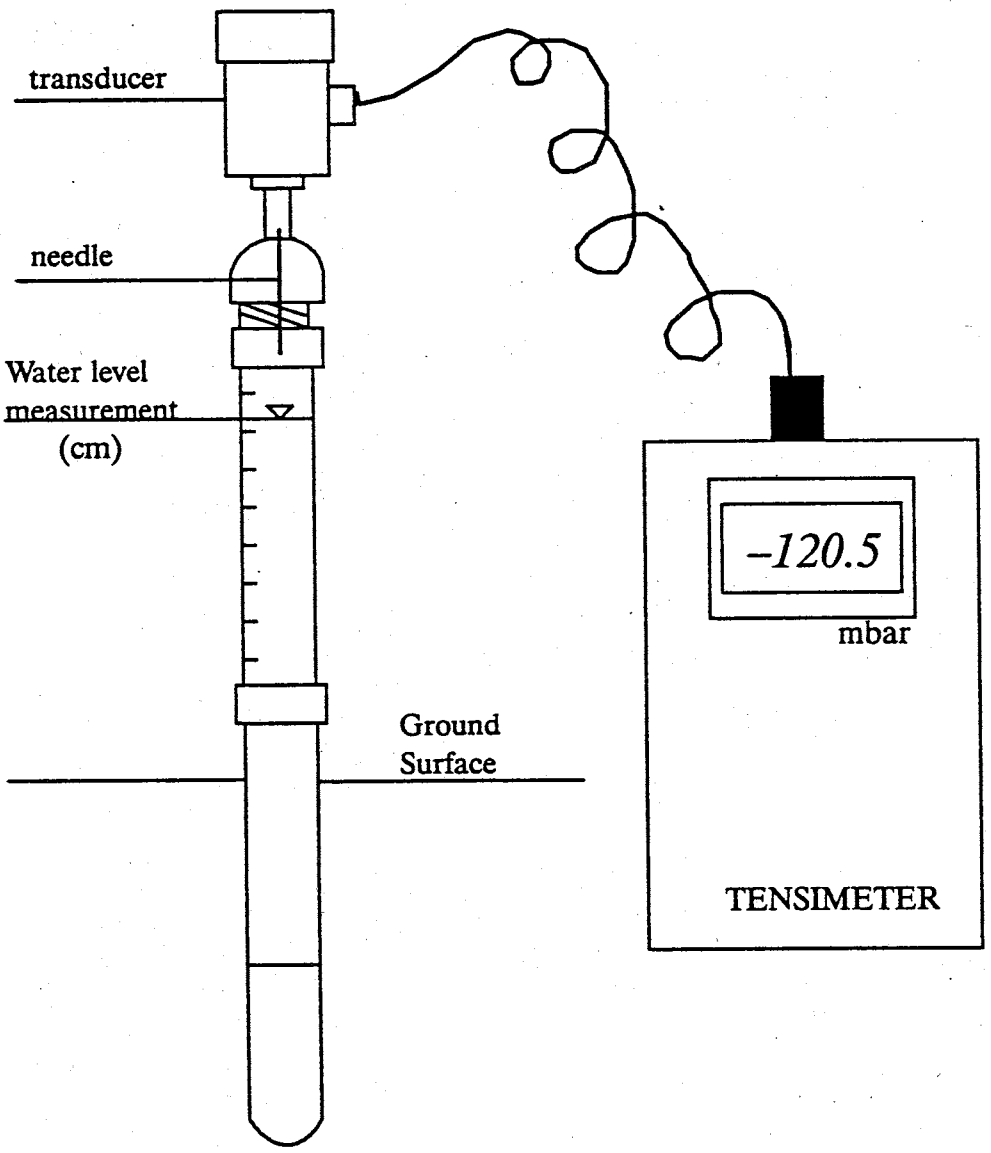

PRESSURE HEAD = Ψ = {C1 x (tensimeter reading) + C2} + water level
where C1 and C2 are conversion/correction values.

Figure 3-2. Pressure head measurement.

detected in the cups. The sludge was either formed by bacterial activity or corrosion of the epoxy about the porous cup. Abnormal amounts of bacteria were not found in the sludge (Kieft, personal communication, 1989) suggesting the epoxy had possibly reacted with the antifreeze to form the buildup. This mixture clogged the pores in the cups and produced near atmospheric conditions in the tensiometer. All the tensiometers at the site were flushed and refilled with water only. This produced much more realistic pressure head data.

3.2.2 Moisture Content Gauge.

Gardner and Kirkham (1952) developed a method of measuring moisture content rapidly and without sample disturbance. The process involved a source of fast neutrons obtained by mixing a radioactive emitter of alpha particles with beryllium. Emitters such as polonium (ibid, 1952), radium (Hillel, 1980b) and americium are available.

The mobile source (within a "neutron probe") is stored within a protective shield. An incorporated computer conducts a standard count of neutrons present in the casing, and this assures the precision of the instrument. The probe is then lowered into an aluminum access tube via a cable incremented with equally spaced clips (Figure 3-3). A known amount of neutrons is emitted from the probe into the surrounding soil at some known depth. They encounter and elastically collide

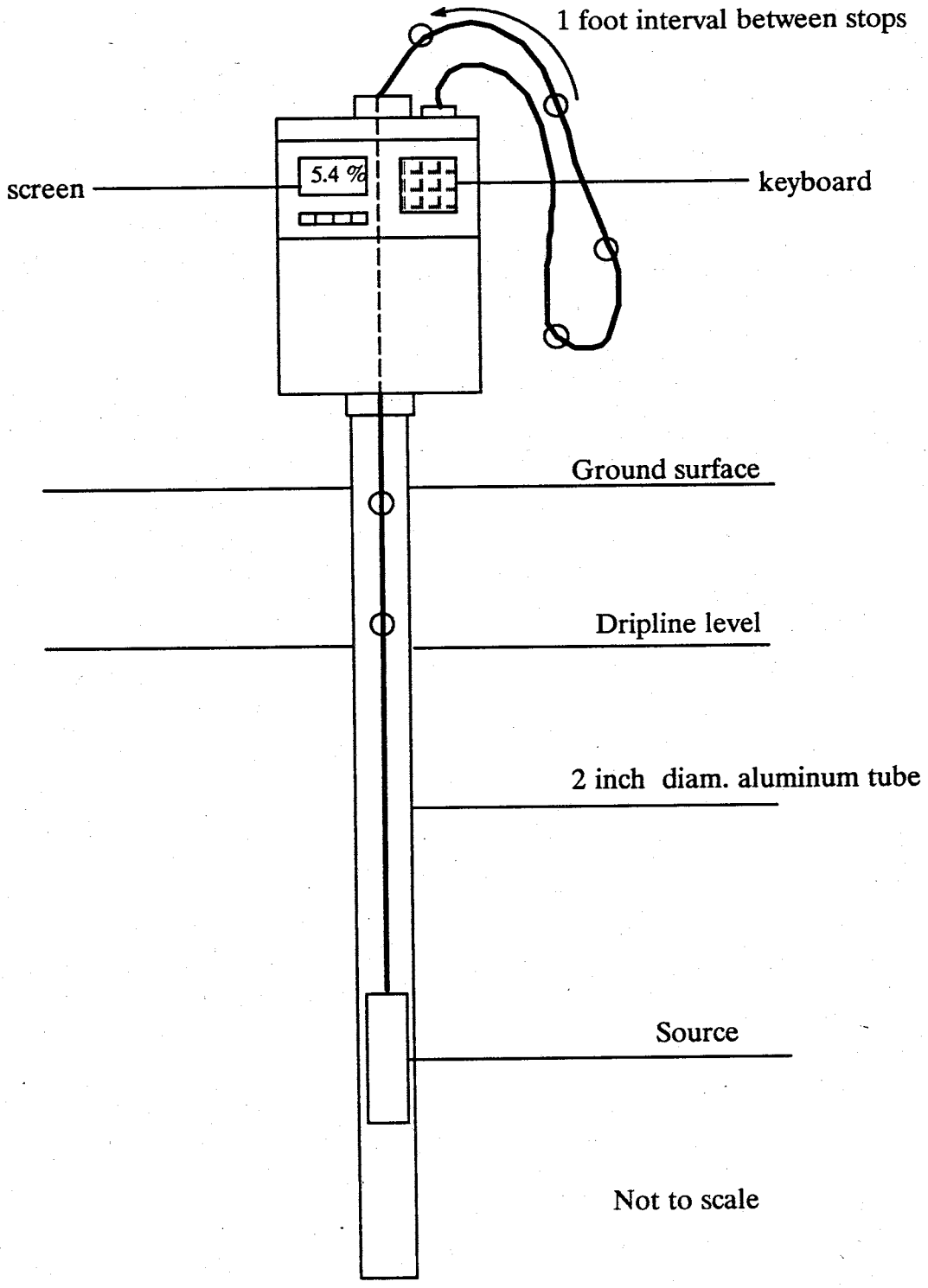

Figure 3-3. Neutron probe/ access tube set-up.

with a number of nuclei. Hydrogen slows these "fast" neutrons more effectively than other common elements (Gardner and Kirkham, 1952). Hydrogen almost always occurs in the form of water but can exist in soil organic matter as well. But this is not a problem considering much water is contained in organic material. The collisions with hydrogen cause neutrons to lose energy and move more slowly. These "slow" particles are detected by the probe over a time period, and this count is converted to a volume per volume measure of moisture content. This was accomplished in our experiment using a calibration (relating count rate and soil wetness) determined by Mattson (1989) for the probe.

Measurements were collected at one foot and half-foot intervals from dripline level to the base of the tubes. The probe is not effective in measuring soil moisture near ground surface. Also, contacts between layers are "smoothed over" during detection of slow neutrons. Volume of cobbles present is not accounted for in measurements of "cobble layer" wetness. The probe determines matrix moisture instead. The technique, however, is nondestructive and is not affected by temperature. Careful positioning of the stops, maintenance of the battery, computer and tubes as well as checks for accuracy permitted collection of reliable and valid data.

3.2.3 Collection of precipitation and temperature data

For this study, rainfall and air temperature data

assisted in general drainage analysis. Precipitation was captured by a tipping bucket rain gauge (Model RG2501, Sierra-Misco). Rainfall entering the 8 inch-diameter collector filled the factory-calibrated bucket assembly, and when the calibrated amount was gathered, the bucket tipped. A contact closure of a reed switch was produced for every one-hundredth of an inch (0.254 mm) of rainfall. Upon each closure, a signal was sent to the data logger and amount of rainfall (in mm, +/- 4% accuracy) was recorded.

The Model 107 temperature probe incorporated thermistors (Fenwal Electronics) which were used to measure air and soil temperature. The CR7 computer converted the probe signals to values of temperature in degrees celsius (+/- 0.2°C accuracy). The data was downloaded to cassette tape which then was interfaced with a personal computer (pc) where data was permanently stored.

3.2.4 Dye Study/Trenching

The qualitative estimation of fluid pathways is also vital in flow field analysis. Several studies have been completed involving application of dyes to an irrigated or ponded field site and subsequent excavation of their trace in the soil in order to provide a visual determination of fluid behavior in the substrata. Ghodrati, et al. (1990) applied Acid-Red 1 (water-soluble, anionic) dye and Dispersed-Orange no.3 dye in solution to eight 1.5 X 1.5 M plots (all loamy

sand to gravelly sand), some of which had disturbed top layers. Four plots were irrigated by sprinkler while the others were ponded. Albrecht, et al. (1989) applied water containing two fluorescent dyes to a small 3 X 9 X 0.9 M compacted earthen liner to examine preferential patterns of water movement through the material. Omoti and Wild (1979) also used fluorescent dyes as solute markers. They wished to determine reasons behind asymmetric leaching of nitrate and chloride in the soil profile.

To characterize the flow field in terms of actual pathways taken by the infiltrating water, a similar qualitative analysis was undertaken at the site. Prior to the drainage phase of the field experiment, three dyes were investigated. Uniformly packed soil columns were assembled containing representative samples from the site. Acid Red 1, Disperse Orange 3 and a blue food dye were each added to individual columns to test their effectiveness during infiltration. The red dye stained the soil well and readily passed through with the water. The Disperse Orange moved through the material but blended in with the soil color making it difficult to trace. The blue dye stained the soil brilliantly (retardation factor = 6) and because it was more noticeable than the red dye, it was ultimately chosen.

This blue food coloring (FD&C no. 1) dissolved readily in water forming an indigo-colored solution. A syringe pump fed the solution into the southern portion of the "main" line

every 15 minutes (water pump activation time) over a 4-day period. A steady quantity of dyed water was applied to the soil through driplines 1-5 (Figure 3-4). During the fifth day, the last day of plot irrigation, the remaining solution was dumped into the water tank and injected into all driplines. Drainage commenced on the sixth day (early September, 1989).

Following intensive drainage monitoring, a series of trenches was completed with a backhoe throughout the 30 X 30 m plot (Figure 3-5). A shallow (1.5 m deep below site datum) SE-NW trench was excavated in three phases. Initially, the channel was dug from the corners of the 30 X 30 m plot to the corners of the irrigated plot during the latter stages of drainage. The second phase brought the trench to the edges of the wooden trench containing the "main" water line. (see Figure 1-2) Finally, the trench became continuous along a SE-NW transect upon removal of the wooden trench. A second trench near Station 12-12 was constructed mid-summer, 1990 and provided a study of instrument performance as suggested by dyed pathways in the vicinity (see Figure 3-4).

3.3 Methods of Analysis

3.3.1 Hydraulic Head/Pressure Head Analysis

Because fluid moves due to a gradient induced by a change in hydraulic head over a distance, it is extremely useful to

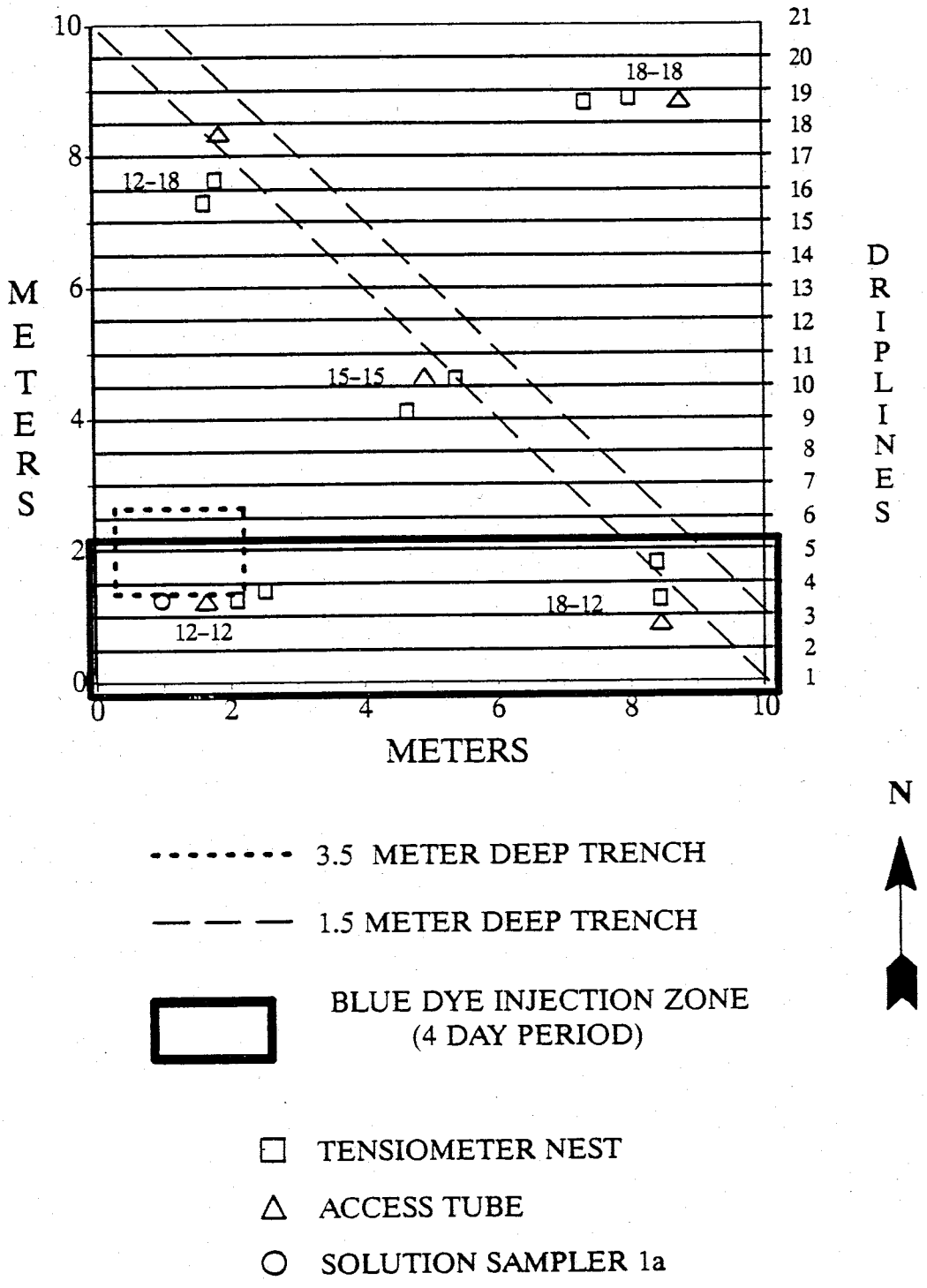

Figure 3-4. 10 x 10 m irrigated plot showing dye injection zone. One soil water sampler is shown as it is relevant to the dye study in the vicinity of station 12-12.

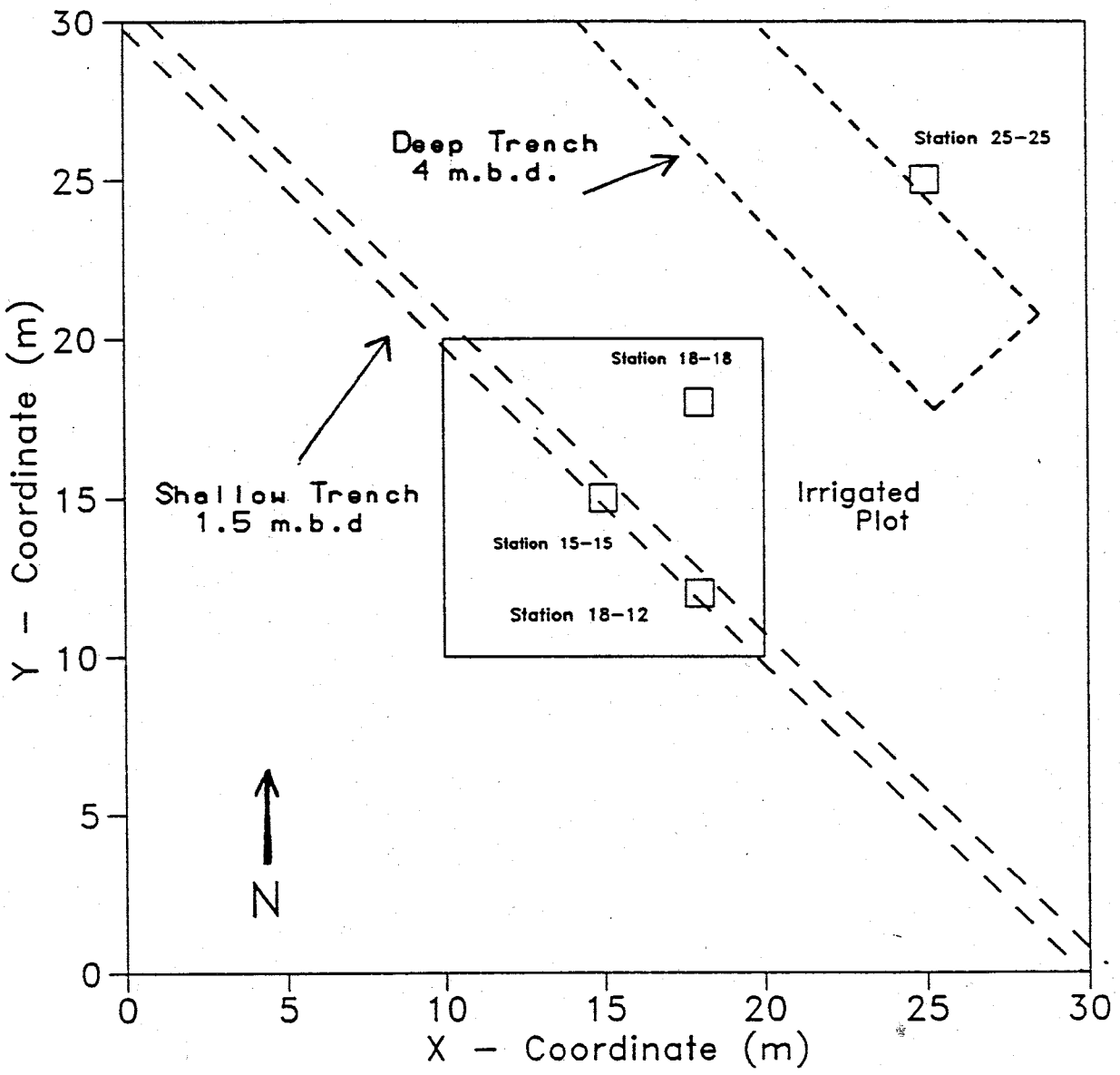

Figure 3-5. Excavated trench locations.

analyze the distribution of hydraulic head with depth, on a site-wide scale. General flow directions can be deduced for the infiltration and drainage events from such a detailed study. In addition, station by station analyses of pressure head distribution can shed light on any discrepancies found in the general head field study.

A number of hydraulic head fields were assembled for vertical transects extending S-N, W-E, SW-NE and SE-NW across the 30 x 30 m plot (Figure 3-6). Two plots were created for each transect. One represents conditions during early September (pre-drainage) while the other represents 16 days of drainage. These drainage period were chosen because we collected data for most of the stations at this time. Also, tensiometers had enough time to equilibrate to draining soil conditions by the 16 day mark.

Most stations had two tensiometers located at about the same depth. The one exhibiting the most consistent and reasonable pressure heads over time was used for the September graphs. Those which showed increasingly negative and stable pressure head values were incorporated into the drainage fields. Data which suggested leaking (gradually less negative pressure head) or clogged (zero or positive psi) tensiometers were not used. Contours for all "fields" were hand drawn and represent intervals of 0.20 meters. In as much as the datum is near land surface, all values of hydraulic head are inherently negative for this experiment, and the vertical

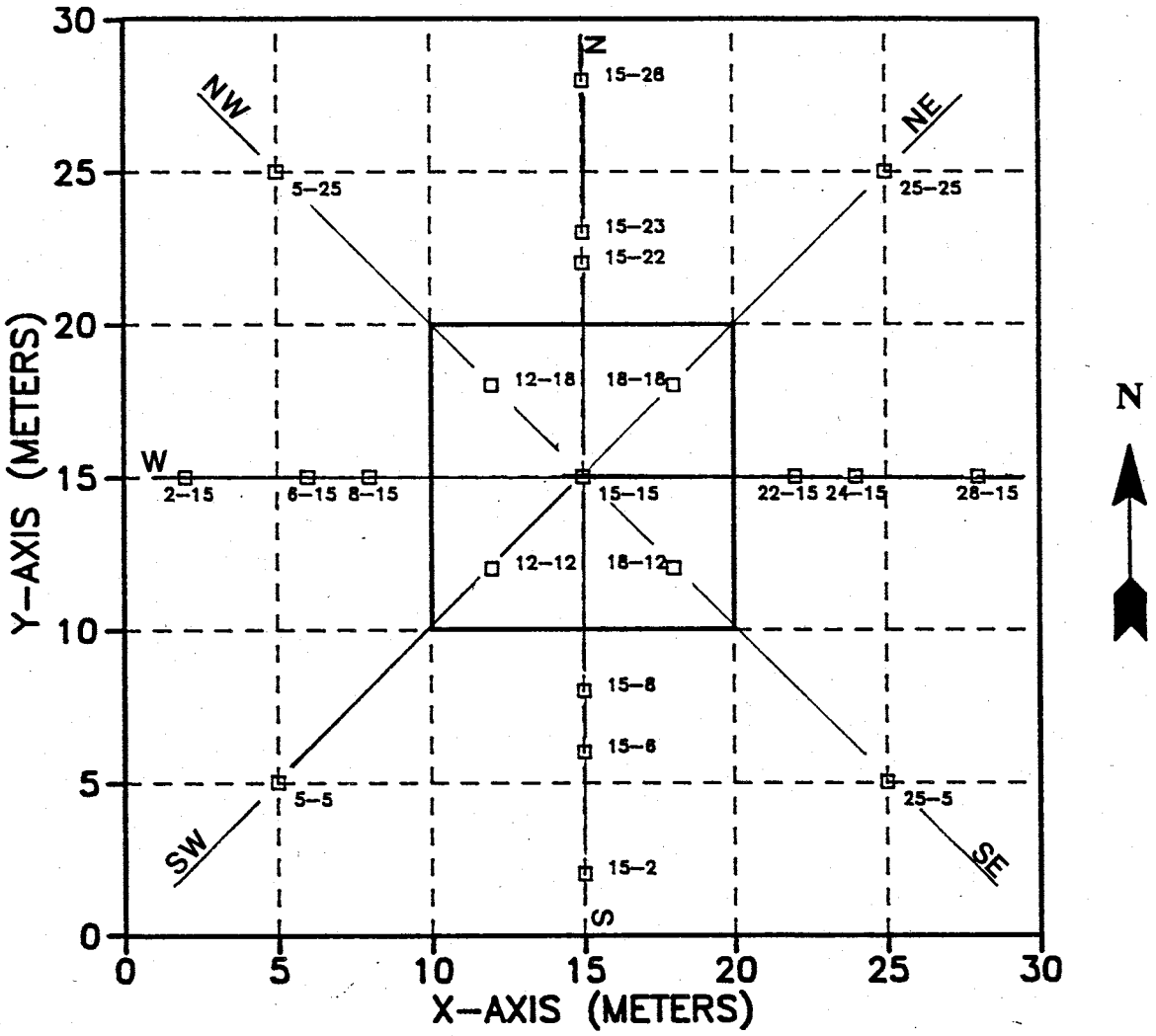

Figure 3-6. Location of four transects for hydraulic head fields.

exaggeration is 5 to 1.

Pressure head profiles were created for each irrigated plot station. Each figure contains one graph for early September (pre-drainage) and one representing conditions after 16 days of drainage. Geologic logs are also included to aid in the analysis of distribution of soil water tension.

The following items are included in head field and/or pressure head profile analysis:

1. Cross-sectional distribution of pressure/hydraulic head with time
2. Geologic controls/ effects on trends in data
3. Sources and sinks for moisture
4. Destination of drained water
5. Explanation of large drops in pressure head over time
6. Problem with zones between stations (uncertainties)
7. Problem of vertical exaggeration (uncertainties)

3.3.2 Moisture Content Distribution

For moisture content data analysis, both plan view and vertical cross-sectional distributions are important in establishing the flow field. To provide a better understanding of site-wide moisture distribution, plan view wetness values were plotted for two different depths at all 21 stations. The Piedmont Slope facies is represented by the 3.0 meter deep plots while the 7.5 meter depth is indicative of the fluvial facies. Figures created for these distributions include an initial (pre-drainage) plot and diagrams created for one, five, ten, twenty, fifty and one hundred days following the start of drainage. All figures have a 2% contour interval, and some values of moisture content were

interpolated for later stages of drainage when data collection was less frequent.

The following items are included in the analysis:

1. Distribution of moisture content with time
2. Spatial variation in geology
3. Anomalous sinks and sources of wetness
4. Presence of preferential flow
5. Speculations on destination of draining moisture

Profiles of moisture content versus depth below datum were completed for five stations within the irrigated plot and nine stations just outside the plot. Analyses of these distributions were undertaken, as needed, to complement the more general plan view moisture content study. The remaining seven (i.e. stations 25-5, 15-2, 5-5, 5-25, 2-15, 5-25 and 15-28) of the outermost stations were not studied, in as much as wetness was largely unaffected by the drainage process. Data collected for the completed graphs include pre-infiltration conditions from January, 1987 (for irrigated plot) and February-March, 1987 for other stations. The initial values for the "1989 plots" were gathered one or two days prior to drainage, depending on the location and data collection schedule.

3.3.3 Unsaturated Hydraulic Conductivity

Once pressure head and moisture content data are collected and analyzed, the data can be used to calculate a third parameter, hydraulic conductivity. Before this calculation is described in detail, a brief review is in

order.

The literature describes a variety of field methods to determine unsaturated conductivity. Three of these require a steady state flux to measure conductivity (K). For the "impeding layer" or "crust" method (Hillel and Gardner [1970]; Bouma, et al. [1971]) a constant head is maintained above a thin artificial or natural crust ($K_{crust} < K_{underlying\ soil}$) until a steady flux into the soil has been obtained (Hendrickx, 1990). Hydraulic conductivity (K) equals the flux rate (q) for a uniform soil where the hydraulic gradient equals unity. For areal measurements of conductivity, the "sprinkler" method is useful. Water is uniformly distributed at a flux less than the saturated hydraulic conductivity for a long period of time. Moisture content and pressure head data are collected at steady state, and K is determined using Darcy's Law. Both of these methods are described in detail by Green, et al. (1986) and Hendrickx (1990).

Thirdly, Stephens (1985) developed the "flow net" method for ponded conditions. Once a steady flux is achieved, pressure head measurements are collected via tensiometers installed close to the ponded source. A flow net is constructed from the data, and stream tubes are drawn. Relative conductivity (K/K_{sat}) is then determined using hydraulic gradient and cross-sectional area of stream tube partitions.

To employ transient data, the "instantaneous profile" or

"drainage flux" test is implemented. This method relies on measuring moisture profiles during a drainage process. This allows us to determine soil moisture flux and, eventually, hydraulic conductivity.

As described above, a number of methods are available for determining hydraulic conductivity in unsaturated soil. Because of its ease in use, the instantaneous-profile (I-P) test (Rose, 1952 (theory) and Watson, 1966 (development)) was utilized to characterize vertical drainage beneath the irrigated plot. This procedure does not require destructive sampling and determines hydraulic conductivity as a function of moisture content. Pressure head, volumetric moisture content, drainage time and depth measurements need to be collected during transient unsaturated flow. Drainage is assumed to be a one-dimensional, downward process. If drainage occurs in the absence of suction gradients, then it occurs under gravity influence only (Hillel, 1980a). In such a system, effects of lateral flow, evaporation, runoff and plant/root water intake are not considered during drainage data analysis. It is also important to note that knowledge of the soil moisture characteristic curves is not necessary, as drainage data alone will suffice.

Development of the I-P test theory incorporates the above assumptions into the general one-dimensional unsaturated flow equation:

$$\frac{\partial \theta}{\partial t} = \frac{\partial}{\partial z} K(\theta) \frac{dH}{dz} \qquad (1)$$

where: θ = moisture content (vol/vol)
t = time (days)
z = depth below datum (cm)
$K(\theta)$ = hydraulic conductivity (cm/day)
H = hydraulic head (cm)

To determine conductivity values at prescribed depths, equation (1) must be integrated across an interval of z:

$$\int_{z_1} \frac{\partial \theta}{\partial t} dz = \left[K(\theta) \frac{dH}{dz} \right]_z = \frac{\partial \theta}{\partial t} Z \qquad (2)$$

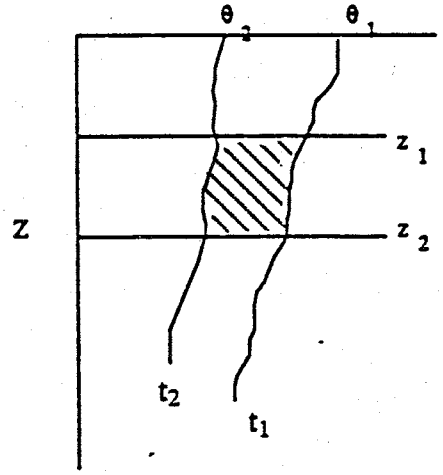

Figure 3-7. Graphical Representation of Equation 2.

Equation (2) indicates that a change in moisture content over time at depth z is due to a change in soil moisture flux through that depth. As conductivity is highly dependent on moisture content, a decrease in moisture over time across an interval of vertical distance (z) likewise produces a decrease in conductivity and gradient. dH/dz represents the average head drop across the shaded region of Figure 3-7. The change in moisture with time integrated over the depth interval is equal to the flux through that interval over that time (equation 2). Therefore, to determine conductivity, $\partial\theta/\partial t$ and dH/dz must first be calculated from measured head and moisture content.

Calculation of Soil Moisture Flux (q)

The time rate of change in moisture content for selected depths is calculated from the measured moisture contents at selected depths. The rate of moisture change ($\partial\theta/\partial t$) is multiplied by the depth interval (dz) across which the decrease in moisture content is measured. For example, in Figure 1-6, the interval between the 86 cm depth and the 116 cm depth is 30 cm (=dz). This value (dz) would be multiplied by the slope of the 116 cm drainage curve ($\partial\theta/\partial t$) at a specified time. The depth which denotes each curve is, by convention, the base of an interval "dz." The data in each curve is indicative of drainage through the interval just

above this base depth.

The flux, q, is obtained from the following equation (Hillel, et al., 1972):

$$q = \left(\frac{dW}{dt}\right)_z = Z\frac{\partial\theta}{\partial t} \qquad (3)$$

where q = soil moisture flux (cm/day)
W = total water content of profile to depth z (cc/cc)
Z = soil depth to which this measurement (q) applies

The soil moisture flux is indicative of not only the flux through the soil depth interval being evaluated but also of the fluxes through the overlying layers. Therefore $dz(d\theta/dt)$ becomes additive from depth interval to interval. Once q has been determined at each depth in the profile, attention is shifted to calculation of hydraulic gradient (dH/dz).

Calculation of Hydraulic Gradient and Hydraulic Conductivity

Collection of pressure head data was described above. These values of head are added to their corresponding depths to produce hydraulic head values. A negative sign is inherent for hydraulic head as both pressure head and elevation head (z) are negative. This number is then plotted against depth producing straight-fitted curves (i.e. Figure 3-8). Hydraulic gradient is the slope (dH/dz) determined at the

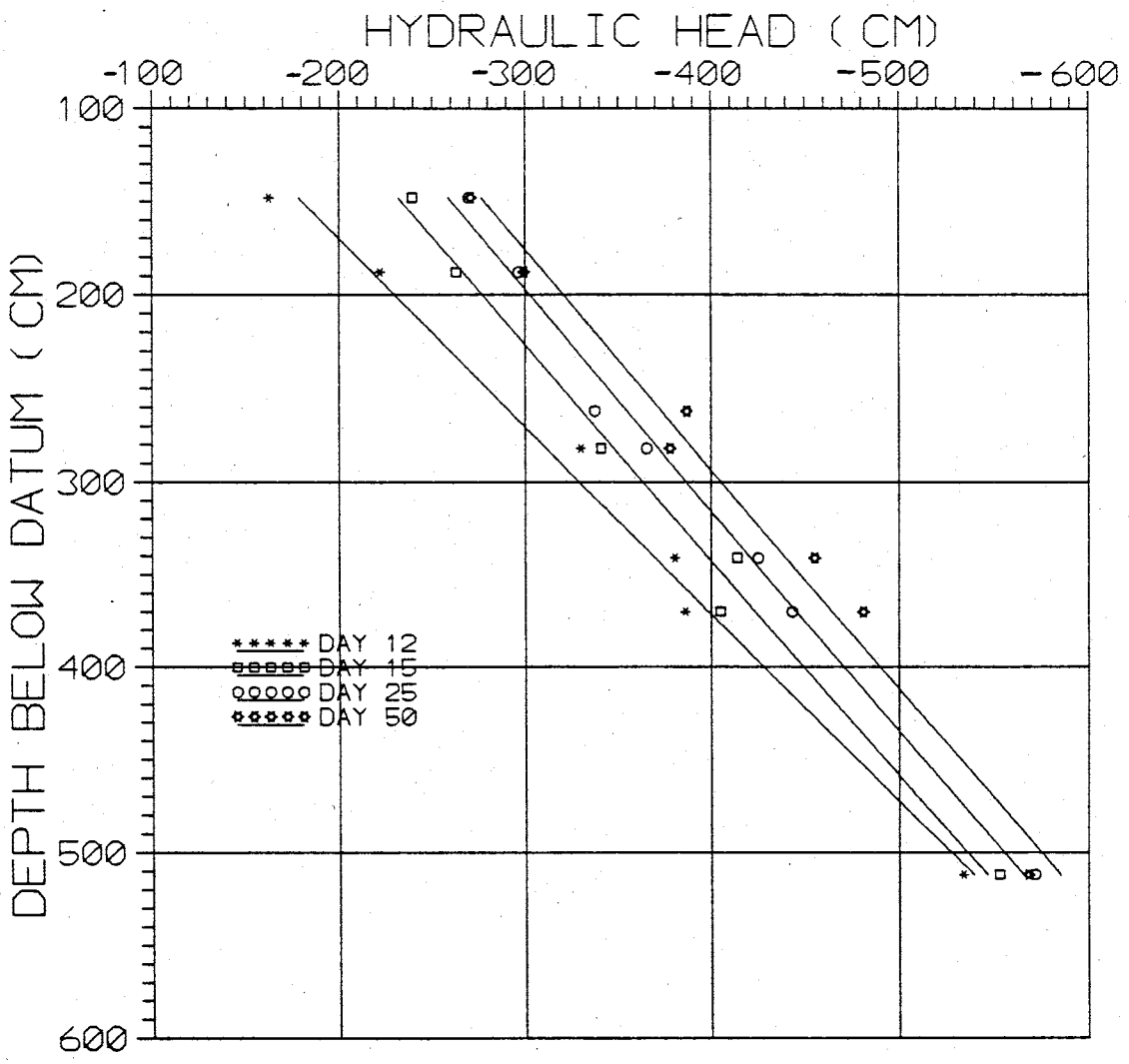

Figure 3-8. Hydraulic head vs. depth below datum--Station 15-15.

point of intersection of a set value of depth and the representative time curve.

Calculation of $K(\theta)$ is based on Darcy's Law. Values of q determined at certain depths are divided by the hydraulic gradient calculated for those depths to give the unsaturated conductivity. Spatial differences in hydraulic conductivity and the exponential fit of K and θ-data can then be used to hypothetically distinguish hydrologic units. Results from Station 15-15 are discussed in detail below.

3.3.4 Uncertainties in Field Data

In order to effectively study and model (numerically) the subsurface flow field, certain uncertainties and data collection limitations must be noted and accounted for. These have a bearing on the moisture content, pressure head, dyed soil and hydraulic conductivity analyses.

For moisture content data collection, the neutron probe has a few shortcomings which affect the data itself. The "zone of influence" in dry soils for the probe is 25 centimeters and increases somewhat in size for wetter regions. Near surface moisture, however, cannot be examined due to this limited zone. The neutron probe tends to "smooth over" sharp contacts between soils, averaging moisture contents. Volume of cobbles is not considered in determination of θ as only matrix wetness is measured. Also, if the "clips" or "stops" on the cable connecting the probe and the machine are moved,

data collected for certain depths can be confused.

Uncertainties can be created in pressure head and subsequently conductivity data by faulty tensiometers or tensimeters. Clogged tensiometer cups prevent water movement from soil to tube, thus creating a stable water level and constant pressure head with time. The cup itself cannot be used for pressure head values less than -0.8 bar. Air entry into the cup occurs at this point. Measurements conducted during daylight hours also reflect bias as increase in temperature result in decrease in suction (Chahal, 1965). Lastly, crooked needle placement during measurement or incorrect tensimeter calibration produce questionable data.

Flow and geologic effects of several varieties can also make data analysis difficult. Lateral flow induced by textural variations and sharp soil contacts may occur at this site. Assumption of unit gradient and pure vertical drainage may or may not apply on a local scale. Macropores, preferential flow along instrumentation and infiltration-induced fluid pathways (Simpson, et al., 1982) provide easy means for moisture distribution which may or may not be detected by the neutron probe and tensiometers. Also, strong rainstorms produced flooding into depressions around stations 18-18 (prior to completion of irrigated plot) and stations 6-15, 24-15 and 28-15 which may have caused anomalous, sudden increases in the moisture content measurements at shallow depths.

3.3.5 Model Descriptions for Physical Properties and Drainage

Once moisture content, pressure head and hydraulic conductivity data were collected and analyzed, two analytical models were utilized to produce a soil characteristic curve fit to the field data and predict the functional relationship between moisture content and conductivity. Soil water parameters necessary for the computations are included below in the modelling results section.

Characteristic Curve

In deriving an equation predicting relative conductivity (K/K_{sat}) based on knowledge of the soil-water retention curve, Mualem (1976) defined a dimensionless water content, Θ. This parameter relates residual water content and saturated water content as follows:

$$\Theta = \frac{\theta - \theta_r}{\theta_s - \theta_r} \qquad (4)$$

where θ_r = residual volumetric water content (cc/cc)
θ_s = saturated volumetric water content (cc/cc)

The parameter Θ was further described as a function of pressure head by van Genuchten (1980):

$$\Theta = \left[\frac{1}{1+(\alpha\psi)^n}\right]^m \qquad (5)$$

where Ψ = pressure head (cm)
α, n, m are coefficients

Equation (5) can be solved for θ, yielding (6):

$$\theta = \theta_r + \frac{\theta_s - \theta_r}{[1+(\alpha\psi)^n]^m} \qquad (6)$$

where m = 1 - 1/n (a simplification from Mualem's soil water retention theory)

These equations were incorporated into a computer code (van Genuchten, n.d.) which allows the soil-water retention model to be fit to experimental moisture content and pressure head data. The program predicts θ_r, θ_s, n, alpha and unsaturated conductivity (K_{sat}).

For the purposes of this project, only drainage data was used, and the model produced a set of fitted data for the characteristic curves discussed in section 4.2.1. For an in-depth application and statistical analysis of parameters including K_{sat}, n and α generated from site data, the reader is directed to Parsons (1988) and Schmidt-Petersen (1991).

Conductivity -- Moisture Content

To predict drainage from field plots, Sisson, et al. (1980) adapted an equation from Brooks and Corey (1964) which relates unsaturated hydraulic conductivity and moisture content:

$$K(\theta) = K_{sat}\left(\frac{\theta-\theta_r}{\theta_s-\theta_r}\right)^{\frac{1}{n_s}} \qquad (7)$$

where n_s is a coefficient different from van Genuchten's "n"

Because the parameters K_{sat}, θ_r and θ_s have been described by Parsons (1988) for many borehole site samples, the only unknown constant is n_s.

Expressing equation (7) in terms of dimensionless K (or relative conductivity, K_r) and moisture content, we now have:

$$K_r(\Theta) = \Theta^{\frac{1}{n_s}} \qquad (8)$$

van Genuchten (1980) described a Brooks and Corey derivation of $K_r(\Theta)$ as:

$$K_r(\Theta) = \Theta^{3+\frac{2}{\lambda}} \qquad (9)$$

where λ = the pore size distribution index
= n_{vg} -1 (where n_{vg} is van Genuchten's "n")

Equating (8) and (9), we now have:

$$\Theta^{\frac{1}{n_s}} = \Theta^{3+\frac{2}{n_{vg}-1}} \qquad (10)$$

$$\frac{1}{n_s} = 3 + \frac{2}{n_{vg}-1} \qquad (11)$$

$$n_s = \frac{1}{3 + \frac{2}{n_{vg} - 1}} \qquad (12)$$

Using values of n_{vg}, K_{sat}, θ_r and θ_s determined by Parsons (1988), a graphical relationship can be produced between K and θ. Unsaturated hydraulic conductivity calculated from equation (7) can then be compared to K-θ graphs created from the instantaneous profile (I-P) test for various depths.

Chapter 4. Basic Conceptual Model of Flow Field

The purpose of this chapter is to develop a conceptual model of the general flow field during drainage. This will be accomplished through analysis of hydraulic head and moisture content distribution throughout the site. Hydraulic head data were gathered from all 21 stations, and four sets of vertical, cross-sectional head fields were developed. Site-wide moisture content data, collected for two depths, each representing a different facies, are included below for variable drainage periods. Both the head fields and "plan view" moisture content distributions are described in separate sections. A summary is presented in section 4.2.

4.1 Hydraulic Head Fields

The purpose of generating head fields is to determine site-wide infiltration and drainage patterns. Four transects were chosen and mark locations of vertical cross-sectional hydraulic head distributions, or head fields. Values for pre-drainage (early September) and drainage (16 days) are displayed. A vertical exaggeration of 5 to 1 was used so the fields could be contoured using a 0.20 M interval, except for Figure 4-1 which shows a normally scaled W-E transect. Unfortunately, data points are too close together in such a figure, making contouring difficult. Each data point (subsurface asterisks) in vertically exaggerated head

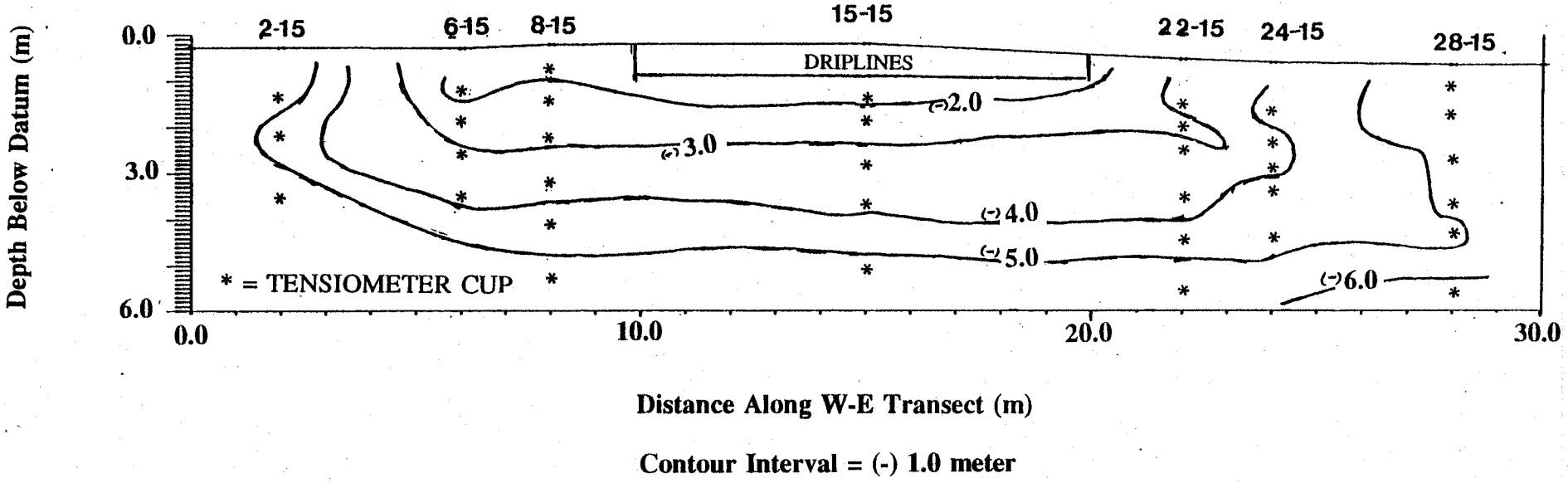

Figure 4-1. Normally scaled W-E trending hydraulic head field.

fields marks the location of the tensiometer cup. For all fields constructed, head data are negative in sign, and the contour interval is (-) 0.2 M. Hydraulic head (and pressure head) data for these points are listed in Appendix D. Flow lines are liberally drawn, considering anisotropy is present, especially on a local scale. However, these flow lines permit general conclusions to be drawn concerning site infiltration and drainage.

Directly beneath the driplines (irrigated plot) vertical infiltration and drainage have apparently occurred. This feature is strongly evident below the western half of the irrigated plot along the W-E transects (Figures 4-2, 4-3). In fact, the vertical flow zone is wider than the source area (driplines). The zone widens with depth, permitting flow with a substantial vertical component to occur during both infiltration and drainage. This flow, however, may have varied on a local scale. Hydraulic head data were not collected for the region between stations 8-15 and 15-15. Geologic data, however, can be helpful in developing these areas where numerical data is not available.

In analyzing the apparent vertical flow, we can use soil borehole information from porous cup sampler (PCS) boring logs developed by Arnet (1991). Refer to Figures 1-4 and 1-5 for their locations and Appendix A for the logs. At a depth of 1.5 feet below datum, a 0.5-1.5 feet thick, pervasive silty clay unit extends from PCS 4 to PCS 17, through the center of

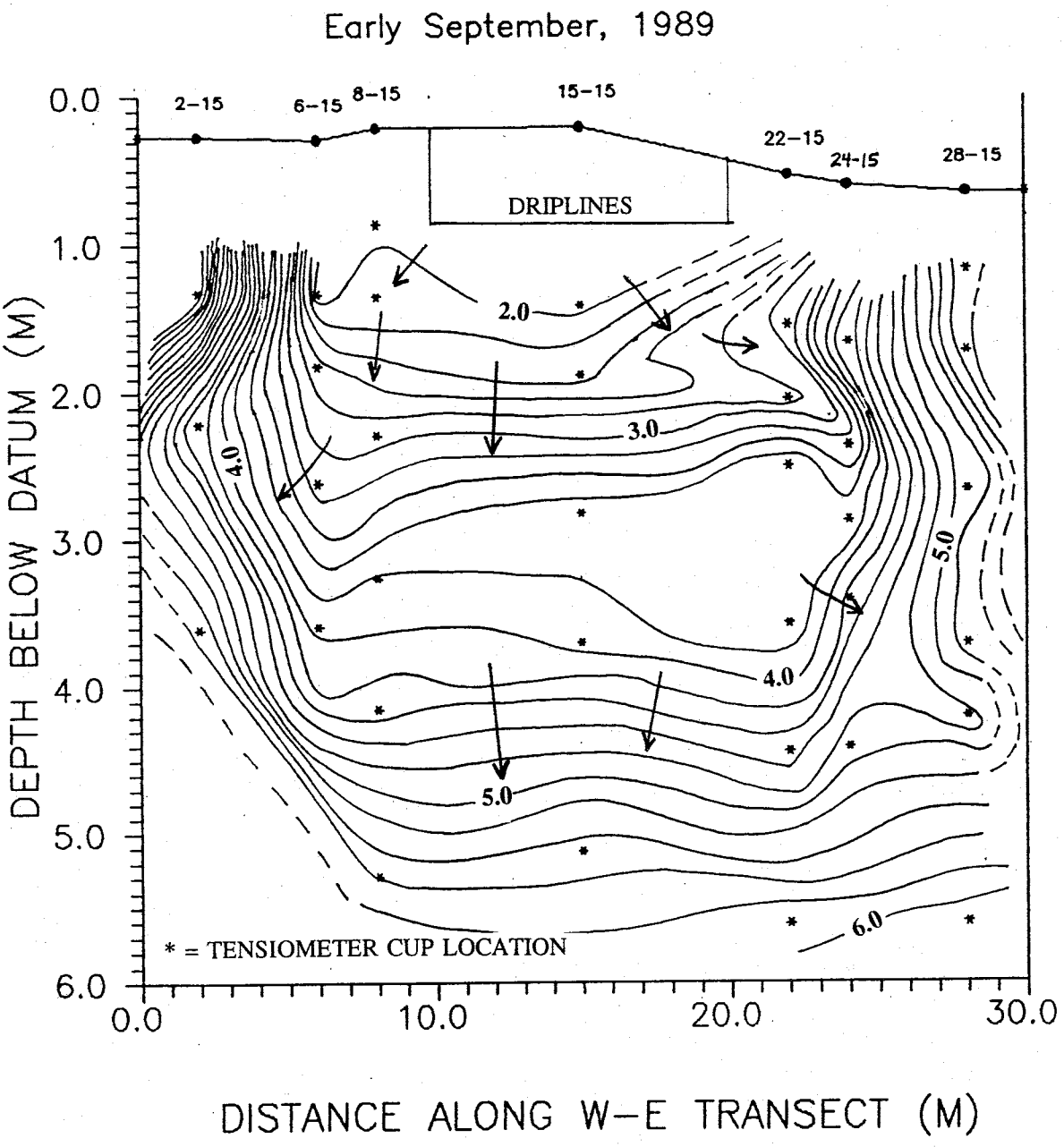

Figure 4-2. Hydraulic Head Field--W-E Transect: Infiltration.

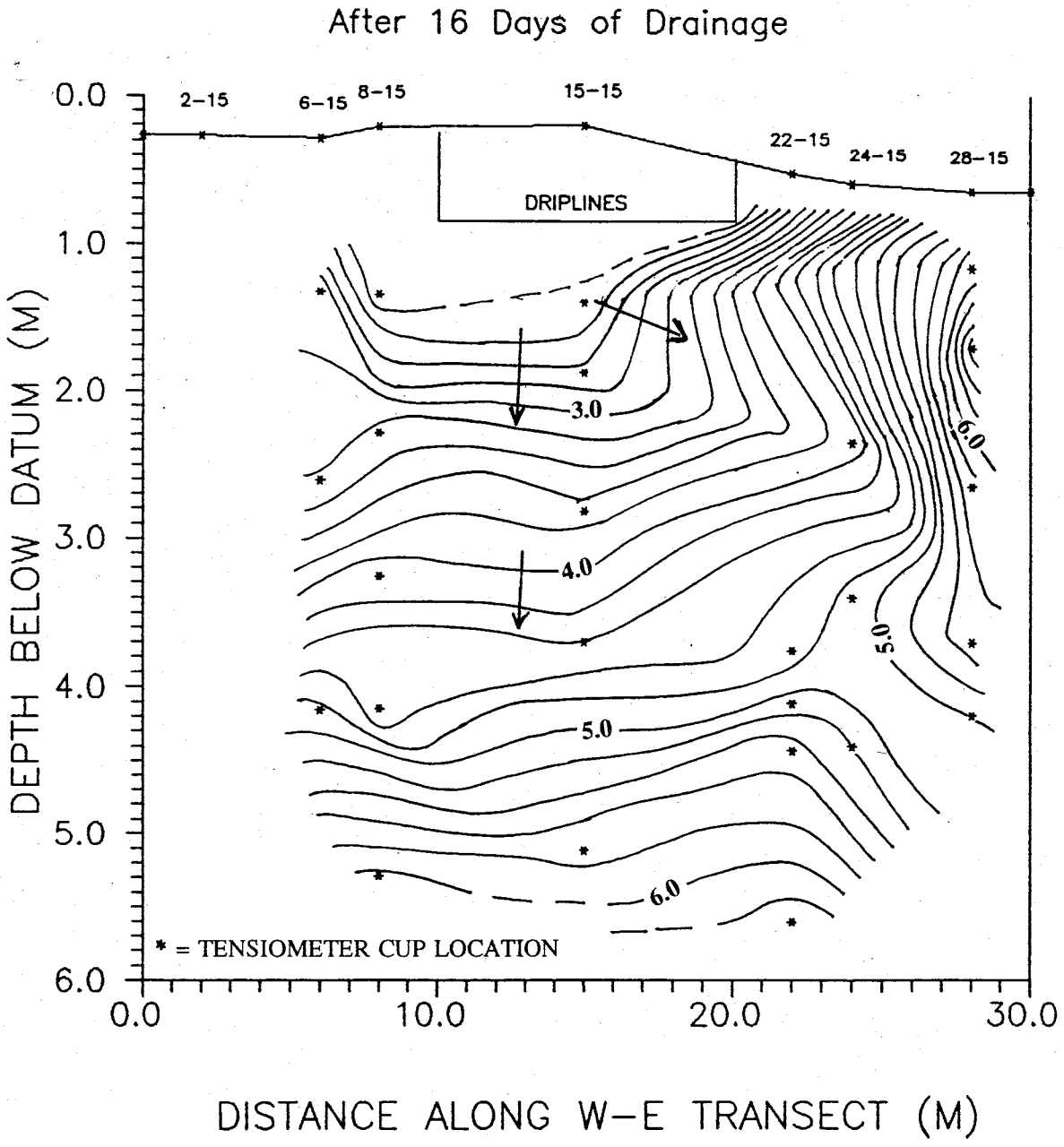

Figure 4-3. Hydraulic Head Field--W-E Transect: Drainage.

the irrigated plot (see Appendix A for these logs). Similarly, in PCS 9 and 13, a 1-1.5 meter thick silty clay occurs around the two meter depth (below datum). Due to high moisture content, the silty clay is more conductive during drainage than underlying cobble and sand layers. Yet, the ability of water to drain from this layer can be restricted by the coarser layer beneath it (Eagleman and Jamison, 1962). The suction exerted by the coarse layer must equal or exceed that of the finer pores in order for water to move from a fine soil to a coarser soil. Therefore, if vertical infiltration or drainage cannot readily occur, water may move along the surface of the coarser soil.

Flow lines deflect from vertically downward both to the west (2-4 MBD) and east (2 and 4 MBD) in Figure 4-2. Southerly deflections also occur between the 2 and 4 meter depths in Figure 4-4. These deflections may have been caused by the presence of coarse material such as cobble layers.

Common to several geologic logs compiled by Parsons (1988), including those for stations 15-15 and 22-15, are shallow (2.5-4 MBD) and deep (5-6 MBD) cobble layers (Pages B1, B4, B13, Appendix B). The log for station 22-15 does not show a shallow cobble layer two meters deep, east of the irrigated plot, where the head field indicates strong lateral flow. However, a cobble layer between 2.3 and 3 meters deep is shown in the ENE borehole log (Page A21, Appendix A). This cobble layer appears continuous with 2.5 and 3.8 meter

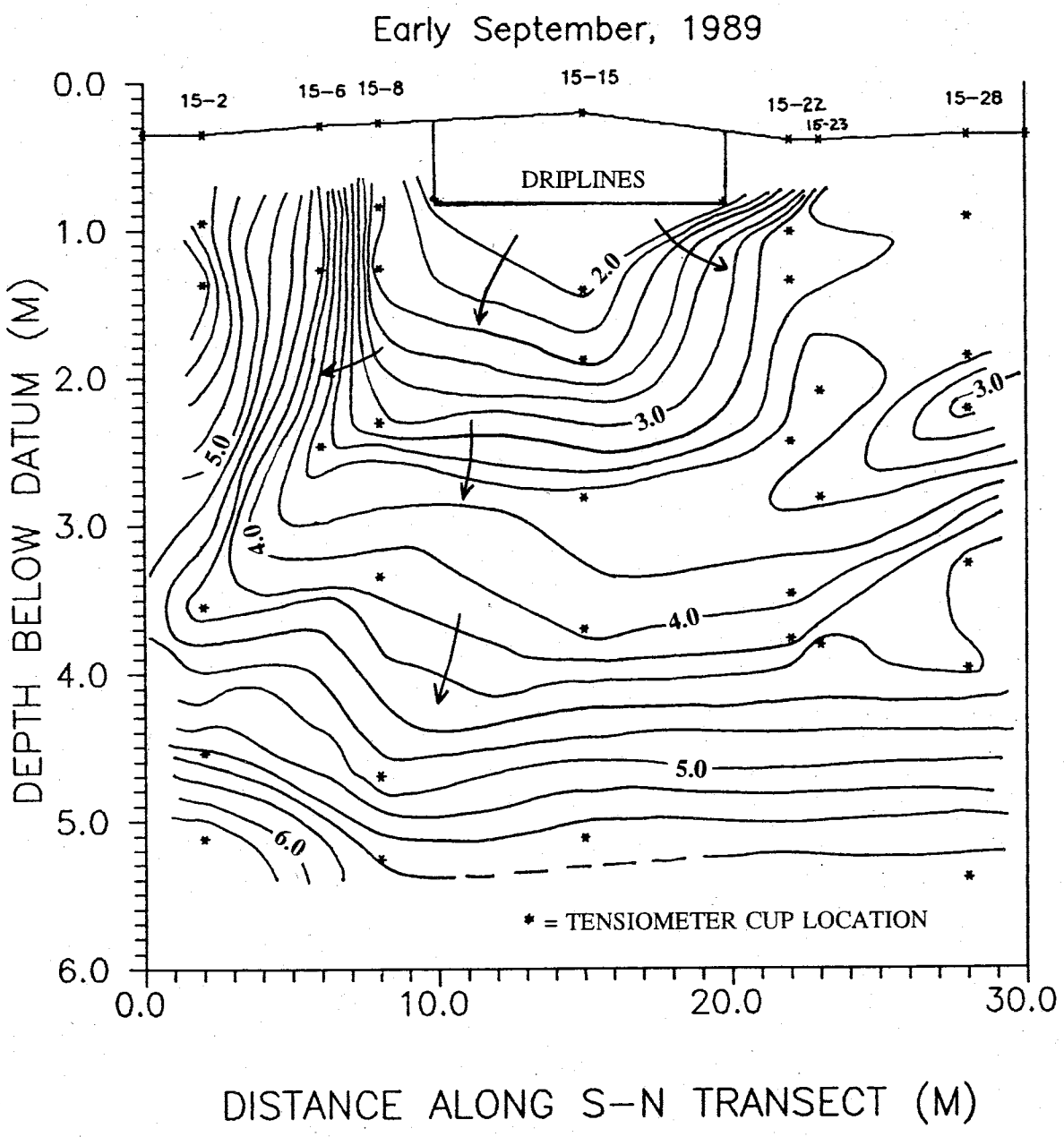

Figure 4-4. Hydraulic Head Field--S-N Transect: Infiltration

deep cobble layers described in borehole logs for stations 15-6 and 15-2, respectively. Depths of this apparently continuous cobble layer correspond to the region of lateral flow described above.

It is useful at this point to define the nature of these cobble layers. As described in section 1.3, cobble layers consist of cobbles suspended in a silty fine sand matrix. These cobble layers can be laterally extensive (3-4 meters deep below the irrigated plot extent) or can pinch out abruptly. For example, the shallow cobble layer (3.75 MBD) in the log for station 18-18 may be laterally continuous with the layer 3.5 meters deep at station 25-25. However, the deep cobble layer at station 18-18 pinches out somewhere between these two station locations.

To better define flow in the region between stations 18-18 and 25-25, a 3.5 meter deep trench was excavated in Spring 1990 (Figure 4-5). Two "wet" regions were mapped above two different cobble layers along the southwestern face of the trench. These wet units consist of silty clay and silty sand. Because the variable matrix material in the cobbles beneath these units was not damp, these is reason to believe lateral infiltration and drainage occurred above the cobble zone.

This lateral migration of moisture is further evidenced by the moisture content profile for station 25-25 (Figure 4-6). A large increase in moisture content is found between 4 and 5 meters deep. Although this depth correlates with the

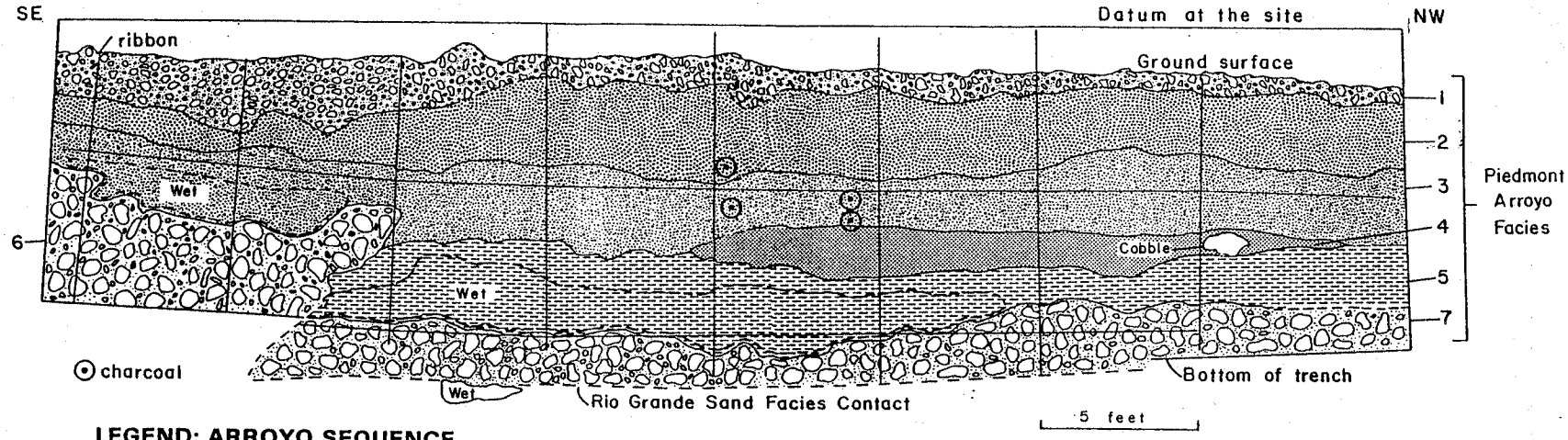

LEGEND: ARROYO SEQUENCE

UNIT 1: A 1 to 2 foot thick continuous silty sand bed with either bedded or suspended sands and gravels. The bedded gravels represent high energy flow. This unit was deposited in the last 200 years.

UNIT 2: A massive and continuous 1 to 3 foot thick silty sand with interbedded subrounded to subangular sands and gravels in bottom half. Bounded by a discontinuity on the top and a scoured surface at the base. This unit contains small fining upward bedded channel deposits.

UNIT 3: A 2 to 3 foot thick silty to sandy clay with little sand and gravel lenses. This unit is characterized by up to 30% clay, scattered pieces of charcoal, entrapped air and a blocky texture. The southern end of this unit became wet due to irrigation experiment.

UNIT 4: A 1½ foot thick distinctly bedded sand and gravel subunit of Unit 3 found on northern side of well. Deposited with substantial amounts of water in a high energy environment. The beds in the lower half of the unit bend down toward the depositional surface. Black hematite and manganese stains are found within this unit.

UNIT 5: A 2 foot thick silty sand with some clay and little lenses of sand and gravel that was interrupted in the southern end of the trench by Unit 6. This unit is characterized by a blocky texture due to its high clay content and low energy depositional environment. Parts of this unit became wet due to the irrigation experiment.

UNIT 6: A high energy debris flow that is seen in southern end of the trench. The debris flow carried cobbles up to 1 foot in diameter suspended in a viscous, fine to coarse sand and gravel matrix.

UNIT 7: An extensive 1 to 3 foot thick high energy debris flow that lies conformably on top of the Rio Grande sands. This unit may represent the last discharge event of the Pleistocene. The unit consists of bedded sand and gravel layers on top of a layer of cobbles suspended in a sand matrix.

Figure 4-5. Arroyo sequence as exposed in SE-NW trending trench. (from Arnet, 1991)

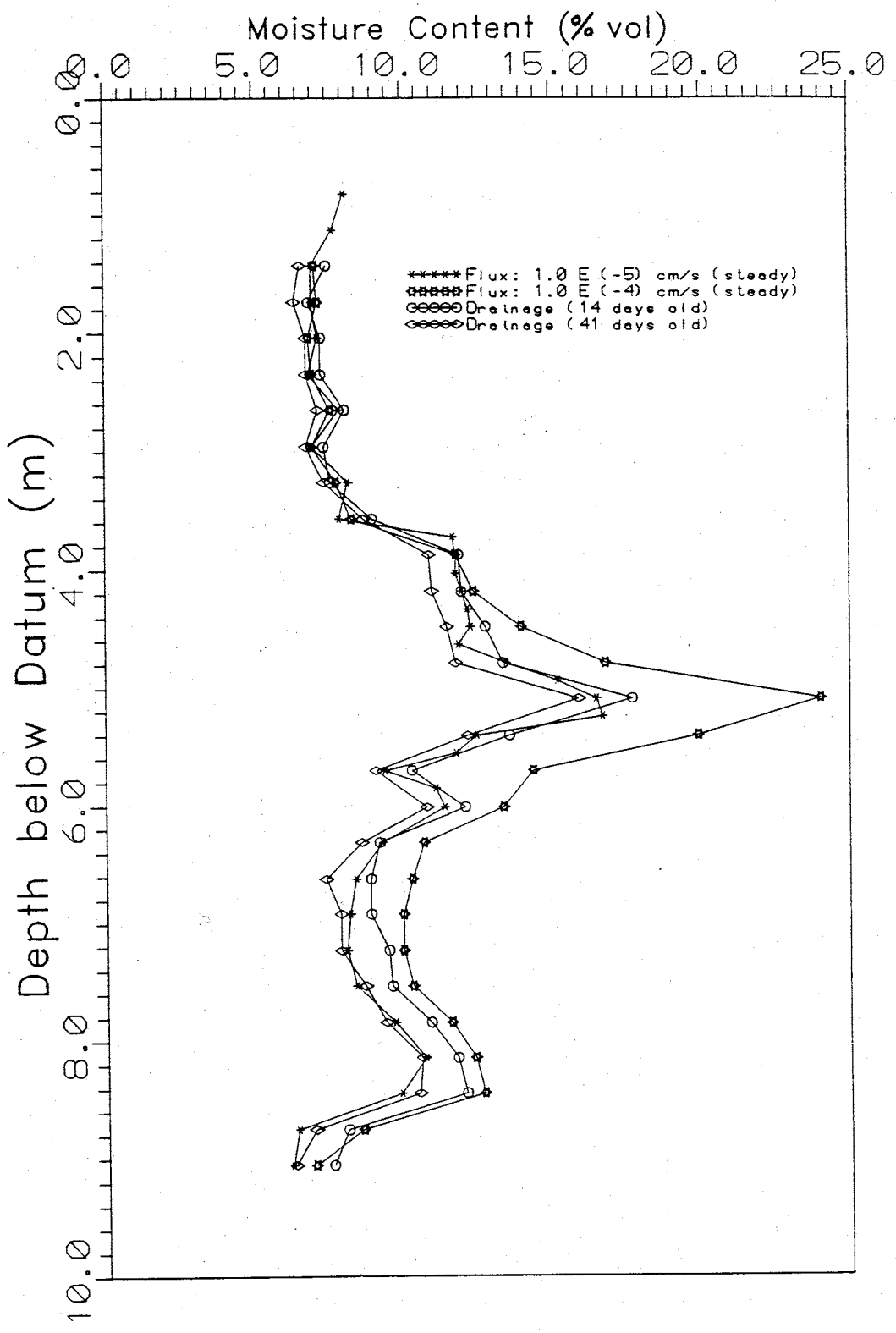

Figure 4-6. Moisture Content Profile--Station 25-25.

presence of silty clay (4.3 MBD in the geologic log at this location), it may be that the cobble layer shown in the trench became thinner or pinched out. The wet regions of the exposed trench wall and the high moisture content logged at station 25-25 suggest water moved along the top of the cobble layers observed in the trench until these layers pinched out; then water moved downward beyond the trench area.

The geologic and moisture content data strongly support the interpretation that lateral flow occurs to the northeast; 3 meters deep in the vicinity of the deep trench and 5 meters deep at station 25-25. The head fields constructed for the SW-NE transect also support this (Figures 4-7, 4-8), although there are not enough data to be definitive. For example, hydraulic head data was not collected between stations 18-18 and 25-25. and between stations 5-5 and 12-12. Moisture content values for station 5-5 did not vary greatly from pre-infiltration values. Therefore, infiltrating moisture apparently did not flow to station 5-5, despite the appearance of the dashed head fields. Therefore, the SW-NE and SE-NW head fields are only helpful in defining flow beneath the irrigated plot. No data was gathered at station 5-5 for the drainage phase (Figure 4-8).

Infiltration and drainage plots for both these diagonal transects suggest vertical flow occurred beneath the 10 x 10m plot. However, a cobble layer is found 3.5 MBD below

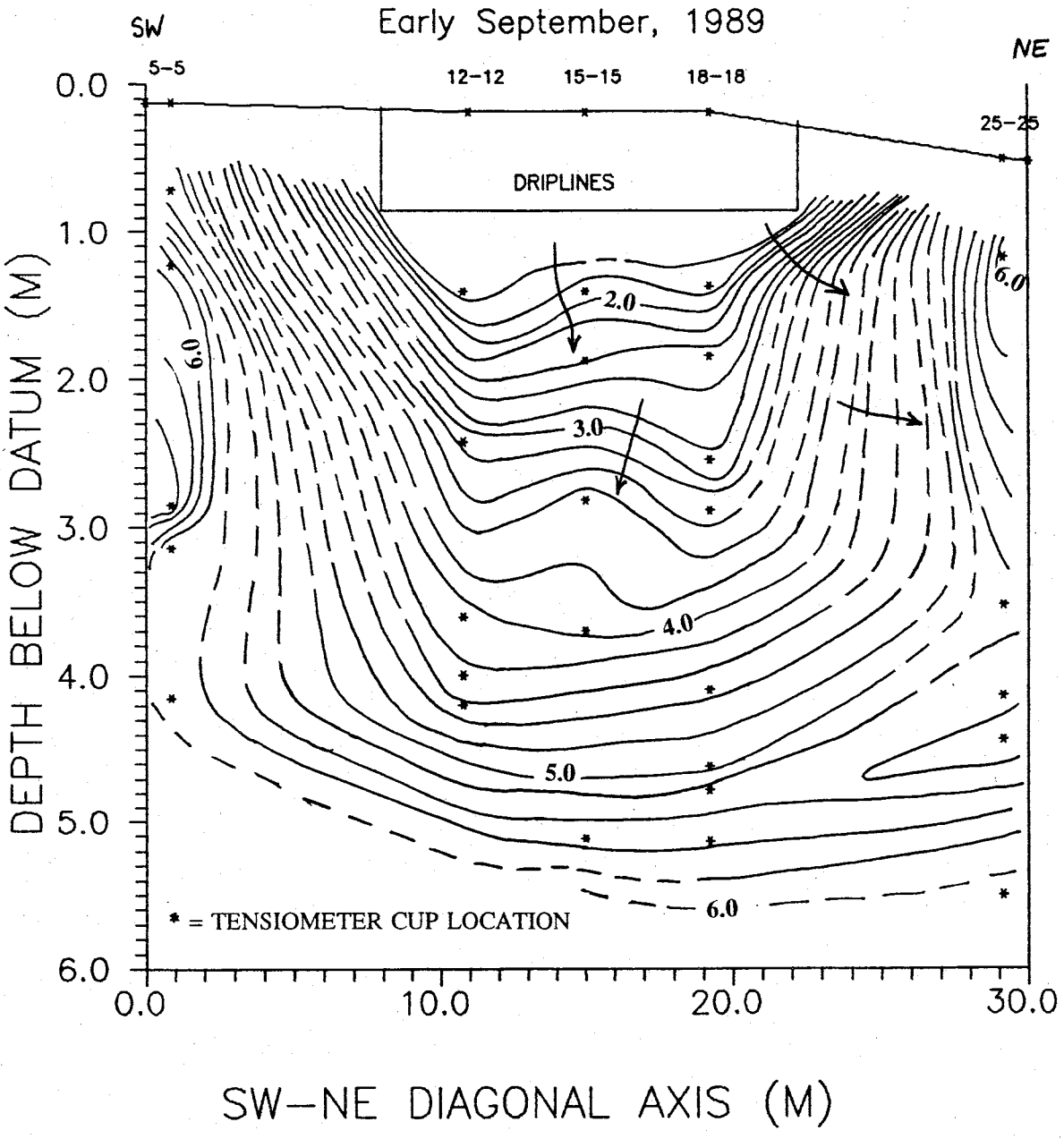

Figure 4-7. Hydraulic Head Field--SW-NE Transect: Infiltration.

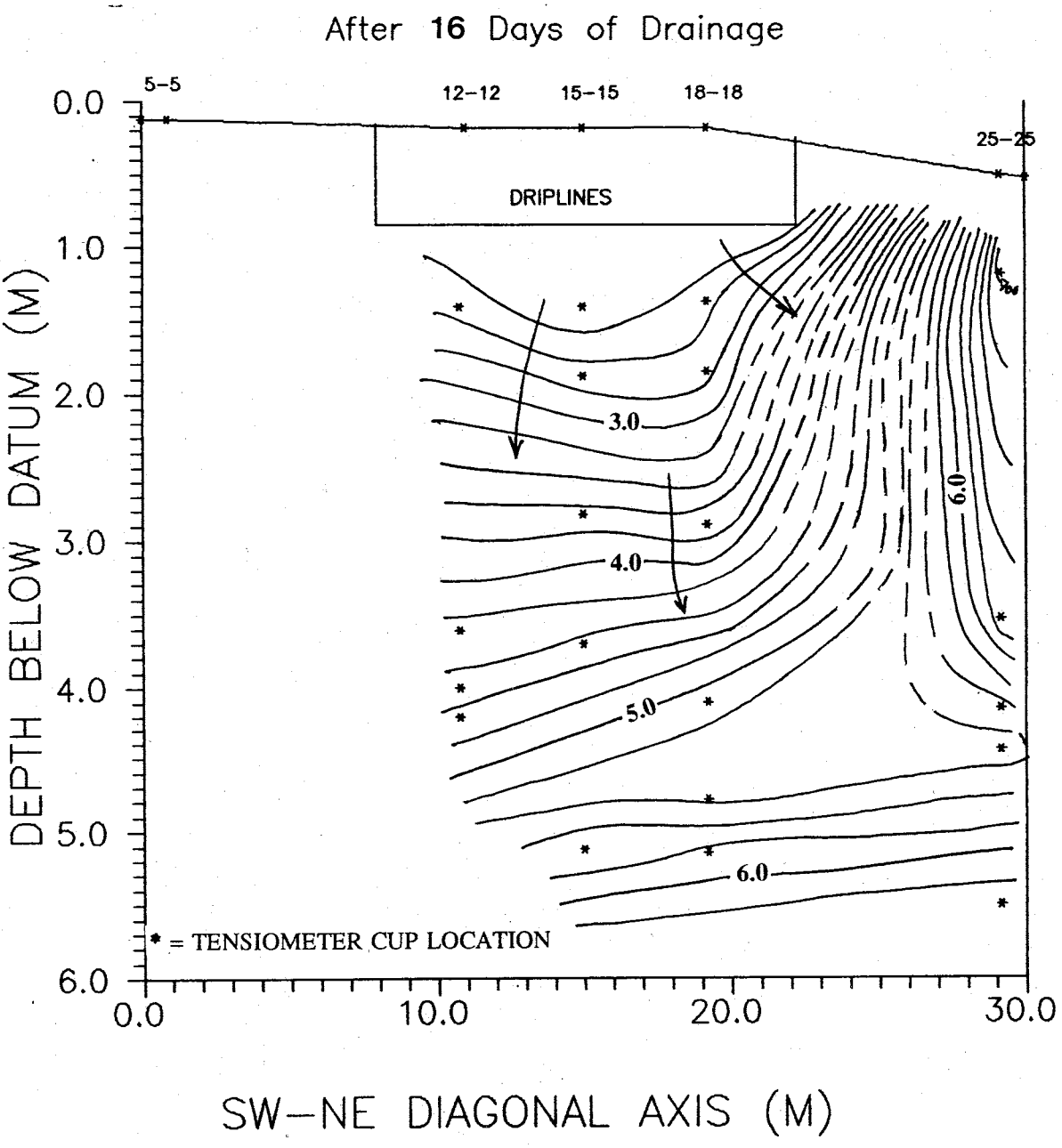

Figure 4-8. Hydraulic Head Field--SW-NE Transect: Drainage.

station 15-15. However, hydraulic gradient decreases from 1.32, between 1.9 and 2.8 meters below datum at station 15-15 to 0.59, between 2.8 and 3.7 meters below datum. Lower gradient suggests the presence of a coarser material (higher conductivity), such as the cobble layer.

Infiltration and drainage fields were constructed for the SE-NW transect across the 30 x 30 m plot (Figures 4-9 and 4-10). Once again, data was not collected from the regions between 25-5 and 18-12 as well as between 12-18 and 5-25. These figures suggest steep (high) lateral gradients in these regions. However, moisture content values were low for stations 5-25 and 25-5 throughout infiltration and drainage. Because hydraulic conductivity is dependent on moisture content, it will be low in these areas. Subsequently, flow rates will be very low.

While large scale infiltration and drainage appear to be vertical, there exist several local anomalies. For example, a lack of data exists four meters below datum beneath station 24-15 (Figure 4-3). Equipotential lines diverge from this area, during drainage, suggesting a small flow divide. A silty clay is logged at the four meter depth in borehole logs for stations 22-15 and 24-15 show a clay layer is present at this depth. As the site drained, clay became a region of relatively high conductivity, compared to surrounding coarser (sandier) layers. Drainage from the clay layer would be more gradual due to its ability to conduct water over a longer

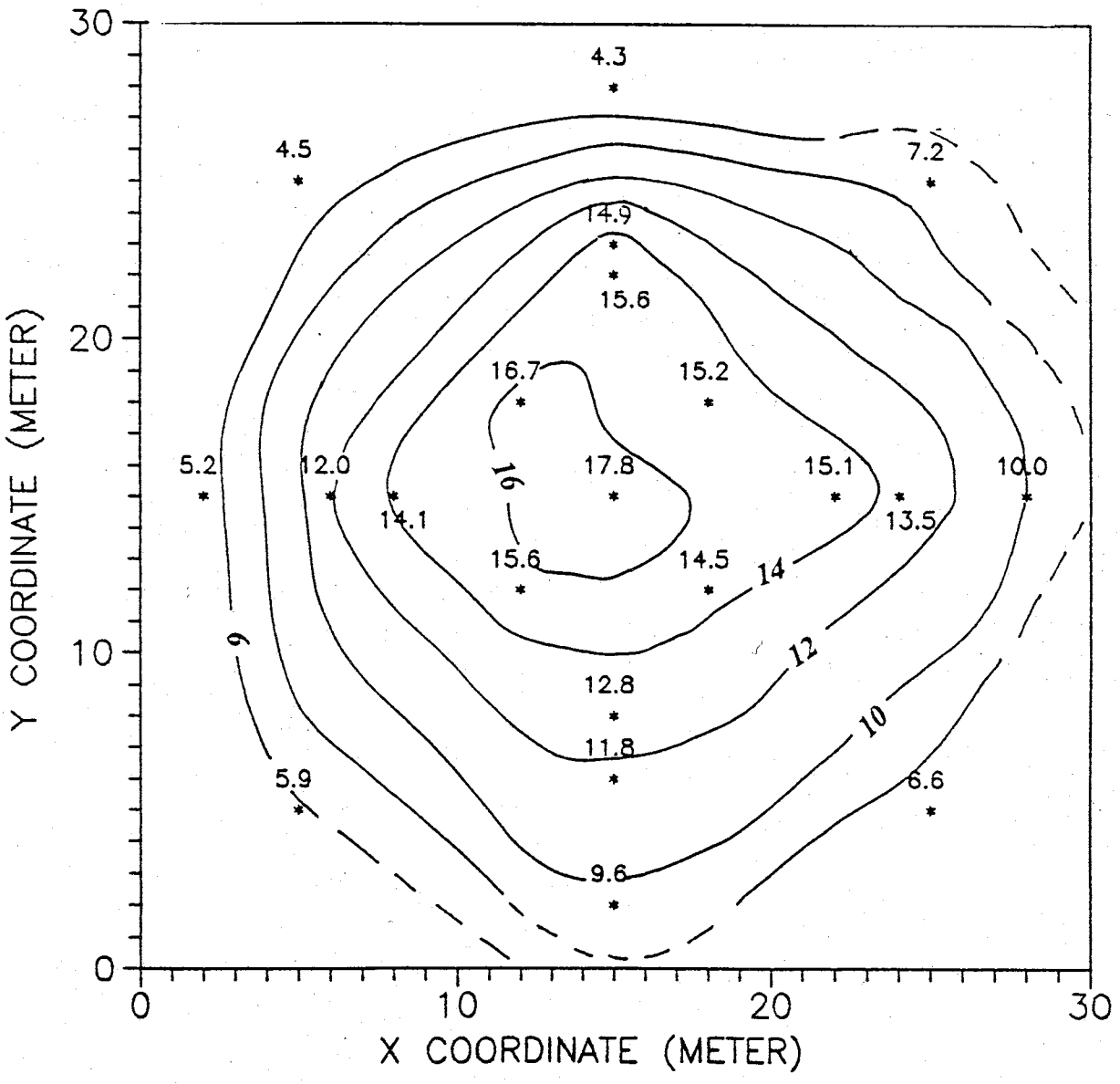

Figure 4-12b. Moisture content distribution (%vol); 3.0 Meters Below Datum; after five days of drainage (contour interval: 2%)

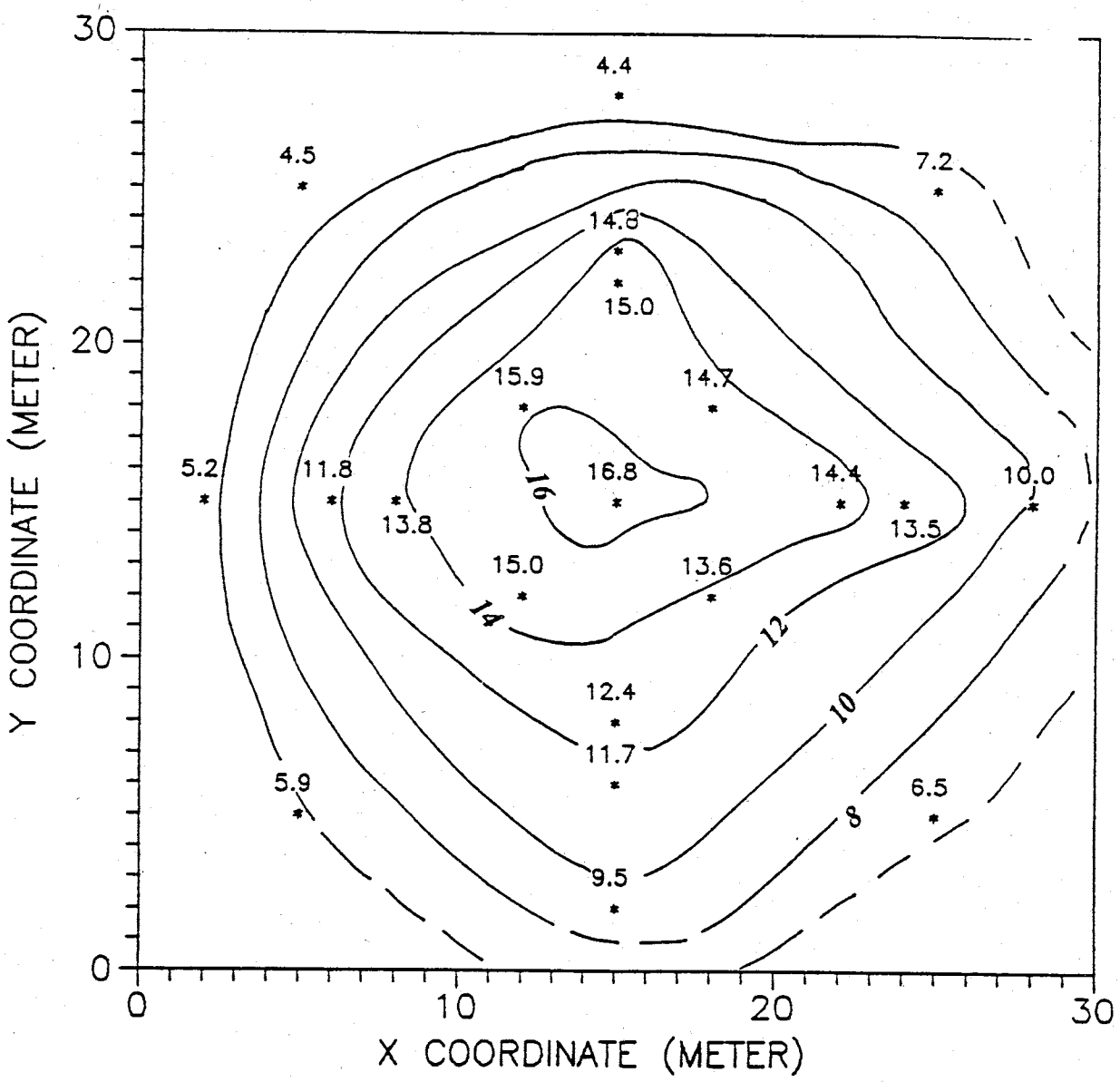

Figure 4-12c. Moisture content distribution (%vol); 3.0 Meters Below Datum; after ten days of drainage (contour interval: 2%)

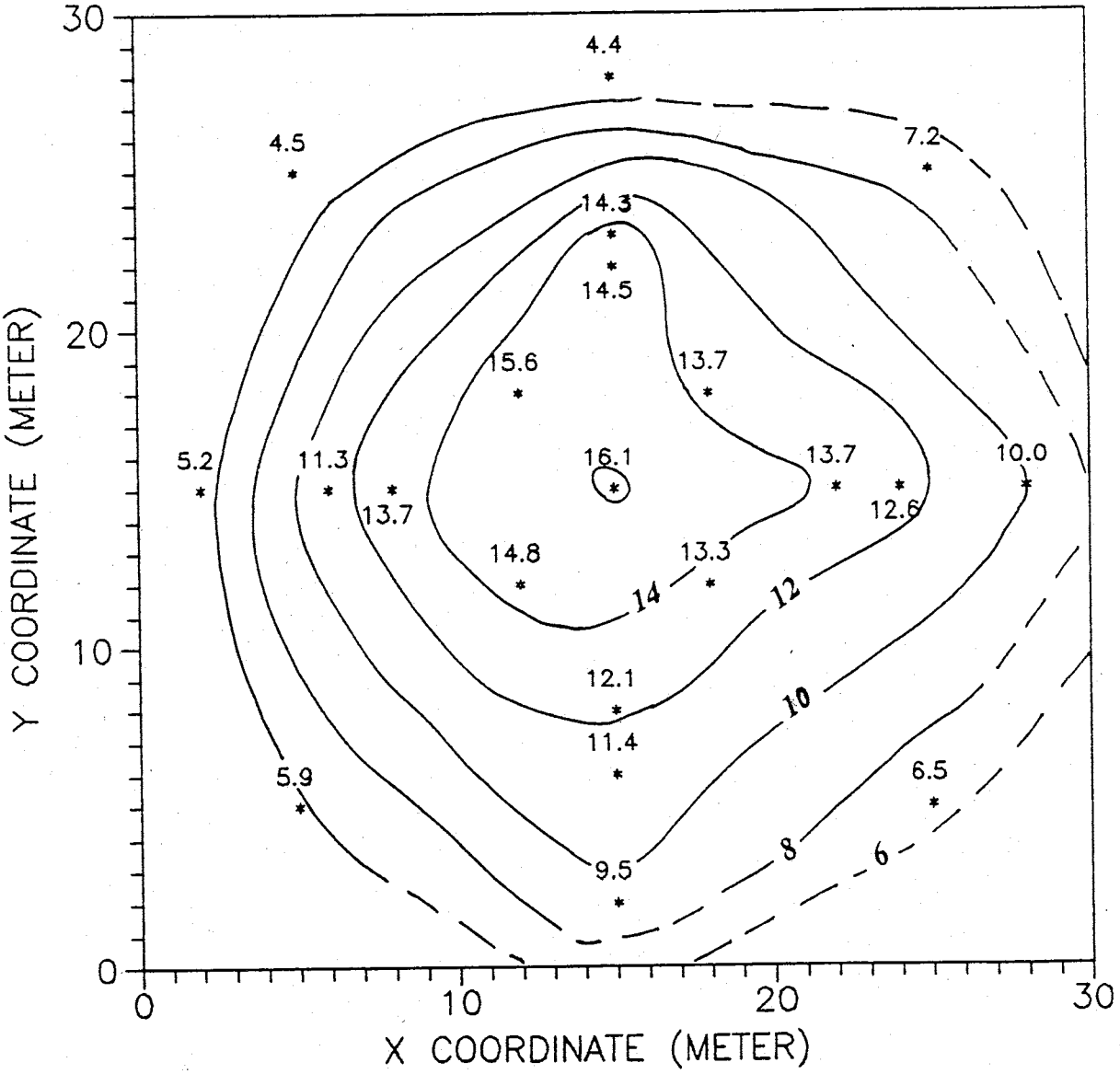

Figure 4-12d. Moisture content distribution (%vol); 3.0 Meters Below Datum; after twenty days of drainage. (contour interval: 2%)

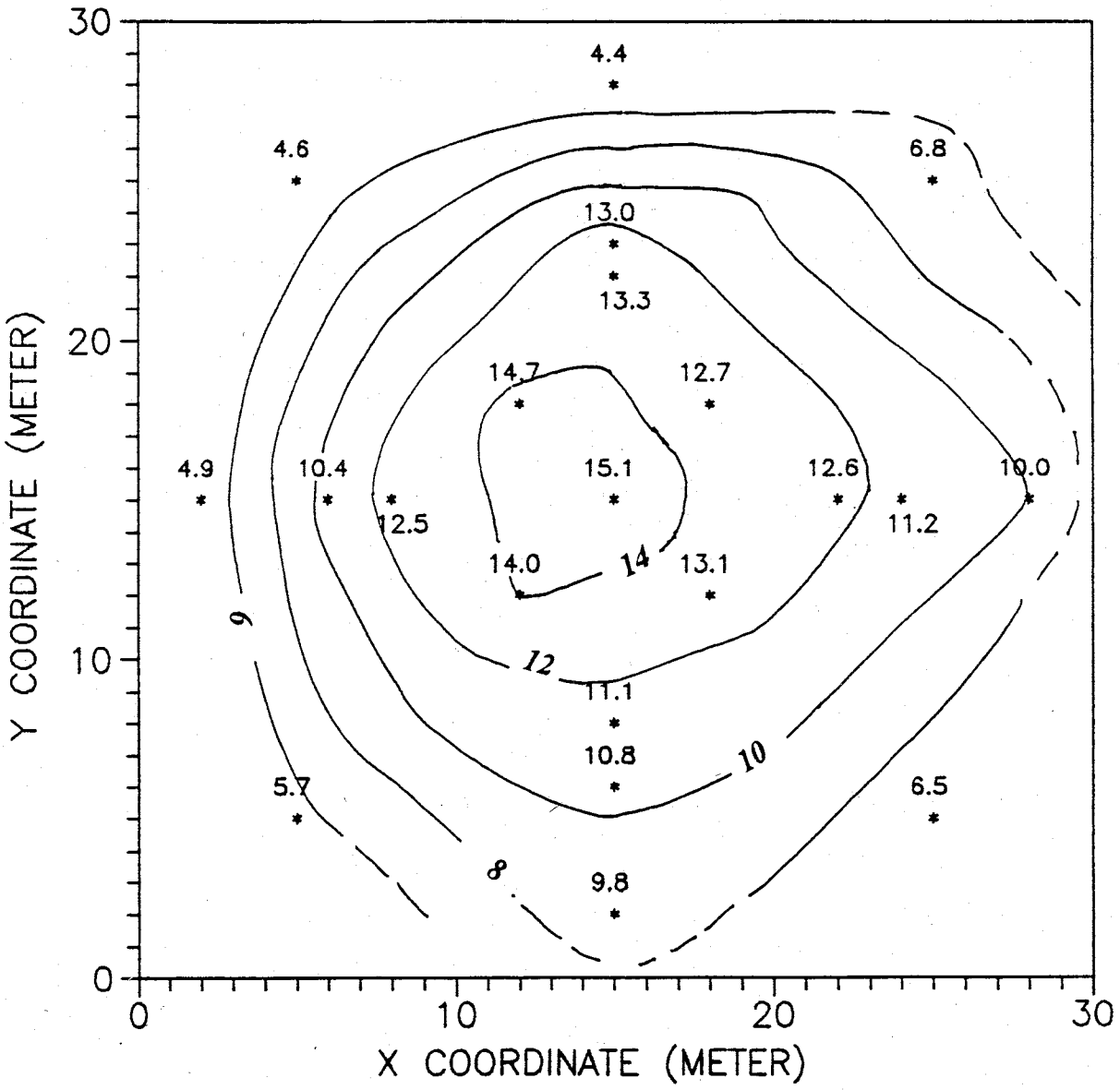

Figure 4-12e. Moisture content distribution (%vol); 3.0 Meters Below Datum; after fifty days of drainage. (contour interval: 2%)

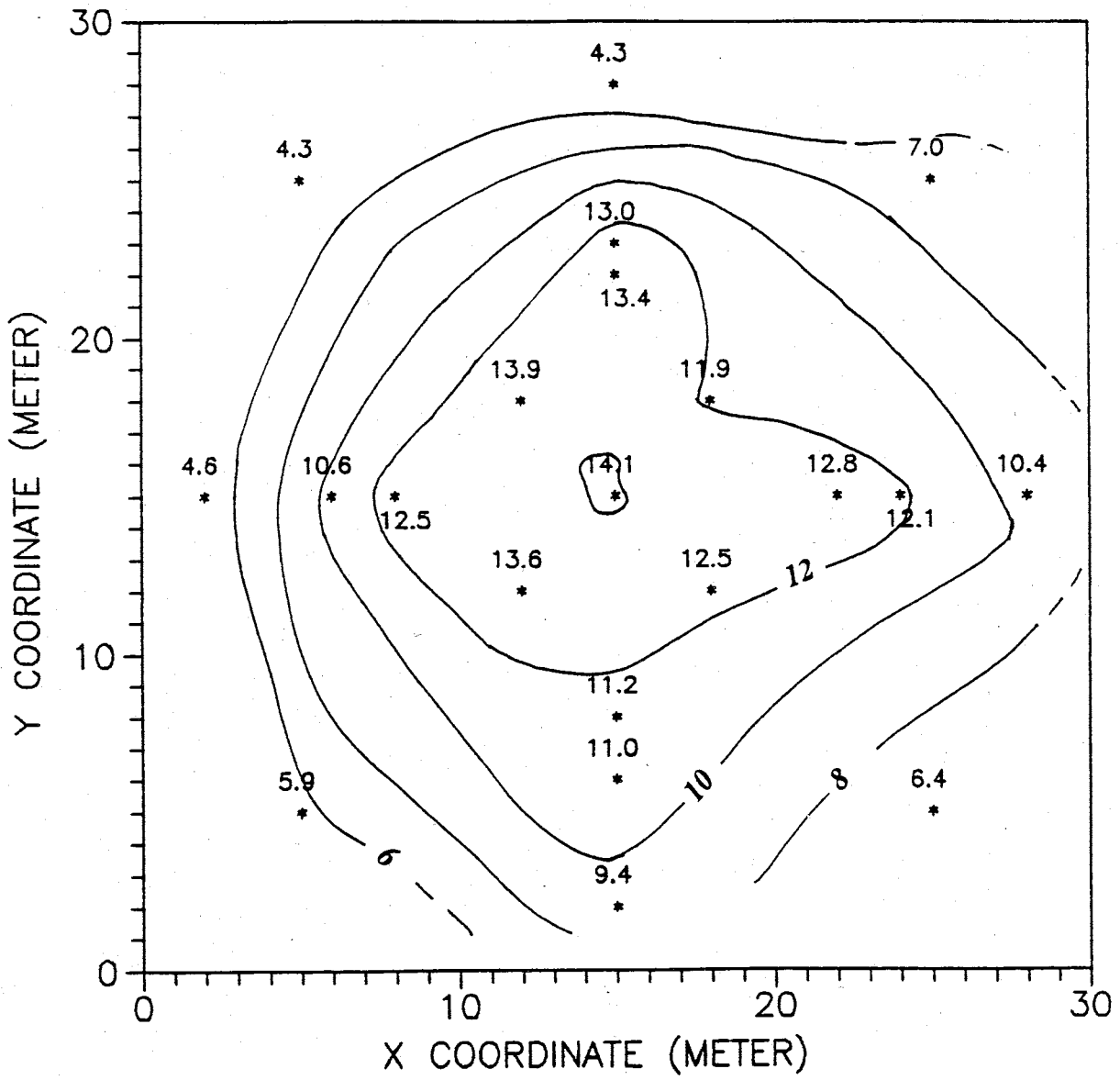

Figure 4-12f. Moisture content distribution (%vol); 3.0 Meters Below Datum; after one hundred days of drainage. (contour interval: 2%)

characterized by pebbly, fine-coarse sand, stations 18-12 and 12-12 by silty fine sand, and station 12-18 by pebbly, cobbly fine-coarse sand. Head fields emphasized these areas experienced general vertical flow, with some lateral flow to the east-northeast. All four values for these stations do not represent saturated conditions for any of the soils. They do suggest an even distribution of moisture to the four corners of the plot during infiltration.

It is during drainage that the moisture content among the four stations just inside the corners of the plot began to show differences. Four quadrants are represented by the four stations. Following five days of drainage, the southeastern portion or quadrant of the irrigated plot area lost the most moisture. The northwestern quadrant lost the least (station 12-18). Essentially, the eastern half of the plot area drained more than the western half, following five days. This was due in part to the effect of lateral flow to the northeast as evidenced by the excavated trench between stations 18-18 and 25-25. Also, piping along instrumentation at station 18-12 may be responsible for the loss in moisture in the southeastern quadrant. Piping is a serious issue in defining the flow field and is discussed in later sections.

The northwestern quadrant lost the least moisture following 100 days of drainage (Figure 4-12f). Following this period, moisture content was essentially equal to that of the center of the site, approximately 14%. The logs for porous

cup samplers 17 and 19 and the geologic log for station 12-18 suggest a cobble layer present at 3 meters below datum. Porous cup sampler logs inside the plot tended to "bottom out" when cobbles were encountered during hand augering of the boreholes. Drainage above three meters in this area was essentially vertical. However, once moisture encountered the cobbles, it may have accumulated above the cobbles until suction built up in the cobble layer to permit water entry into its pores from above.

Moisture was released at roughly the same rate during each drainage period (five days, ten days, etc.) from the vicinities of stations 6-15 and 8-15. This moisture, although not substantial, probably drained downward into the plot. See Figure 1-7 for geologic descriptions. A cobble layer is present at the three-meter depth, but the uniform moisture profiles for both stations at this depth suggest moisture did not accumulate above the cobbles (Figures 4-13 and 4-14). Note that initial and drainage profiles are shown. See Figure 1-7 for geologic descriptions. The three to six meter depth in both stations' profiles reflected the greatest increase in moisture over the two year (1987-1989) infiltration period. The head field generally supports lateral, downward flow in this region (Figure 4-2).

Moisture content values for stations 15-22, 18-18 and 22-15 were virtually the same after five days of drainage (Figure 4-12b). However, these areas lost moisture at different rates

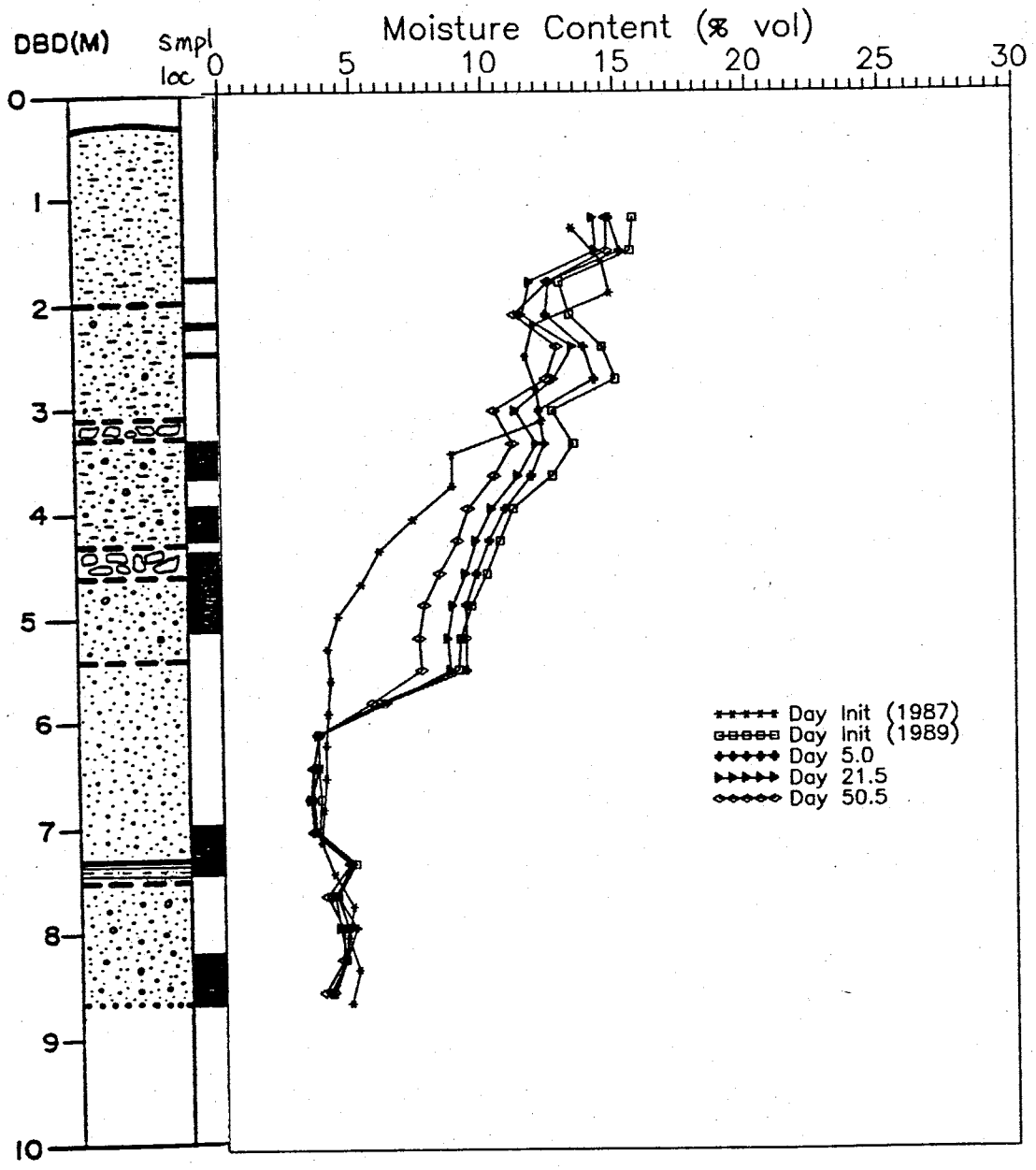

Figure 4-13. Moisture Content Profile--Station 6-15

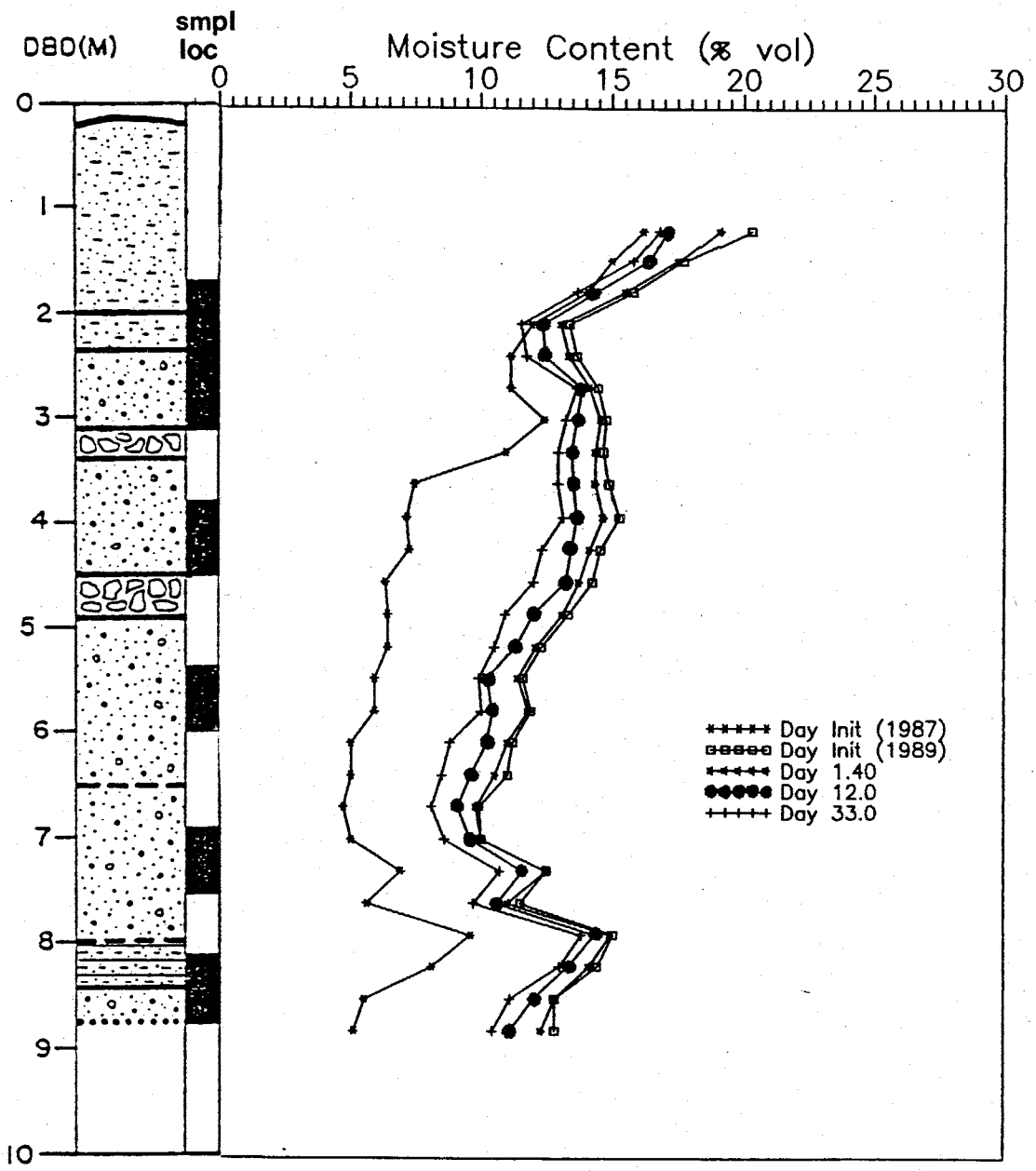

Figure 4-14. Moisture Content Profile--Station 8-15.

after this time. These three locations are characterized by fine-med sand (1% pebbles), fine-coarse sand (30% pebbles) and silty, fine-coarse sand (10% pebbles), respectively. The effect of this variable texture is evident after twenty and fifty days of drainage, when moisture content values are equal for stations 18-18 and 22-15. These are in turn less than that for 15-22. The coarser (pebbly) material drained more moisture, more rapidly than the finer material. Finally, after 100 days of drainage, the three locations are distinct in terms of moisture content (Figure 4-12f). The soil layer at this depth may be horizontally continuous on a regional scale, but local textural variations allowed it to drain differently over time.

In general, radial distribution of moisture persisted after 100 days of drainage. Moisture content values for nearly half of the station locations are between 12 and 14%, suggesting the regional soil layer at the three-meter depth is approaching a more uniform wetness. This effect may only propagate a short distance further, considering the outermost stations do not show effects from infiltration or drainage. The range in moisture content may not narrow further owing to local variations in texture.

7.5 Meter Depth

The general pattern of moisture at 7.5 meters depth was nonuniform (Figures 4-15a through 4-15f). All values of

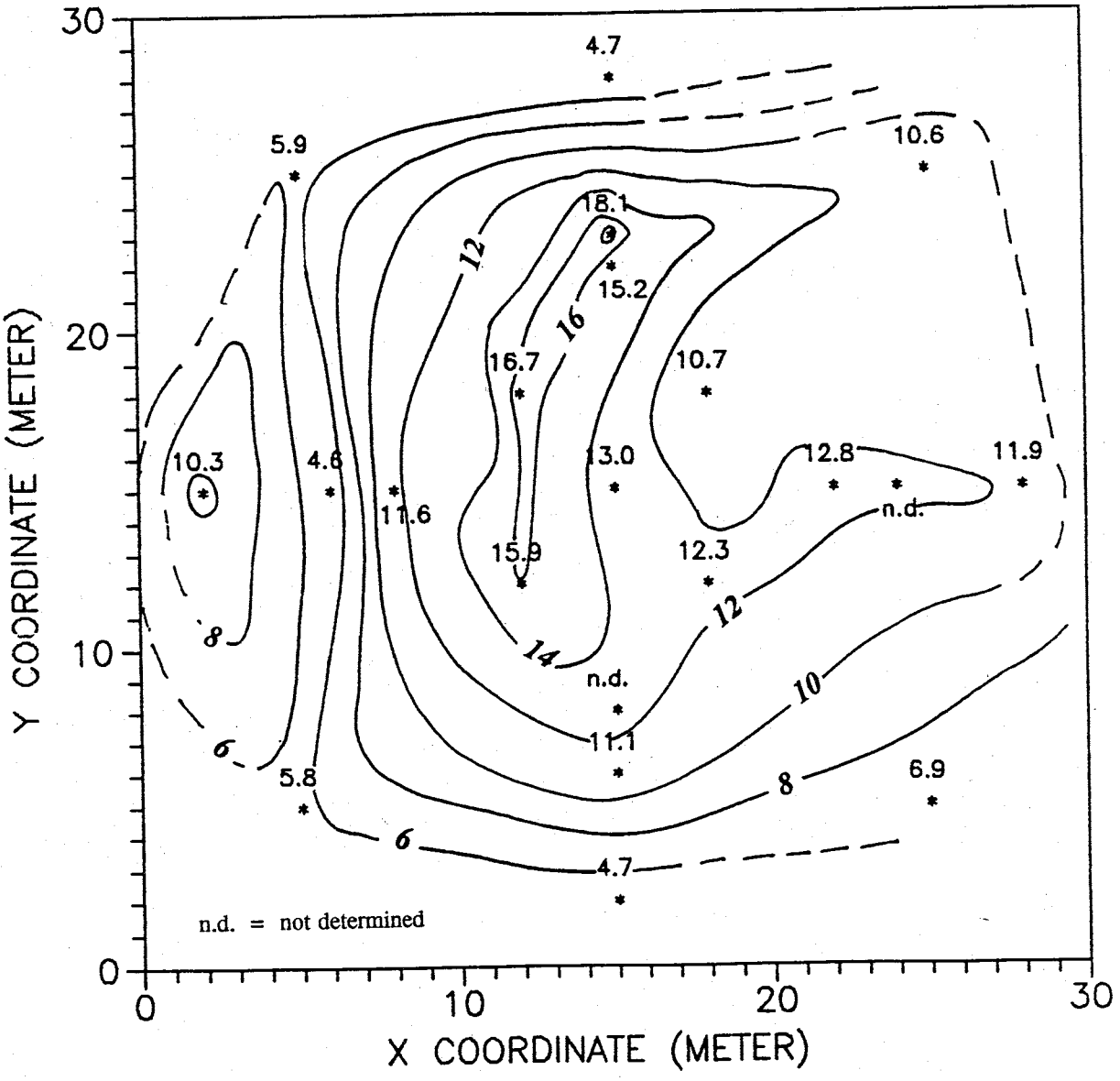

Figure 4-15a. Moisture content distribution (%vol); 7.5 Meters Below Datum; one day prior to drainage. (contour interval: 2%)

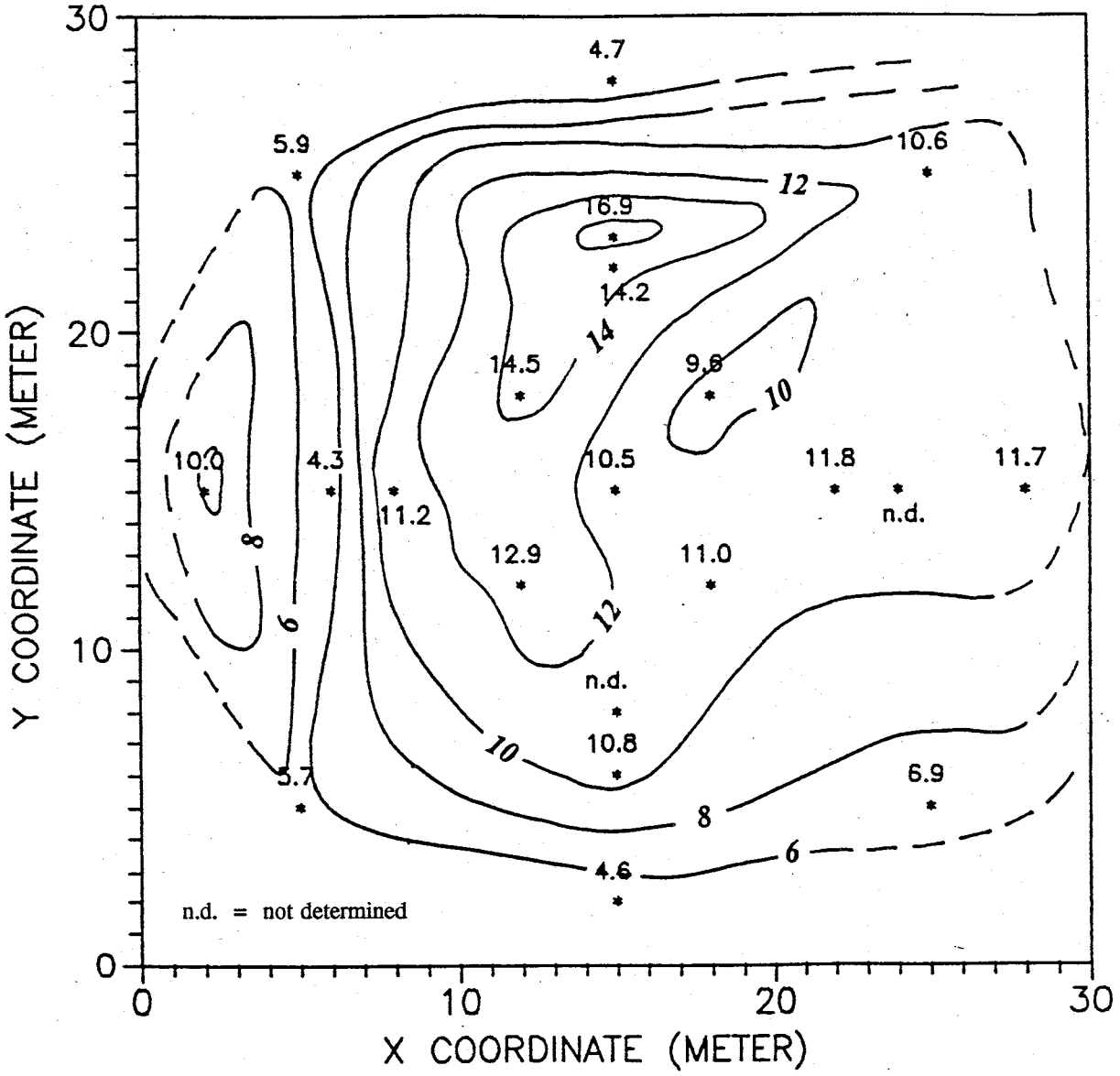

Figure 4-15b. Moisture content distribution (%vol); 7.5 Meters Below Datum; after five days of drainage. (contour interval: 2%)

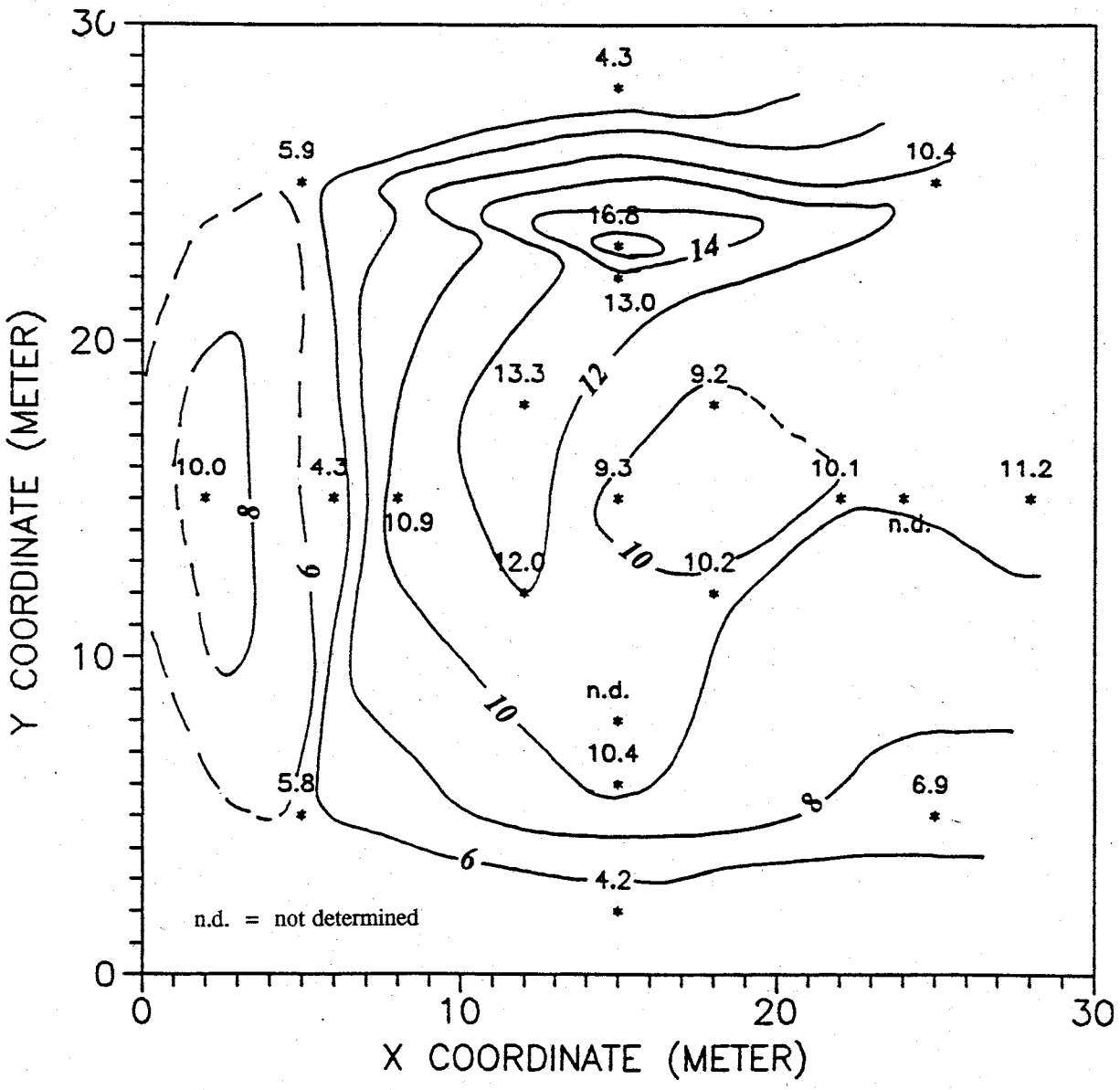

Figure 4-15c. Moisture content distribution (%vol); 7.5 Meters Below Datum; after ten days of drainage. (contour interval: 2%)

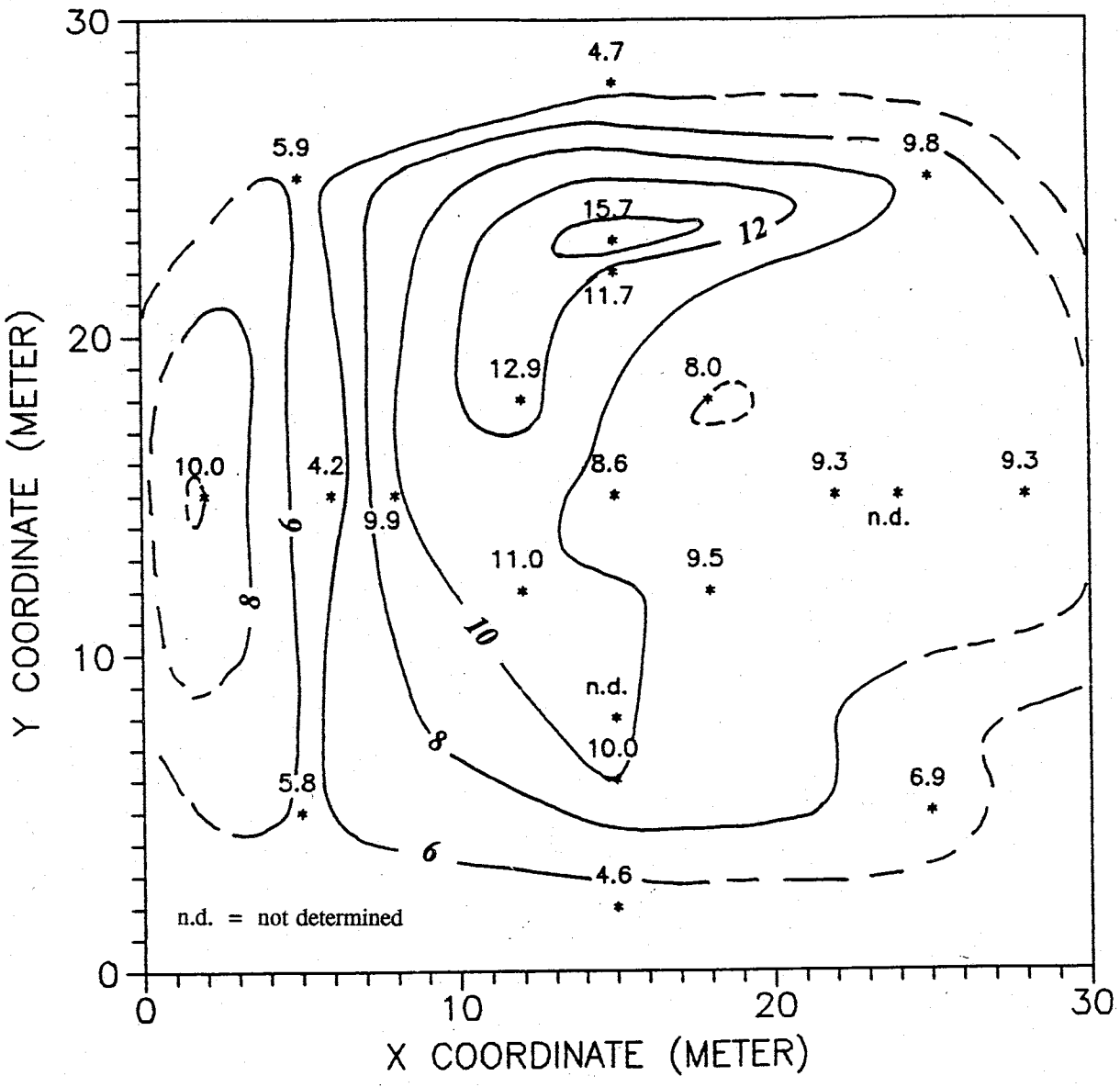

Figure 4-15d. Moisture content distribution (%vol); 7.5 Meters Below Datum; after twenty days of drainage. (contour interval: 2%)

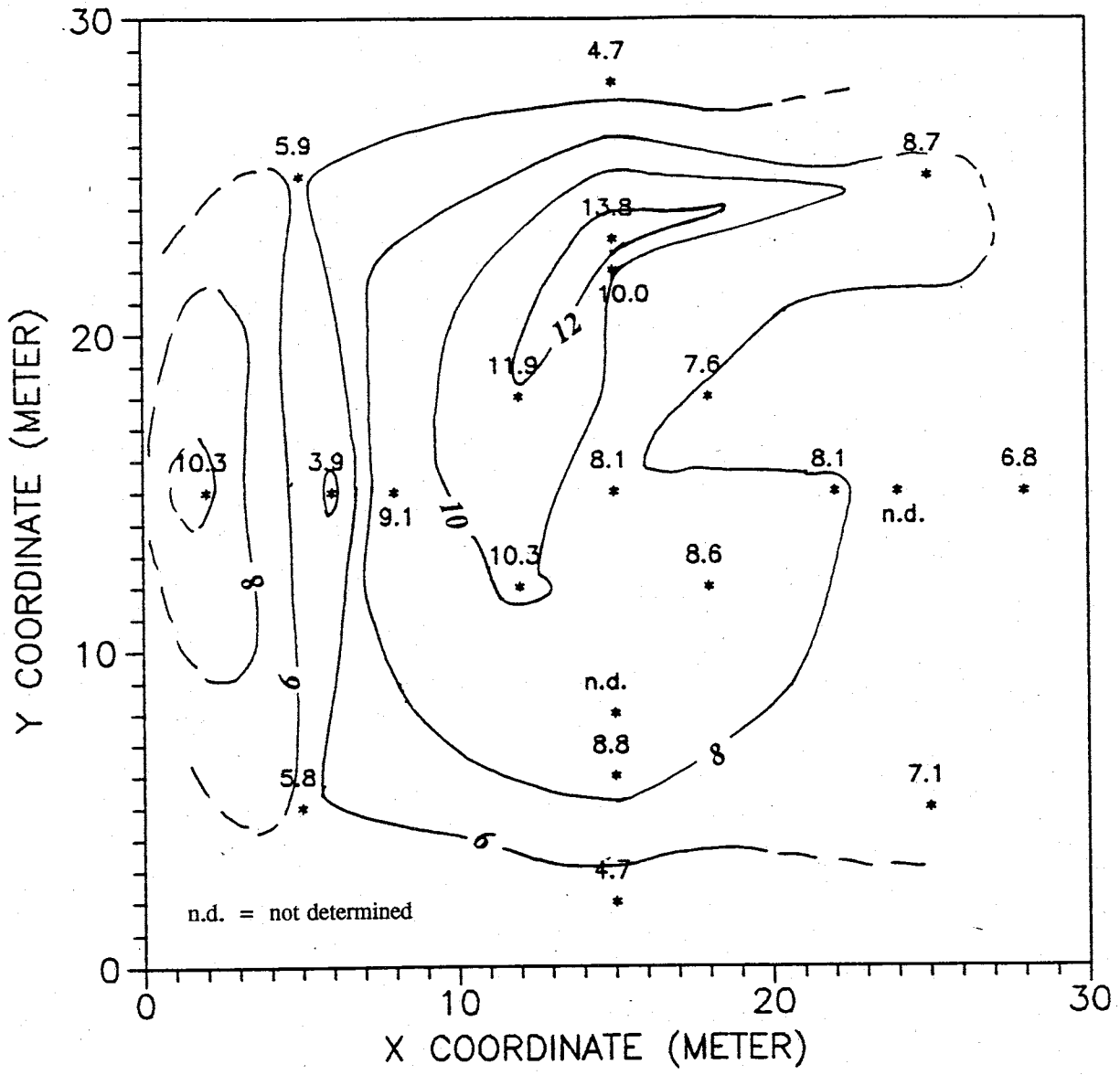

Figure 4-15e. Moisture content distribution (%vol); 7.5 Meters Below Datum; after fifty days of drainage. (contour interval: 2%)

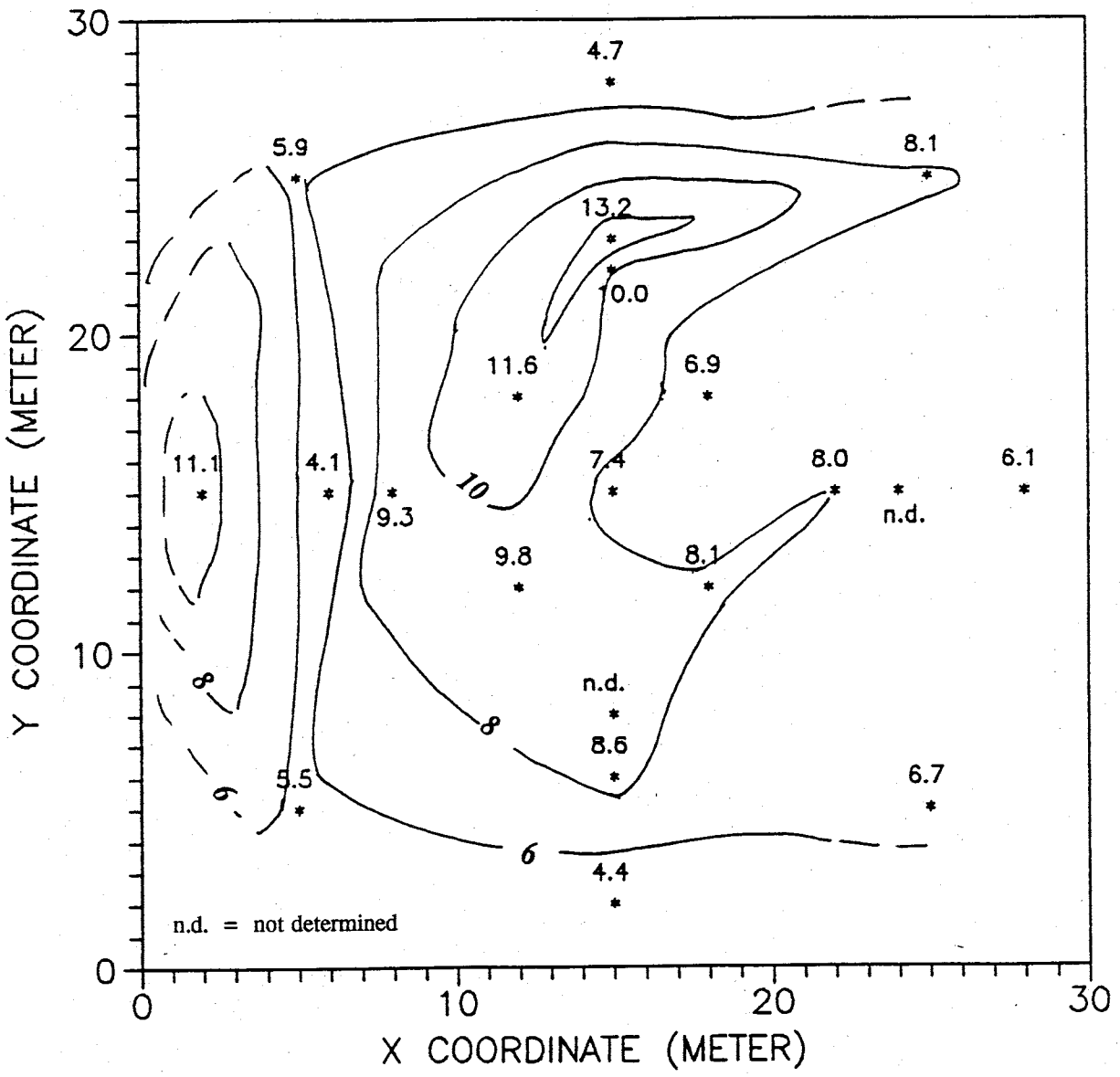

Figure 4-15f. Moisture content distribution (%vol); 7.5 Meters Below Datum; after one hundred days of drainage. (contour interval: 2%)

moisture content were measured within the fluvial facies, predominated by fine-med, fine-coarse sand. Pressure head data was not collected from this depth, so hydraulic head fields were not constructed. Thus, any conceptual flow model details developed below are based on moisture content and geologic data only.

The highest values of moisture content existed along a strip extending from station 12-12, northward to 12-18 and northeastward to 15-23 (Figure 4-15a). The moisture content profile for station 12-12 displays a noticeable increase in moisture at the 7.5 meter depth (Figure 4-16). This may be due to vertical drainage from shallower depths.

Moisture content steadily decreases in the profile above the 7.5 meter depth. However, uniform drainage profiles are shown for the cobble layer (4.8 to 5.8 MBD) and the pebble layer (5.8 to 6.5 MBD). Samples were not collected in this region. These layers may drain similarly because they contain similar matrix material. Measurements of moisture content may reflect drainage of this material (silty fine-coarse sand?), in spite of the presence of cobbles or pebbles.

Similar fining downward stratigraphy occurs at station 18-12 (Figure 4-17). Also, the unit at 7.5 meters deep is comprised of silty fine to coarse sand. The moisture content profiles are similar between stations for the cobble layer/pebble layer/silty fine to coarse sand sequences. However, it is possible an impeding layer prevented moisture

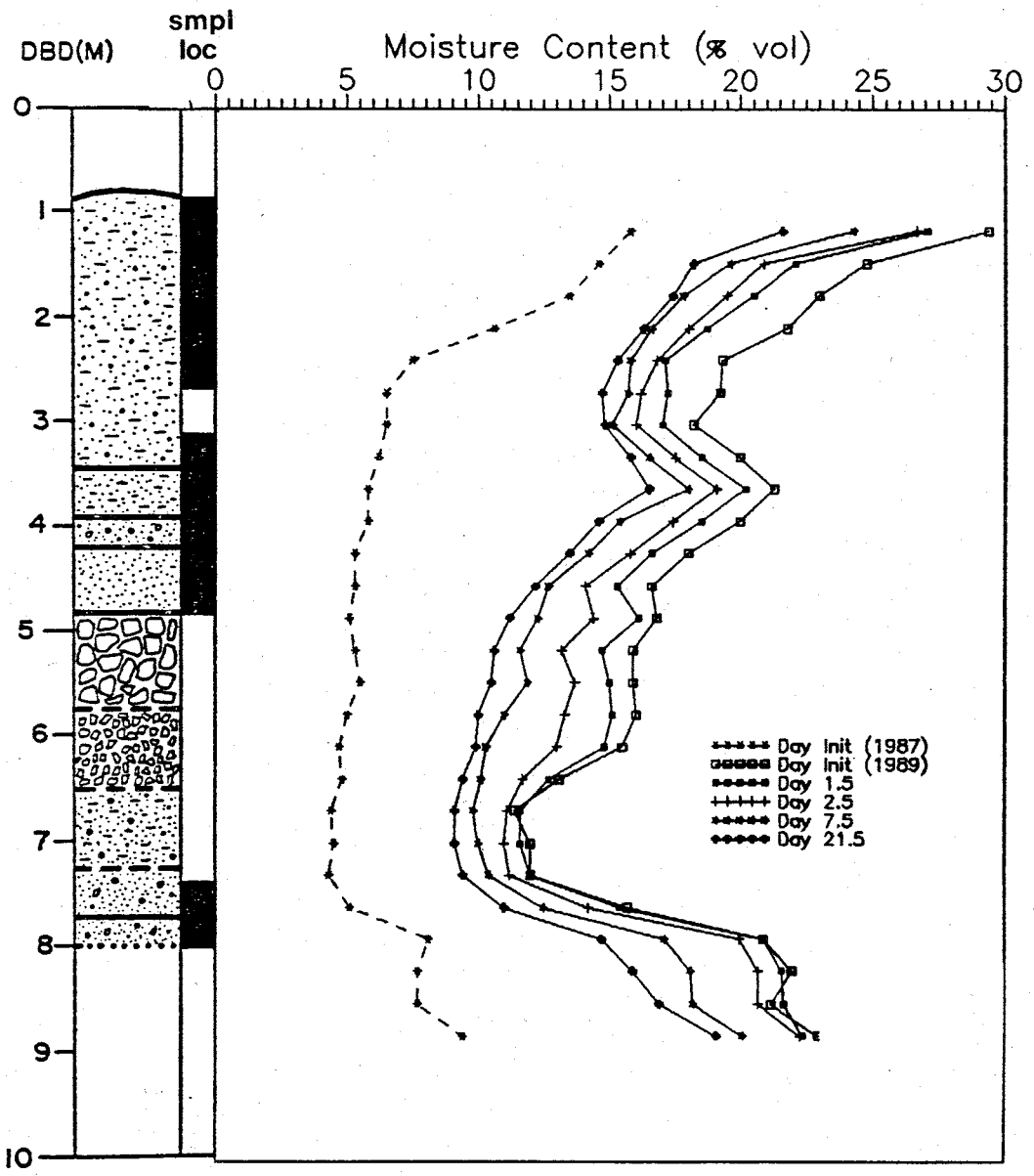

Figure 4-16. Moisture Content Profile--Station 12-12.

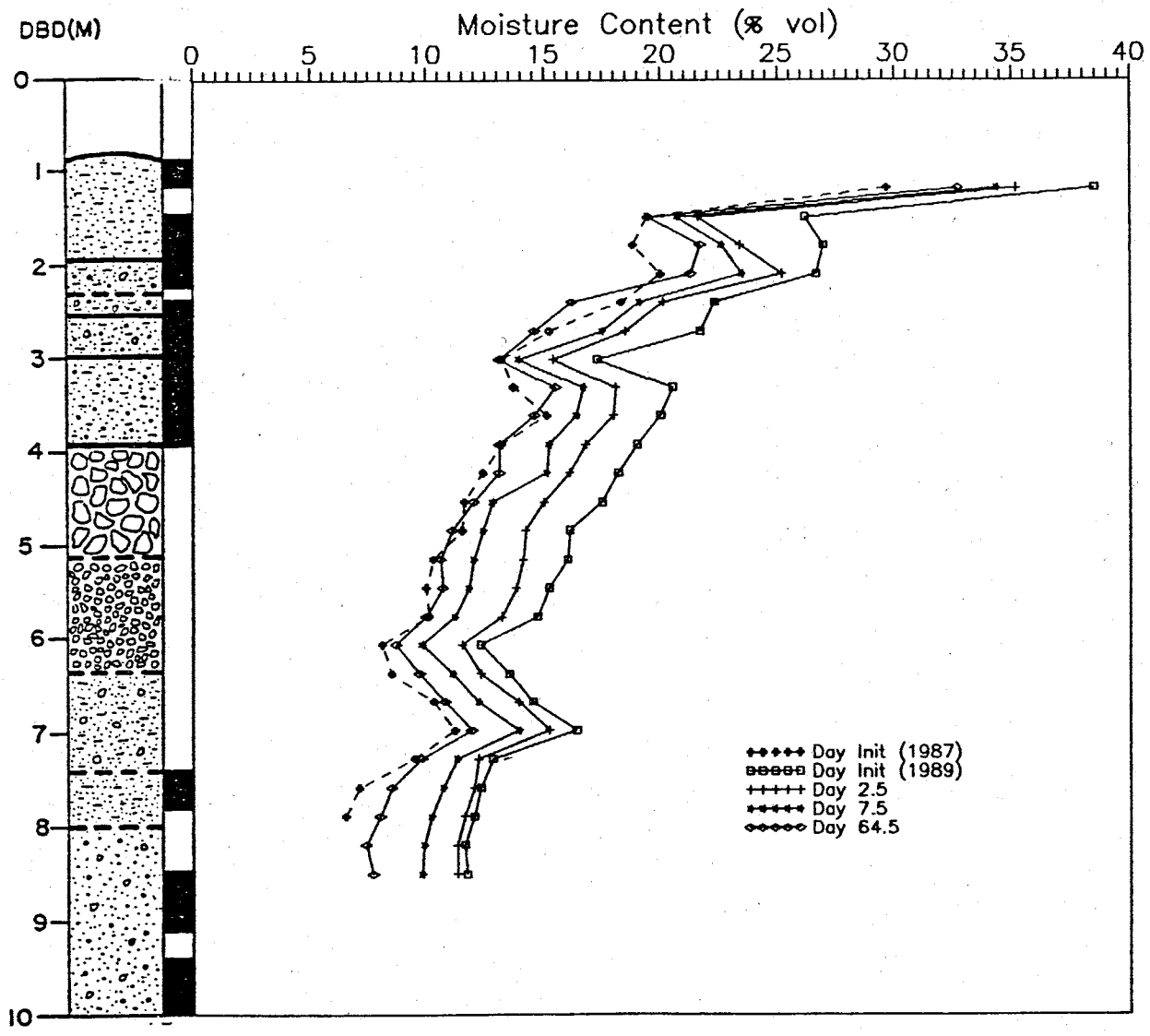

Figure 4-17. Moisture Content Profile--Station 18-12.

from reaching the 7.5 meter depth at station 18-12. Therefore, moisture content values at station 12-12 are higher than those at station 18-12 due to uninterrupted vertical flow to the 7.5 meter depth.

The northwestern corner of the irrigated plot (station 12-18) and the north-central region (station 15-23) of the site showed the highest values of moisture prior to and following one hundred days of drainage. Green silty clay exists just below the 7.5 meter depth at station 12-18 and between 7 and 8 meters deep at station 15-23, based on geologic log information. Moisture may have preferentially vertically drained into the clay from shallow depths at station 12-18. This moisture may have been distributed into thicker portions of the clay. The thick clay did drain gradually, and the destination of this moisture is still uncertain due to limited geologic information. If the underlying material was sand, then it is possible only a fraction of the sand could have conducted water being delivered to it (i.e. fingers may result) (Hillel and Baker, 1990). However, this is part of infiltration theory and may or may not be applicable here, depending on existing preferential pathways.

The driest region of the 7.5 meter deep plan view diagrams follows a north to south trend, in the western half of the site. Moisture did not propagate to the three meter nor the 7.5 meter depth at stations 5-5 and 5-25. Also, the

vicinity of station 6-15 was abnormally devoid of moisture. The water content profile on the west side of the site showed little change in antecedent moisture due to infiltration or drainage at this depth (Figure 4-13). During infiltration, this area was bypassed as water moved laterally and eastward along a cobble layer, 4.5 MBD. Apparently, water also drained vertically downward through a thick (three meter) fine-coarse sand, just east of this area. The sand unit is shown in the geologic log for station 8-15 (Figure 4-14).

Moisture content was unusually high at station 2-15, at the 7.5 meter depth. This value, however, did not decrease during drainage. It is probably indicative of antecedent conditions. A strong, pre-infiltration rainfall event could be the source of this moisture.

Among the outer three eastern stations (25-25, 28-15, 25-2), stations 25-25 and 28-15 reflected drainage of laterally infiltrated moisture. Moisture content in the northeastern area (station 25-25) decreased from 10.6% to 8.1%, while the far eastern area (station 28-15) decreased in moisture from 11.9% to 6.1% (Figure 4-15f). The east-northeast dipping soil layers, especially cobble layers in the vicinity of station 18-18, may have permitted preferential spread of infiltrating moisture, whereas the remaining outer edges of the site did not show effects of the infiltration event. Once infiltration was terminated, this moisture most likely drained vertically, beyond the limit of the instrumentation.

4.3 Summary

The purpose of this broad base analysis of hydraulic head and moisture content data from both infiltration and drainage events was to establish a basic conceptual understanding of flow within the substrata. Hydraulic head fields for all four transects suggested vertical flow was dominant directly beneath the irrigated plot. Head fields for the south to north and west to east transects also reflected the influence of cobble layers on the flow field. Lateral flow appeared more prevalent during infiltration while vertical flow predominated during drainage. However, data was sparse in certain regions (i.e. between station locations), and local textural variations could enhance lateral flow. Thus, only general conclusions can be drawn from these head fields.

Another analysis was performed using plan view moisture content distributions. Regional, site-wide drainage patterns were displayed in these diagrams. Three-meter deep figures represented the Piedmont Slope facies. Although this facies is extremely heterogeneous, a radial distribution of moisture suggested the predominance of vertical drainage in the center of the site. Also, moisture contents fell into a narrower range across the site with time. Very nonuniform distribution of moisture content occurred at the 7.5 meter depth, possibly due to the presence of impeding layers. In general, drainage was controlled by local variations in soil texture and layering.

The importance of these local variations must be examined more closely to understand their impact on infiltration and drainage from an impounded source. This more intensive analysis can fill in the gaps in the head fields and plan view moisture content distributions. Our understanding of site-wide infiltration and drainage can only improve through such an analysis. The following study of dye traces in soil layers can provide a qualitative estimation of textural and instrumentations influence on the flow field.

Chapter 5. Dye Study

5.1 1.5 Meter Deep Trench

The first dye study area was located in the southeastern corner of the irrigated plot (Figure 5-1). This 2.5 X 4.0 M region encompassed portions of six driplines. This area is expanded in Figure 5-2. Eight cross-sections or "cuts" are displayed. Each of these cuts or transects contained one or more "sections" which were cleaned of backhoe marks, brushed, drafted (noting dye paths and geology) and, in some cases, photographed. The stippled pattern in each cross-section represents dyed soil.

The first excavation and drafting performed was along the "lateral" sections (note Figure 5-2). Before the wooden trench was removed, sections A3 and C1 were exposed. Section A3 is located 0.46 M northwest from the southeastern border of the study area while C1 was 1.57 M away. Flow through the lateral region A3 was primarily saturated in nature, as the dyed water moved around silty clay. Locations of clay correspond to areas, 10 to 20 cm below driplines, devoid of dyed soil (Figure 5-3). However, thick layers of clayey sandy silt as well as thin layers of silty sandy fine gravel were dyed an intense blue from southeasterly, laterally flowing water. Toward the base of the section, the dyed fluid broke into large lobes, penetrating finer material. Flow through finer material may have commenced during the early stages of

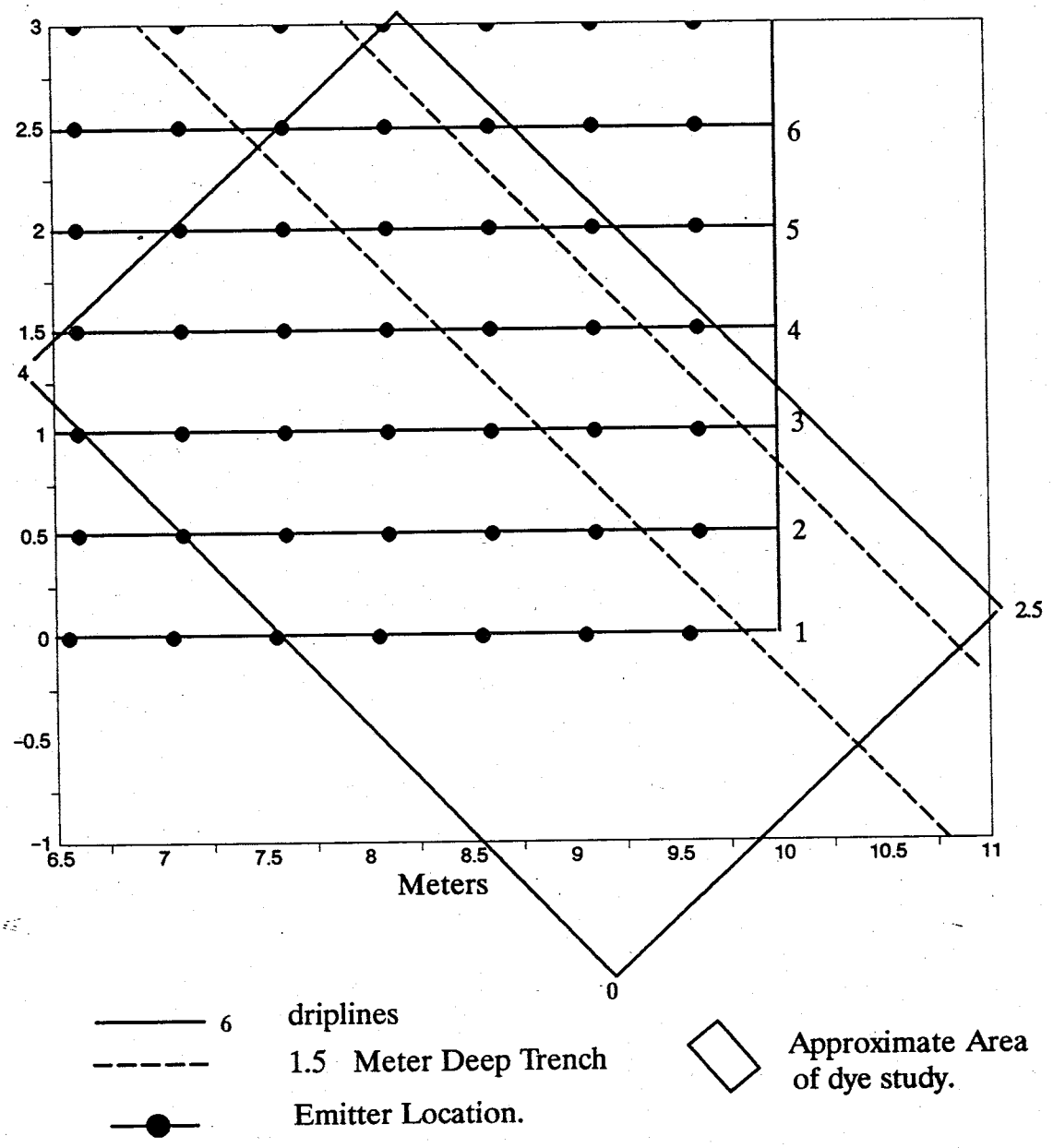

Figure 5-1. Southeast Corner of Irrigated Plot.
(See Figure 5-2 for diagram of 2.5 X 4.0 M Study Area)

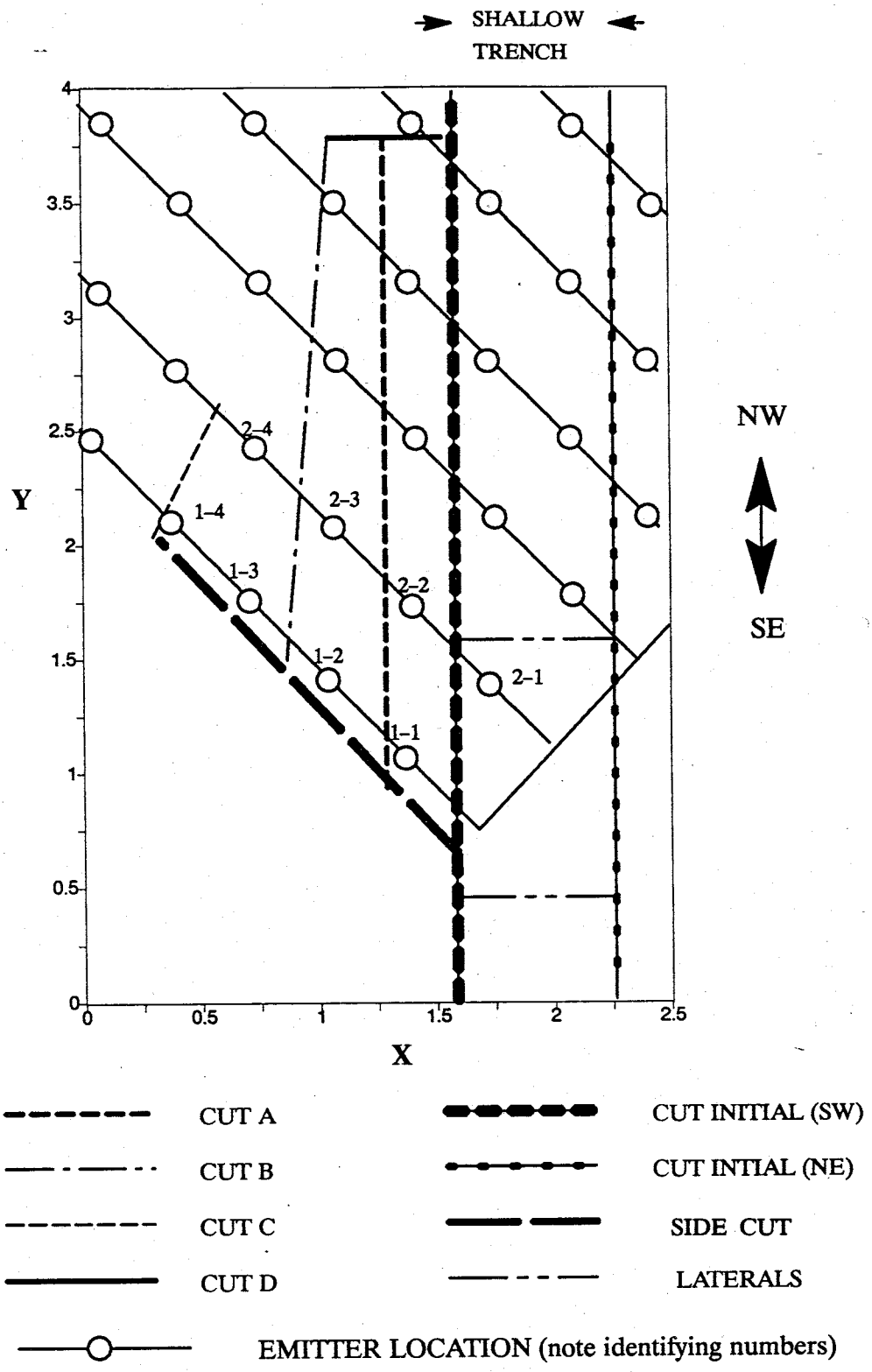

Figure 5-2. Locations of Excavations in Dye Study Area. (Both axes are in meters.)

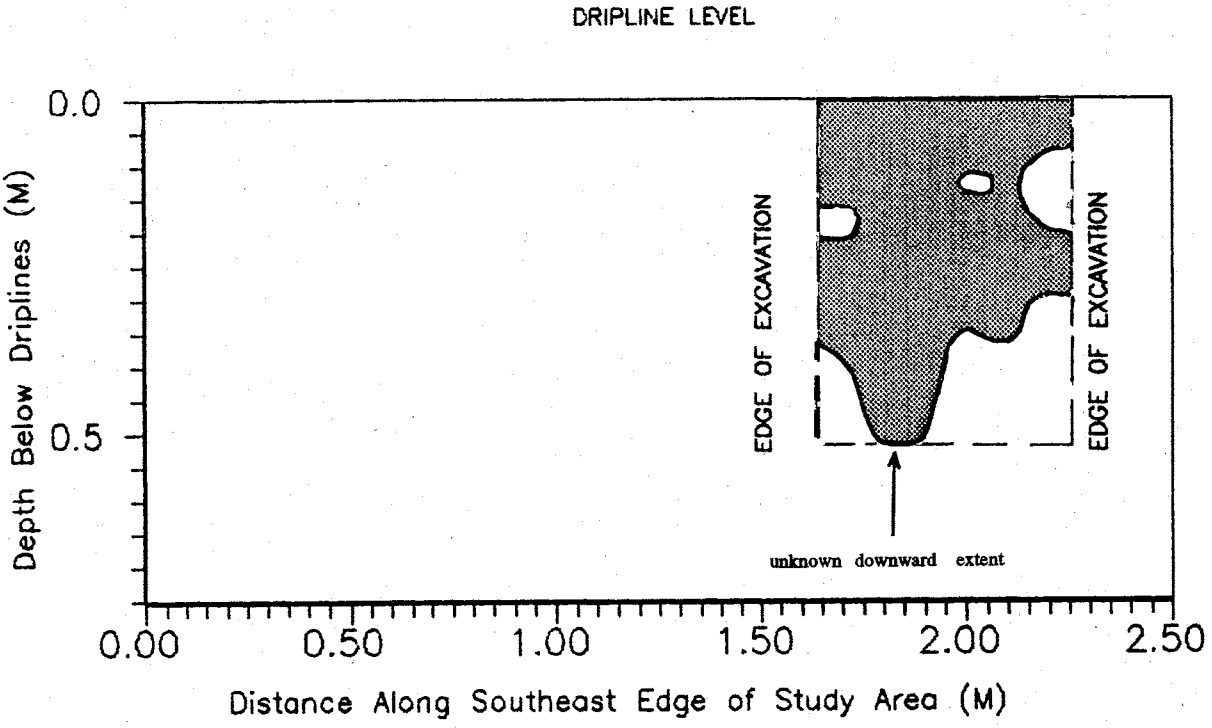

Figure 5-3. Cross-section of Dye Extent--Section A3

drainage. Fine textured layers tend to impede infiltration but could promote drainage of overlying, coarser layers (Hillel and Talpaz, 1977).

For section C1, saturated flow was prevalent in the upper 10 cm of the zone (due to proximity to driplines), but became more unsaturated toward the base (Figure 5-4). The bean-shaped white spot in this figure was composed of sand and pebbles. A large cobble (blue tinged on edges only) was found just below the left lobe of dye. Soil in the right dyed lobe was similar in nature to that found in the dyed pathway near the base of A3.

The third cut was along the northeast face of the trench (Figure 5-5). Each number along the top of the figure refers to the point of intersection between that dripline and the trench. Also note that when dripline locations are referenced, the two-dimensional region, in the vicinity of its intersection with the trench, is the subject of the reference.

The thick zone of dye in the southeastern part of this cross-section was primarily due to ponding effects in the wooden trench. Approximately 10 gallons of water was applied to the plot every 15 minutes. This water may not have had time to infiltrate in some areas of the plot, and thus, may have "backflowed" into the wooden trench, forming a small pond. The water eventually soaked in, but this produced virtually saturated conditions in the vicinity of the "main" line. The dyed front spread laterally to the southeast (in

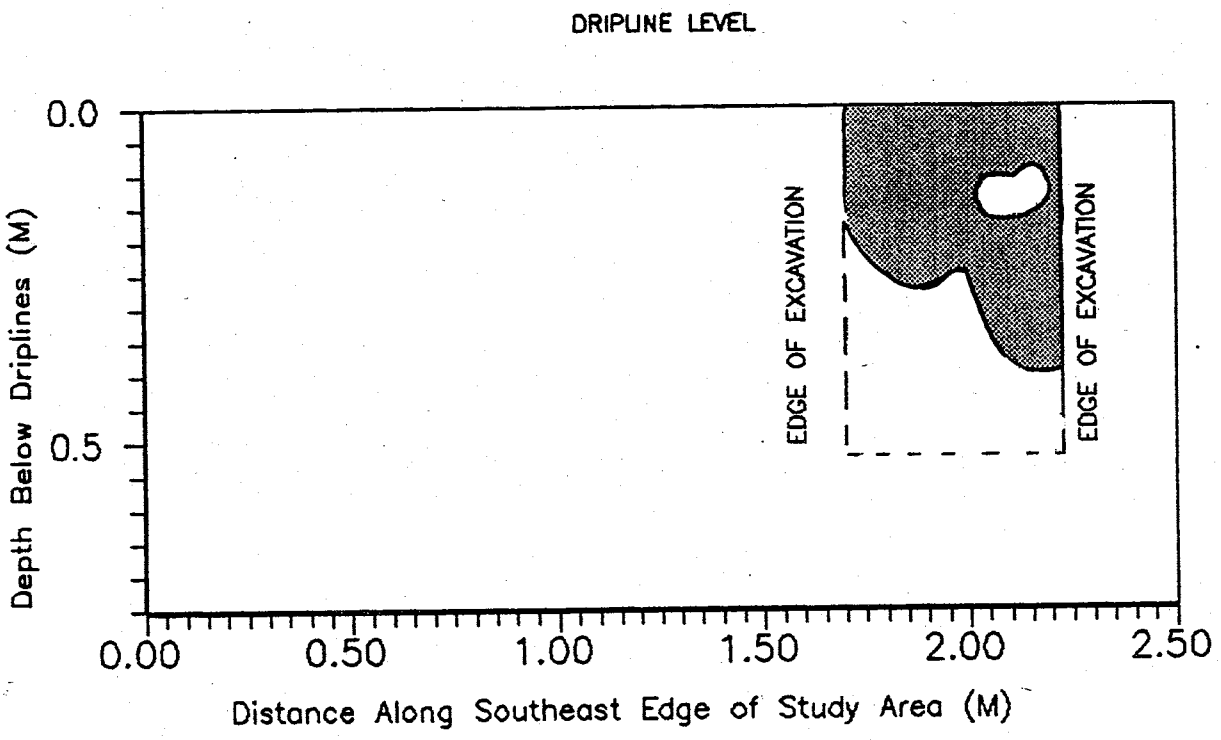

Figure 5-4. Cross-section of dye extent--Section C1
(Y = 1.57 M)

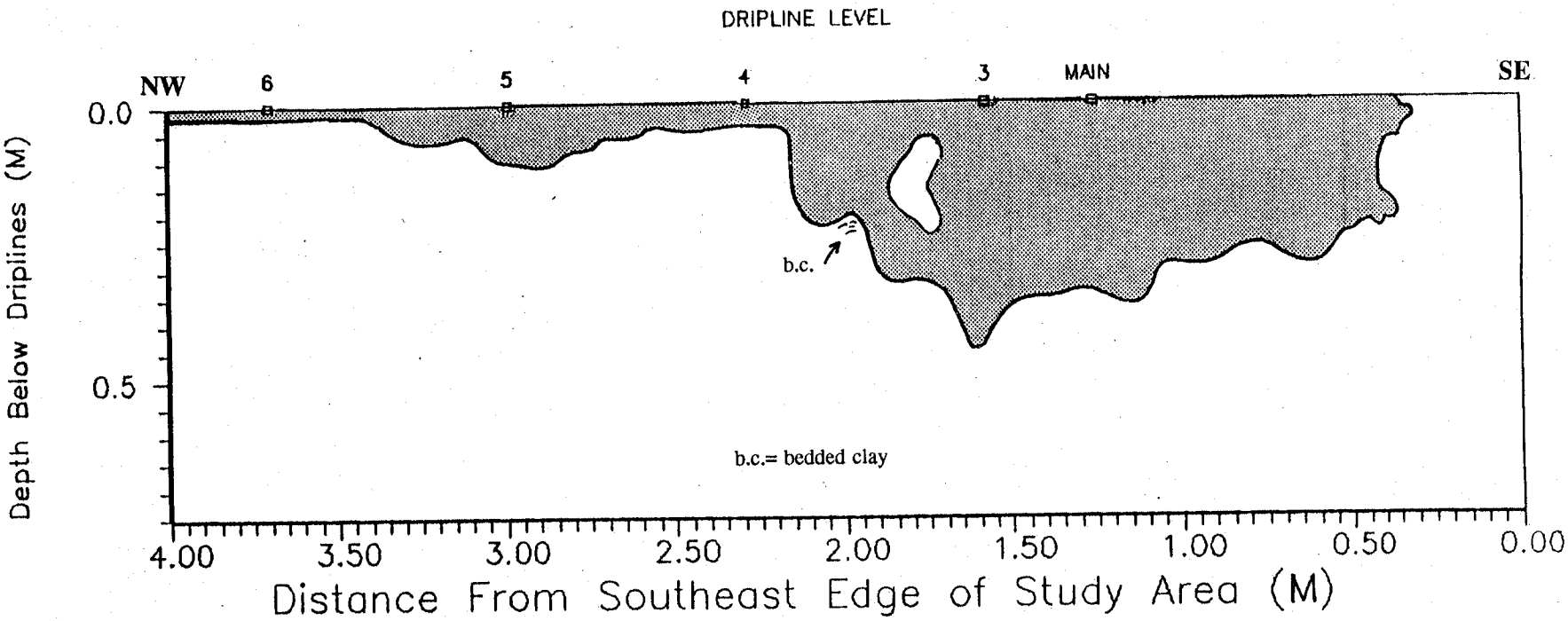

Figure 5-5. Cross-section of dye extent--Northeast Face: Cut Initial

two dimensions) along and through coarse layers, while seeping vertically into the underlying clayey silt layer. Beyond the wooden trench and to the southeast, some moisture was pulled upward (above dripline level) by capillary forces into finer (clayey silt) layers overlying coarse material.

The deepest penetration of dye along this transect was 45 centimeters below dripline 3 (Figure 5-5). The spreading of the dye appears to be an almost radial phenomenon in the vicinity of the main line. However, a small soil region, composed of silty sand overlying gravelly sand, is devoid of dye and found near dripline 3.

It was difficult to ascertain if these soils were coincidentally bypassed or not. The first emitter on dripline 3 was found in the proximity of this area and may not have produced steady flow due to damage. This region, on the other hand, may have been simply bypassed due to preferential flow through the coarse layers to the left (missing the bedded clay--denoted as "b.c.") and from the strong pulse of moisture around the main line. The first emitter on dripline 4 may have contributed significantly to flow producing the lobe just northwest of the bedded clay. Material consisting of coarse sand and medium gravel persisted upwards to this dripline's level. Large, interconnected pores forming channels could have accounted for the very wet conditions here (Simpson, et al., 1982).

Unlike the southeastern end, the northwestern end of the

transect (Figure 5-5) showed dye present only in fine cover sand in the vicinity of the driplines and in the underlying sandy silt. Although participating in the 4-day injection period, the region about dripline 5 shows dye penetrated only a short distance. Once again, this could have been due to a clogged emitter and/or lateral flow. Also, the dye may sorb more easily to finer soils such as the fine cover sand versus underlying gravelly sandy lenses.

The fourth transect was along the original southwest face of the trench (Figure 5-6). The expansive region of dyed soil to the southeast was also associated with the slightly ponded conditions around the main line. Dyed water penetrated and evenly stained soils ranging from bedded clay to coarse pebbles and gravel before breaking into lobes having wavy fronts. The water traveled vertically 50 cm through clayey silt before becoming impeded by small, thin coarse sand-gravel lenses. The water also avoided a large cobble as it flowed more laterally into layers of sand and fine gravel.

While water flow in the vicinity of dripline 1 was somewhat radially distributed, flow about dripline 2 was more laterally directed. A lens of bedded clay was bypassed completely. Also, the dyed front terminated sharply at a coarse/fine soil boundary, 20-25 cm below dripline 2. This silty sand/clayey silt contact is continuous to the northwest and explains the orientation of the dyed soil below dripline 4. Lateral flow is suggested by the small isolated patch of

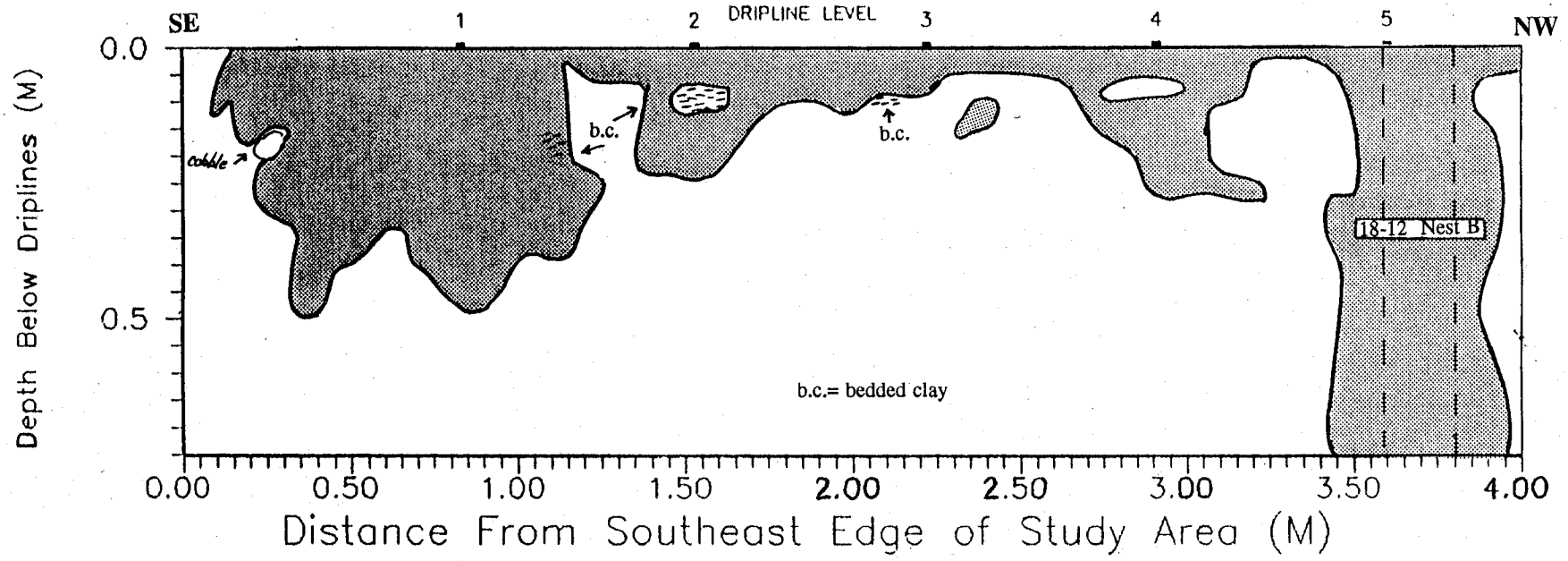

Figure 5-6. Cross-section of dye extent--Southwest Face: Cut Initial.

dyed soil near dripline 3. In terms of emitter uniformity, those in the vicinity of driplines 2 and 4 appear to have contributed nearly equal amounts of flow.

Water apparently passed along the interior of the tensiometer nest B at Station 18-12. Bentonite seals and backfill in the shallow portions of the profile were not sufficient to deter water movement along the tubes. The extent of the piping is unclear, but a 5-meter deep tensiometer removed from the nest was stained blue along its length. Preferential pathways here may have drawn flow from dripline 4. This may explain the lack of dyed soil between driplines 4 and 5, along both the northeast and southwest faces of the trench.

Cut A revealed a narrow, deep zone of dyed soil below dripline 1 (Figure 5-7). A nearby emitter may have contributed all or part of flow in this region (see also Figure 5-2). A pulse of dyed water penetrated the cover sand initially, then silty sand, followed by sandy, pebbly gravel and clayey, sandy silt. The depth of the base of dyed soil here was undetermined. The exposed, smooth dye trace is indicative of flow through the extensive clayey silt. The infiltrating water avoided a circular lens of bedded clay and protruded slightly to the northwest along the coarse sandy gravel.

While the regions of dyed soil beneath driplines 1 and 3 are similar in size and extent, the region beneath dripline 2

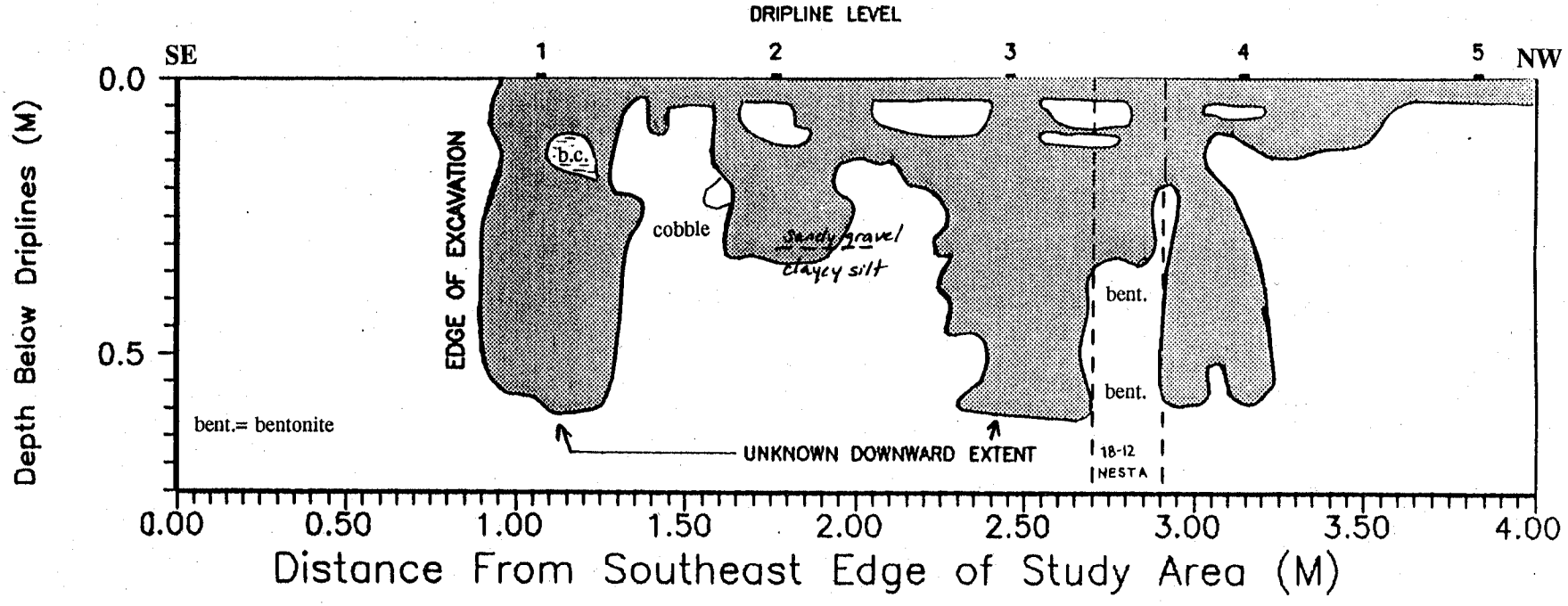

Figure 5-7. Cross-section of dye extent--Southwest Face: Cut A

is only half as extensive. Dyed water may have flowed laterally here, as the bare area just below dripline 2 is composed of the same soil which was dyed to either side. However, the lower boundary of the dyed soil does not mark a contact; rather, it lies below the contact marking the base of the sandy gravel mentioned above. If lateral flow occurred along the contact during irrigation, then drainage may have caused the water to move vertically from the coarse layer into the underlying fine layer. This phenomenon is also described by Hillel and Talpaz (1977) and Bybordi (1969).

Dyed water infiltrated to an unknown depth (over 75 cm) below dripline 3 and did not move preferentially along tensiometer nest A (Figure 5-7). Two layers of bentonite in the annulus outside the tensiometers prevented channeling of infiltration. This observation suggested that these tensiometers would provide unbiased values of pressure head. Undyed, shallow portions of soil, found below driplines 3 and 4, suggest that there were lateral flow components through the cover sand. This flow eventually channelled downward near the tensiometer nest (station 18-12). Finally, a small isolated zone of dyed soil below dripline 5 signifies some preferred flow paths, perhaps toward the sink at tensiometer nest B.

Based on the above cross-sectional analyses of dye traces, tensiometer nest A appeared to have performed adequately while nest B experienced piping. An analysis of pressure head or hydraulic head data collected from each nest

is necessary to establish the impact of the piping. Figures 5-8 A and B show hydraulic head data (elevation head plus pressure head) gathered from shallow tensiometers of both nests. Tensiometers of near equal elevation heads were compared, assuming these tensiometers were emplaced into the same soil layer. Time equal to zero days signifies a date just prior to the beginning of the second infiltration flux (approximately equal to 8.64 cm/day). This span of days was chosen to represent both the infiltration and drainage cycles and allow any effects from piping to be determined during those cycles. Noise in the data is due to tensiometric response to system perturbation from the increased flux and subsequent initiation of drainage.

Because elevation heads are virtually the same, the graphs represent changes not only in hydraulic head, but in pressure head as well. During the period zero to eighty days, line 1 (nest B) showed lower values of pressure head than those for line 2 (nest A). However, between days 80 and 123 (beginning of drainage: September 3, 1989), lines 1 and 2 suggested similar wetting behavior. Following 123 days, and during the drainage phase, hydraulic head did vary from nest to nest but not consistently to suggest impact from piping.

Deeper tensiometers found at 4.31 m and 4.32 m were also compared (Figures 5-9 A and B). In these graphs, line 1 (nest A) becomes distinct from line 2 (nest B) beginning at day 80 and continuing up until 200 days. Opposite behavior is

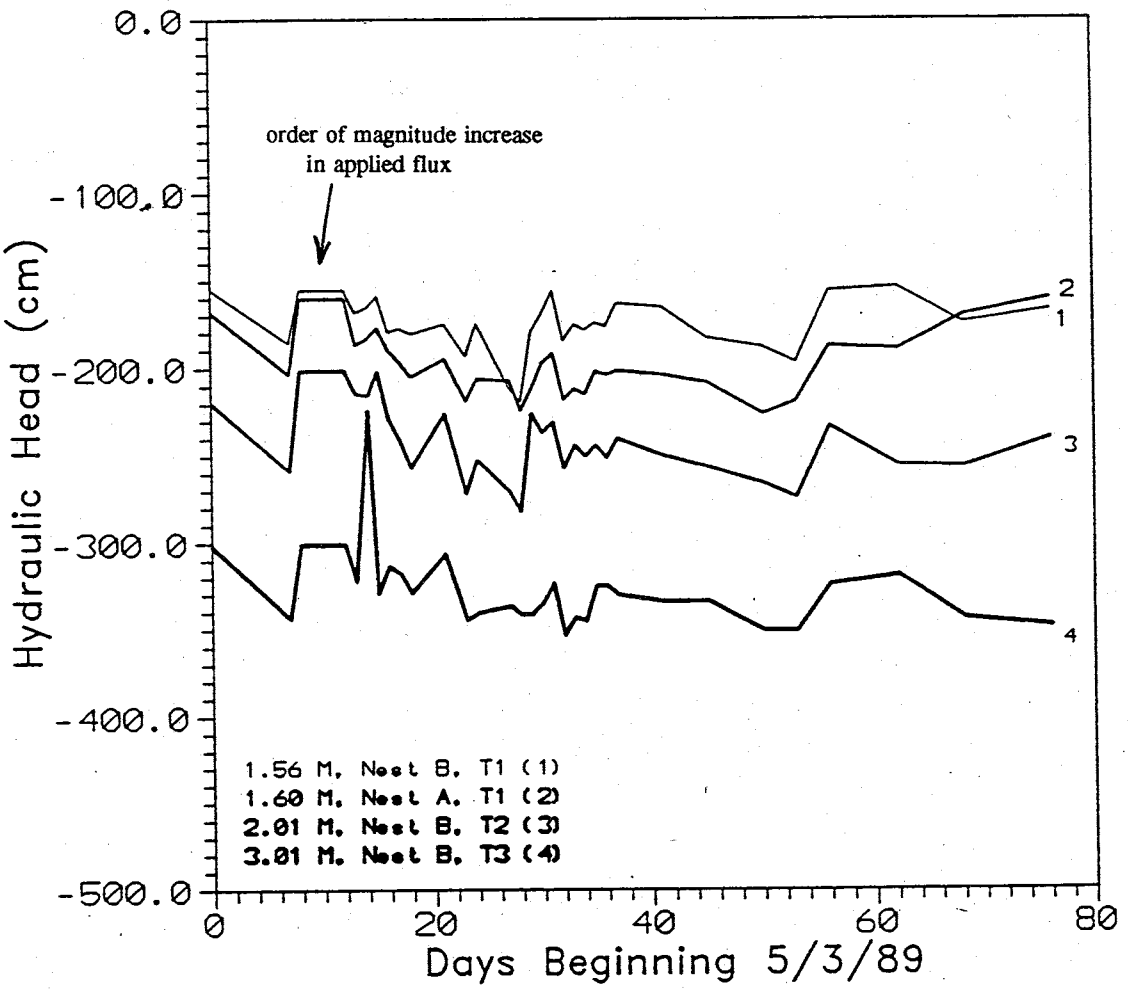

Figure 5-8a. Hydraulic head (cm) vs. Time (days): Station 18-12; Infiltration

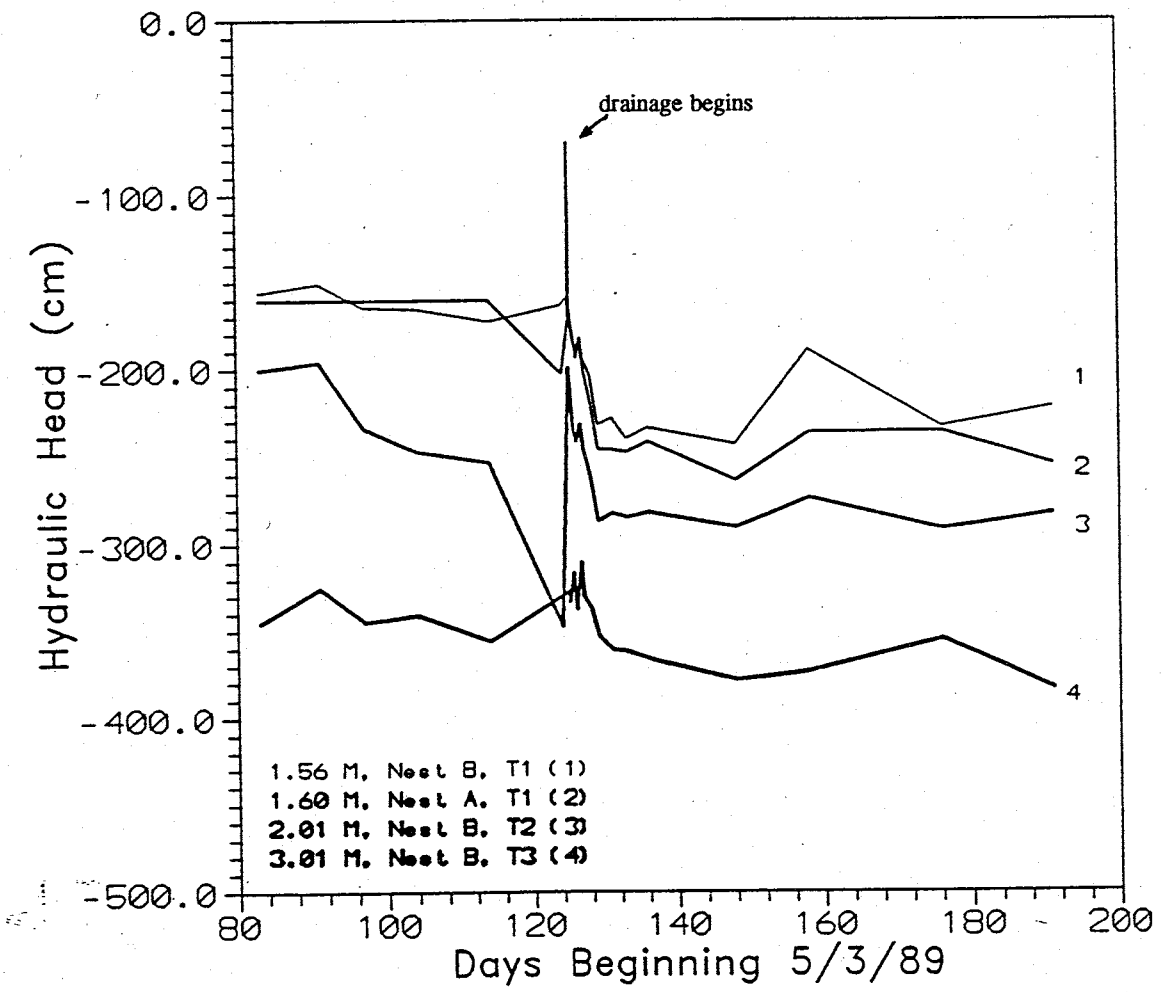

Figure 5-8b. Hydraulic head (cm) vs. Time (days): Station 18-12; Infiltration/Drainage

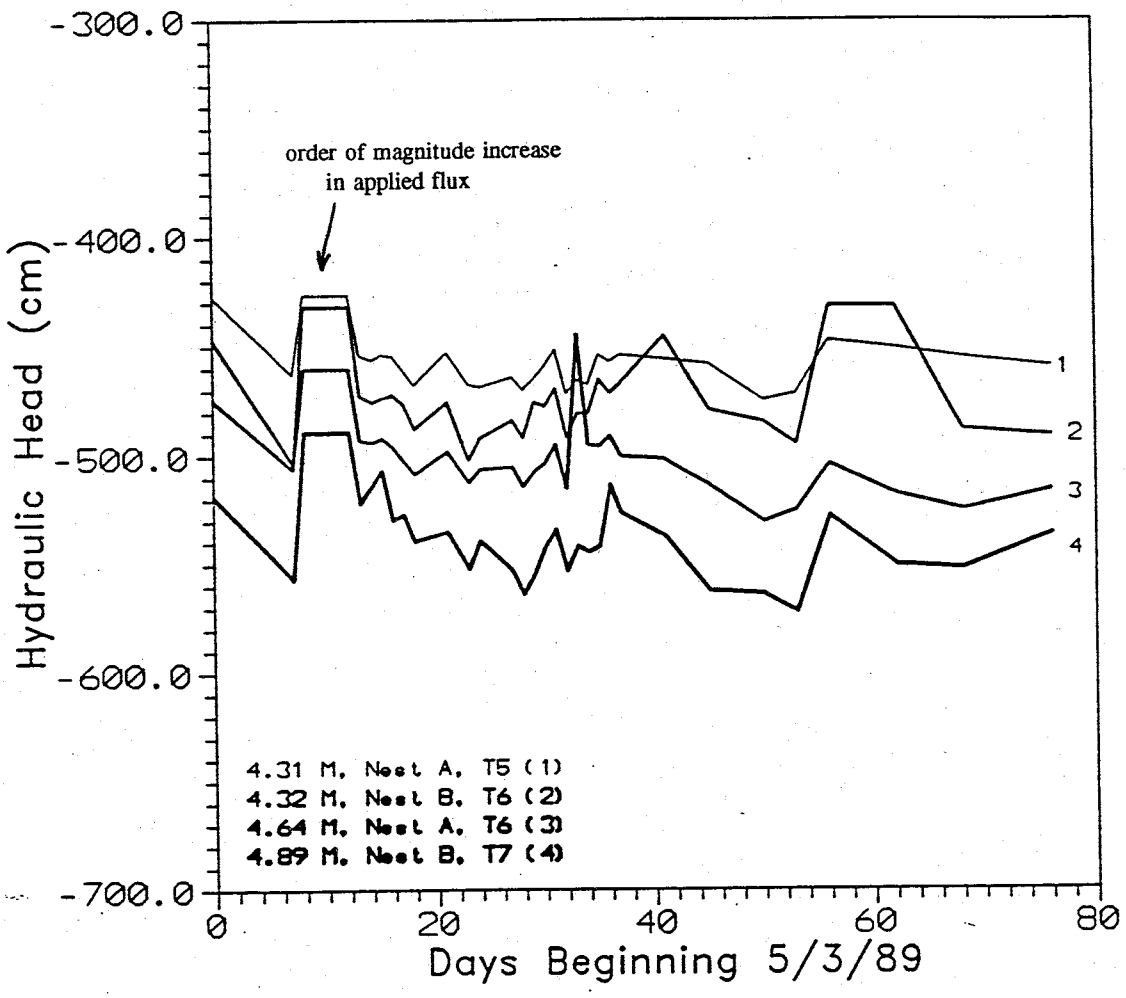

Figure 5-9a. Hydraulic head (cm) vs. Time (days): Station 18-12; Infiltration

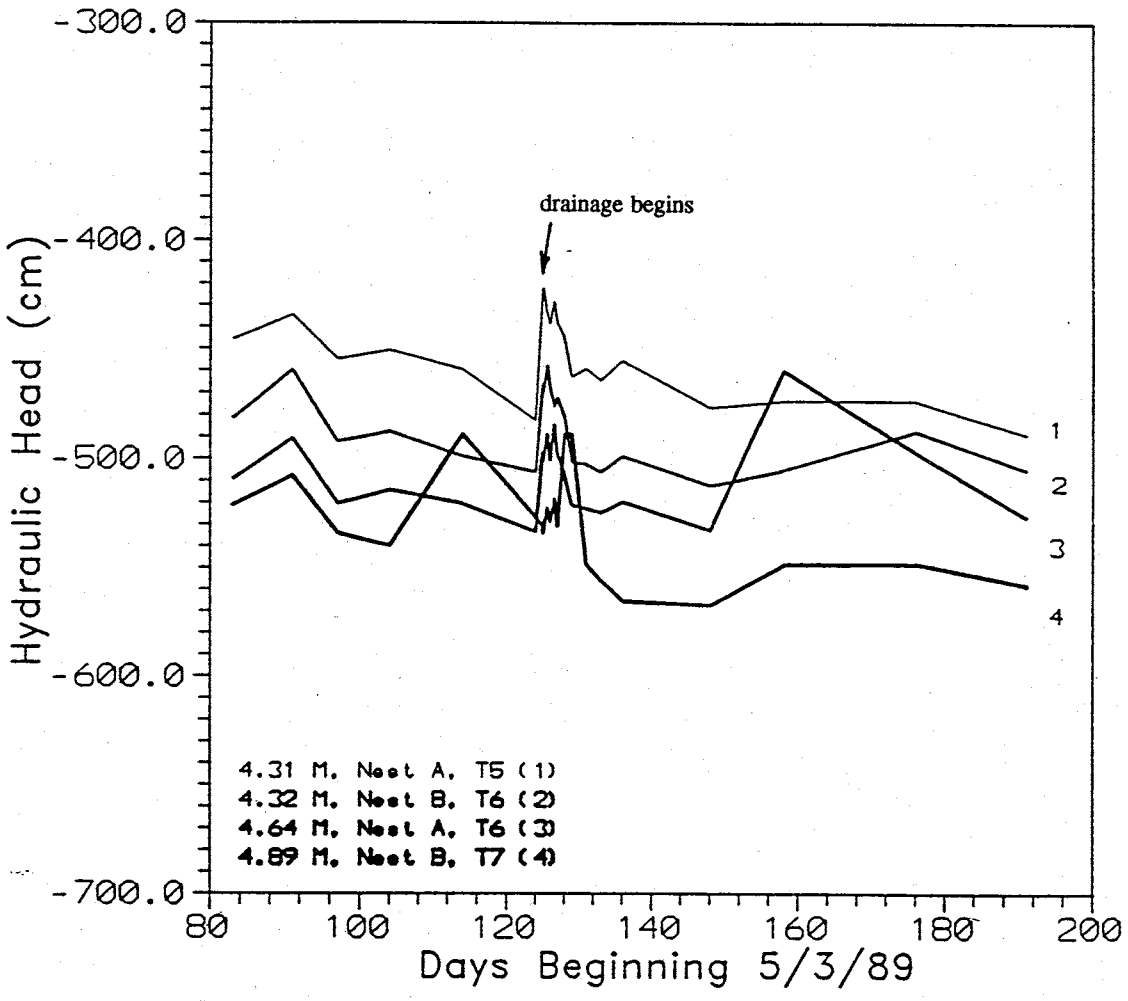

Figure 5-9b. Hydraulic head (cm) vs. Time (days): Station 18-12; Infiltration/Drainage

indicated, as nest A maintains less negative values of pressure head than nest B. Even though blue dye coated the deep tensiometer from nest B, piping does not appear to have affected the data. It could be that a deep layer of bentonite or other fine material, found just above the cup, may have inhibited downward flow. In conclusion, the general effects of channelling may have been present during infiltration and drainage in the two shallow and two deep tensiometers, but the effects could have been masked by redistribution of moisture during drainage.

The fifth transect, cut B, is oriented at a slight angle north of the SE-NW main trench (note Figures 5-2 and 5-10). The dripline crossover points are therefore closer together. The dye trace extended down to 65 cm and deeper below dripline level. A wavy dye front marks an extensive zone of dyed soil in the southeastern portion of the cut. Flow through this area may have been primarily vertical, as the dyed fluid bypassed a number of irregular lenses of silty, sandy gravel, found in the upper 25 cm of the profile. The dyed water penetrated these lenses and then proceeded into the pervasive clayey silt. The front was not smooth, however, and this may have been due once again to local textural variability producing preferential broad "fingering" of the dye trace.

Preferential pathways for flow may have developed along the outer walls of the neutron probe access tube. Clean bentonite was still intact along the tube. However, additional

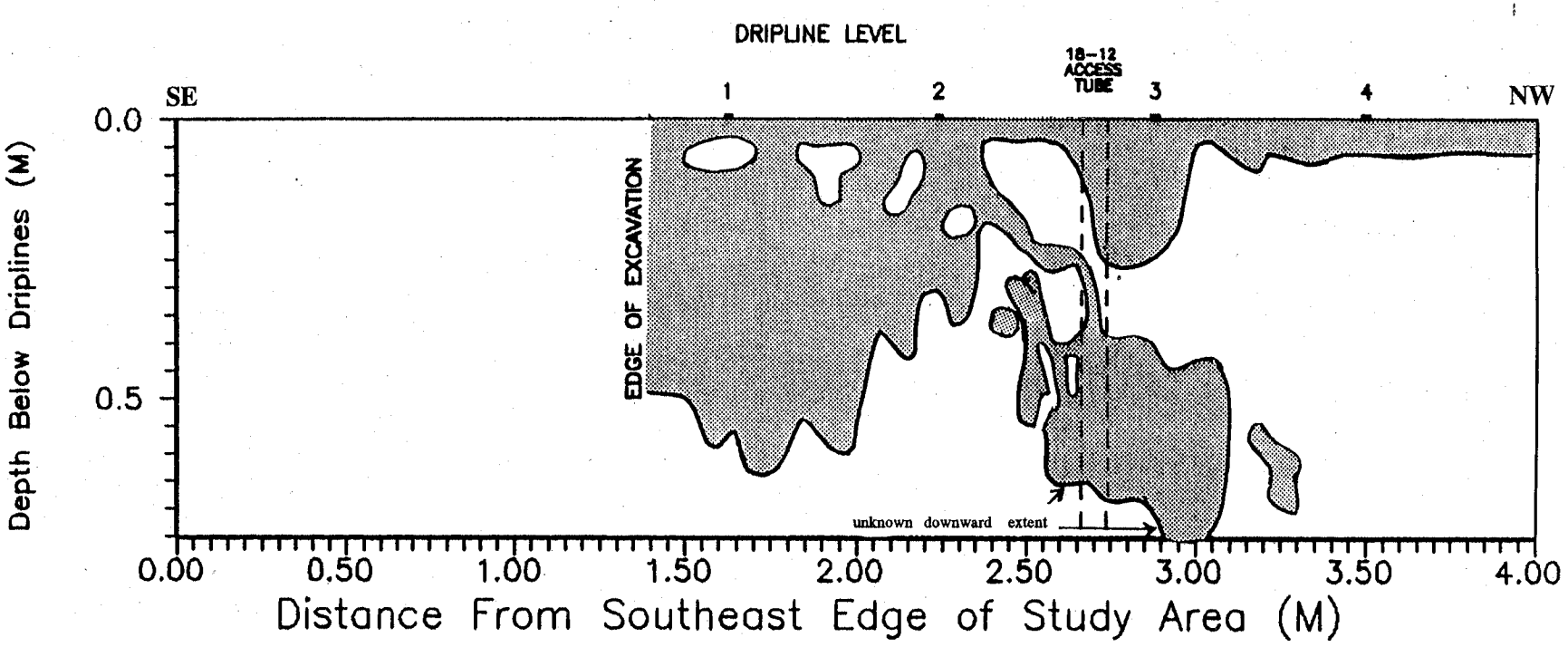

Figure 5-10. Cross-section of dye extent--Southwest Face: Cut B

blue-stained bentonite was smeared onto the metal tubing, suggesting lateral flow of dyed water around the tube and northwestward (in two dimensions) into the clayey silt. Some of this water also moved vertically downward, along the access tube. The dye trace is of unknown downward extent below the trench floor.

The closest emitter to cut B is along dripline 4 (see Figure 5-2). Little dyed soil was found in this area. One can infer that either the emitter was disabled or that substantial lateral gradients swept the dyed water away.

One cross-section was excavated parallel to dripline 1 (Figure 5-11). Its intersection with cuts A and B are shown. The emitter locations (from dripline 1) are actually 10 cm away (out from the page) from this "side cut." It is puzzling that dyed soil is not present directly in the vicinity of emitter one, while dyed soil is prevalent around "dripline 1" in Figure 5-7. Three-dimensional flow is inferred as the dyed water may have been initially channelled away from the wall and then back toward this side cut. Lenses of bedded clay were common at the 15 cm depth (Figure 5-11), in the vicinity of dripline 1. Dyed water avoided these lenses, but soil became dyed beneath them.

A change in texture from fine clayey silt to coarser gravelly clayey silt may account for the unstable dye trace in the eastern region of the side cut. Flow from fine to coarse layers promotes wetting front instabilities (Raats, 1973).

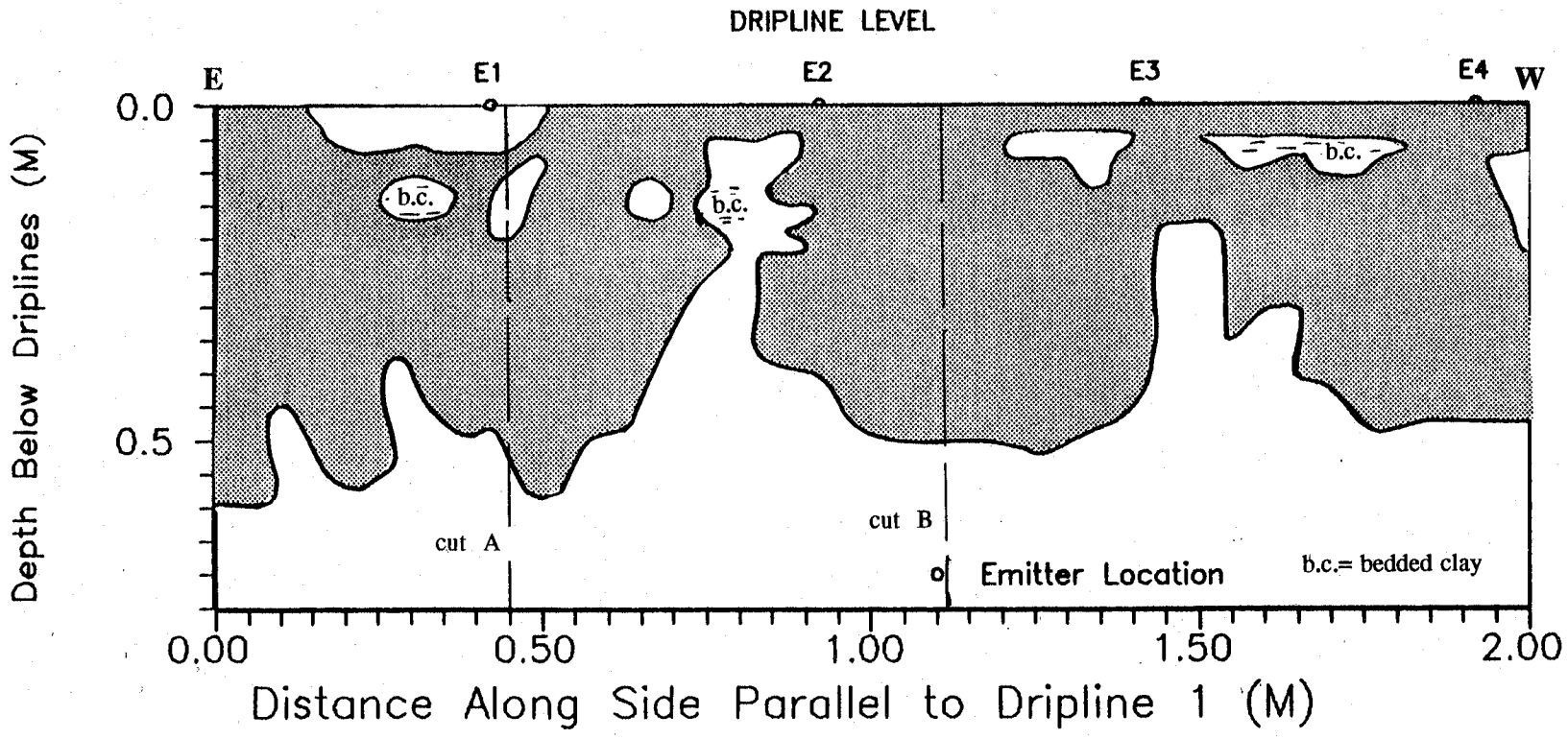

Figure 5-11. Cross-section of dye extent: Side Cut (parallel to dripline one)

Also, Parsons (1988) assigned a saturated conductivity value of 2.5×10^{-4} cm/s to the region containing the clayey silt. The applied flux rate was approximately 1.0×10^{-4} cm/s. Because the flux rate is less than the K_{sat} of the clayey silt, instabilities can occur. The wetted depth along the "side cut" is relatively consistent, possibly suggesting application of fairly uniform flux.

Another large zone of dyed soil is present midway between emitters 2 and 3, along the side cut. The front is rather smooth, indicating a more uniform texture in the clayey silt along the cut. The soil appears to be dyed by flow from both emitters. The T-shaped undyed region in the side cut to the right of the cut B intersection seems continuous with the undyed region in cut B just below dripline 1 (Figure 5-10). Dyed water again avoided a section of bedded clay between E3 and E4, but penetrated a smaller clay lens due west. Flow was channelled through this small lens and into a silty sand. This silty layer was dry upon excavation while the underlying clayey silt was damp. During drainage the silty sand layer may have released some moisture to the finer layer.

Figures 5-12 and 5-13 are of cut D and section C3C (cut C), respectively. An emitter (number 5-5) on dripline 5 is located practically on top of cut D (note Figure 5-2). Dye penetrated to about the 10 cm depth, immediately adjacent to the emitter. Dye was also visible in a zone 50 cm deep. This dye pattern and the one in section C3C suggest dye spread

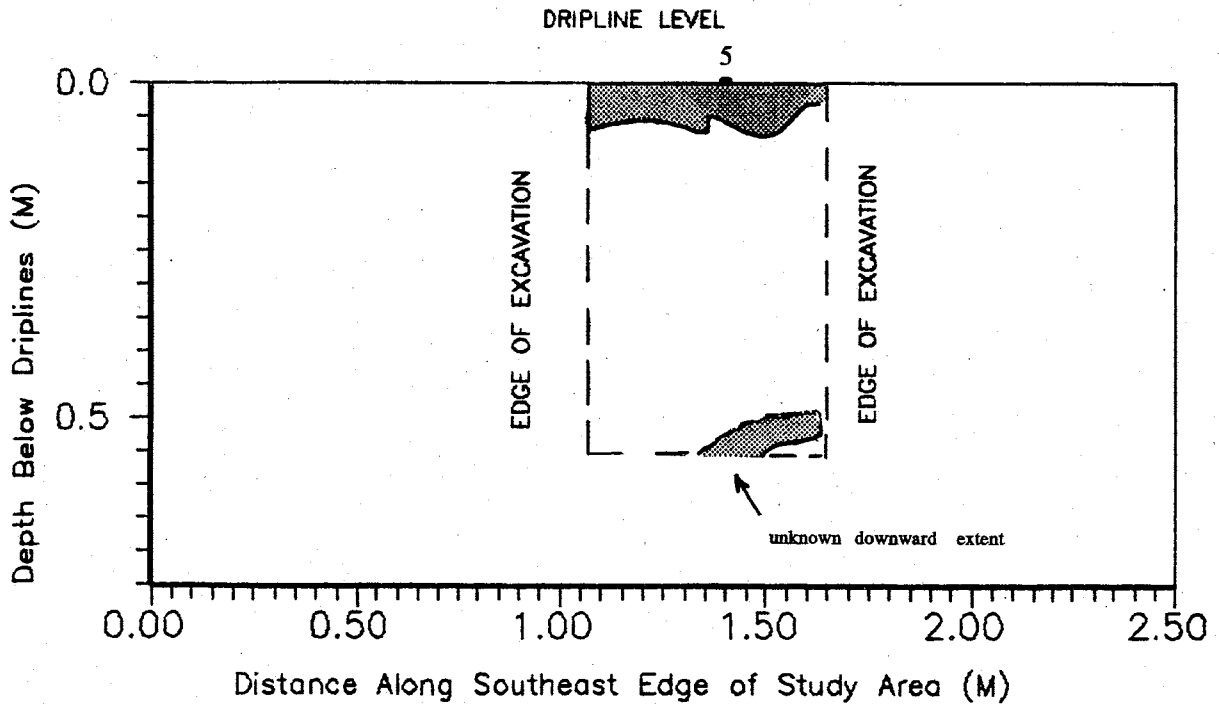

Figure 5-12. Cross-section of dye extent: Cut D (Y = 3.80 M)

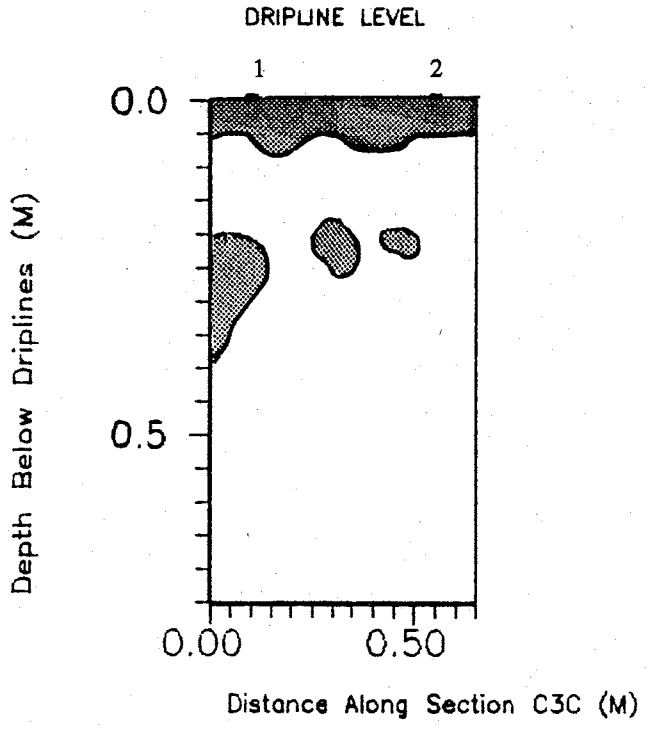

Figure 5-13. Cross-section of dye extent: Cut C (Section C3C)

uniformly in the cover sand and the shallow soil. Preferential flow also carried the dye to greater depths as shown by isolated patches of dyed soil.

2.5 Meter Deep Trench

The second dye study area was located along the southern wall of the 2.5 M deep trench, excavated near Station 12-12. The schematic of the dye trace relative to instrumentation is shown in Figure 5-14. Note that the width of the backfill is not to scale and that dripline 4 here is actually 30 cm north of the south wall.

Figure 5-14 primarily illustrates dyed fluid behavior in the vicinity of tensiometer nest A, neutron probe access tube and solution sampler 1a. There was no evidence that preferential flow occurred along either the neutron probe access tube or tensiometer nest A. Although the water eventually flowed laterally and vertically, as unsaturated flow became more pronounced in deeper portions of the profile, shallow channelling of water along these instruments had been successfully deterred.

On the other hand, preferential flow at sampler 1a did occur. Dyed fluid coursed through the discontinuous, fractured bentonite and silica flour seals. Lateral components of flow were induced as the front encountered a thick silica flour seal at the base of sampler 1a. This type of flow along the sampler stem can produce abnormally high

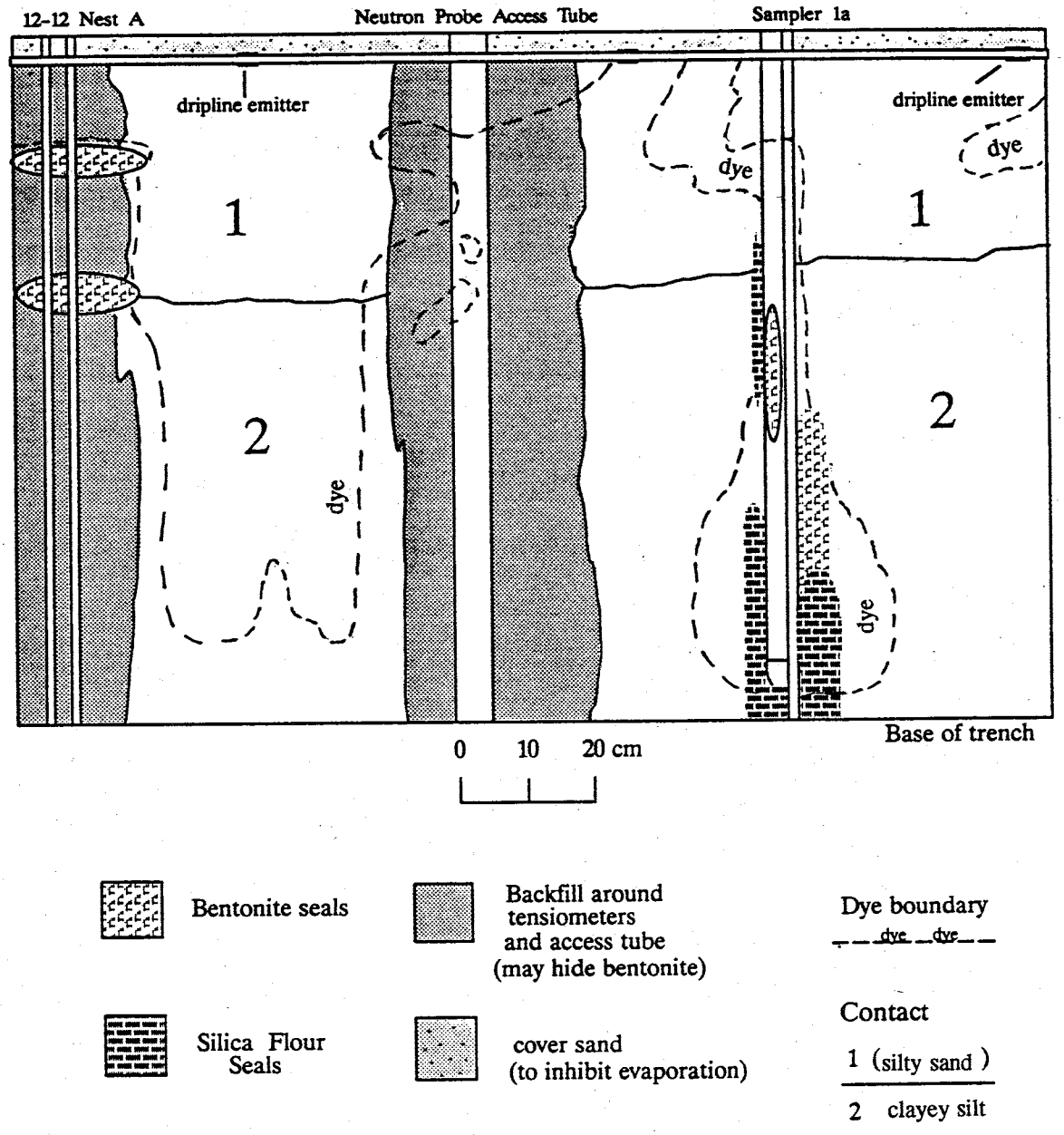

Figure 5-14. Dye patterns in the vicinity of tensiometer nest, neutron probe access tube and solution sampler--south wall of 2.5 meter deep trench

water velocities around the cup and therefore allow tracers to show up too quickly. For more information on pore water velocities and sampler performance, consult Grabka (1990).

It is interesting to note, however, that in Figure 5-14 the depth of dye penetration in soil (about 80 cm) is very similar to that found at sampler 1a. This could have been due to presence of similar soils, with similar affinity for dye sorption. Successful deterrence of vertical flow around the access tube and tensiometers may have concentrated flow in this area. Another source, such as soil disturbance (from drilling?) or roots may also be responsible for deep progression of the dye front.

5.3 Summary

During the last few days before drainage commenced, a blue dye was injected into the southern quarter of the irrigated plot, via the dripline system. The goal of this study was to analyze dyed fluid pathways in order to assess instrument performance and the effect of texture and soil layering on the shallow flow field. In terms of instrument performance, preferential fluid flow along the access tube and tensiometer nest B, station 18-12, was indicated. High values of moisture content collected at shallow depths (Figure 4-18) may be explained by increased flow along the access tube, as indicated by the dye experiment (see Figure 5-10). Also, dyed fluid flow suggested preferential flow along the tensiometer

nest (B), although hydraulic head data (and pressure head data) only roughly support this. Flow broke through bentonite seals around soil water sampler 1a, near station 12-12. Enhanced flow along the sampler stem can bias measurements of velocity, determined during the solute transport experiment, for the soil surrounding this sampler.

The dye study also indicated that emitter uniformity may be in question. For example, northwestern regions of Figure 5-5 and the cross-section in Figure 5-12 show little dyed soil, in spite of close proximity emitters. But lateral gradients or variable soil textures may have caused dyed water to move away from these areas and toward the sink at tensiometer nest B.

The dye study was particularly useful for determining, on a local scale, the influence of texture and soil layering on the shallow flow field. In regions of saturated flow, found only in the vicinity of the main line of the irrigation system, dyed fluid passed laterally through coarse layers (gravelly sand) while largely avoiding lenses of clay. Macropores, both unnatural (due to poorly packed instruments) and natural also provided pathways for preferential moisture movement. Sharp dye fronts terminating at coarse over fine layer boundaries suggested pseudosaturated conditions. However, once drainage commenced, the dyed fluid front was pulled downward into underlying, finer material.

Progress of vertical flow and drainage, in general,

through the thick layer of clayey silt at the base of the shallow trench is indicated by a wavy dye trace. Thin lenses of silty, gravelly sands, found in the thick silt layer, inhibited unsaturated flow, causing the front to change shape. These soils may have also had a higher affinity for dye sorption as opposed to the coarser soils. Also, lateral flow through the clayey silt is indicated by detached pockets of dyed soil.

Although the dye study area was small compared to the three-dimensional extent of the experimental site, the small scale influence of texture and layering is extremely important, especially if, for example, we are examining contaminant movement on the same scale. To assess more completely the role of these features on a local scale, a number of pressure head and moisture content profiles were constructed from stations within the irrigated plot. Observations made from these profiles are presented in chapter 6.

Chapter 6. Distribution of Hydraulic Gradient and Moisture Content

The dye study emphasized the importance of texture and soil layering on the flow field. The scale of study is much smaller than that used in hydraulic head field and plan view moisture content analyses. However, the study shows local scale lateral and vertical flow occurred through variable soil types and across both sharp and gradational layer boundaries. If the flow behavior exhibited by the dye is any indication of behavior in other parts of the 10 x 10 m plot, then local scale distribution of hydraulic gradient and moisture content must be investigated.

There are two goals for this investigation. First, this analysis will determine if the regional conceptual model developed above is adequate to describe subsurface flow or if local variability must be incorporated. Trends in the data will be analyzed as they may indicate particular textures or layers. Thus, the second goal will be to compare these trends to geologic information, allowing confirmation or adjustments to geologic description and interpretation.

6.1 Local Scale Observations

Table 3 summarizes vertical hydraulic gradients (i) calculated for various depths at each irrigated plot station. Tensiometer cup locations, denoted by filled circles, as well as hydraulic head data are provided in Appendix D. Gradients

Table 3. Summary of hydraulic gradients. Solid arrows indicate infiltration gradients. Dashed arrows indicate drainage gradients.

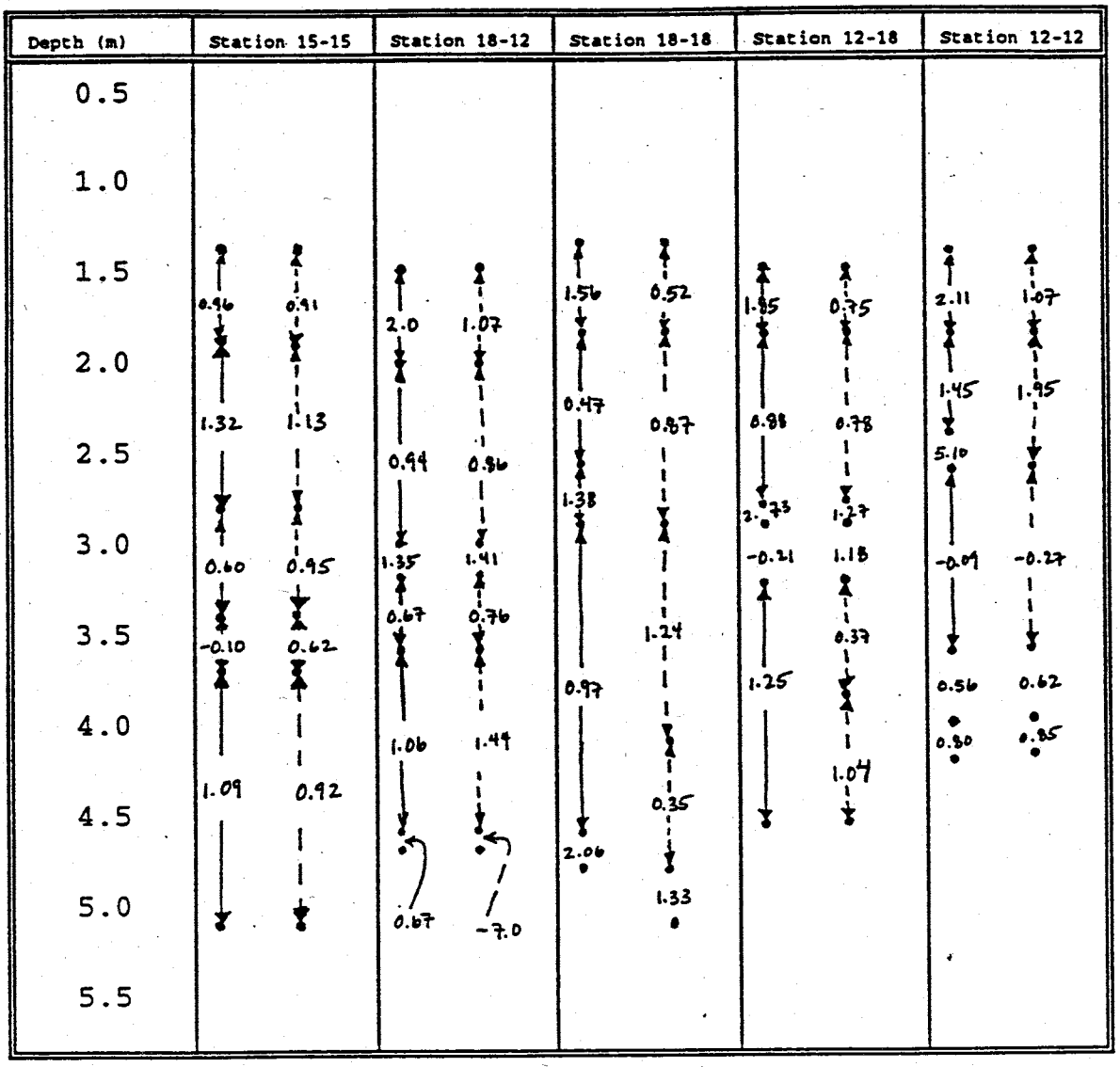

range from -7.0 to 2.11. Negative gradients indicate an increase in hydraulic head (becoming more positive) over an increase in depth.

Unit gradient can be approximated as a range between 0.8 and 1.20 (Stephens, 1990, personal communication). When the gradient equals or nearly equals unity, one-dimensional flow is indicated, and the soil moisture flux (q) approximately equals the unsaturated hydraulic conductivity (K_{unsat}). K_{unsat} is a function of moisture content. Therefore, if unit gradient is established across several layers in a soil profile, flux and K_{unsat} are equal among these layers. Changes in moisture content with depth will thus reflect texture: high moisture content will indicate silts and clays; low moisture content will indicate sands and gravels.

Extremes in gradient also indicate other types of flow. Gradients larger than 1.20 suggest strong downward flow with perhaps less propensity for lateral flow. Similarly, small gradients ($0.0 < i < 0.8$) indicate flux rates through the soil are small; lateral flow may be more significant in this case.

For all 10 x 10 m plot stations, shallow hydraulic gradients, calculated for the 1.4 - 2.0 meter depth interval, are for the most part nearly equal to or greater than unity, indicating strong vertical flow occurred. In the center of the plot (station 15-15), the gradient did not change appreciably between infiltration and drainage as opposed to other regions. Both the southeastern and southwestern areas

experienced high soil moisture flux (i > 1). The dye study showed that preferential flow along instruments may have caused high flux at station 18-12. The study also emphasizes that dye penetrated deeply at station 12-12, and this validates the high gradients measured.

Distribution of gradients between 2.0 and 2.75 MBD suggested vertical flow increased in magnitude in the southwestern (station 12-12) and central areas of the plot and slightly decreased in other regions. The geologic log for station 15-15, shown with drainage profiles (Figure 6-1), displays a coarse over fine layer sequence in this depth interval. This layering system supports the calculated high gradient. However, the log for station 12-12 does not indicate soil layering (Figure 6-2). A change in texture is indicated by d_{10} sizes, with an increase in grain size shown for the interval 2.08 - 2.69 MBD (Table 4). Thus, the effects of layering and texture on the flow field are evident at this depth in central and southwestern regions of the site.

Propagation of vertical flow is signified in the southwestern and central regions of the shallow profile by drying front locations, or DFL's. Drying fronts are tracked by examining the early drainage profiles and noting at what depth and time the soil profile has "felt" the effects of drainage. After 0.5 day of drainage, the DFL at station 12-12 has progressed 2.69 meters. The DFL at station 15-15 moved an additional 1.5 meters beyond this point, after the same amount

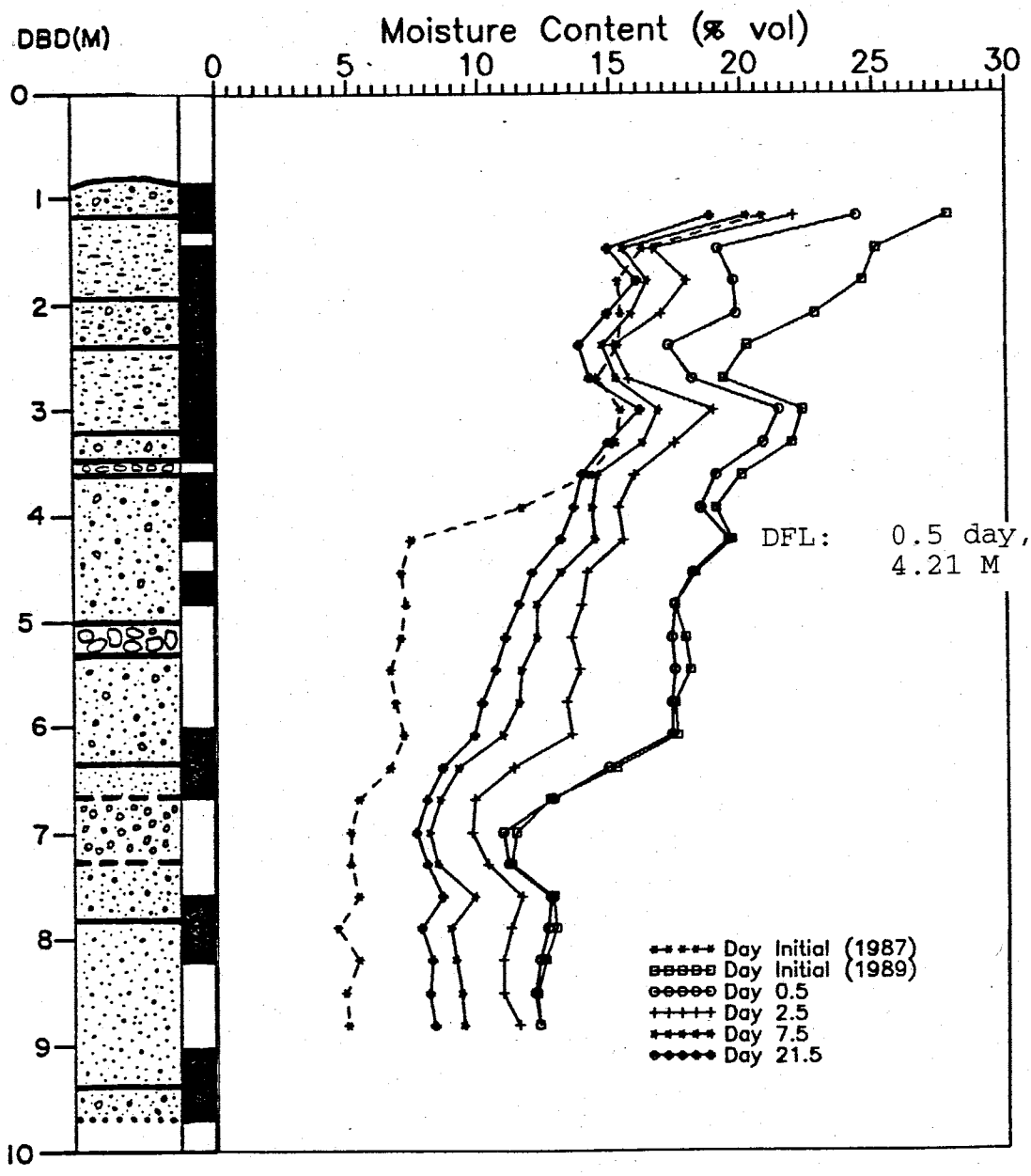

Figure 6-1. Drainage Profiles--Station 15-15. "Day Initial (1987)" refers to January 25-26, 1987. "Day Initial (1989)" refers to August 24-25, 1989 (11 days prior to drainage).

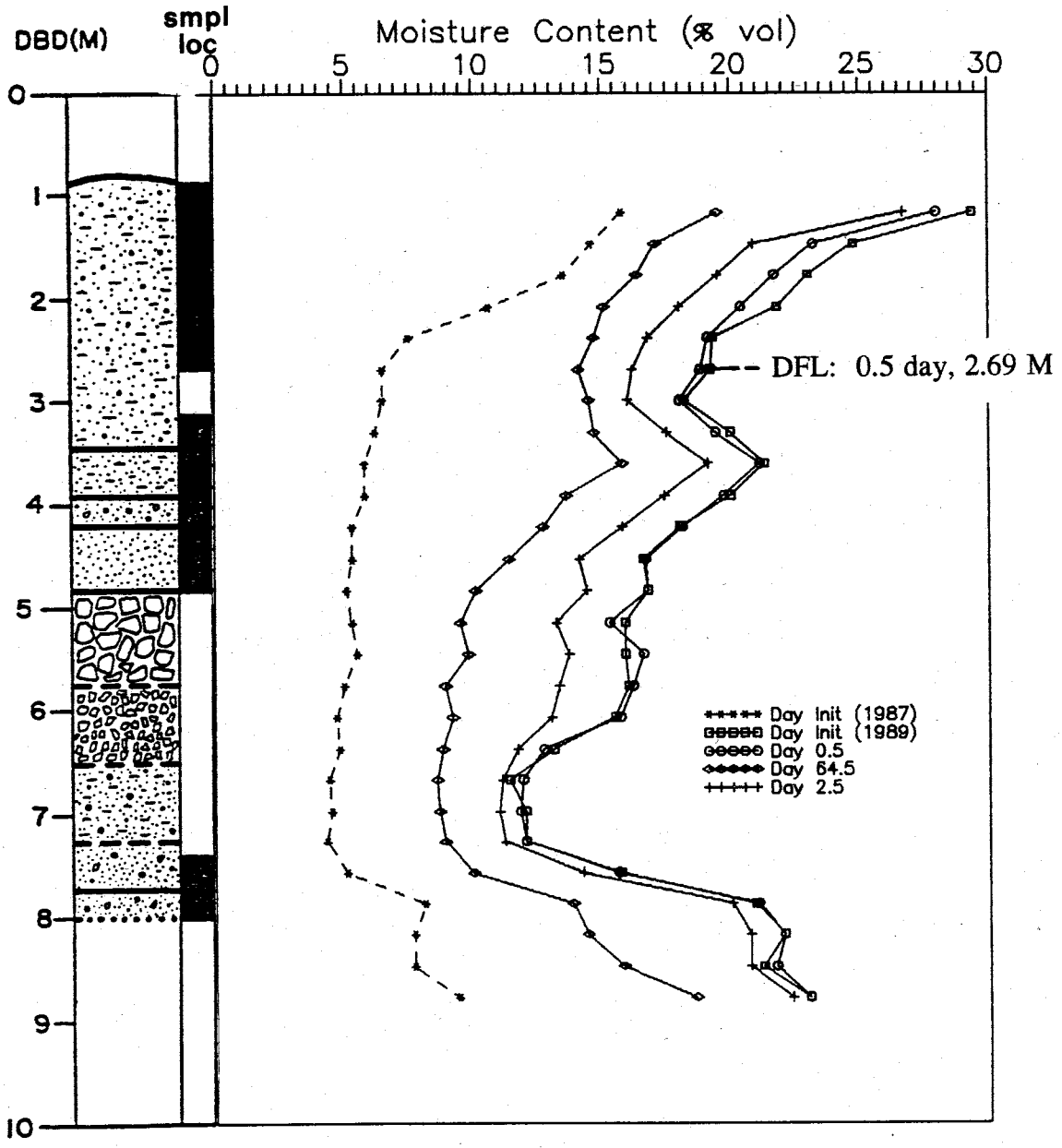

Figure 6-2. Drainage Profiles--Station 12-12. "Day Initial (1987)" refers to January 25-26, 1987. "Day Initial (1989)" refers to August 24-25, 1989 (11 days prior to drainage).

Table 4. d_{10} Sizes for Various Soil Depths--10 x 10 m Plot Stations. (from Parsons, 1988)

Station	Depth B.D. (M)	d_{10} (mm)	Station	Depth B.D. (M)	d_{10} (mm)
15-15	0.86-1.16*	0.158	18-12	0.86-1.16	1.02×10^{-3}
	1.47-1.93	2.10×10^{-3}		1.47-1.93*	1.32×10^{-3}
	2.08-2.38	4.20×10^{-3}		1.93-2.23*	2.41×10^{-1}
	2.99-3.15	1.15×10^{-2}		2.38-2.54*	4.98×10^{-1}
	3.15-3.45	0.185		2.54-2.84*	2.07×10^{-3}
	3.60-3.91*	0.157		2.84-2.99*	2.93×10^{-3}
	3.91-4.21*	0.168		2.99-3.60	2.12×10^{-3}
	4.52-4.82	0.209		3.60-3.91*	3.61×10^{-3}
	6.04-6.35	0.144		7.41-7.87	4.53×10^{-2}
	6.35-6.65	0.113	12-18	1.47-2.38	1.94×10^{-2}
	7.57-7.87	0.193		2.38-2.69	3.31×10^{-2}
	7.87-8.18	0.155		2.84-3.15	1.83×10^{-2}
12-12	0.86-1.32	7.70×10^{-4}		3.91-4.67	0.130
	0.86-1.47	8.62×10^{-4}		5.74-6.04	0.156
	1.47-2.08	1.80×10^{-3}		7.57-7.87	0.191
	2.08-2.69	4.74×10^{-2}		7.87-8.18	3.12×10^{-4}
	3.30-3.91	7.56×10^{-2}		8.18-8.48	0.176
	3.45-3.60	4.90×10^{-2}		8.63-8.94	0.152
	3.91-4.21*	0.158	18-18	1.62-2.23	4.82×10^{-2}
	4.21-4.82	6.00×10^{-2}		2.23-2.84	0.127
	7.41-7.72	0.107		3.15-3.76	0.194
	7.72-8.02	4.68×10^{-2}		4.06-4.82	7.50×10^{-2}
	8.78-9.09	0.184		6.35-6.65	0.156
*tensiometer borehole sample				6.65-7.11	0.134

of time. Although more layers were present to affect flow in the center of the plot, overall shallow vertical flow was more rapid here at station 12-12.

Texture once again played a role in terms of interaction between cobble layers and the flow field. Both the hydraulic head fields and the northeastern deep trench (Figure 4-5) emphasized the presence of lateral infiltration, and perhaps drainage, along the surface of the 3-4 meter deep cobble layer, which persists throughout the soil profile. During infiltration, downward flow was impeded at the 3.5 meter depth at station 15-15 and at the 3.0 meter depth at station 12-18. Cobble layers, as shown in geologic logs, provided this impedance. However, gradients applying to drainage of these depths suggest these layers vertically drained their moisture to some extent. Lateral infiltration or drainage is not evident for the 3-4 meter depth interval at station 18-18. Data was not collected within this interval so resulting gradients represent an average for layers in this interval.

Between 3.6 and 4.5 MBD, in the central, southeastern and northwestern regions of the irrigated plot, hydraulic gradients ranged from 0.92 to 1.44. Near unit gradient existed for infiltration in the northeast (station 18-18), but this number decreased during drainage, to 0.35, for the 4.1 to 4.6 meter depth interval. Drainage profiles for this station suggested moisture increased above the cobble layer (3.75 MBD) (Figure 6-3). While this moisture may have drained through

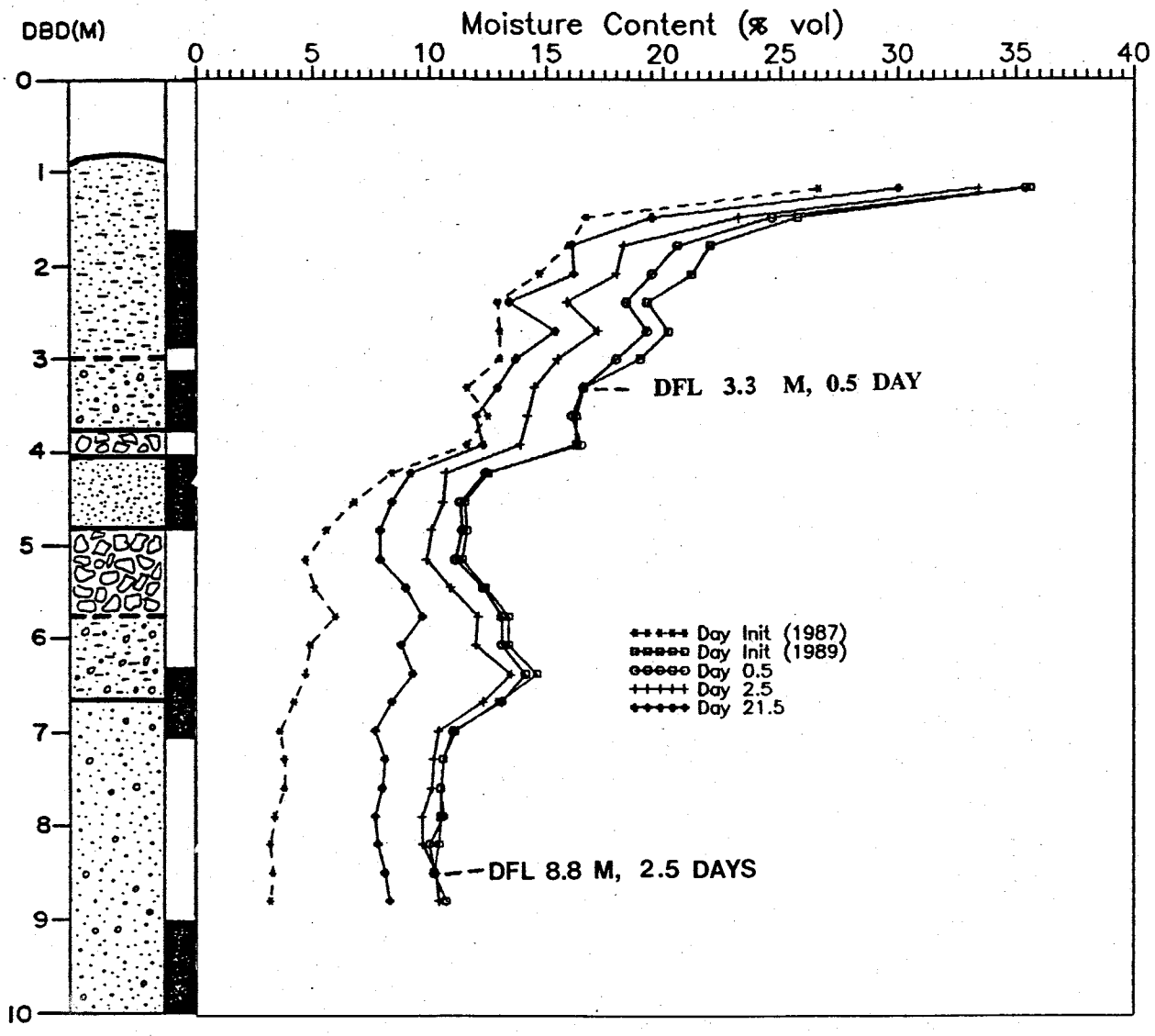

Figure 6-3. Drainage Profiles--Station 18-18. "Day Initial (1987)" refers to January 25-26, 1987. "Day Initial (1989)" refers to August 24-25, 1989 (11 days prior to drainage).

the shallow (silty sandy?) cobble layer, the low gradient and low range of moisture content in this 0.5 meter thick interval suggest this moisture may not have vertically progressed to the deeper cobble layer.

Low gradients for both infiltration and drainage events were calculated for the 3.6 - 4.2 meter depth interval at station 12-12 (southwest). Moisture increased greatly from the initial moisture profile at the 3.6 meter depth (Figure 6-2) The uniform original (1987) profile does not indicate presence of an impeding layer or texture which would cause moisture content to increase as it did. However, the log describes a poorly sorted, pebbly layer present at the four meter depth (see geologic log description, Appendix B). This layer may have provided impedance to downward flow. Once drainage began, vertical flow increased, and with time, the profiles shown in Figure 6-2 began to assume the shape of the original (1987) profile.

Drainage profiles, in general, were constructed to better define the drainage event for the irrigated plot soil profile (examples: Figures 6-1 through 6-5). Additional profiles for these stations are found in Appendix C. The five sets of profiles show a number of similarities and differences which are related to soil texture, soil layering, instrumentation and perhaps dripline uniformity. All five figures show that the wettest layers were at the top of the soil profile, in the vicinity of the driplines. The uppermost layer(s) at station

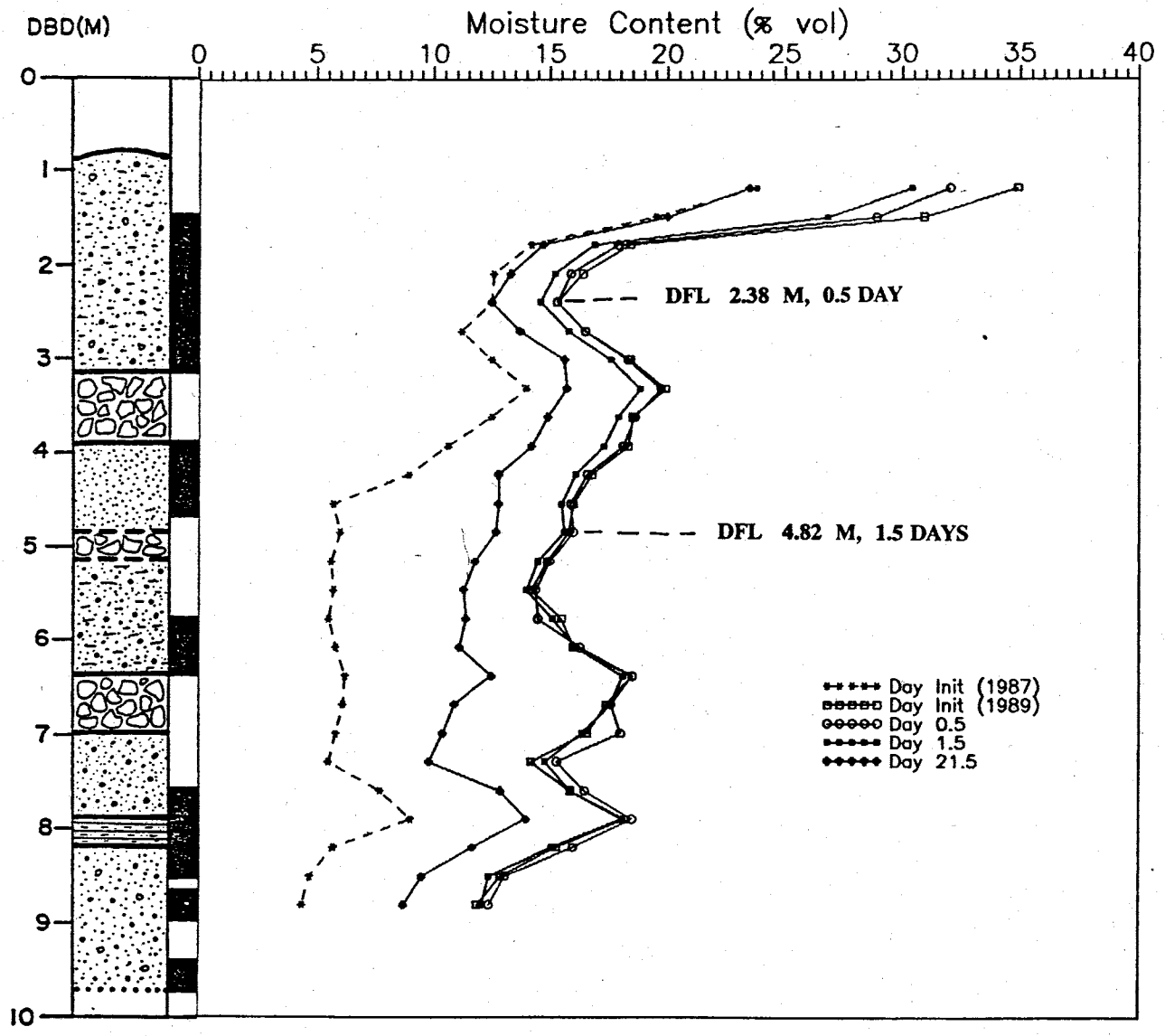

Figure 6-4. Drainage Profiles--Station 12-18. "Day Initial (1987)" refers to January 25-26, 1987. "Day Initial (1989)" refers to August 24-25, 1989 (11 days prior to drainage).

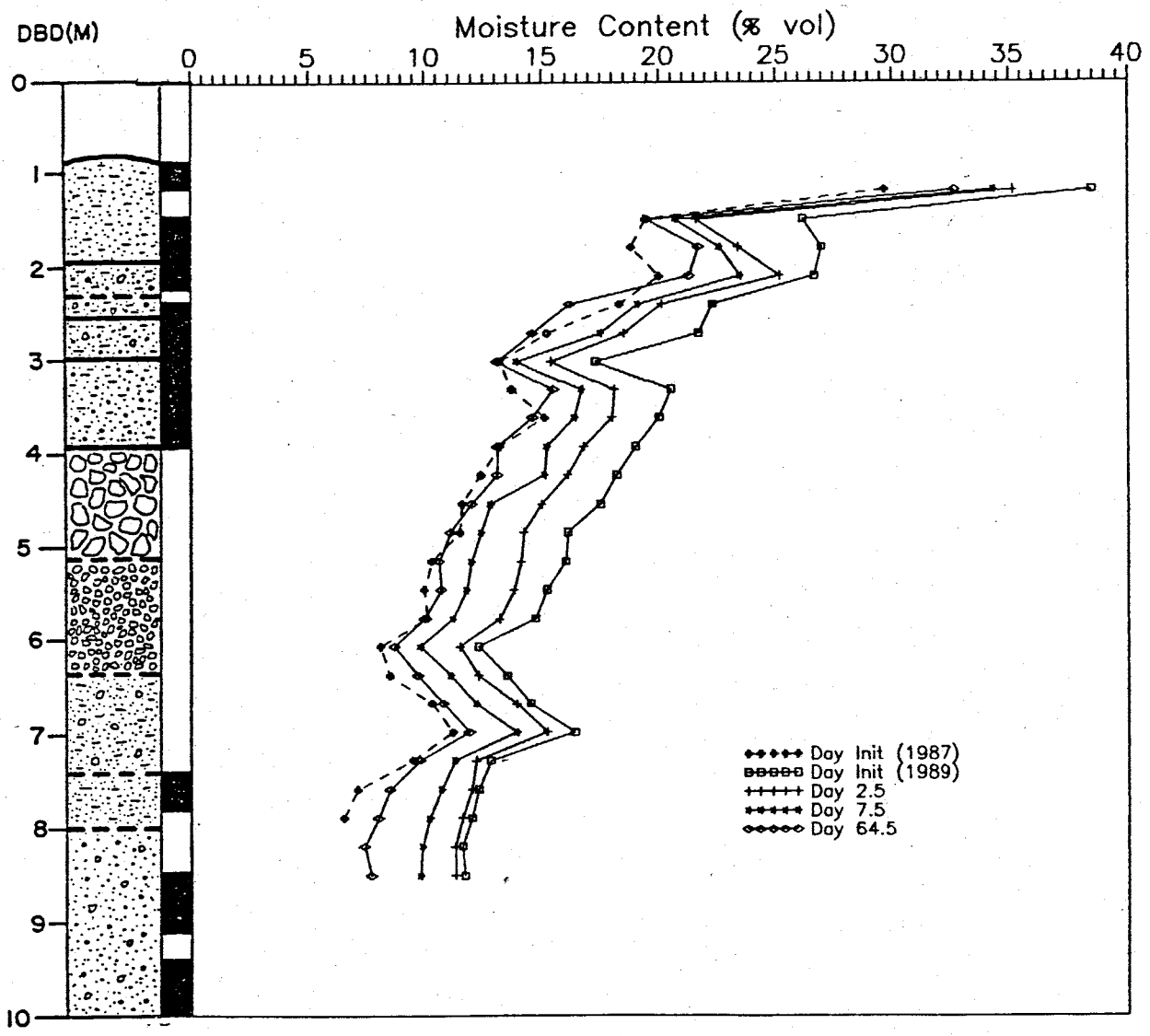

Figure 6-5. Drainage Profiles--Station 18-12. "Day Initial (1987)" refers to January 25-26, 1987. "Day Initial (1989)" refers to August 24-25, 1989 (11 days prior to drainage).

15-15 retained the least amount of moisture. This observation is supported by d_{10} data, as the shallow layer here is also the coarsest among all five stations. Therefore, the initial (1989) profile for station 15-15 is a good indication of texture, especially considering unit gradient persisted during infiltration.

Initial (1987) profiles plotted for station 15-15, 18-18 and 12-18 are very similar in character. Moisture content is high between dripline level and the four-meter depth. This moisture content decreases drastically at this depth to roughly 5-6% vol/vol. Mattson (1989) reported that a portion of the 10 x 10 m plot was inundated with rainwater before being covered with fill. This may explain the initially high moisture content in this region. However, it is also possible that the gravels (or cobbles) retained water above them over time. To solve this problem, late time drainage data must be compared to the initial (1987) data.

Drainage characteristics for all five areas of the plot are included in Table 5. The data show that the central and northern regions of the plot drained below individual 1987 profiles, to the 3.6 meter depth, following 64.5 days of drainage. Thus, it appears the early flooding of the site greatly affected the initial site characterization. Drainage below the 1987 profile for station 18-12 also occurred but these instances were not limited to shallow layers. Also, moisture content in very shallow layers at this station

Table 5. General Drainage Characteristics.

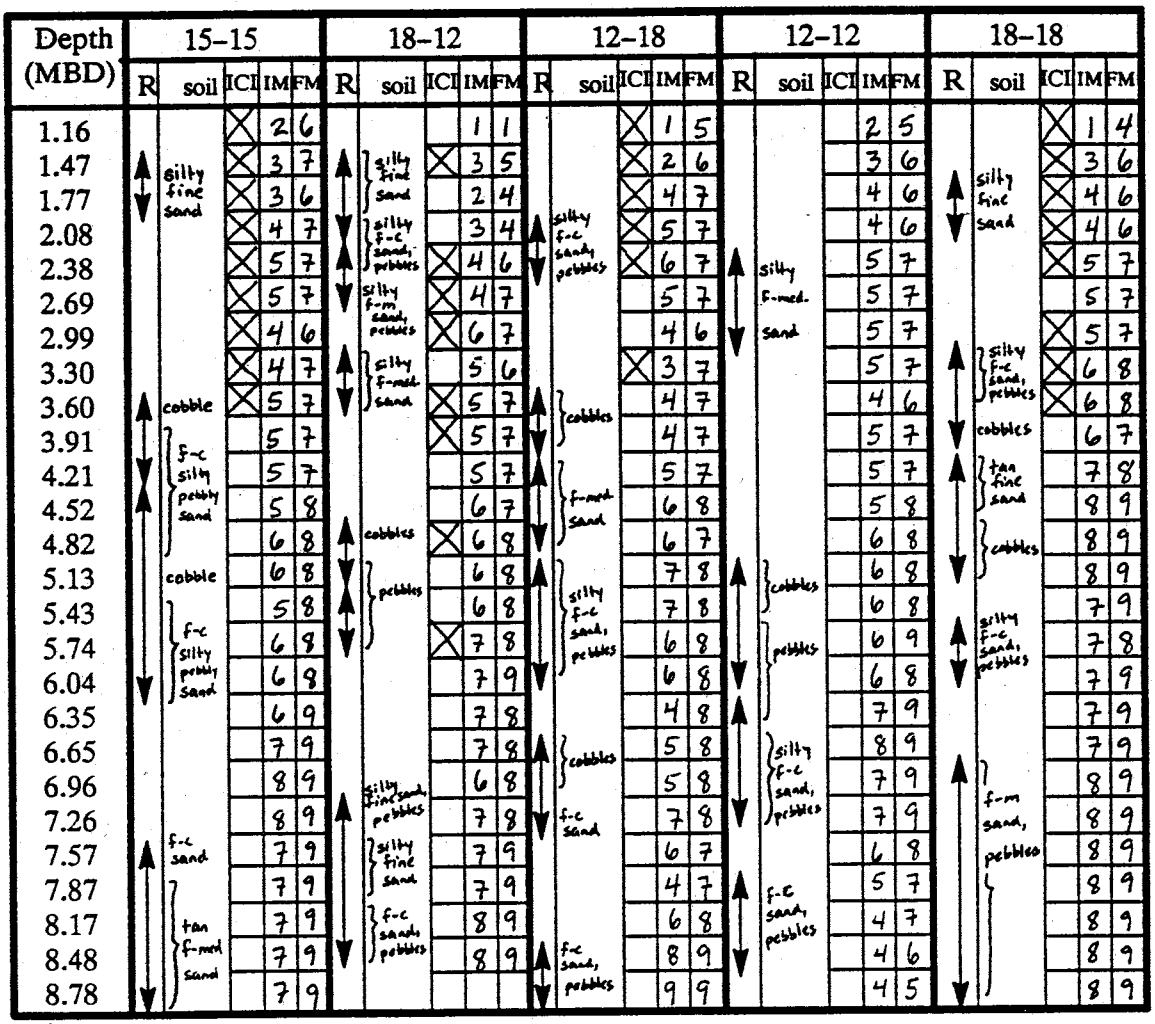

LEGEND:

R: Range (as denoted by arrows) of uniform distributions of moisture content.

ICI: Initial condition index: "X" -- Unit drained to or below station's 1987 profile (by 64.5 days)

no "X" -- Unit did not drain to station's 1987 profile

IM: Initial Moisture Index (moisture content—1989 profile)

FM: Final Moisture Index (based on profile at 64.5 days)

USE RANKING:

1 — >30%
2 — 27-30%
3 — 24-27%
4 — 21-24%
5 — 18-21%
6 — 15-18%
7 — 12-15%
8 — 9-12%
9 — 5-9%

remained highest for the plot, following 64.5 days.

Profiles for station 18-12 reflect shape characteristics shared by many of the profiles through the 10 x 10 m plot. Moisture content is highest in the shallow layers. A sharp decrease is shown between 2 and 3 meters below datum. Moisture content again increases with depth. Between 4 and 6 MBD, moisture content gradually decreases or becomes uniform with depth. Peaks again occur in the profile between the 6 and 8 meter depth interval.

Alternating increases and decreases which are common from station to station may be related to instrumentation. Joints in each access tube as well as bentonite plugs at the 3 and 6 meter depth, for instance, at station 18-12, may have created bias in moisture content measurements. Moisture content may have been channelled around bentonite. Thus, the zone of influence of the moisture probe may have intercepted only a portion of moisture present.

In the southeastern portion of the plot (station 18-12), moisture content decreased with depth between 4 and 6 meters. This depth interval is characterized by a cobbles/pebbles/ silty fine to coarse sand package. Soil samples were not collected in this region, so it is uncertain why specific layers are implied (Figure 6-5). Hydraulic gradient data is inconclusive in determining lateral or vertical flow. But, this uniform decrease in moisture content, as well as the general moisture profile, resembles that of station 15-15, for

the same depth interval. Thus, a pebbly sand, which coarsens with depth may exist at station 18-12, similar to the unit found at station 15-15.

Uniform moisture content distributions are found in several regions and depths of the irrigated plot, as shown in table 5. Soils present at various depths are listed as well. One-to-one correspondence between soil layer and uniform moisture content, on average, does not occur. Several layers appear to drain similarly, including cobble layers. As explained above, in section 1.3, the matrix of these layers may resemble the soil found above or below them. As a result, a "cobble layer" may be more of a stony soil which drains the same amount of moisture as layers above and below do.

6.2 Summary

In addressing the goals described at the beginning of this chapter, the following can be concluded:

- The regional conceptual flow model is acceptable if that is the scale of interest. Many of the drainage curves are similar in character. Unit hydraulic gradient is most prevalent at the center of the plot, where the regional model shows primarily vertical flow. Northeasterly regional lateral flow is further supported by mass moisture losses in this area.

- In different areas of the soil profile, certain sets of soil layers were smoothed by hydraulic gradient data. Unit hydraulic gradient can suggest vertical flow across several layers. However, small scale effects are effectively removed. The scale of the original problem must coincide with the scale of the analysis.

- Soil sampling was not complete in some of the borehole logs. Size and extent of cobble layers are only inferred in some areas. Data showed that shallow cobble layers

affect flow on a regional and local scale, while deeper cobble layers (below 4 meters), on a local scale, resemble stony soils, containing matrix material composed of silty sands found above and below it.

- Vertical flow propagated at different rates through the soil profile. This is vital in small scale studies.
- Effects of coarsening/fining and sorting are recognizable on a local scale. These effects should be incorporated into large scale studies, especially where the regional picture is unclear.

The bottom line in this study is that the scale of the problem must first be addressed. Then, the scale of analysis can be established. In this experiment, moisture content data was collected in far greater quantities and depths than tensiometric data. Moisture content data analysis thus improved our knowledge of the small scale flow field, while the tensiometric data were more helpful for the regional study.

Although unit gradients were established for several layers at a time in the soil profile, this assumption can be useful in other studies. A key assumption in the instantaneous profile test is one-dimensional vertical flow. Although lateral flow occurred in a number of areas at the study site, the hydraulic head data supports the presence of vertical flow, especially in the center of the plot. Because of this, moisture content data and pressure head data collected from station 15-15 will be used to calculate values of unsaturated hydraulic conductivity with depth.

Chapter 7. Unsaturated Hydraulic Conductivity

7.1 Results

The instantaneous profile (IP) test was described in chapter 3 under analysis methodology. Values of hydraulic conductivity are determined for individual soil layers by analyzing moisture content and pressure head data gathered during the drainage phase of the experiment. Five sets of data were available for this test, from five irrigated plot stations. However, results and discussion of station 15-15 data are presented below. This station was chosen because vertical flow and drainage were most prevalent at this location, as indicated by hydraulic head fields which were described in chapter 4. Vertical drainage is a key assumption incorporated into the IP test, as explained in chapter 3.

Moisture content data was collected at station 15-15 at depths below datum ranging from 116 cm to 513 cm. All monitoring intervals are 30-31 cm or multiples of this value. Measurements were taken three times a day for the first week of drainage, daily for the next two weeks, then weekly, then monthly. The study here is limited to the first 150 days of drainage as most of the water drained from the site by this time.

Tensiometer depths used in this study ranged in depth from 148 cm to 370 cm below datum. These depths, or elevation heads, are inherently negative, as they are measured below

site datum. These values combined with pressure head produce a value of hydraulic head. Change in hydraulic head over an interval of depth is the hydraulic gradient. Examination of the depths of pressure head (Ψ) and measurements of moisture content (θ) shows that because tensiometer depths are not coincident with depths of water content measurements, hydraulic gradient measurements must be estimated or interpolated for most of the depth intervals.

Figures 7-1a and 7-1b show drainage curves assembled for various depths. These curves were included in the determination of soil moisture flux (q) as they yielded $d\theta/dt$. (Note equation 1, chapter 3.) Most of the drainable moisture at each layer was released by 20 days. The next 100 days or so were marked by little or no measurable moisture loss with depth. Note that day 11.62 represents September 4, 1989.

Moisture content was highest at the shallow depth of 1.16 meters (below datum). Note that driplines were 0.86 meter below datum. A significant amount of moisture remained at this depth after 150 days, perhaps resting on an impeding layer of some kind. Both the 1.47 and 1.77 meter curves (Figure 7-1a) represent a single unit, as indicated in the geologic log (Figure 6-1). However, textural differences produced nonuniform drainage and thus the different curves. The fourth curve (2.08 meters) showed drainage to a low θ for coarse sand and pebbles. Vertical gradients caused moisture to pass into the silty sand below. Similar behavior was noted

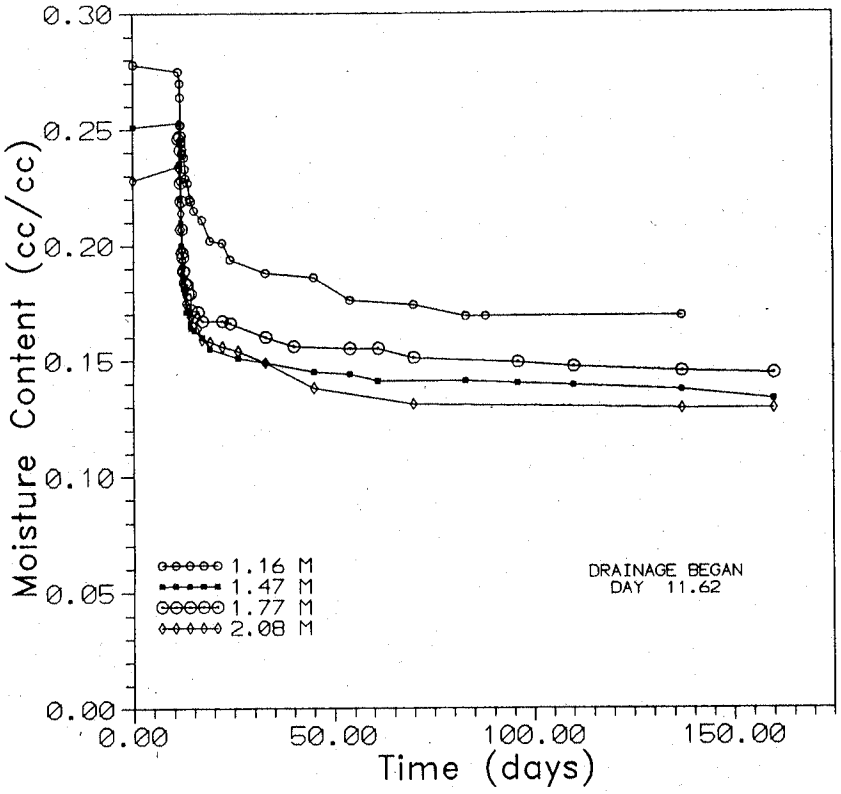

Figure 7-1a. Drainage Curves for Various Depths: Station 15-15

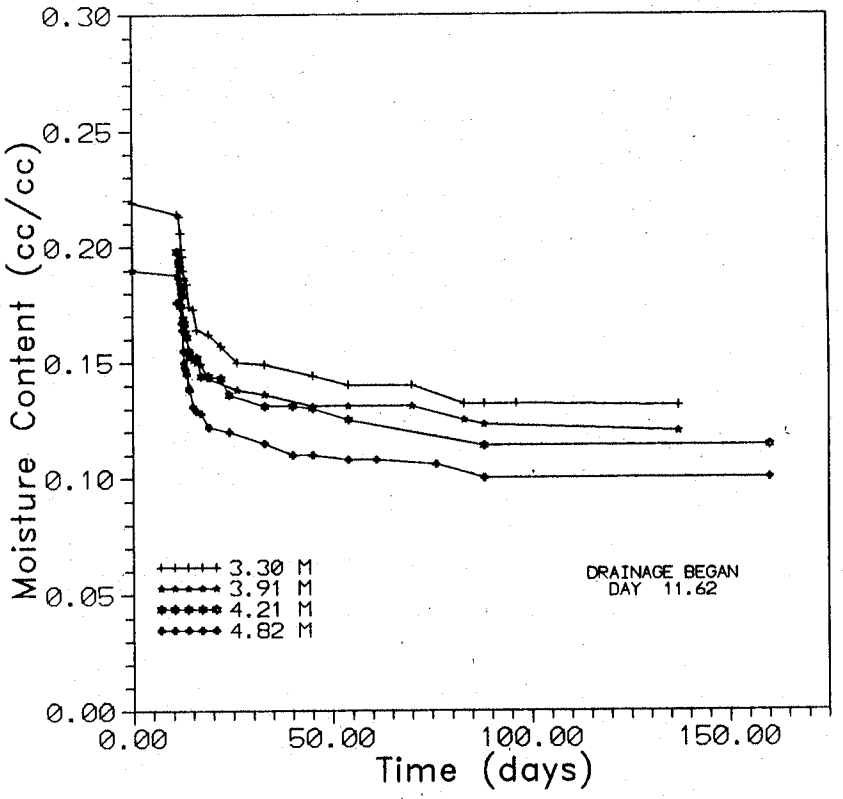

Figure 7-1b. Drainage Curves for Various Depths: Station 15-15

in drainage curves presented by Hillel, et al. (1977).

The 3.3 meter curve signified wet conditions above a cobble layer. Lateral flow along the surface of the cobble layer may have removed infiltrating moisture from the system. The remaining curves were produced by data from a single draining unit (pebbly sand). Once again differential moisture release and storage was due to textural variations.

Table 6 contains some of the calculated values of soil moisture flux (q). The numbers in parentheses represent depths below datum of moisture content measurements collected between dripline level and the deepest tensiometer depth. Depth intervals (dz) are listed as well. Slopes ($\partial\theta/\partial t$) of the eye-fitted drainage curves (Figures 7-1a and 7-1b) are multiplied by corresponding dz values. Integration across any interval dz (i.e., 0 to Z) gives the soil moisture flux (Equations 2,3).

Values of hydraulic gradient and hydraulic conductivity are listed in Table 7. Soil moisture fluxes are listed, and in general, they decrease with time at each depth interval. However, hydraulic gradient values do not necessarily decrease with time. In some cases, they increase toward the end of the drainage event. This is due to breakdown of tensiometers as they may leak (break seals) over time. Fewer tensiometers are then available for pressure head measurement, and they produce a biased value of gradient.

Table 6. Sample of Calculated Soil Moisture Fluxes: Station 15-15

Days Since Drainage Began	dz* (cm)	$\partial\theta/\partial t$ (day^{-1})	$-dz(\partial\theta/\partial t)$ cm/day	$q=dz(\partial\theta/\partial t)$ cm/day
0.13	(116) 30	0.0890	2.67	2.67
	(147) 31	0.1700	5.17	7.84
	(177) 30	0.1600	4.67	12.51
	(208) 31	0.1100	3.44	15.95
	(238) 30	0.0780	2.33	18.28
	(269) 31	0.0120	0.36	18.64
	(299) 30	0.0220	0.67	19.31
	(330) 31	0.0280	0.87	20.18
	(360) 30	0.0110	0.33	20.51
	(421) 61	0.0110	0.67	21.18
	(452) 31	0.0120	0.36	21.54
	(513) 61	0.0035	0.21	21.75
0.38	30	0.0083	0.25	0.25
	31	0.0750	2.33	2.58
	30	0.0830	2.50	5.08
	31	0.0750	2.33	7.41
	30	0.0750	2.25	9.66
	31	0.0500	1.55	11.21
	30	0.0330	1.00	12.21
	31	-0-	-0-	12.21
	30	0.0500	1.50	13.71
	61	0.0280	1.69	15.40
	31	0.0125	0.39	15.79
	61	0.0035	0.21	16.00

*Number in parentheses is depth below datum, in cm

Table 7. Values of Hydraulic Gradient (J) and Hydraulic Conductivity (K)--Station 15-15
q = soil moisture flux; w.c. = water content; (Drainage began day 11.62)

z(cm)	Days	q(cm/day)	J (cm/cm)	K (cm/day)	W.C. (cm/cm)	z(cm)	Days	q(cm/day)	J (cm/cm)	K (cm/day)	W.C. (cm/cm)
	11.75	2.6700	1.16	2.3017	0.257		11.75	15.9500	1.16	13.7500	0.222
	12	0.2500	1.13	0.2212	0.245		12	7.4100	1.13	6.5575	0.203
	13	0.7500	0.97	0.7732	0.231		13	2.4700	0.97	2.5464	0.175
	14	0.4100	0.94	0.4362	0.221		14	1.0700	0.94	1.1383	0.170
	15	0.1500	0.90	0.1667	0.215		15	0.5700	0.90	0.6333	0.163
116	17	0.0600	0.72	0.0833	0.211		17	0.3600	0.72	0.5000	0.160
	20	0.0100	0.63	0.0159	0.202		20	0.0480	0.63	0.0762	0.158
	25	0.0200	0.67	0.0299	0.193		25	0.0740	0.67	0.1104	0.154
	35	0.0050	0.73	0.0068	0.188		35	0.0600	0.73	0.0822	0.147
	50	0.0340	0.95	0.0358	0.181	208	50	0.0480	0.95	0.0505	0.137
	60	0.0038	0.81	0.0047	0.176		60	0.0260	0.81	0.0321	0.134
	75	0.0120	1.04	0.0115	0.172		75	0.0300	1.04	0.0288	0.131
	90	0.0000	1.02	0.0000	-		90	0.0057	1.02	0.0056	0.130
	100	0.0000	1.00	0.0000	-		100	0.0076	1.00	0.0076	0.130
	130	0.0000	0.95	0.0000	-		130	0.0055	0.95	0.0058	0.129
	150	0.0000	0.92	0.0000	-		150	0.0067	0.92	0.0073	0.129
	11.75	7.8400	1.16	6.7586	0.227		11.75	18.2800	1.16	15.7586	0.199
	12	2.5800	1.13	2.2832	0.196		12	9.6600	1.13	8.5487	0.177
	13	2.3000	0.97	2.3711	0.175		13	2.6600	0.97	2.7423	0.158
	14	0.7100	0.94	0.7553	0.167		14	1.2000	0.94	1.2766	0.154
	15	0.1900	0.90	0.2111	0.163		15	0.5700	0.90	0.6333	0.153
	17	0.1100	0.72	0.1528	0.16		17	0.5000	0.72	0.6944	0.149
	20	0.0280	0.63	0.0444	0.154	238	20	0.0870	0.63	0.1381	0.146
147	25	0.0380	0.67	0.0567	0.152		25	0.0740	0.67	0.1104	0.138
	35	0.0150	0.73	0.0205	0.148		35	0.0690	0.73	0.0945	0.138
	50	0.0370	0.95	0.0389	0.144		50	0.0500	0.95	0.0526	0.133
	60	0.0170	0.81	0.0210	0.141		60	0.0280	0.81	0.0346	0.132
	75	0.0120	1.04	0.0115	0.141		75	0.0380	1.04	0.0365	0.132
	90	0.0024	1.02	0.0024	0.14		90	0.0057	1.02	0.0056	0.132
	100	0.0023	1.00	0.0023	0.14		100	0.0162	1.00	0.0162	0.131
	130	0.0023	0.95	0.0024	0.138		130	0.0055	0.95	0.0058	0.128
	150	0.0054	0.92	0.0059	0.134		150	0.0067	0.92	0.0073	0.128
	11.75	12.5100	1.16	10.7845	0.233		11.75	18.6400	1.16	16.0690	0.191
	12	5.0800	1.13	4.4956	0.203		12	11.2100	1.13	9.9204	0.185
	13	2.3900	0.97	2.4639	0.183		13	3.4400	0.97	3.5464	0.165
	14	0.7100	0.94	0.7553	0.179		14	1.4400	0.94	1.5300	0.158
	15	0.3000	0.90	0.3333	0.169		15	0.6300	0.90	0.7000	0.155
	17	0.2200	0.72	0.3056	0.167		17	0.6100	0.72	0.8472	0.15
	20	0.0280	0.63	0.0444	0.167		20	0.1120	0.63	0.1778	0.148
	25	0.0580	0.67	0.0866	0.165	269	25	0.0820	0.67	0.1224	0.145
177	35	0.0320	0.73	0.0438	0.157		35	0.0840	0.73	0.1151	0.141
	50	0.0390	0.95	0.0411	0.155		50	0.0510	0.95	0.0537	0.136
	60	0.0170	0.81	0.0210	0.155		60	0.0290	0.81	0.0358	0.135
	75	0.0250	1.04	0.0240	0.151		75	0.0450	1.04	0.0433	0.134
	90	0.0047	1.02	0.0046	0.149		90	0.0081	1.02	0.0079	0.131
	100	0.0066	1.00	0.0066	0.148		100	0.0177	1.00	0.0177	0.131
	130	0.0045	0.95	0.0047	0.145		130	0.0070	0.95	0.0074	0.129
	150	0.0067	0.92	0.0073	0.144		150	0.0091	0.92	0.0099	0.128

Table 7. (continued) Values of Hydraulic Gradient (J) and Hydraulic Conductivity (K)--Station 15-15; q = soil moisture flux; w.c. = water content; (Drainage began day 11.62)

z(cm)	Days	q(cm/day)	J (cm/cm)	K (cm/day)	W.C. (cm/cm)	z(cm)	Days	q(cm/day)	J (cm/cm)	K (cm/day)	W.C. (cm/cm)
	11.75	19.3100	1.16	16.6466	0.223		11.75	21.1800	0.95	22.2947	0.194
	12	12.2100	1.13	10.8053	0.216		12	15.4000	0.94	16.3830	0.190
	13	3.6300	0.97	3.7423	0.194		13	5.1400	0.97	5.2990	0.167
	14	1.5200	0.94	1.6170	0.189		14	3.2600	0.95	3.4316	0.156
	15	0.7800	0.90	0.8667	0.182		15	1.0400	0.88	1.1818	0.152
299	17	0.8000	0.72	1.1111	0.175	421	17	1.3300	0.72	1.8472	0.145
	20	0.1120	0.92	0.1217	0.168		20	0.2010	0.92	0.2185	0.144
	25	0.0990	0.89	0.1112	0.166		25	0.1970	0.89	0.2213	0.136
	35	0.0930	0.86	0.1081	0.161		35	0.1310	0.86	0.1523	0.131
	50	0.0580	0.95	0.0611	0.155		50	0.1230	0.64	0.1922	0.127
	60	0.0420	0.76	0.0553	0.151		60	0.0620	0.76	0.0816	0.123
	75	0.0500	1.04	0.0481	0.149		75	0.0890	1.04	0.0856	0.118
	90	0.0081	1.02	0.0079	0.147		90	0.0089	1.02	0.0087	0.114
	100	0.0200	1.00	0.0200	0.147		100	0.0216	1.00	0.0216	0.114
	130	0.0093	0.95	0.0098	0.144		130	0.0110	0.95	0.0116	0.114
	150	0.0114	0.92	0.0124	0.143		150	0.0128	0.92	0.0139	0.114
	11.75	20.1800	1.16	17.3966	0.212		11.75	21.5400	0.95	22.6737	0.182
	12	12.2100	1.13	10.8053	0.206		12	15.7900	0.94	16.7979	0.178
	13	3.8300	0.97	3.9485	0.186		13	6.1000	0.97	6.2887	0.154
	14	2.1300	0.94	2.2660	0.176		14	3.7500	0.95	3.9474	0.142
	15	0.8100	0.90	0.9000	0.173		15	1.0400	0.88	1.1818	0.139
	17	0.8200	0.72	1.1389	0.164		17	1.3900	0.72	1.9306	0.131
	20	0.1620	0.92	0.1761	0.160		20	0.2510	0.92	0.2728	0.129
330	25	0.1530	0.89	0.1719	0.152	452	25	0.2130	0.89	0.2393	0.124
	35	0.1060	0.86	0.1233	0.148		35	0.1390	0.86	0.1616	0.120
	50	0.0720	0.95	0.0758	0.142		50	0.1400	0.64	0.2188	0.114
	60	0.0420	0.76	0.0553	0.140		60	0.0640	0.76	0.0842	0.112
	75	0.0690	1.04	0.0663	0.137		75	0.0980	1.04	0.0942	0.110
	90	0.0081	1.02	0.0079	0.132		90	0.0089	1.02	0.0087	0.106
	100	0.0208	1.00	0.0208	0.132		100	0.0216	1.00	0.0216	0.106
	130	0.0100	0.95	0.0105	0.131		130	0.0110	0.95	0.0116	0.106
	150	0.0120	0.92	0.0130	0.131		150	0.0152	0.92	0.0165	0.105
	11.75	20.5100	0.95	21.5895	0.200		11.75	21.7500	0.95	22.8947	0.172
	12	13.7100	0.94	14.5851	0.194		12	16.0000	0.94	17.0213	0.171
	13	4.7700	0.97	4.9175	0.169		13	6.1000	0.97	6.2887	0.153
	14	2.5400	0.95	2.6737	0.160		14	4.8300	0.95	5.0842	0.136
	15	0.8900	0.88	1.0114	0.154		15	1.4200	0.88	1.6136	0.131
	17	0.8800	0.72	1.2222	0.147		17	1.7300	0.72	2.4028	0.123
	20	0.1810	0.92	0.1967	0.144		20	0.3710	0.92	0.4033	0.120
	25	0.1630	0.89	0.1831	0.142	513	25	0.3350	0.89	0.3764	0.112
360	35	0.1310	0.86	0.1523	0.137		35	0.1820	0.86	0.2116	0.109
	50	0.0890	0.64	0.1391	0.128		50	0.1450	0.64	0.2266	0.103
	60	0.0420	0.76	0.0553	0.126		60	0.0690	0.76	0.0908	0.102
	75	0.0690	1.04	0.0663	0.126		75	0.0980	1.04	0.0942	0.101
	90	0.0089	1.02	0.0087	0.120		90	0.0089	1.02	0.0087	0.098
	100	0.0216	1.00	0.0216	0.120		100	0.0261	1.00	0.0261	0.098
	130	0.0110	0.95	0.0116	0.119		130	0.0160	0.95	0.0168	0.096
	150	0.0128	0.92	0.0139	0.118		150	0.0187	0.92	0.0203	0.094

Two groups of gradients are presented in Table 7. Individual lines graphed in Figure 3-8 are comprised of seven data points. These points were gathered into two groups and graphed into two better-fitted lines (not shown). Thus, two sets of gradients were produced. Tensiometric data collected from the five irrigated plot stations prior to drainage produced a gradient close to one (Figure 7-2). This graph lent credence to the grouping of points into two lines as both sets of gradients approached one. Hydraulic gradient values in the second set (at greater depths than those of set one) are all less than one, indicating the presence of an impeding layer at or below the 360 cm depth (Hillel, et al. 1972). At this depth, an impeding layer could produce a lateral component to soil moisture flow.

Conductivities are tabulated next to corresponding values of moisture content at each depth below datum (Table 7). Note that values of K initially increase with depth. This is so for drainage which is uniform with depth (Black, et al., 1968). In general, K decreased sharply with small decreases in θ. Small increases in K toward the end of the drainage period are misleading as there were problems with tensiometric data at this time.

The last flux applied to the irrigated plot was approximately 1.0×10^{-4} cm/sec which is equivalent to 8 to 9 cm/day. This value is much less than 300 cm/day, an approximate saturated conductivity of the silty sand between

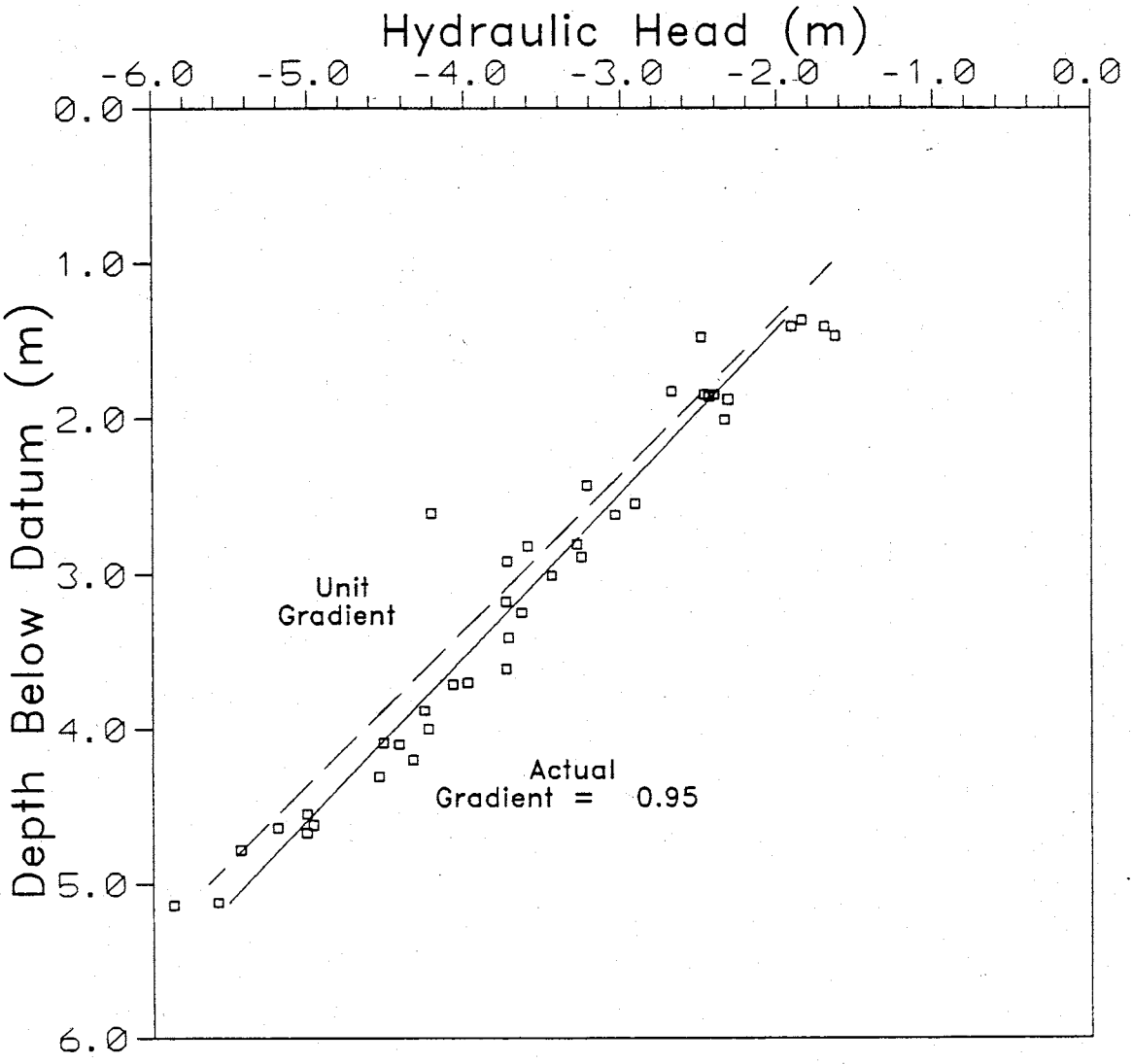

Figure 7-2. Pre-drainage Hydraulic Head Gradient--Irrigated Plot Stations. Each (□) represents a tensiometric measurement.

0.86 and 1.16 meters below datum. However, the dye study showed that ponded conditions existed at the southeastern corner of the 10 x 10 m plot. Drainage fluxes may have been higher in this area than 8-9 cm/day. However, individual values of soil moisture flux, given in Table 6, suggest drainage occurred at rates less than the water application rate. It is also possible that zones of shallow saturated soil were not within range of neutron probe measurement activity.

For each depth studied, a semilog graph of K vs. θ was produced (Figure 7-3a,c). For each depth interval, a straight line was fit to the data using the equation:

$$\ln K = \ln A + B\theta \qquad (13)$$

where A and B are empirical constants.

Table 8 contains values of ln A and B (slope).

In Figure 7-3a, the 116 cm curve is distinct from those for the other three depths. This suggests a change in texture between 116 cm and 147 cm, and supports the different drainage histories shown in Figure 7-1a. A smaller soil moisture flux was measured at the 116 cm depth (=2.67 cm/day) compared to the 147 cm depth (=5.17 cm/day) during early drainage time. Thus, based on K-θ curves and drainage curves, it appears the soil at the 116 cm depth is much siltier than that found

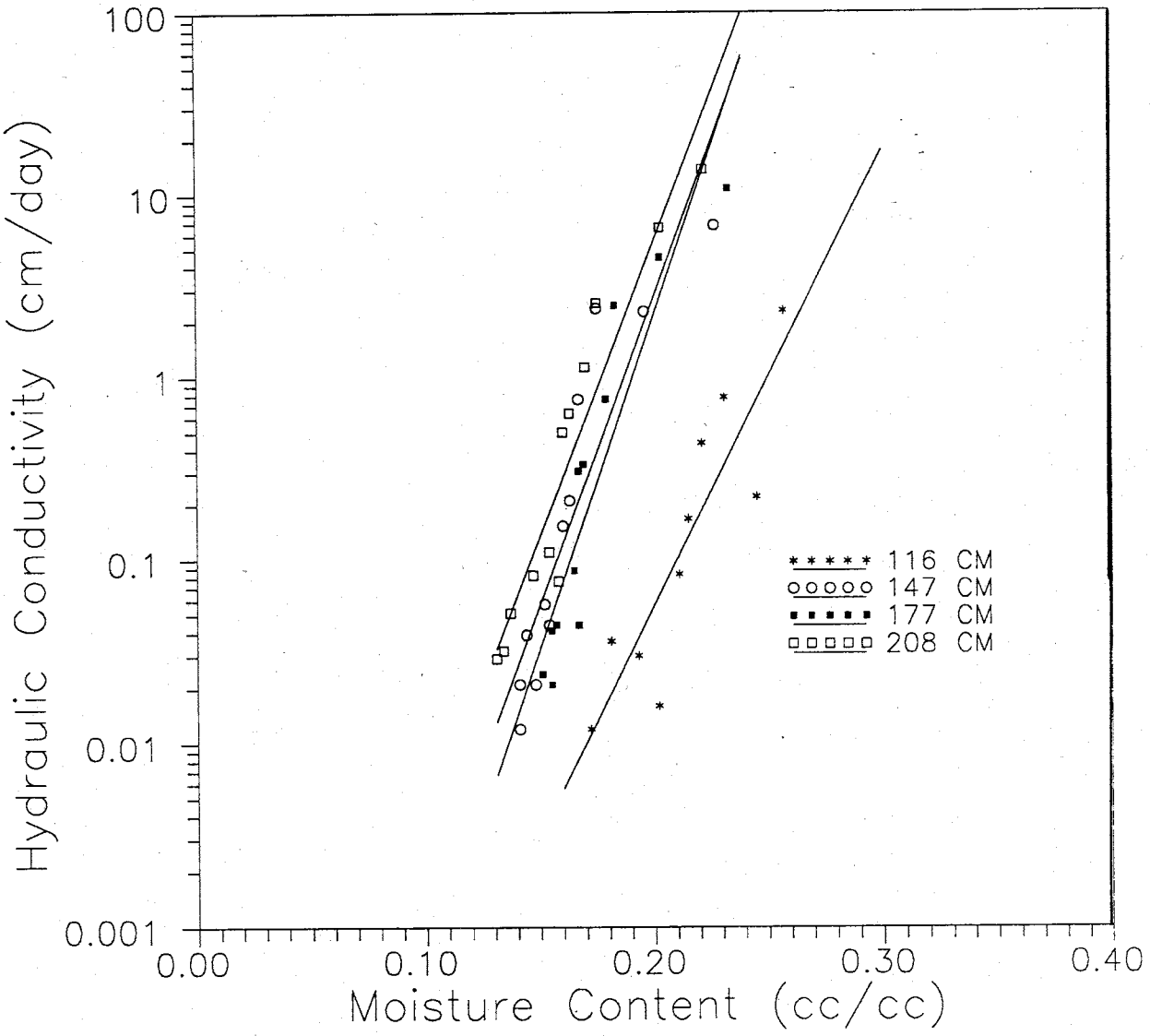

Figure 7-3a. Hydraulic Conductivity vs. Moisture Content for various depths at Station 15-15

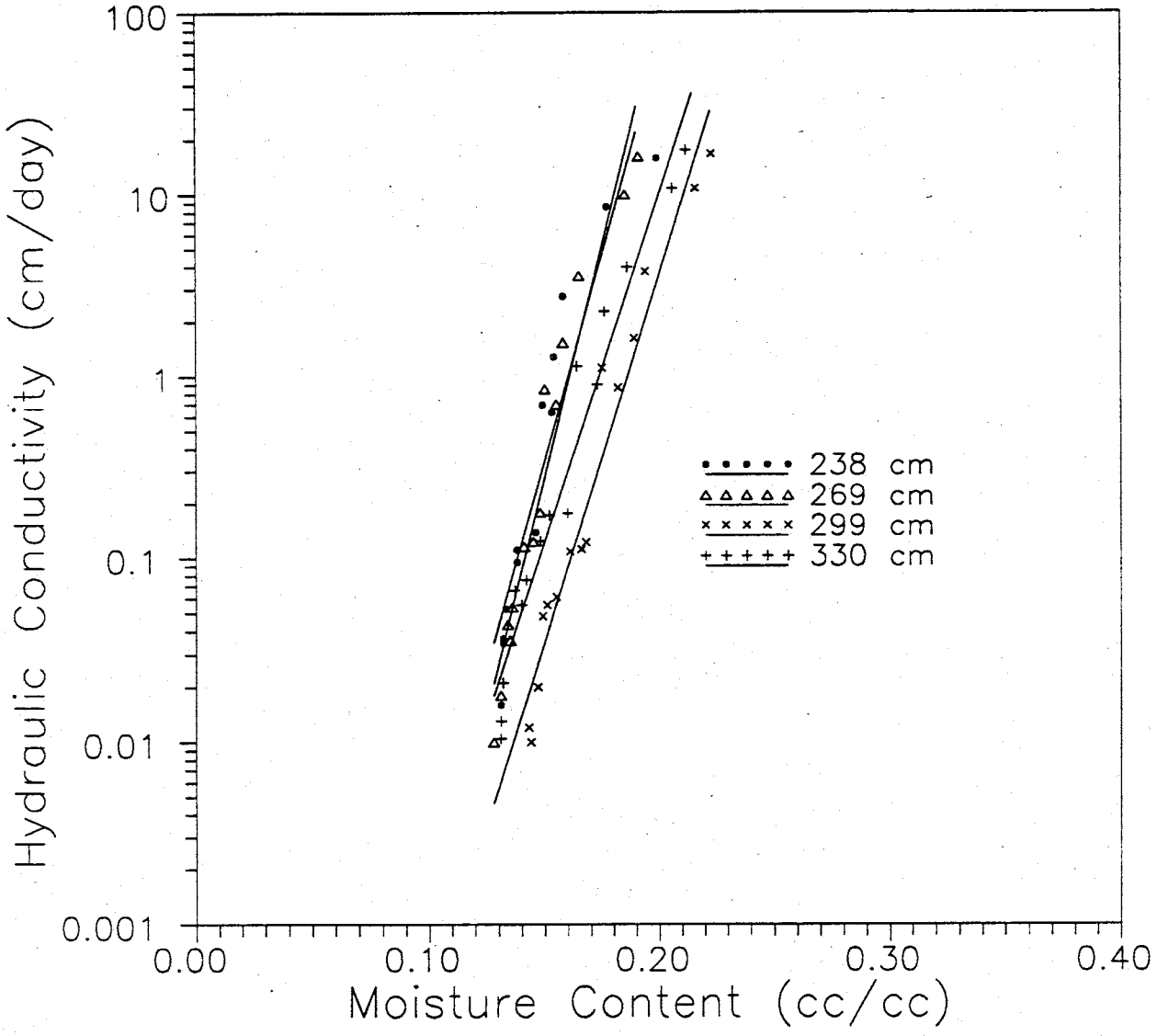

Figure 7-3b. Hydraulic Conductivity vs. Moisture Content for various depths at Station 15-15

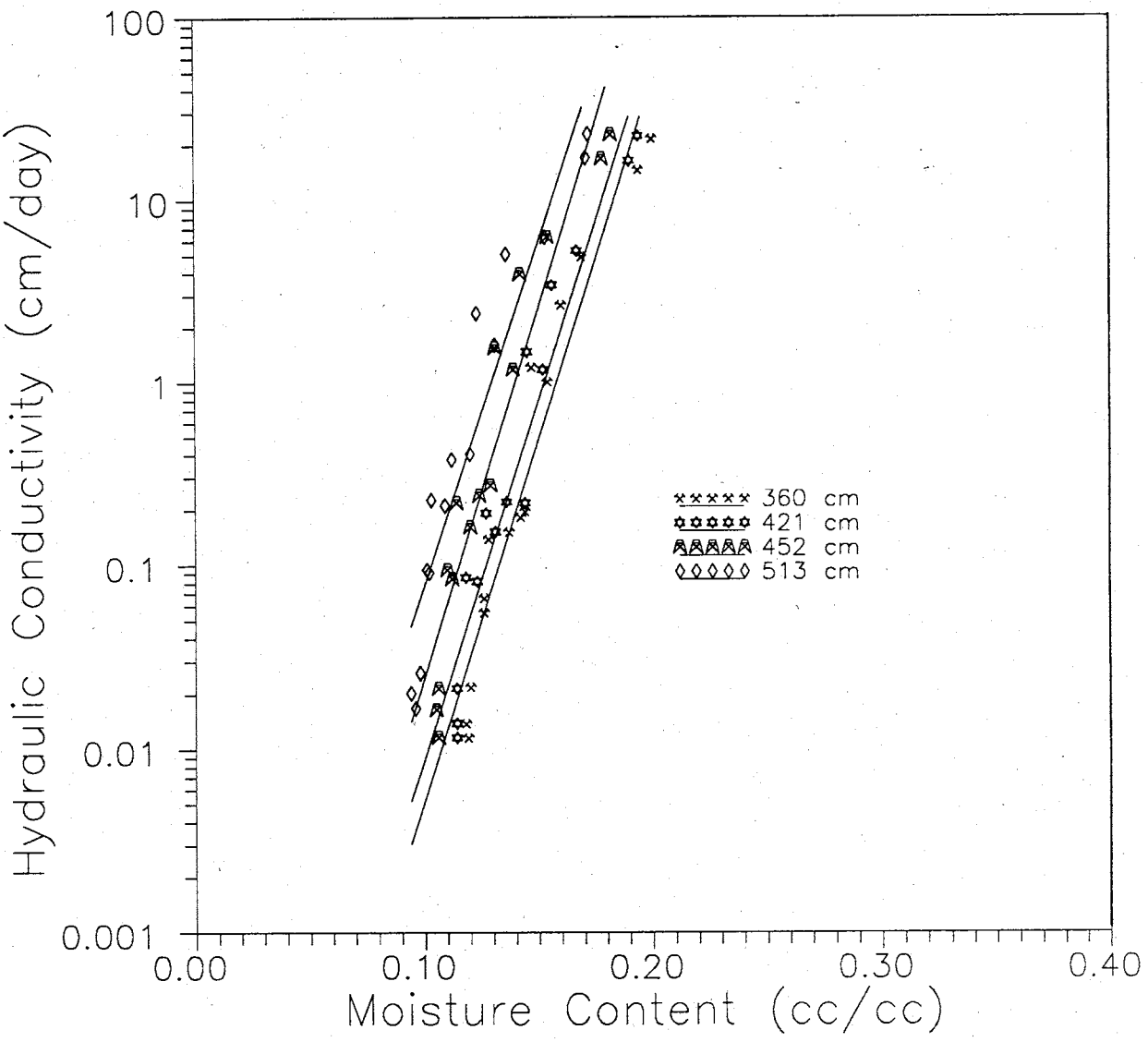

Figure 7-3c. Hydraulic Conductivity vs. Moisture Content for various depths at Station 15-15

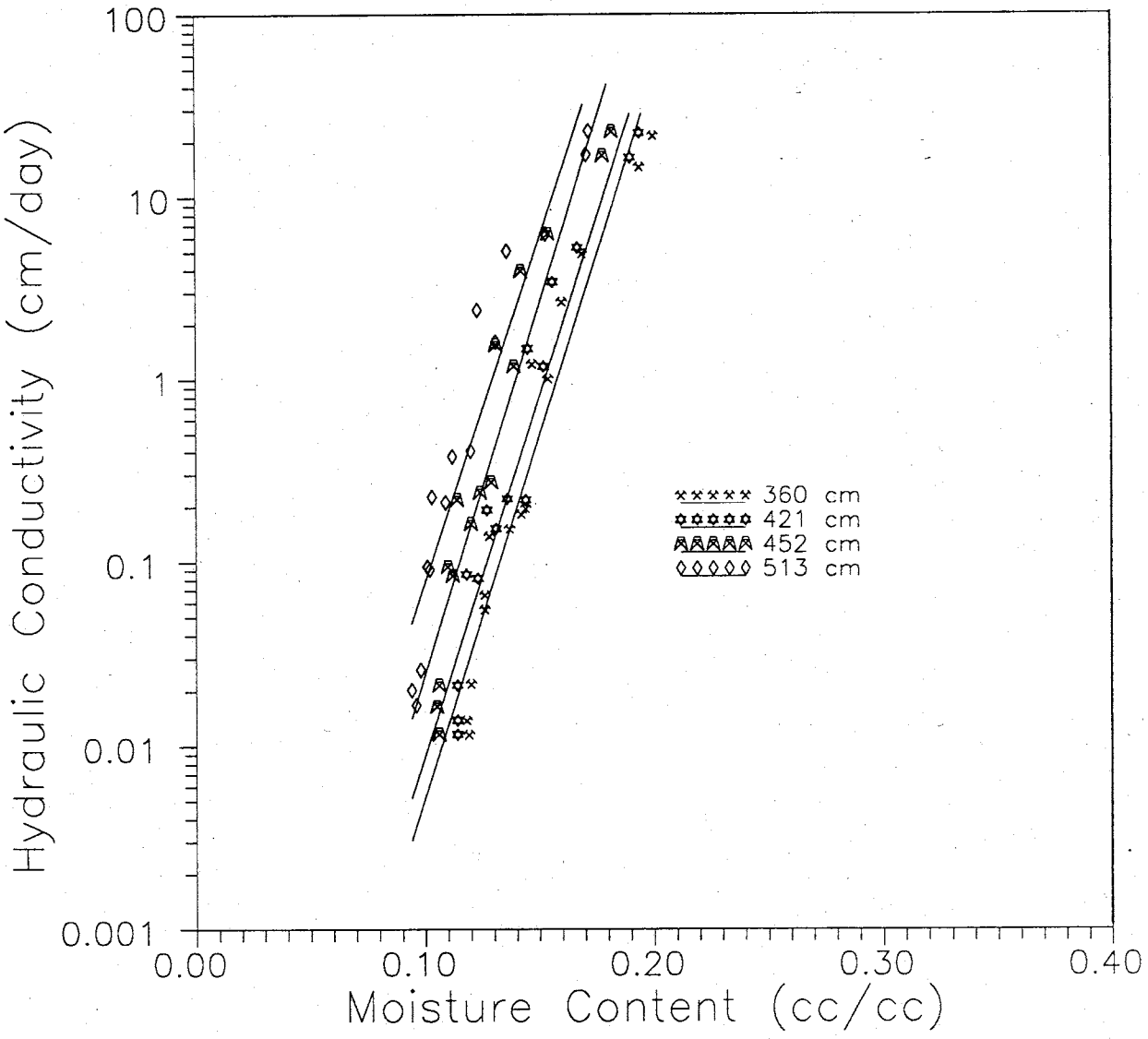

Figure 7-3c. Hydraulic Conductivity vs. Moisture Content for various depths at Station 15-15

Table 8. Coefficients from exponential fit--Station 15-15

Depth Below Datum	Ln A	B
116 cm	-14.35	57.36
147 cm	-14.44	77.12
177 cm	-15.95	83.53
208 cm	-13.10	73.93
238 cm	-16.68	104.07
269 cm	-18.87	117.14
299 cm	-17.17	92.14
330 cm	-15.24	87.63
360 cm	-14.28	90.35
391 cm	(use 421 cm)	(use 421 cm)
421 cm	-13.68	89.64
452 cm	-12.98	92.75
482 cm	(use 513 cm)	(use 513 cm)
513 cm	-11.20	86.45

between 147 and 208 cm. The soil (116 cm deep) is wetter and drains moisture more slowly than the soils beneath it.

The steepest slope (B) is indicated for the 269 cm depth line. Drainage data show a 6.8% loss in moisture over a 300 day period. This indicates that either this layer was not significantly wet initially or that lateral flow supplied water to this unit during drainage. Although the I-P assumes no lateral flow, the effects in a layered profile must never be ruled out.

The slopes generally increase as depth increases, indicating a large drop in conductivity for a small drop in moisture content. The soils also generally become coarser-grained with depth. Moisture content also decreases with depth. When saturated large pores begin to lose water, drainage rates are initially very high and then decrease because so much moisture is drained during early time. These rates equal conductivity where the hydraulic gradient equals unity. Thus, during steady infiltration, conductivity would be constant at all depths, even though moisture content is low, deep in the profile. During one-dimensional vertical drainage, less moisture initially drains from deeper (coarser) portions of the profile. Consequently, the slope of the K-θ curves are steeper.

7.2 Discussion

It is the purpose of the discussion to explore additional site information which may aid in the understanding and visualization of the flow field. Boundary effects and

uncertainties will also be described.

Moisture content profiles for station 15-15 are displayed in Figure 7-4. Locations of the Piedmont Slope facies and Rio Grande fluvial facies are also noted. In general, the Piedmont Slope facies soils are primarily silty, pebbly sands while Rio Grande fluvial sediments are primarily clean sands and pebbly sands. If one-dimensional vertical drainage occurred and the soils coarsen downward, then one would expect moisture content to decrease with depth. This is the case, in general, except the slopes of the K-θ graphs do not necessarily increase with depth.

Regions of nearly constant slope (B) are graphed next to the moisture content profiles. The slope increases sharply at the 238 and 269 cm depths. However, this slope then decreases to 92.14 and, with depth, begins to increase once again. This trend is seen in the drainage profiles as the moisture content decreases sharply at the 238 cm depth and increases again at the 299 cm depth.

It appears that two zones of slight ponding or moisture buildup were present in the shallow profile, one above the 238 cm depth and one above the 360 cm depth. Moisture content values do not imply that saturated conditions existed in these areas. However, one would expect the moisture content of the finer layer (between 238 and 269 cm) to be much higher, considering it is between two coarse layers. The coarse layers should effectively suppress the finer layer's drainage.

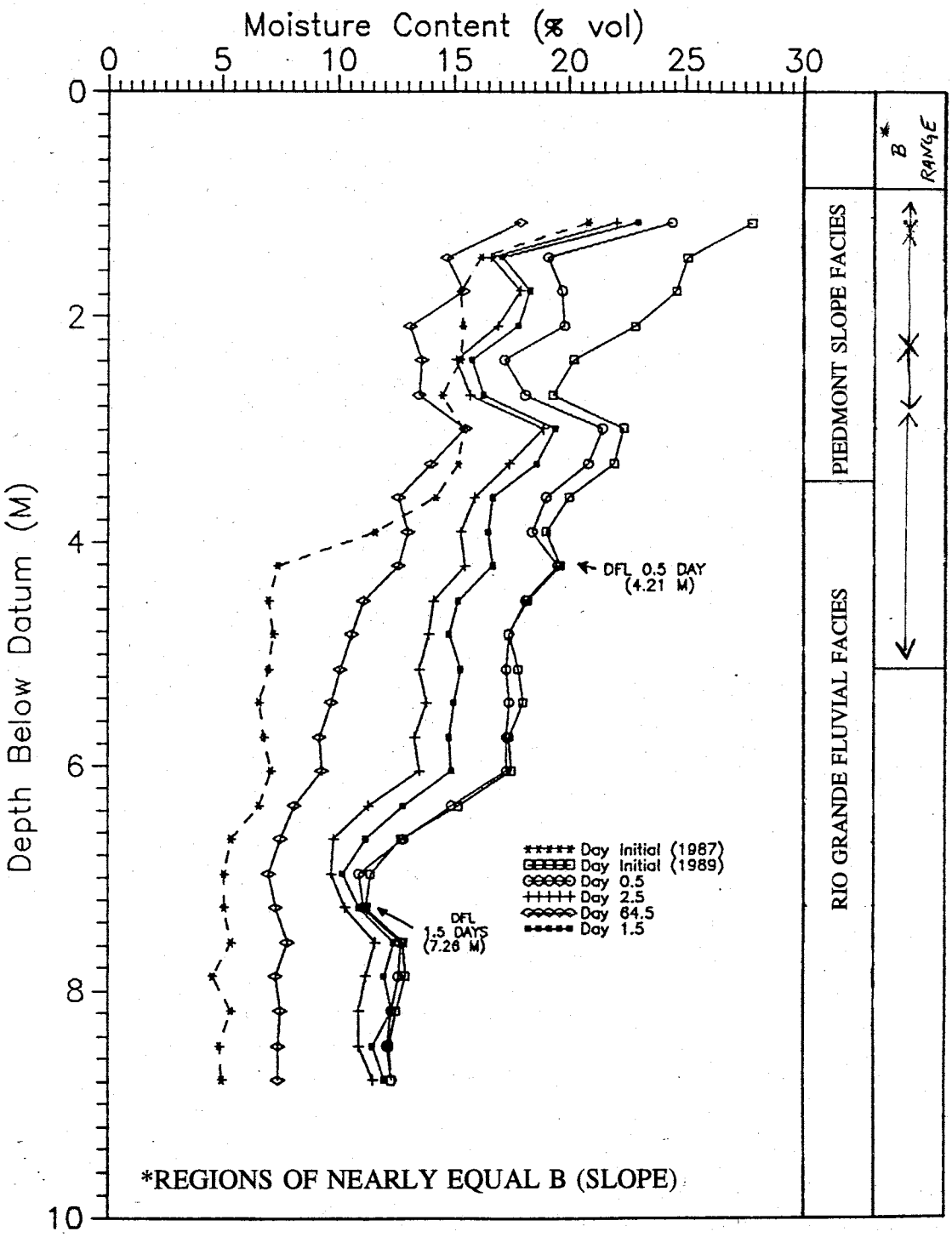

Figure 7-4. Comparison of Moisture Content Profile and Geologic Units-Station 15-15.

One of two scenarios are possible to explain this anomaly. Lateral flow may have removed moisture before it could drain downward to the finer layer. Secondly, this layer may have been mislabeled as red-brown sand with silt, or its borders with other soils may be in question. It may be much coarser than described. The steep K-θ slope and low range of moisture content support the presence of a coarser layer.

The propensity for lateral flow and drainage, at least on a local scale, is very great in the Piedmont Slope facies. Conversely, drainage is more uniform with depth in the Rio Grande fluvial facies. The correlation between coarsening textures in the lower facies and K-θ slopes is much more consistent and predictable than the upper facies.

The coefficient B is analogous to β in the following empirical equation (Libardi, 1980):

$$K=K_o \exp[\beta(\theta-\theta_o)] \qquad (14)$$

where K_o = hydraulic conductivity during steady infiltration
β = fit parameter
θ_o = moisture content during steady infiltration

Because values of coefficient A are so small, it is difficult to consider them as conductivities relative to K_o in equation (13). If the site was saturated, then K_o is equivalent to K_s and θ_o is equivalent to θ_s. As $\theta \longrightarrow \theta_o$ then $K_o \longrightarrow K_s$ in the above equation.

If upper portions of the irrigated plot were saturated, values of K and θ just prior to drainage should resemble those from Table 7. They, in fact, do not. For example, note in Table 7 that at 116 cm below datum, θ = 0.257 after 0.13 day of drainage. The value of moisture content prior to drainage was 0.275. Using equation (20), K_o = 6.46 cm/day. This is far below laboratory measured K_s for the 116 cm depth, 300 cm/day. However, the value correlates well with the applied flux rate, 8-9 cm/day.

As the instantaneous profile test suggests, rapid measurements of θ and Ψ should be taken to accurately describe the drainage event. When moisture content is measured, the value reflects the wetness of the soil at that instant. Pressure head may or may not reflect soil water suction at the instant of measurement as tensiometers have an equilibration lag time.

To assess the sensitivity of the calculation to changes in pressure head, the following example using data from station 15-15 will be studied. At z_1 = 341 cm, pressure head equals -39.5 cm. At z_2 = 370 cm, pressure head is -16.0 cm. Finally, at z_3 = 512 cm, pressure head is -21.7 cm. The gradient calculated for the region z_1 to z_3 is .94 (slope of the H vs. z line). A 50% increase in Ψ (i.e. becoming more negative) for all three points results in a 3% decrease in gradient. Increasing one value only produces an 8.5% decrease (increasing Ψ_1); 3% decrease (increasing Ψ_2) and a 6%

increase (increasing Ψ_3) in gradient. Hydraulic gradient, in this case, is most sensitive to the change in pressure head at 341 cm. However, all the increases and decreases in gradient are small considering the pressure head was greatly increased. The altered values of gradient are still rather close to unity. Therefore, conductivity will not vary considerably.

In the determination of unsaturated conductivity and hydrologic units, sources of error must be considered. Ponding developing around driplines was discussed above. Excess water present in the site produces higher moisture content and higher soil moisture fluxes. Although the I-P test does not assume effects from flow along layers, this seepage can return flow to draining layers producing anomalous drainage patterns and mass balance errors. Because few tensiometers are available for this study, linearity in pressure head and hence hydraulic head is assumed. Hydraulic gradients thus may not reflect flow across individual layers but across several layers. Gradient was also estimated for the 116 and 513 cm depths as tensiometers were not emplaced above or below these depths at station 15-15. Small changes in moisture content on the order of a few tenths of a percent are within the error limits of the neutron probe. Refilled tensiometers require time to reequilibrate with the soil water. Measurements of pressure head taken during this time will be less negative (or more close to atmospheric) than usual. Finally, if the instrumentation was not packed well

during installation, water could have piped along the tubing as shown by dyed water flow along the soil water sampler near station 12-12 (Figure 5-14). The tensiometer nest and access tube were well emplaced here, indicating that if both stations 12-12 and 15-15 were constructed using the same procedure and care, water piping at 15-15 may not be a factor in moisture content measurements.

Using the lab and field parameters determined by Parsons (1988), analytical equation (7) was used to determine values of unsaturated hydraulic conductivity for different values of moisture content. Numerical and graphical results for this analysis and generated characteristic curves (equation 6) are presented below. Comparisons are made between field data and model results where possible.

Chapter 8. Predicting Soil Hydraulic Properties

The purpose of this chapter is to use analytical methods to determine soil moisture characteristic curves and unsaturated hydraulic conductivity. Equations and methods are described in chapter 3. Characteristic curves will be compared to field data (pressure head and moisture content) while calculated K-θ curves will be compared to results from the instantaneous profile test. A discussion of these comparisons follows the results section.

8.1 Characteristic Curves

Station 15-15

Figure 8-1 shows two moisture retention curves for two depths at station 15-15. The 1.47 meter depth represents a silty fine sand while a "cobble layer" was found at the other location (5.1 MBD). Values of θ_r (residual moisture content) and θ_s (saturated moisture content) were estimated from similar soil parameters determined at other stations by Parsons (1988) and from some field data (see Table 9). Only alpha and n-values from the Mualem model (van Genuchten, 1980) were permitted to vary, in equation (6). The program (RET.C) produced fitted curves to the field data.

A fairly good fit resulted for the 1.5 meter depth. However, the curve resembles that for a sand layer though the d_{10} size for this depth suggests a very fine silt (Friedman and

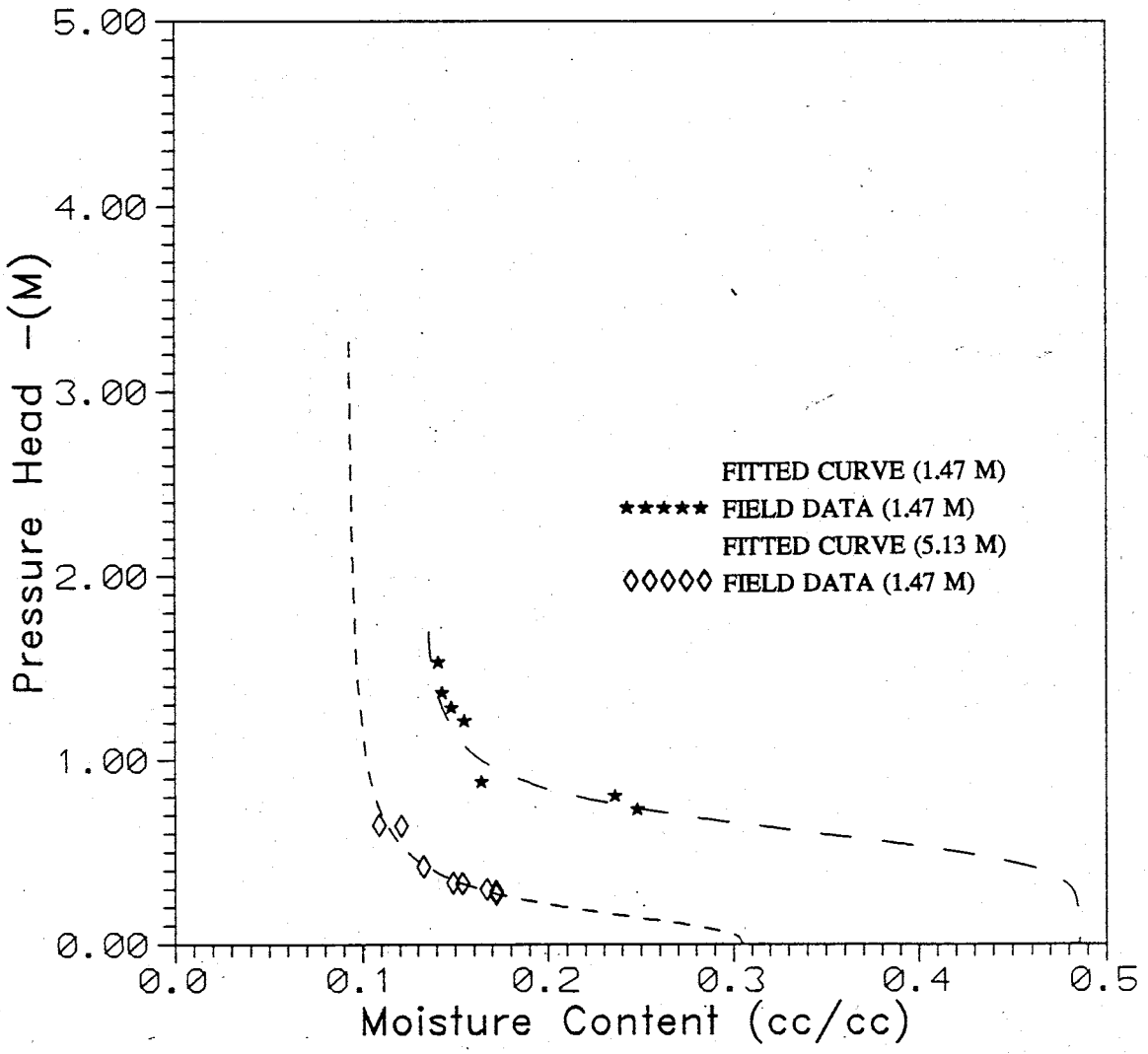

Figure 8-1. Characteristic Curve--Station 15-15.

Table 9. Parameters for characteristic curve development; Stations 15-15 and 18-18. The superscript "f" implies a result from curve fitting.

Station	Depth	Soil	θ_r	θ_s	θ_r^f	θ_s^f	r^2
15–15	1.47 M	silty fine sand	0.134	0.485	—	—	0.907
	5.13 M	"cobble layer"	0.092	0.305	—	—	0.995
18–18	1.45 M	silty fine sand	0.107	0.457	0.096	0.242	0.987
	4.57 M	fine sand	0.052	0.400	—	0.126	0.967

Sanders, 1978; see Table 4). Therefore, a better fit may have resulted if more parameters were allowed to vary. Also, vertical and lateral redistribution of moisture may have affected the actual field data. Nonuniform drainage is suggested by the profiles shown in Figure 6-1. The unit drained in uneven spurts, and this is not characteristic of a fine-grained material. As described in chapter 7, lateral redistribution of moisture may be responsible for this anomaly, or there may be error in its physical description (i.e. it may be coarser than described).

The curve generated for the 5.1 meter depth fit very well to the experimental data (r^2 = 0.995). Low values chosen for θ_r and θ_s appeared to be reasonable and indicative of the coarse nature of the material. The drainage profiles showed that the "cobble layer" at this depth behaved similarly to the

coarse sand and pebble layers above and below the cobbles (Figure 6-1). These layers drained fairly uniformly, and the hydraulic head fields, described in chapter 4, suggest vertical drainage at this depth.

Station 18-18

Figure 8-2 exhibits two fitted curves constructed for the 1.45 and 4.57 meter depths. For the shallow depth, the values of θ_r and θ_s were not fixed. Initial values of parameters were estimated, and these and final results are given in Table 9. The initial value for θ_r was a good choice, but the program produced a value of θ_s which was small for a silty sand. Once again, though, the field data used could be slightly biased due to extensive lateral flow during the early stages of drainage.

The characteristic curve for 4.6 meters below datum is oddly shaped for a sand. θ_s was permitted to vary here while θ_r remained constant. The computer generated a very low value of θ_s used to fit the curve. Note in Figure 6-3 that this unit was not very wet prior to drainage and lost only a few percent by day 64.5. Even so, despite the low values of saturated moisture content produced by the computer, a large increase in moisture content could occur as pressure head reaches 0 cm. Thus, the curve in Figure 8-2 would resemble that for a sand. More pressure head data in the wet range of this soil would have permitted a more realistic fit.

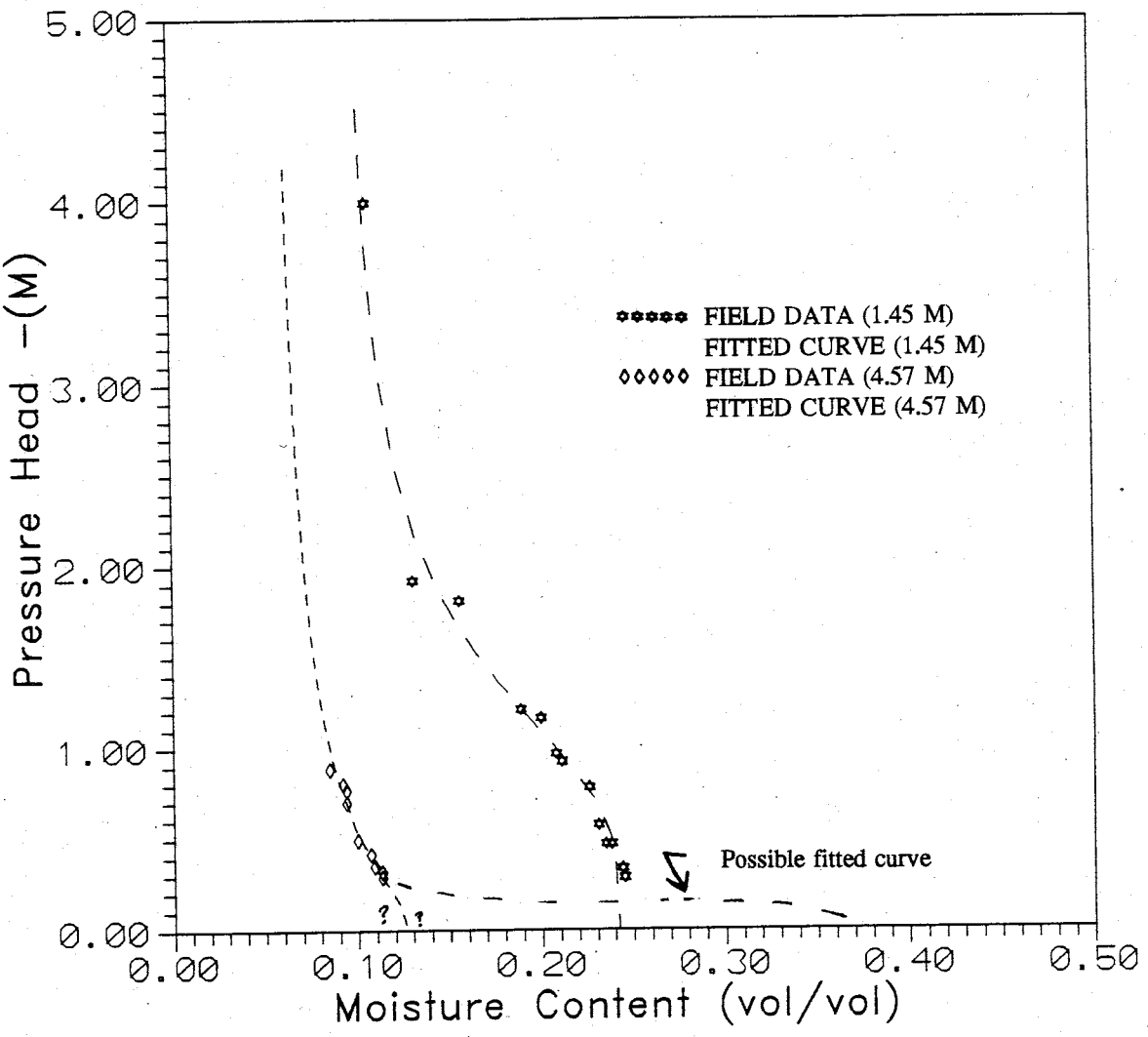

Figure 8-2. Characteristic Curve--Station 18-18

8.2 van Genuchten -- Sisson Model Results

Figures 8-3a through 8-3c show K-θ results from equation (8), described above in section 3.3.5. Values of K_{sat}, θ_r, θ_s and n_s used in this equation are included in Table 10. The interval from 0.86 to 5.13 meters below datum was studied as

Table 10. Parameters for Station 15-15: Development of K-θ Graphs.

Layer	Depth Range (m)	θ_r	θ_s	K_{sat} (cm/day)	n_{vg}	n_s
1	0.86-1.16	0.076*	0.335*	300	1.3282*	0.1010
2	1.16-1.96	0.134***	0.447*	84.6*	1.3779*	0.1206
3	1.96-2.4	0.129***	0.362*	527*	1.8604*	0.188
4	2.4-3.2	0.097*	0.432*	285.1*	1.310*	0.106
5	3.2-5.0	0.063*	0.300*	1036.8*	1.3972*	0.124
6	5.0-5.3	0.092*	0.305*	3024*	2.714**	0.240

*values from other stations in field study plot

**fitted values from computer-fitted characteristic curve

***field residual

I-P test data from this region is directly comparable to K-θ graphs created from I-P test for various depths (see Figures 7-3a,c). Solid lines or those lines connecting symbols

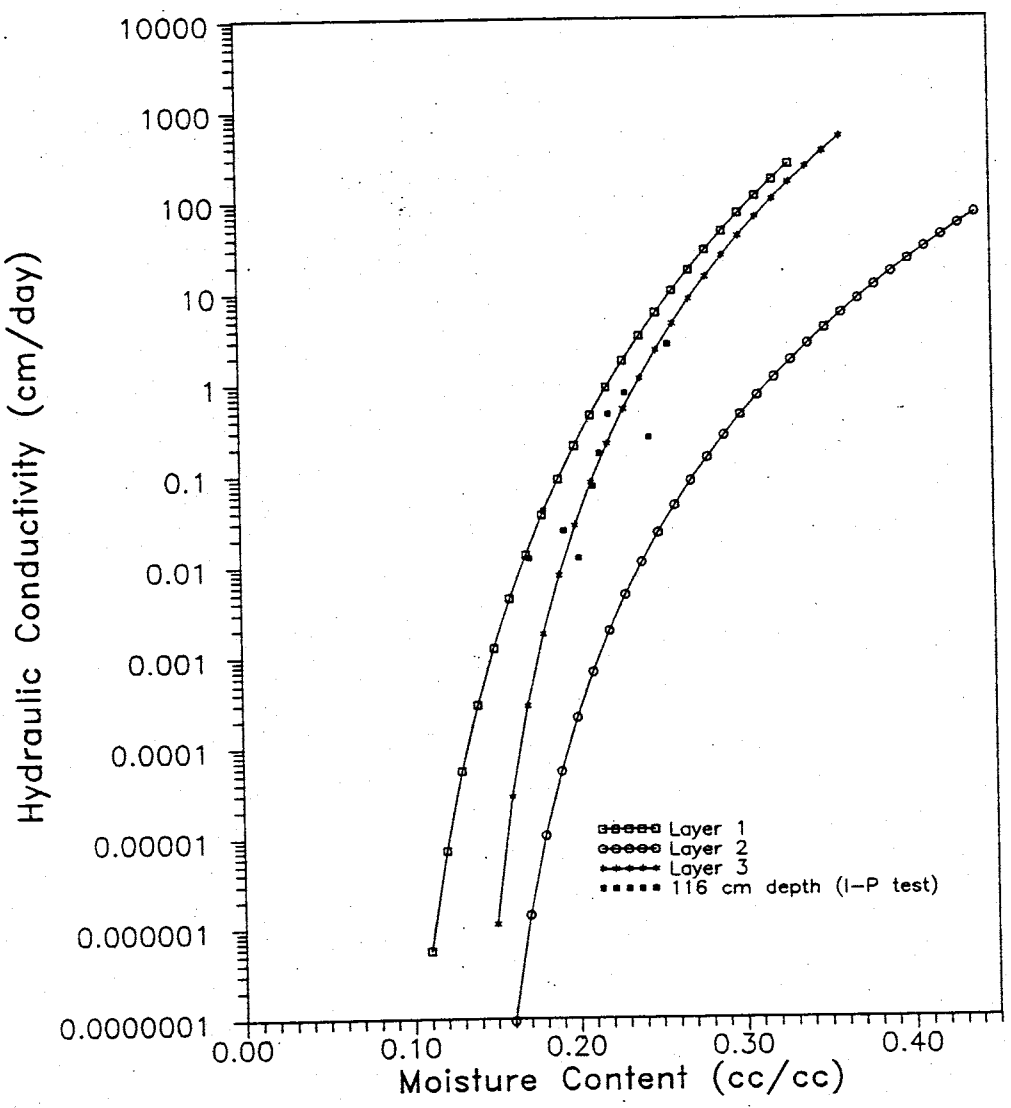

Figure 8-3a. Predicted Curves--Sisson Method; Hydraulic Conductivity vs. Moisture Content

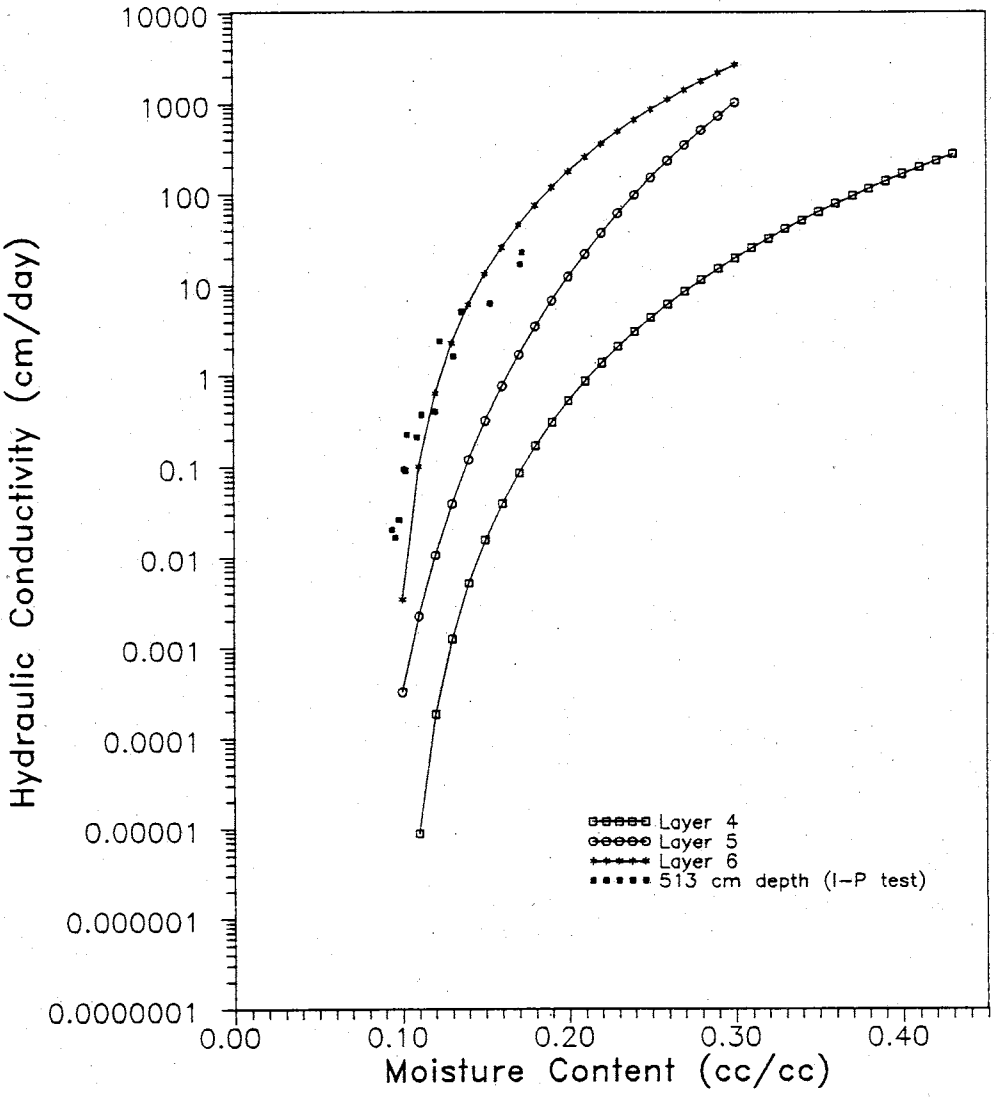

Figure 8-3b. Predicted Curves--Sisson Method; Hydraulic Conductivity vs. Moisture Content

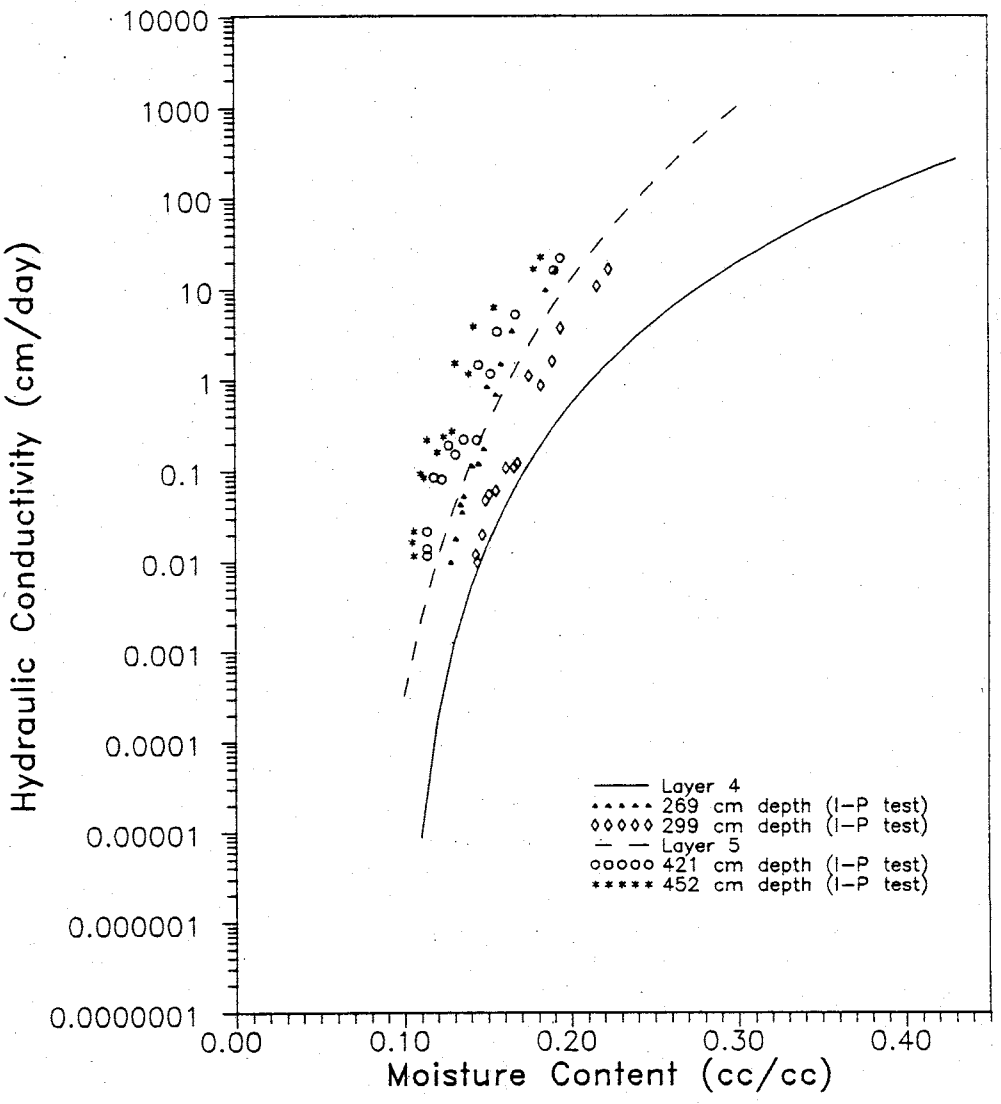

Figure 8-3c. Predicted Curves--Sisson Method; Hydraulic Conductivity vs. Moisture Content

represent predicted values of K as a function of moisture content while data from the I-P test is displayed as individual symbols. Only station 15-15 is examined here.

In Figure 8-3a, three curves (Layers 1-3) and I-P test data for the 116 cm-depth are presented. The 116 cm-depth was chosen as it produced an unusual K-θ graph (Figure 7-3a). The I-P test data primarily cluster around the curve for Layer 3. Both curves for Layers 1 and 3 show similar trends, while the curve for Layer 2 is more distinct. The geologic log shows that Layer 1 and 3 are comprised of similar soils. Thus, there is very good agreement between generated K-θ curves (based on parameters in Table 10) and the I-P data (based on field drainage data).

The three curves shown in Figure 8-3b are individually distinct. However, the slope, in general, increases from right to left, or from Layer 4 to Layer 6. The increase in slope (and in grain size) is comparable to the patterns shown in K-θ graphs generated from the I-P test data. Additionally, very good agreement is shown between the graph for Layer 6 and I-P data determined for the 513 cm depth. As described above, Layer 6 is probably more of a stony soil rather than a full layer of cobbles.

Finally, in Figure 8-3c, I-P data from the 269 cm depth cluster around the graph of layer 5 as opposed to layer 4. This suggests the soil at the 269 cm depth is coarser than described. This anomaly was evident in K-θ curves generated

from I-P test data. Slightly better agreement exists between data from 299 cm and the solid line (layer 4). Discrete coarse over fine zones may thus be present in the 269 to 299 cm interval.

8.3 Discussion

As described above, characteristic curves were developed using field data and soil parameters such as θ_s and θ_r. For station 15-15, θ - Ψ data represented the first sixty-five days of drainage. Due to tensiometer lags during equilibration periods, only Ψ - data which became more negative with time were used along with corresponding θ - values. Neither θ_s nor θ_r were permitted to vary for each depth. This resulted in two very different fits.

The agreement between field data collected from the shallow silty sand and the fitted curve, for the 1.47 meter depth at station 15-15, was reasonable (r^2 = 0.907; note Table 9). Changing the two moisture content parameters may have produced a closer fit. A very good value of r^2 (=0.99) and thus fit was generated for the other depth. Soils similar in compositions to those found at the two depths, yet located in other portions of the irrigated plot, yielded parameters (i.e. saturated moisture content) which were used to fit curves. The r^2 values suggest that such an application is acceptable.

Good fits resulted for both depths at station 18-18. A slightly better fit resulted for the silty fine sand as

opposed to the deeper fine sand (see Table 9). However, the final (fitted) values of saturated moisture content for both layers are not very realistic for these soils. The curves fit nicely to the field data, but their shapes are not very comparable to standard curves for these soil types.

A sensitivity analysis was conducted for the methods which determined, via analytical equations, the relationship between K and θ. Equation (8) was used for $K(\theta)$ and included the constants n_{vg}, K_{sat}, θ_s and θ_r. Using values from Table 10 (Layer 1) for all these constants, we can fix a value of moisture content to determine K. For instance, if $\theta = 0.25$, then K = 8.07 cm/day. Even though the 116 cm deep values of $K(\theta)$ from the I-P test did not cluster around the line for layer 1 (Figure 8-3a), the model, using a pre-drainage value of $\theta = 0.25$, predicts a K-value very close to the applied flux rate (~ 8 cm/day). Again, this suggests that good choices for soil parameters allow reliable calculations of $K(\theta)$.

In terms of individual variations in soil parameters, we see a very large increase (239%) in unsaturated conductivity (K_{unsat}) from 8.07 to 27.32 cm/day when the value n_{vg} is increased by 25%. If $n_{vg} \leq 1$ then, unsaturated conductivity cannot be determined. The parameter θ_s becomes more important if it is <u>decreased</u>. Reducing this value from 0.335 to 0.300 (10% decrease) produces a 274% decrease in $K_{unsat}(\theta=0.25)$. Problems can still arise based on initial choices of K_{sat} as

this value can vary over an order of magnitude, from soil to soil, likewise allowing a 10-fold change in $K_{unsat}(\theta=0.25)$. Thus, the Sisson--van Genuchten method, while producing very good results, is most sensitive to small variations in n_{vg} and θ_s. Also, values of K_{sat} must be reliable.

Chapter 9. General Discussion

9.1 Factors Controlling Moisture Distribution

Several soil layers in the central, eastern and northern regions of the plot drained below the initial 1987 profile (see Table 5). This initial condition for the infiltration phase was influenced by antecedent moisture from rainfall. This moisture primarily affected the moisture content of the alluvial fan facies soils. Much of this antecedent moisture was readily drained. Drainage of layers in the southwestern area of the irrigated plot did not exceed the 1987 profile (station 12-12). This was due in part to very low initial values of wetness and large amounts of water added to this section during infiltration.

An emitter test was performed to determine if variable amounts of moisture were being applied to the plot. Driplines 1 and 2 (Figure 3-4) were used. A garden hose connected the lines to a water faucet. Water was passed through the lines at a high rate for several minutes. Out of 42 emitters, one did not function. Of the remaining functioning (41) emitters, 33 passed very uniform amounts of water. Exact volumes are not available.

The emitter test did not conclusively establish or disprove uniform application of moisture. However, the plan view moisture content analysis showed symmetrical (two-dimensional) distribution of moisture content, suggesting

rather uniform distribution of applied flux.

The dye study also suggested nonuniform flux distribution. Preferential pathways were created around instrumentation in both the southeastern and southwestern portions of the plot as shown in the dye study (chapter 5). These pathways also create bias in moisture content data analysis and interpretation, primarily on a local scale. Also, the nearly saturated conditions at the eastern-southeastern edge of the plot may have been due to high infiltration/application rates relative to the normal rates applied by other emitters.

Throughout this report, the role of cobble layers in fluid distribution has been described as very influential. The hydraulic head fields developed for late stage infiltration show lateral flow occurring along these layers. These fields, as well as drainage profiles for the irrigated plot, indicate the presence of a cobble layer (silty sand matrix), 3-4 meters in depth, which influences infiltration and drainage in the site. However, another layer, present at the 5-6 meter depth, may be more of a stony soil, sharing similar geologic and hydraulic characteristics as overlying and underlying soils. Hydraulic head fields have also indicated that vertical flow is most prevalent at the center of the irrigated plot. If we look at the irrigated plot as a whole, this central area is surrounded for several meters by sources of moisture. As we move to the corners of the plot,

we move closer to drier regions. These dry regions, outside the irrigated area, can only become wetter if lateral flow is present. These lateral flow gradients thus become stronger the more one moves from the center of the irrigated plot.

Layering also influenced moisture movement in the irrigated plot. Drainage profiles for several irrigated plot stations suggest the presence of both sharp and gradational soil contacts. Coarse layers provided impedance to flow and if wetted, drained vertically and fairly rapidly into underlying finer layers. Fine-grained materials such as clayey silts and sandy clays captured much draining water and released it gradually. Textural variations increased the complexity of flow in single layers as well. Preferential fluid pathways (across layer boundaries) were created by poorly packed instruments and by natural or infiltration-induced macropores or fingering channels in the soil.

In summary, a number of factors, including those listed above, have strongly influenced fluid movement at the site. These factors must be considered in modelling studies and in general quantification of seepage from impoundments. Unfortunately, complex models tend to simplify the physical (conceptual) model to the point where factors such as texture and heterogeneity are missed. It would be quite a challenge to represent all the physical characteristics of the site in a three-dimensional mathematical model.

9.2 Relevance to Vadose Zone Monitoring

In general, the instrumentation at the field site as well as the data collection procedures aided in providing a good conceptual flow field model. As with all field sites, however, certain changes and/or additions to the monitoring system could have been effected to improve the portrayal of the flow field.

To begin with, many of the instruments were buried within the site. Driplines located 86 cm below site datum could not be periodically checked for emitter uniformity. On the other hand, it is difficult to quantify exactly the leakage through a defective liner beneath an impoundment. Therefore, buried driplines are more representative of an actual (perhaps buried) tailings pile.

Because of their depth (up to 8.8 meters), neutron probe access tubes were difficult to remove for maintenance. A few tubes experienced some corrosion as wet bentonite reacted with the aluminum. These tubes were cleaned using a scratcher brush. This process adequately removed buildup in the tubes and permitted reliable data collection.

Tensiometers were easily removed from the soil. Before the second infiltration experiment, a green-black sludge was discovered in the cups (see section 3.2.1). This problem was remedied by purging the tensiometer cups throughout the site. After this episode and especially during the drainage test, the tensiometric measurements were not delayed further, save

for occasional refills and equilibration periods.

It is extremely important to maintain and test this equipment periodically. This significantly controls the amount of error introduced into the data. Propagation of error is produced by unexpected spatial variability in observations, instrument and data collection problems, data interpolation and smoothing and incorporation of this smoothed data into various integration and differentiation steps (Flühler, et al., 1976). This amplification of error can be curbed early by careful attention to instruments and data collection.

Once error is controlled as much as possible, more attention can be focused on improvement of the monitoring network. Figure 9-1 shows the layout of the site including proposed locations for access tubes and tensiometer nests. Circles containing an "X" indicate positions of new tensiometer nests and an access tube. These particular stations could have been placed to improve our understanding of the ENE trending geologic gradient's role in fluid flow. The three "X" stations and the two southeastern ones (1 and 2) would have better defined the extent of lateral flow and vertical drainage just outside the confines of the irrigated plot.

Finally, access tubes 3 and 4 would have allowed further quantification of the preferential channelling of moisture deep in the soil profile from the southwest (station 12-12),

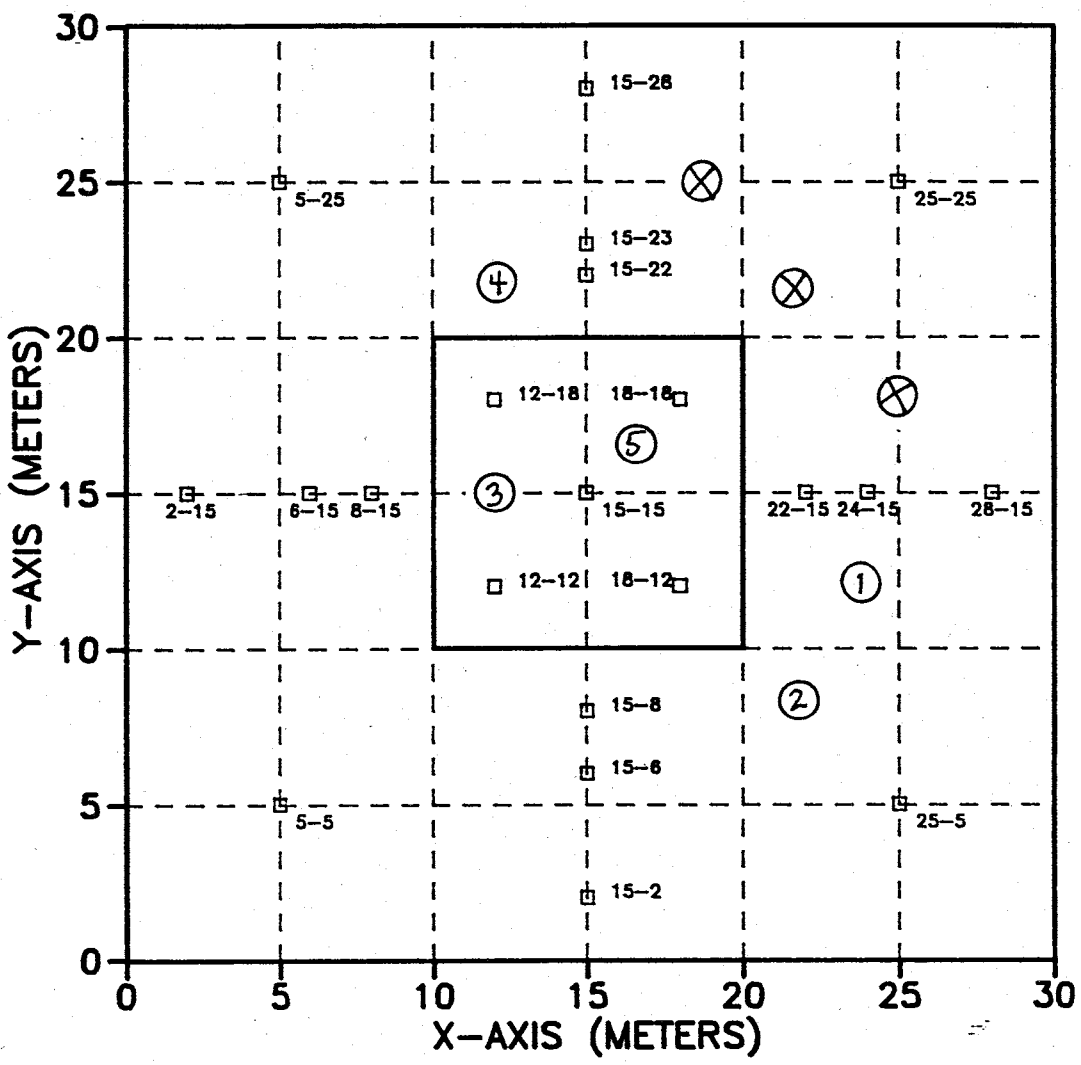

Figure 9-1. 30 x 30 M Plot. Circles represent proposed locations of instrumentation.

northward to the vicinity of stations 12-18 and onward to the north-northeast (station 15-23). Data from access tube 5 would have also enhanced our knowledge of the natural gradient as well as determined the dominance of vertical or lateral flow in this portion of the irrigated plot. As the site, in general, was extensively trenched and later overturned, these proposals were not implemented. However, it would have proved an invaluable exercise.

Chapter 10. Summary and Conclusions.

Beginning in early 1987, a field experiment was conducted to simulate seepage from an impoundment into a layered soil profile. A drip irrigation system was used for water application over a 10 x 10 meter plot. A flux rate of approximately 1.0×10^{-5} cm/s was used until May, 1989 at which time the rate was increased an order of magnitude. The new rate was still 10 times less than the average K_{sat} of soil layers. Infiltration continued until early September, 1987. A dyed solution was injected into the water lines and across portions of the irrigated plot for a period of five days. Following this short test, the pump was shut off, and drainage commenced. Moisture content and pressure head were monitored via neutron logging equipment and tensiometers until early June, 1990. Several trenches were excavated throughout the 30 x 30 meter site beginning in October, 1989 and continuing in several phases through June. Several stages of small scale geology and dye trace mapping extended through August.

A variety of objectives were accomplished during this experiment utilizing substantial amounts of field and laboratory data. The dye and drainage tests were the focus of this phase of the field study. As listed in the objectives section, it was important during these analyses to determine late stage infiltration and drainage dyed fluid pathways and distributions of θ and Ψ, and to utilize one-dimensional

analytical models to generate K-θ and θ-Ψ graphical relationships.

In meeting these objectives, this portion of the multi-faceted experiment yielded the following conclusions:

1. Dyed fluid pathways are a good qualitative indicator of instrument performance. Piping along instrumentation at station 18-12 explains anomalous θ and Ψ measurements.

2. Extensive regions of dyed soil suggested that local ponded conditions existed in shallow portions of the site. These zones were not necessarily detected by the probe. All values of θ measured were less than saturated moisture contents for the shallow layers.

3. Analysis of moisture content distribution showed that applied flux through emitters was rather uniform on a site-wide scale. Local anomalies persisted as indicated by the dye study.

4. Preferential flow occurred in the subsurface due to loosely packed instruments, macropores induced by high infiltration rates around emitters, fingering through coarse soil underlying finer material and impeding layers (pebbles, cobbles) throughout the profile.

5. Moisture content and pressure head generally do support the fact that coarse layers drain rapidly while finer materials drained gradually.

6. The instantaneous profile test is a good method for determining <u>in situ</u> unsaturated hydraulic conductivity at the site despite the high propensity for lateral flow.

7. Unit gradient can be assumed for the profile beneath the irrigated plot. This generality can be incorporated into the I-P test. If local gradients are less than 0.8 and/or greater than 1.20, then they could greatly affect drainage.

8. Wavy dye traces as well as distribution of moisture content and pressure head during drainage of a single layer signify textural changes within the layer. Poor sorting, high percentage of clay, macropores or impeding effects did not promote uniform drainage.

9. Fluid flow, as evidenced by the dye study, did not have an affinity for a particular soil especially at shallow depths. Both thinly bedded silty clay and large cobbles were stained blue in some areas and unstained in others.

10. Moisture did not accumulate above the five-meter deep "cobble layer." Silty matrix material, similar in character and drainage behavior to overlying soils, may account for this absence of moisture.

11. Vertical and lateral drainage occurred in many regions of the irrigated plot. Vertical drainage occurred through uniform sandy or silty soils until impeding layers (cobbles/ pebbles) or water sinks (clays) were encountered. At many of these stations, lateral flow occurred along the upper surface of the 3-3.5 meter deep cobble layer.

12. Significant lateral flow occurred to the east-northeast due to the slope of the soil layers in this direction. Another important system of lateral drainage existed at the 7.5-8.0 meter depth, in the western-northwestern region of the irrigated plot in which water drained into a thick clay and was gradually released.

13. Moisture content data collected for six of the eight outside stations (2-15, 5-25, 15-28, 25-5, 15-2 and 5-5) did not show any effects from infiltration or drainage.

14. Characteristic curves and graphical relationships between K and θ were determined using analytical equations. Results compared very favorably to strictly field-generated drainage data.

15. The instrumentation in general provided good data for a flow field analysis. The dye study coupled with the data analysis proved that substantial lateral flow existed at the site both during infiltration and drainage.

16. If a ponded mill tailings pile was capped and abandoned here, solute-laden moisture would flow laterally toward the east-northeast as well as eventually vertically toward the water table. Although the instrumentation penetrated only one-third of the vadose zone, the uniformity of the river sands (clean f-med. Rio Grande sediments) would allow easy passage of moisture from such a pile into the water table. Study of moisture content profiles in these sands suggests this possibility of vertical drainage.

Chapter 11. Recommendations

If a similar site was chosen for a vadose zone flow and transport experiment, several things could have been done differently to improve data collection procedures and results. These include the following:

* Concurrent measurements of moisture content and pressure head would be collected to more accurately define the flow regime during drainage.

* Tensiometers could be emplaced at depths similar to those corresponding to moisture content measurements. Thus, many tensiometers are needed especially between existing station locations to the east-northeast of the irrigated plot.

* To improve characterization of layering at the site, tensiometers and access tubes could be installed horizontally along layers, providing the site is large enough and layers are thick enough to allow adequate trenching and instrumentation emplacement. This would also correct the uncertainties brought about in gradient calculations and neutron probe measurements in which soil-soil contacts are "smoothed over."

* Driplines were deep enough so moisture measurement by a neutron probe was adequate. Time domain reflectometry could be installed in a similar site to better quantify the amount of moisture infiltrating from rainstorms.

* The entire site could be covered by a tent or similar enclosure to keep out rain and sunlight. This would permit more pressure head measurements to be collected regardless of time of day and season.

* If possible, deeper coring beneath the irrigated plot could be conducted to improve our knowledge of the geologic fabric. More deep trenching along the outer portions of the site would enhance our understanding of the facies boundaries and character of the cobble layers. A detailed study of the matrix between cobbles is

warranted due to the importance of the cobbles as an impeding layer to draining moisture.

Although much field work and many data analyses were undertaken at the site, several other tests could be conducted. These tests were not completed due to time and instrument constraints. They would, however, complement well the infiltration and drainage flow field analyses.

Using data that has already been collected and stored, the following studies could be accomplished:

* Determine water and/or solute mass balance in the site incorporating precipitation, evaporation, dripline flux, soil water sampler and well level data.

* Calculate or predict the amount of groundwater recharge due to infiltrated water. It would also be important to determine if solutes arrived at the water table. For future (similar) sites, more sampling/monitoring wells would be needed.

* Two or three-dimensional modelling could be undertaken using soil parameters, moisture content, pressure head and conductivity data. Understanding of the boundary conditions and complex geologic framework are absolutely necessary to predict flow at the site. This type of study would be valuable for unsaturated flow code validation.

* Other methods of determining field hydraulic conductivity, especially the flow net method (Stephens, 1985) could be implemented to characterize the flow field.

Other studies were not completed due to extensive site soil disturbance. If this experiment is repeated the following analyses should not be neglected:

* Horizontal plan view as well as two-dimensional vertical dye distribution would improve our knowledge of preferential flow pathways in the subsurface. The dye study could also have lasted longer, incorporating deeper trenching to search for the dye traces.

* Because of the importance of texture changes within individual units, a more detailed study of grain size variability is warranted. This could include more soil column studies using undisturbed cores from the field site.

Chapter 12. References.

Albrecht, K.A., B.L. Herzog, L.R. Follmer, I.G. Krapac, R.A. Griffin and K. Cartwright. 1989. Excavation of an Instrumented Earthen Liner: Inspection of Dyed Flow Paths and Morphology. **Hazardous Waste and Hazardous Materials** 6(3):269-279.

Arnet, P. 1991. Field Simulation of Waste Impoundment Seepage in the Vadose Zone: Geologic and Hydrologic Characterization of the Vadose Zone With Respect to Fluid Transport. Unpublished M.S. Independent Study Paper, New Mexico Institute of Mining and Technology, Socorro, New Mexico.

Aylor, D. and J-Y Parlange. 1973. Vertical Infiltration Into a Layered Soil. **Soil Sci. Soc. Am. J.** 37:673-676.

Bear, J. 1979. **Hydraulics of Groundwater** McGraw-Hill Publishing Co., New York, 569pp.

Black, T.A., W.R. Gardner and G.W. Thurtell. 1968. Prediction of Evaporation, Drainage and Soil Water Storage For a Bare Soil. **Soil Sci. Soc. Am. Proc.** 33:655-660.

Bloomfield, R.A. and R.J. Seibel. 1981. Bureau of Mines Research in Mine Waste Disposal Technology, In "Mine Waste Disposal Technology" pp. 2-7. Bureau of Mines Information Circular 8857, Bureau of Mines Technology Transfer Workshop, Denver, Colorado.

Bouma, J., D.I. Hillel, F.D. Hole and C.R. Amerman. 1971. Field Measurement of Unsaturated Hydraulic Conductivity By Infiltration Through Artificial Crusts. **Soil Sci. Soc. Am. Proc.** 32:362-364.

Bouma, J. 1973. Use of Physical Methods to Expand Soil Survey Interpretations of Soil Drainage Conditions. **Soil Sci. Soc. Am. Proc.** 37:413-421.

Brooks, R.H. and A.T. Corey. 1964. **Hydraulic Properties of Porous Media.** Hydrology Paper No. 3. Colorado State University, Fort Collins, Colorado.

Bybordi, M. 1969. Vertical Movement of Water in Stratified Porous Material. 2. Transient Stages of Drainage to a Water Table. **Water Resources Research.** 5(3):694-697.

Chahal, R.S. 1965. Effect of Temperature and Trapped Air on Matric Suction. **Soil Science.** 100:262-266.

Corey, A.T. and R.H. Brooks. 1975. Drainage Characteristics of Soils. **Soil Sci. Soc. Am. Proc.** 39:251-255.

Dane, J.H. and P.J. Wierenga. 1975. Effect of Hysteresis on the Prediction of Infiltration, Redistribution and Drainage of Water in a Layered Soil. **J. of Hydrology.** 25:229-242.

Eagleman, J.R. and V.C. Jamison, 1962. Soil Layering and Compaction Effects on Unsaturated Moisture Movement. **Soil Sci. Soc. Am. Proc.** 26:519-522.

Flanigan, K. 1989. Field Simulation of Waste Impoundment Seepage in the Vadose Zone: Non-reactive Solute Transport Through a Stratified, Unsaturated Field Soil. Unpublished M. S. Independent Study Paper, New Mexico Institute of Mining and Technology, Socorro, New Mexico.

Flühler, H., M.S. Ardakani and L.H. Stolzy. 1976. Error Propagation in Determining Hydraulic Conductivities From Successive Water Content and Pressure Head Profiles. **Soil Sci. Soc. Am. J.** 40:830-836.

Friedman, G.M. and J.E. Sanders. 1978. **Principles of Sedimentology.** John Wiley and Sons, New York, 792pp.

Gardner, W. and D. Kirkham. 1952. Determination of Soil Moisture By Neutron Scattering. **Soil Science.** 73: 391-401.

Ghodrati, M. and W.A. Jury. 1990d. A Field Study Using Dyes to Characterize Preferential Flow of Water. **Soil Sci. Soc. Am. J.** 54:1558-1563.

Grabka, D.P. 1991. Field Simulation of Waste Impoundment Seepage in the Vadose Zone: Multiple-Tracer Transport Experiment In a Stratified, Heterogeneous, Unsaturated Field Soil. Unpublished M. S. Independent Study Paper, New Mexico Institute of Mining and Technology, Socorro, New Mexico.

Green, R.E., L.R. Ahuja and S.K. Chong. 1986. Hydraulic Conductivity, Diffusivity and Sorptivity of Unsaturated Soils: Field Methods. **Chapter 30. Methods of Soil Analysis: Part 1: Physical and Mineralogical Methods-Agronomy Monograph No. 9.** Soil Sci. Soc. Amer./Amer. Soc. Agron. pp. 771-798.

Green, W.H. and G.A. Ampt. 1911. Studies on Soil Physics: I. Flow of Air and Water Through Soils. **J. Agr. Science.** 4:1-24.

Hendrickx, J.M.H. 1990. Determination of Hydraulic Soil Properties. **Chapter 3. Processes in Hillslope Hydrology.** John Wiley & Sons. pp. 43-92.

Hillel, D.I. and W.R. Gardner. 1970. Measurement of Unsaturated Conductivity and Diffusivity by Infiltration Through an Impeding Layer. **Soil Science.** 109(3):149-153.

Hillel, D.I., V.D. Krentos and Y. Stylianou. 1972. Procedure and Test of an Internal Drainage Method For Measuring Soil Hydraulic Characteristics in situ. **Soil Science.** 114:395-400.

Hillel, D.I. and H. Talpaz. 1977. Simulation of Soil Water Dynamics in Layered Soils. **Soil Science.** 123:54-62.

Hillel, D.I. 1980a. **Applications of Soil Physics.** Academic Press, Inc. 385pp.

_____ 1980b. **Fundamentals of Soil Physics.** Academic Press, Inc. 413pp.

Hillel, D.I. and R. Baker. 1990. Laboratory Tests of a Theory of Fingering During Infiltration into Layered Soils. **Soil Sci. Soc. Amer. J.** 54:20-31.

Libardi, P., K. Reichardt, D.R. Nielsen and J.W. Biggar. 1980. Simple Field Methods For Estimating Soil Hydraulic Conductivity. **Soil Sci. Soc. Amer. J.** 44:3-7.

Lucia, P.C., J.M. Duncan and H.B. Seed. 1981. Summary of Research on Case Histories of Flow Failures of Mine Tailings Impoundments. In "Mine Waste Disposal Technology" pp. 46-53, Bureau of Mines Information Circular 8857, Bureau of Mines Technology Transfer Workshop, Denver, Colorado.

Marthaler, H.P., W. Vogelsanger, F. Nichard and P.J. Wierenga. 1983. Pressure Transducer For Field Tensiometers. **Soil Sci. Soc. Am. J.** 47(4):624-627.

Mattson, E.D. 1989. Field Simulation of Waste Impoundment Seepage in the Vadose Zone: Experiment Design and Two-dimensional Modelling. Unpublished M. S. Independent Study Paper, New Mexico Institute of Mining and Technology, Socorro, New Mexico.

McWhorter, D.B. and D.K. Sunada. 1977. **Groundwater Hydrology and Hydraulics** Water Resources Publications, 290pp.

Miller, D.E. and W.H. Gardner. 1962. Water Infiltration Into Stratified Soil. **Soil Sci. Soc. Am. Proc.** 26:115-119.

Mualem, Y. 1976. A New Model For Predicting the Hydraulic Conductivity of Unsaturated Porous Media. **Water Resources Research.** 12(3):513-522.

Nyhan, J. and B. Drennon. 1989. Measurement of Soil-Water Tension in a Hydrologic Study of Waste Disposal Site Design. **Los Alamos Publication: LA-11460-MS.**

Omoti, U. and A. Wild. 1979. Use of Fluorescent Dyes to Mark the Pathways of Solute Movement through Soils Under Leaching Conditions: 2. Field Experiments. **Soil Science.** 128(2):98-103.

Parsons, A.M. 1988. Filed Simulation of Waste Impoundment Seepage in the Vadose Zone: Site Characterization and One-dimensional Analytical Modelling. Unpublished M.S. Independent Study Paper, New Mexico Institute of Mining and Technology, Socorro, New Mexico.

Raats, P.A.C. 1973. Unstable Wetting Fronts in Uniform and Nonuniform Soils. **Soil Sci. Soc. Am. Proc.** 37:681-685.

Richards, L.A. 1954. Multiple Tensiometers For Determining the Vertical Component of the Hydraulic Gradient in Soil. **Soil Science.** 18:7-10.

Richards, S.J. 1965. Soil Suction Measurements With Tensiometers. In **Methods of Soil Analysis** pp. 153-163, Monograph 9, Amer. Soc. Agron., Madison, Wisconsin.

Rose, C.W., W.R. Stern and J.E. Drummond. 1965. Determination of Hydraulic Conductivity as a Function of Depth and Water Content For Soil in situ. **Aus. J. of Soil Research.** 3:1-9.

Rubin, J. 1967. Numerical Method for Analyzing Hysteresis-Affected, Post-Infiltration Redistribution of Soil Moisture. **Soil Sci. Soc. Am. Proc.** 31:13-20.

Rudolph, D.L. 1990. Nonreactive Solute Transport in Unsaturated Sand and Gravel: Cape Cod Field Tests. Characterization of Transport Phenomena in the Vadose Zone. April 2-5, 1991. Workshop sponsored by Soil Science Society of America, American Geophysical Union. University of Arizona, Tucson, Arizona.

Schmidt-Petersen, R. 1991. Field Simulation of Waste Impoundment Seepage in the Vadose Zone: Horizontal Spatial Variability of the Geologic and Hydrologic Properties of an Alluvial Fan Facies. Unpublished M.S. Independent Study Paper, New Mexico Institute of Mining and Technology, Socorro, New Mexico.

Simpson, T.W. and R.L. Cunningham. 1982. The Occurrence of Flow Channels in Soils. **J. Environmental Quality.** 11(1):29-30.

Sisson, J.B. and M. Th. van Genuchten. 1980. Simple Method for Predicting Drainage From Field Plots. **Soil Sci. Soc. Am. J.** 44:1147-1152.

Stephens, D.B. 1985. A Field Method to Determine Unsatuatd Hydraulic Conductivity Using Flow Nets. **Water Resources Research** 21(1):45-50.

van Genuchten, M. Th. 1980. A Closed Form Equation for Predicting the Hydraulic Conductivity of Unsaturated Soils. **Soil Sci. Soc. Am. Proc.** 44(5):892-898.

van Genuchten, M. Th. n.d. RETC, unpublished manuscript, U.S. Salinity Laboratory, Riverside, California.

Warrick, A.W., D.O. Lomen and A. Islas. 1990. An Analytical Solution to Richards' Equation For A Draining Soil Profile. **Water Resources Research.** 26(2):253-258.

Watson, K.K. 1966. An Instantaneous Profile Method For Determining the Hydraulic Conductivity of Unsaturated Porous Materials. **Water Resources Research.** 2(4):709-715.

Watson, K.K. 1967. A Recording Field Tensiometer With Rapid Response Characteristics. **Journal of Hydrology.** 5:33-39.

APPENDICES TO

FIELD SIMULATION OF WASTE IMPOUNDMENT SEEPAGE IN THE VADOSE ZONE:

LATE STAGE INFILTRATION AND DRAINAGE IN A HETEROGENEOUS, PARTIALLY SATURATED SOIL PROFILE

by

Ann M. Stark

Submitted in Partial Fulfillment of

the Requirements for the Degree of

Master of Science in Hydrology

Department of Geoscience

New Mexico Institute of Mining and Technology

Socorro, New Mexico

April, 1992

APPENDICES

APPENDIX A: Porous Cup Sampler (PCS) Geologic Logs

NOTE: Refer to Figures 1-4 and 1-5 for all porous cup sampler locations.

KEY TO BORING LOGS

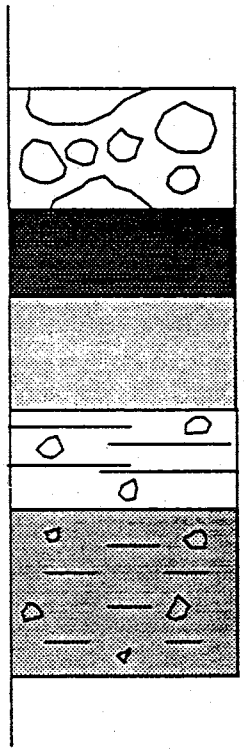

Cobbles and/or gravel layer

Clay and silty clay

Fine to medium sand

Silty fine sand, little gravel

Fine to coarse sand, little silty sand, little gravel

Site datum is at 0 meters

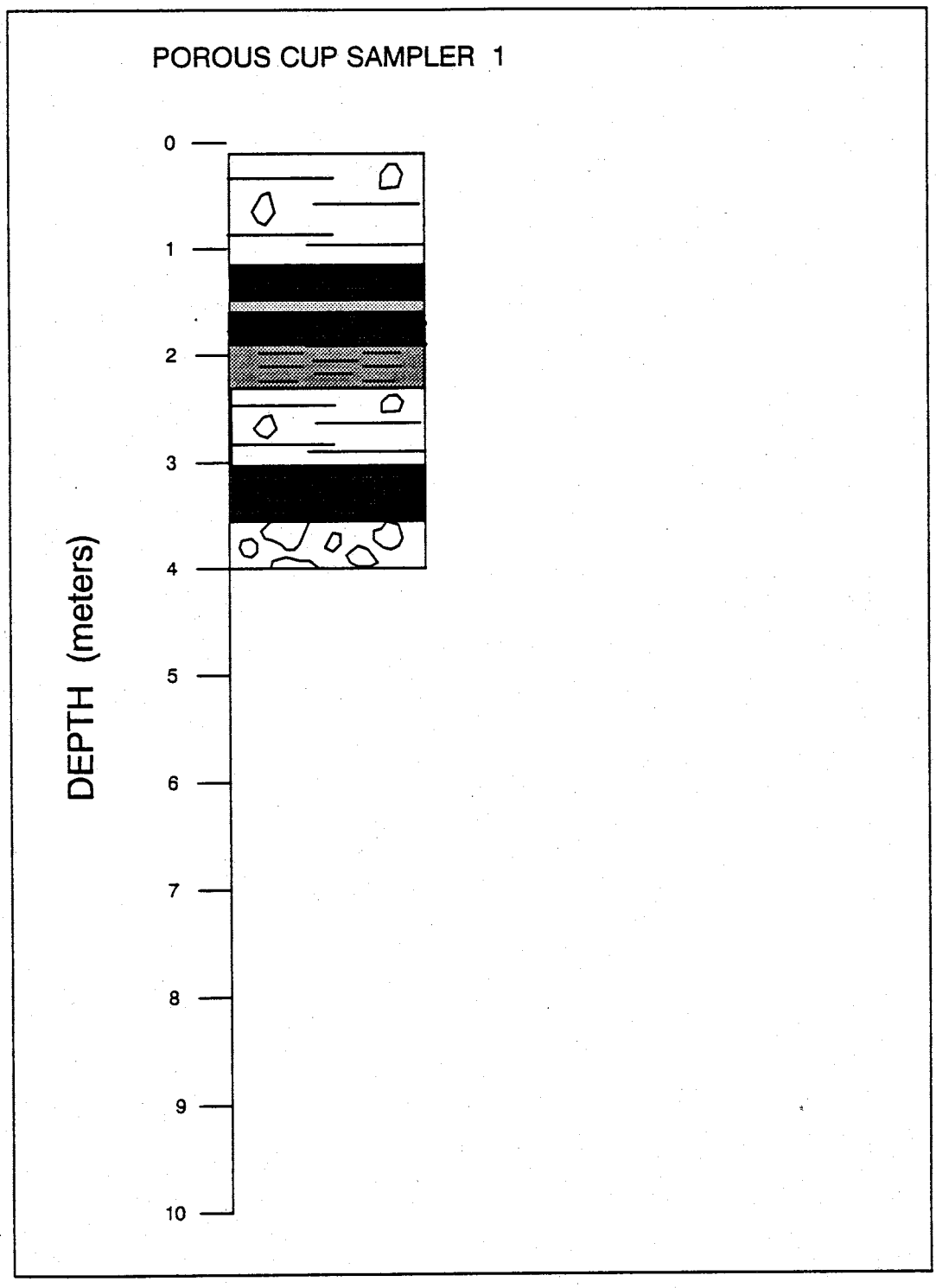
POROUS CUP SAMPLER 1
DEPTH (meters)
0
1
2
3
4
5
6
7
8
9
10

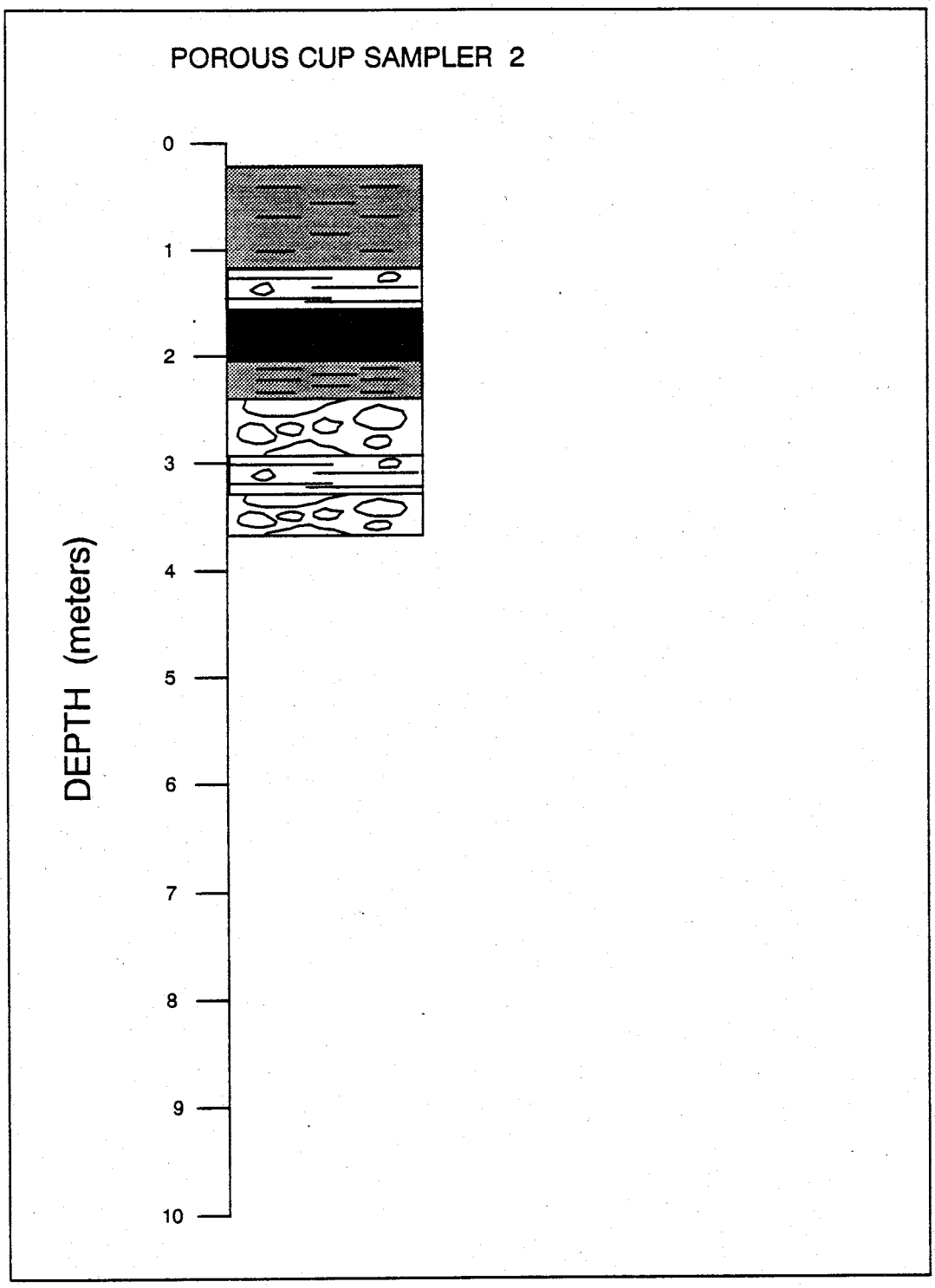
POROUS CUP SAMPLER 2
DEPTH (meters)
0
1
2
3
4
5
6
7
8
9
10

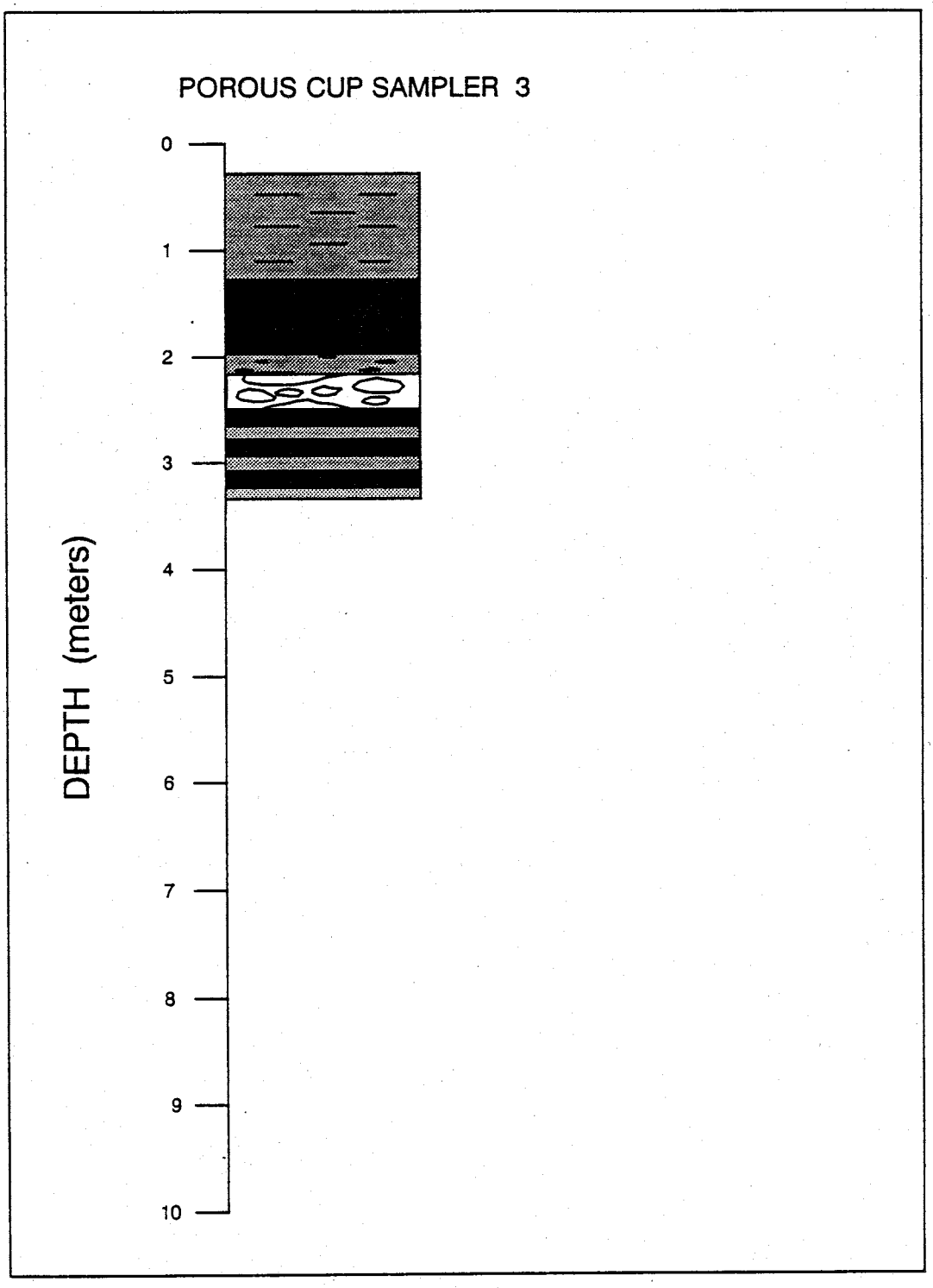
POROUS CUP SAMPLER 3
DEPTH (meters)
0
1
2
3
4
5
6
7
8
9
10

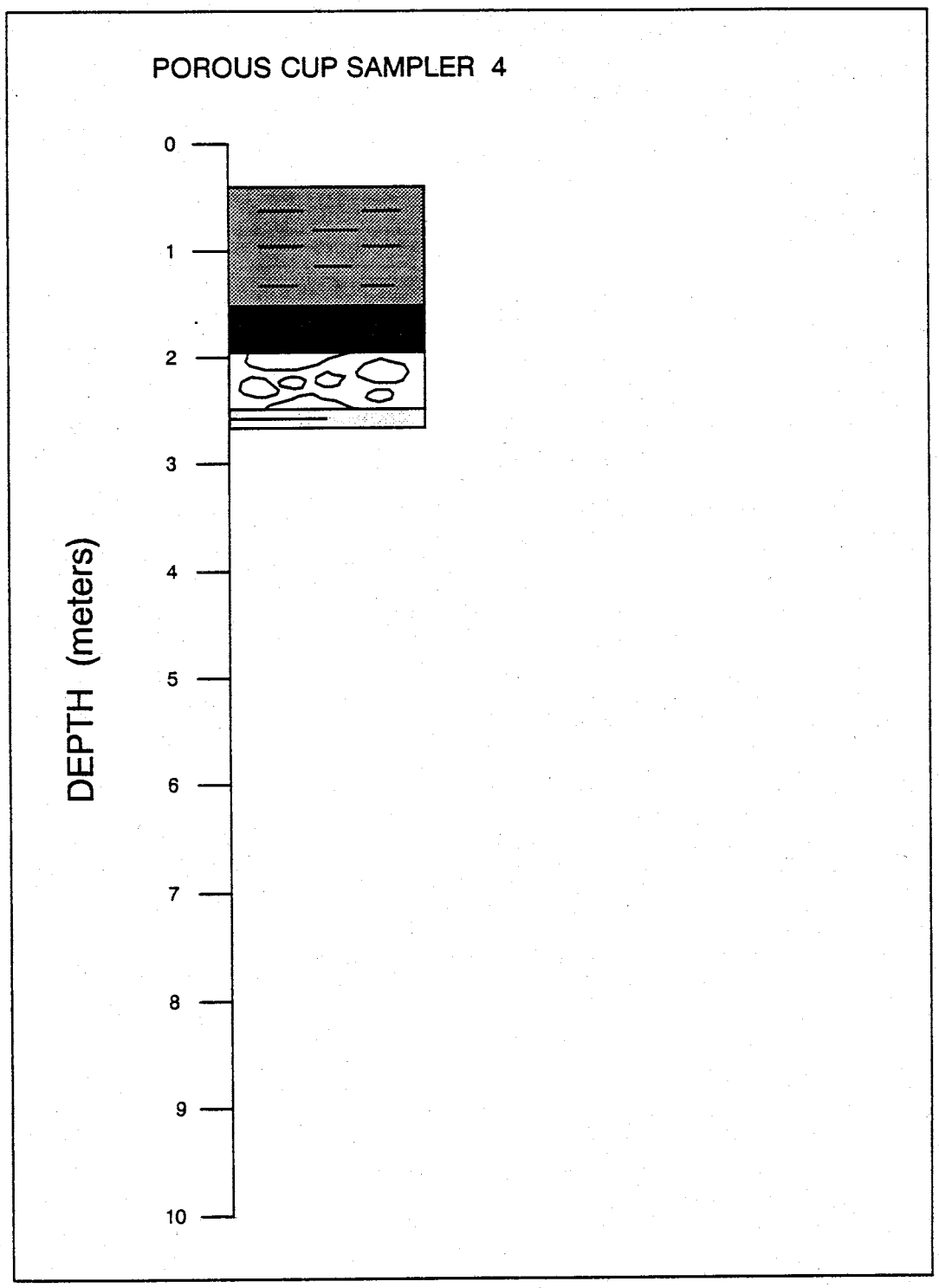
POROUS CUP SAMPLER 4
DEPTH (meters)
0
1
2
3
4
5
6
7
8
9
10

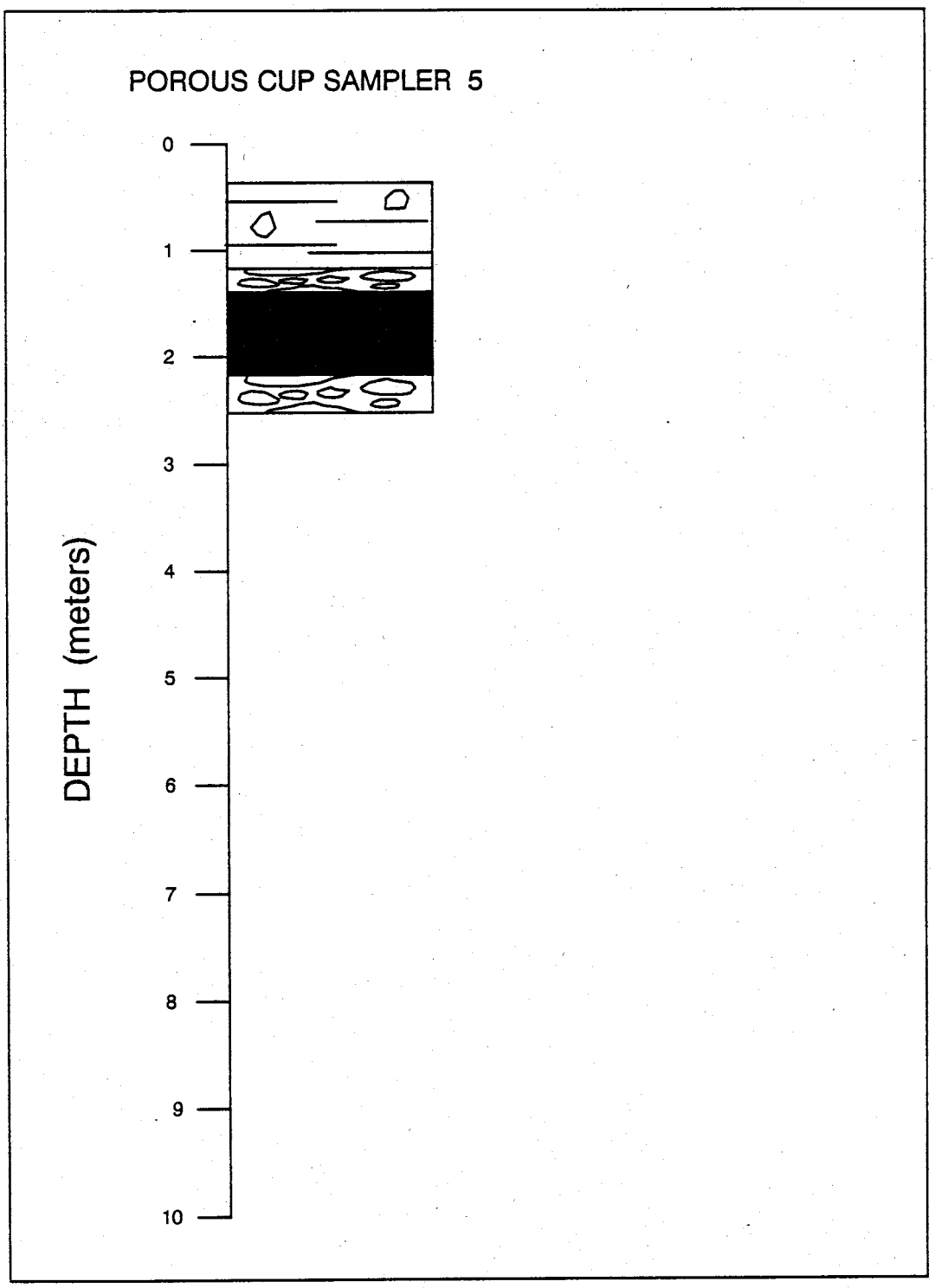
POROUS CUP SAMPLER 5
DEPTH (meters)
0
1
2
3
4
5
6
7
8
9
10

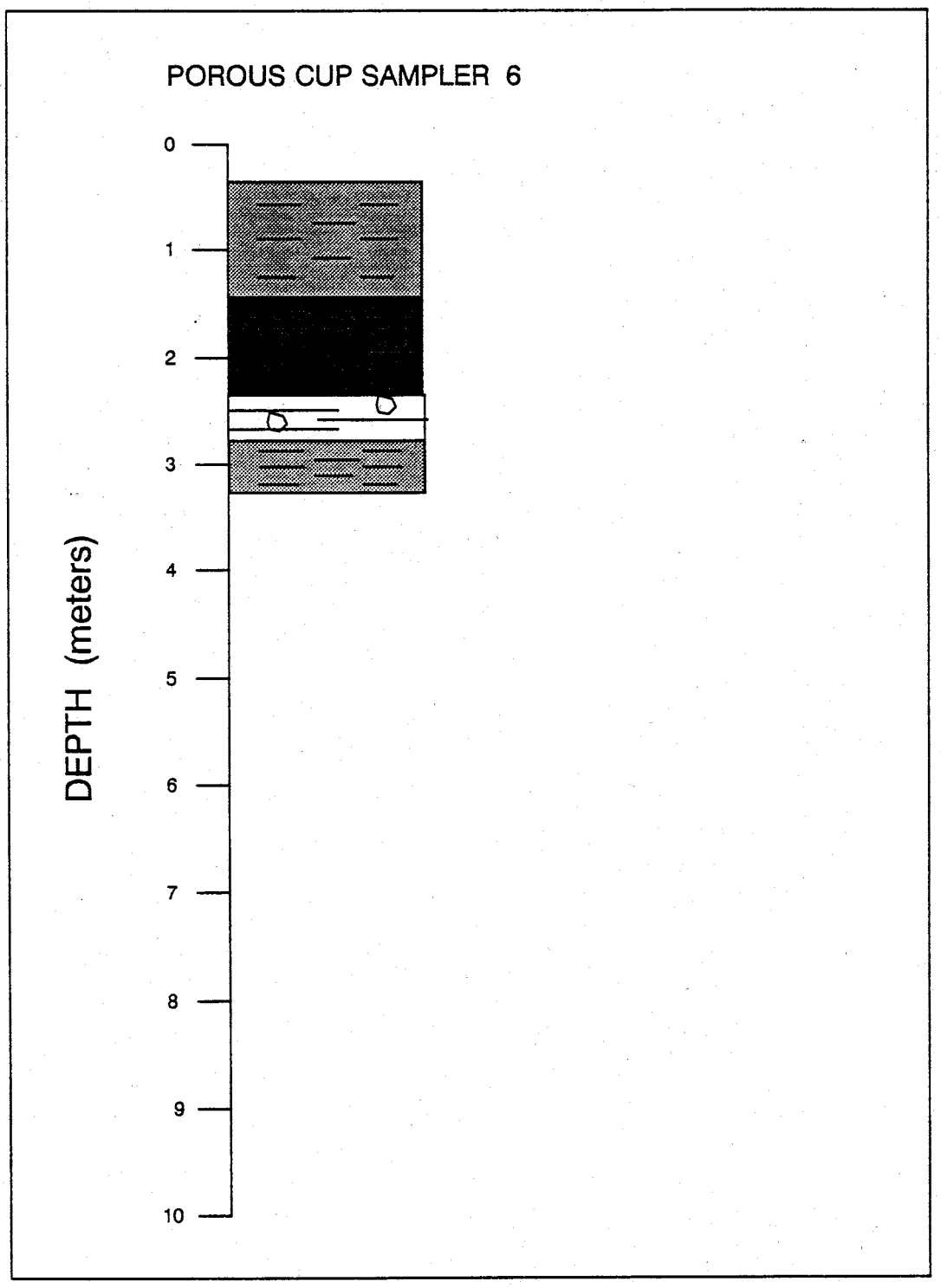
POROUS CUP SAMPLER 6
DEPTH (meters)
0
1
2
3
4
5
6
7
8
9
10

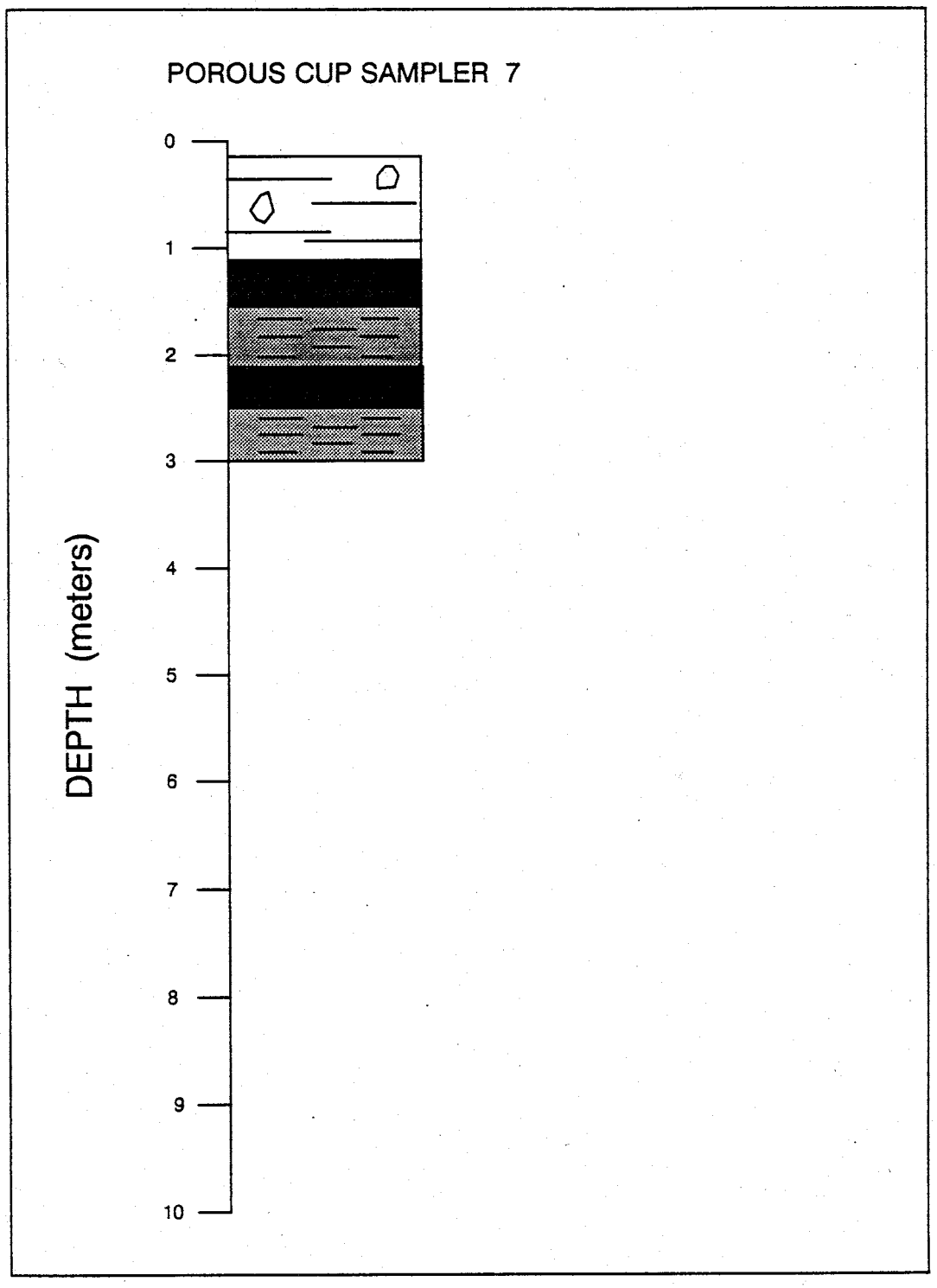
POROUS CUP SAMPLER 7
DEPTH (meters)
0
1
2
3
4
5
6
7
8
9
10

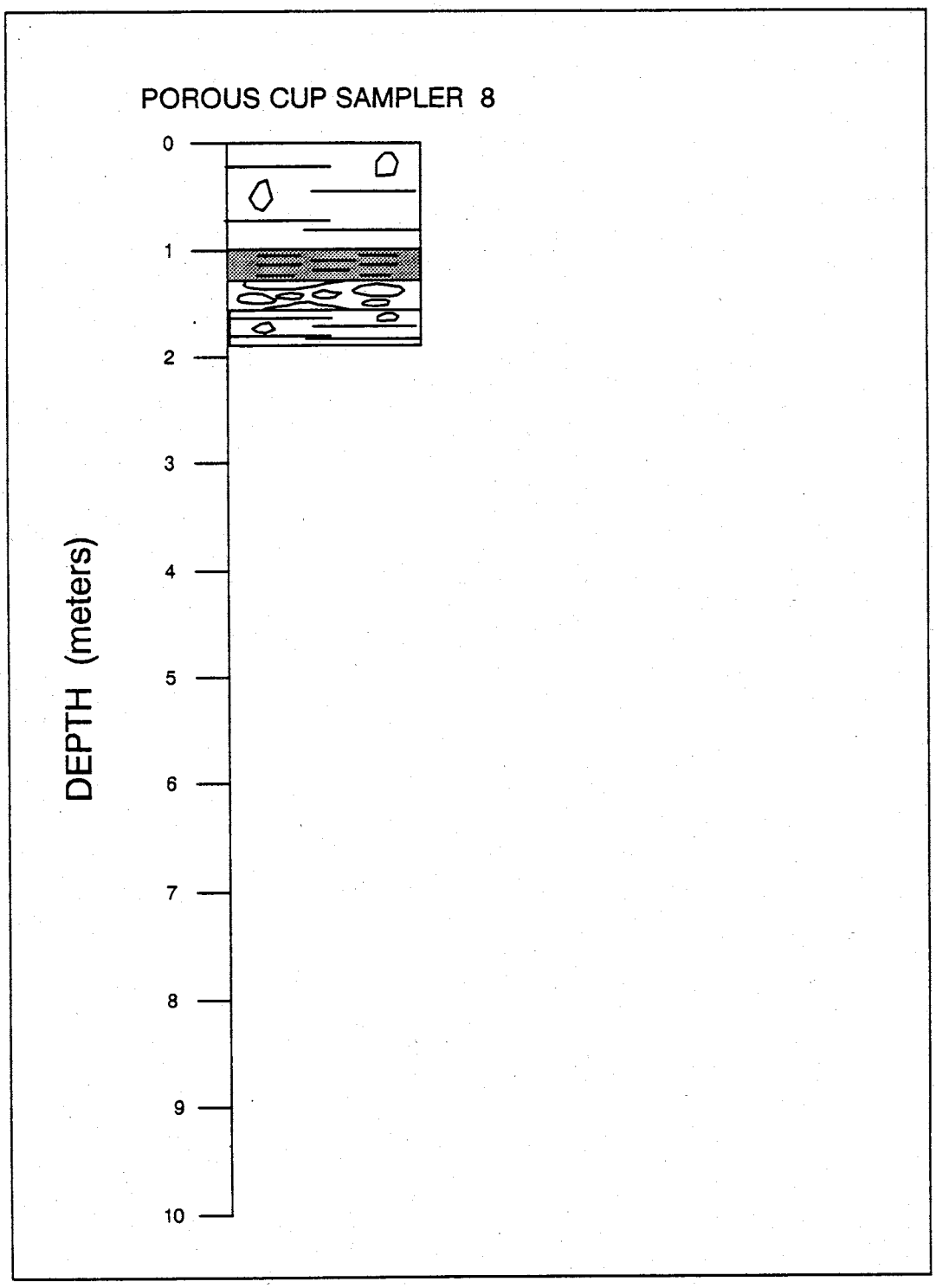
POROUS CUP SAMPLER 8
DEPTH (meters)
0
1
2
3
4
5
6
7
8
9
10

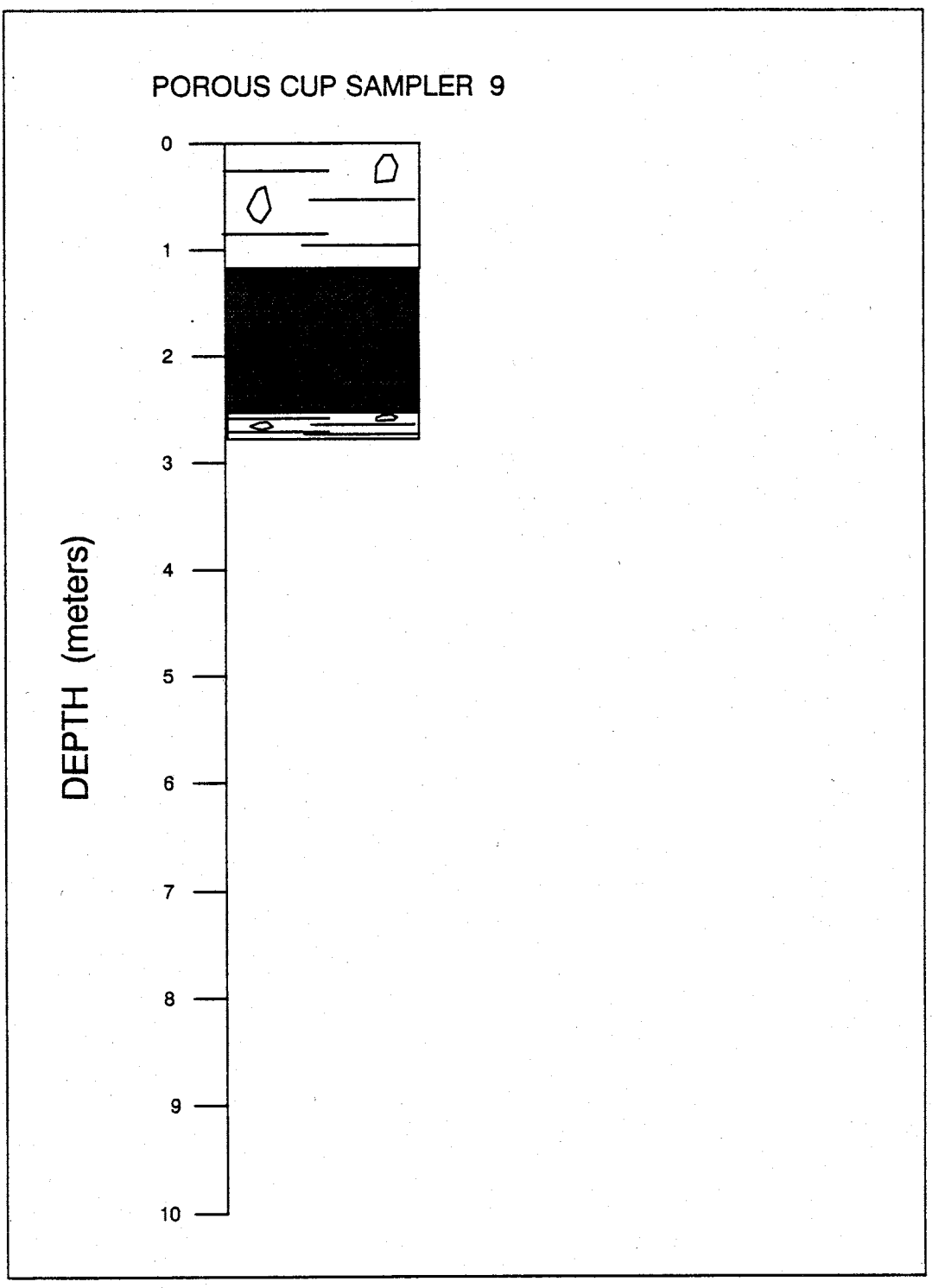
POROUS CUP SAMPLER 9
DEPTH (meters)
0
1
2
3
4
5
6
7
8
9
10

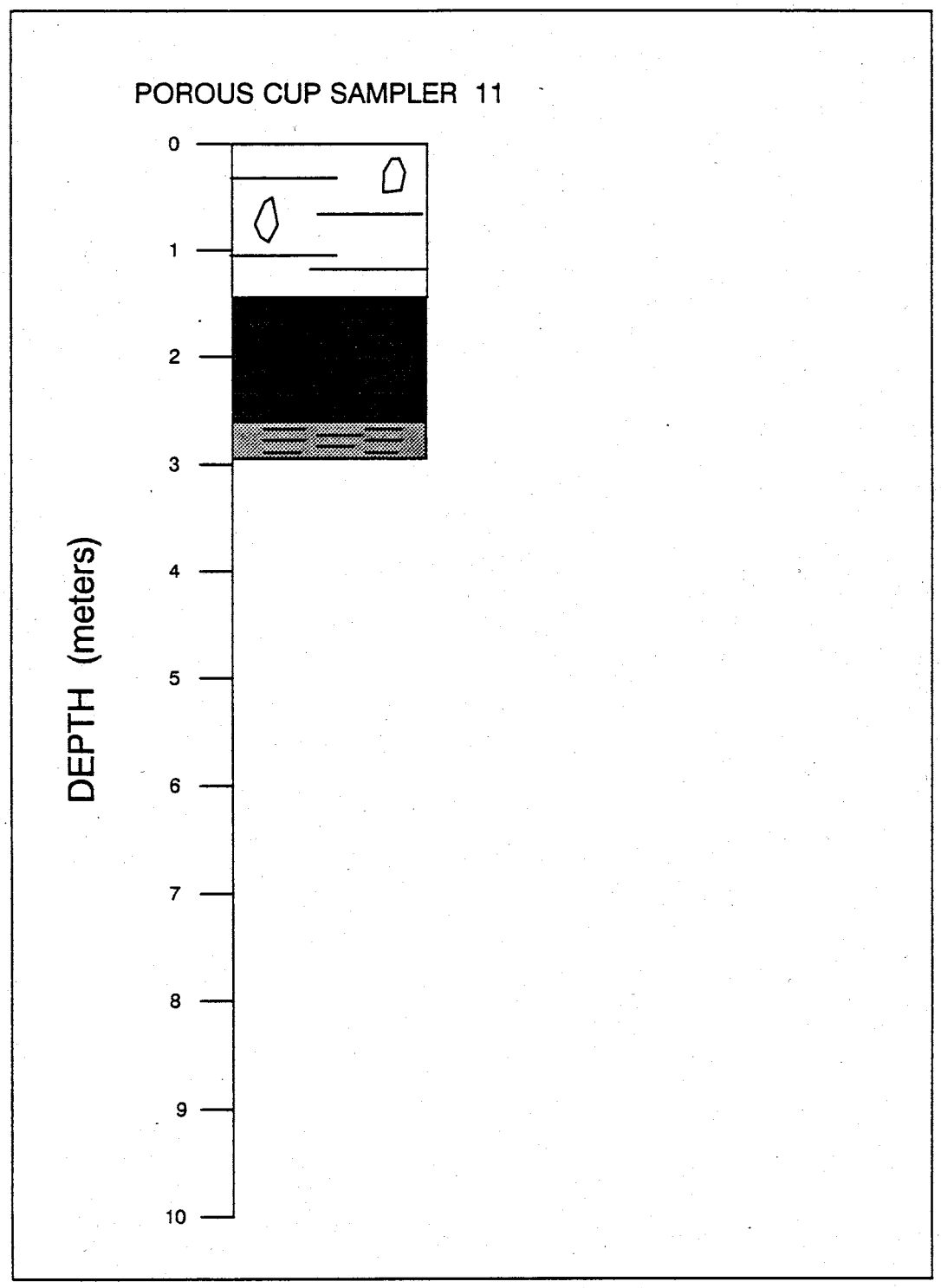
POROUS CUP SAMPLER 11
DEPTH (meters)
0
1
2
3
4
5
6
7
8
9
10

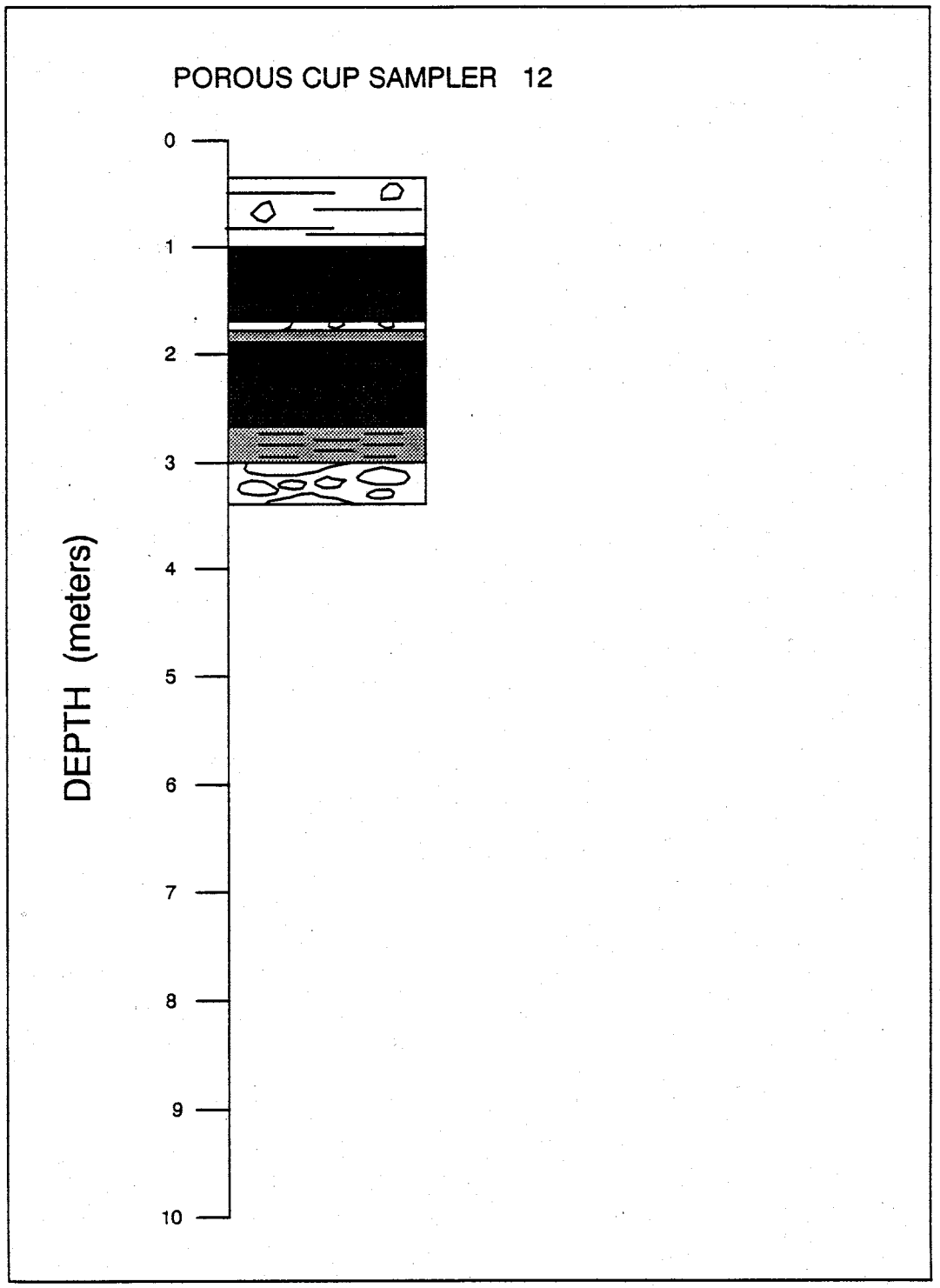
POROUS CUP SAMPLER 12
DEPTH (meters)
0
1
2
3
4
5
6
7
8
9
10

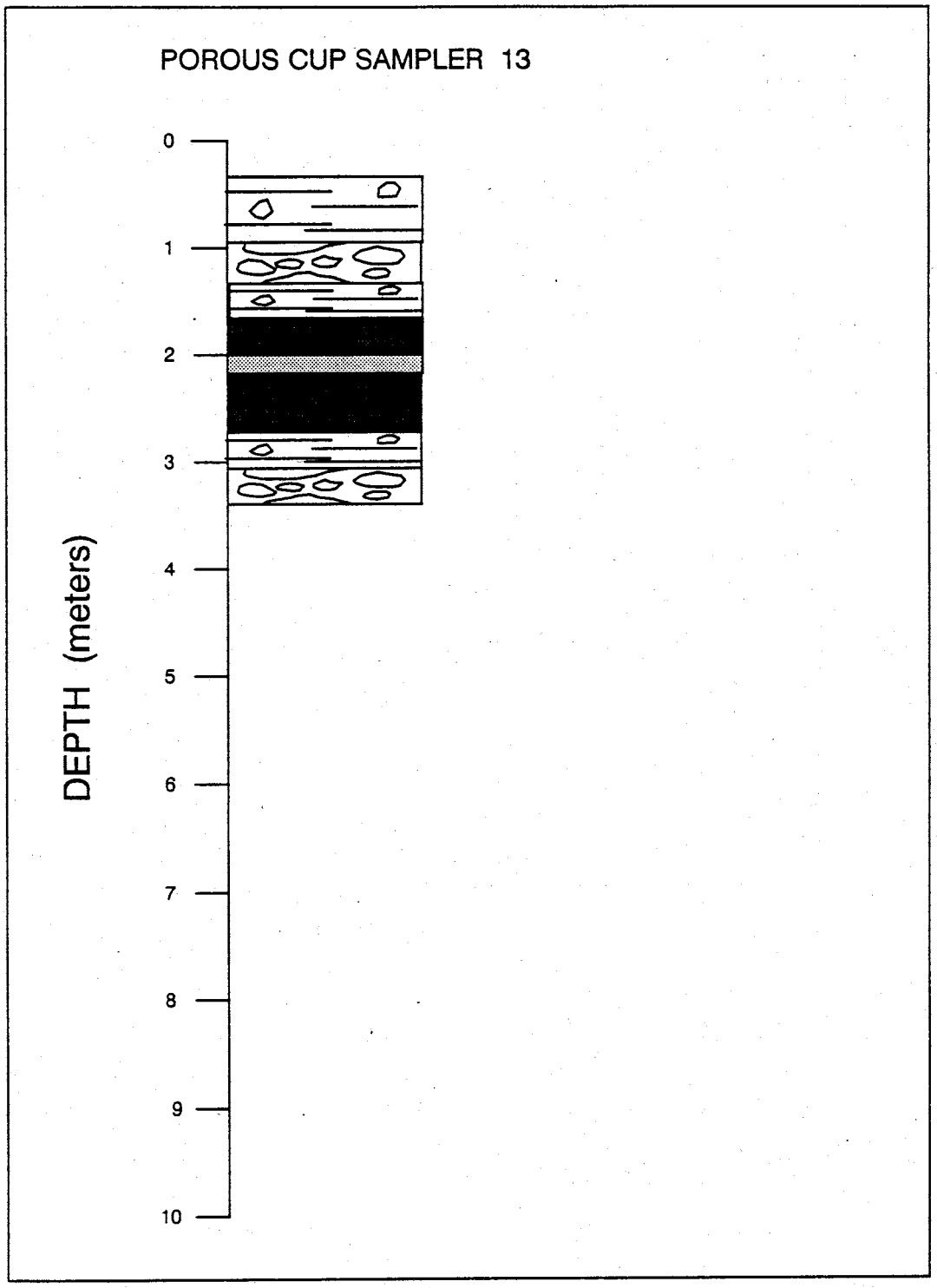
POROUS CUP SAMPLER 13
DEPTH (meters)
0
1
2
3
4
5
6
7
8
9
10

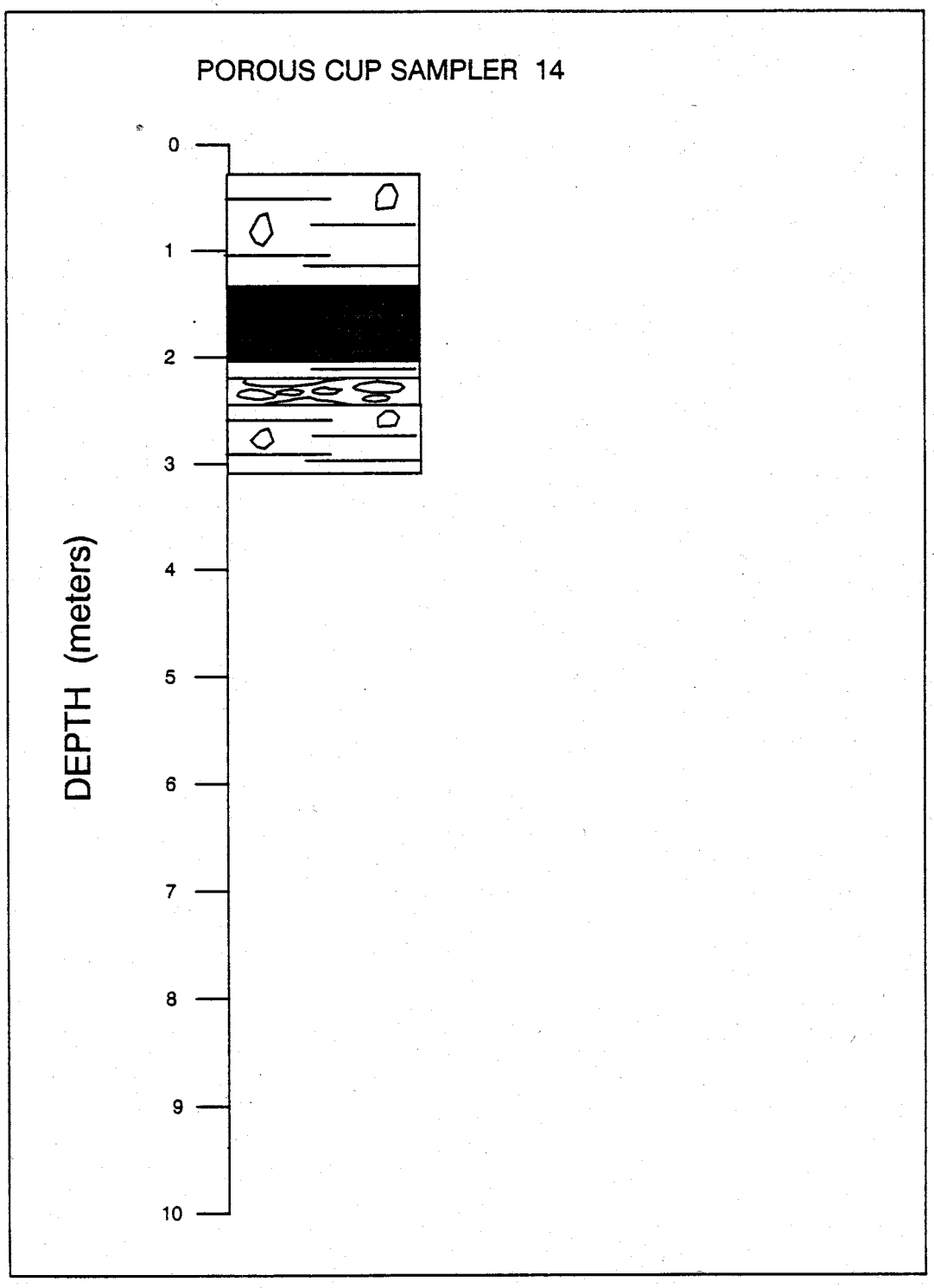
POROUS CUP SAMPLER 14
DEPTH (meters)
0
1
2
3
4
5
6
7
8
9
10

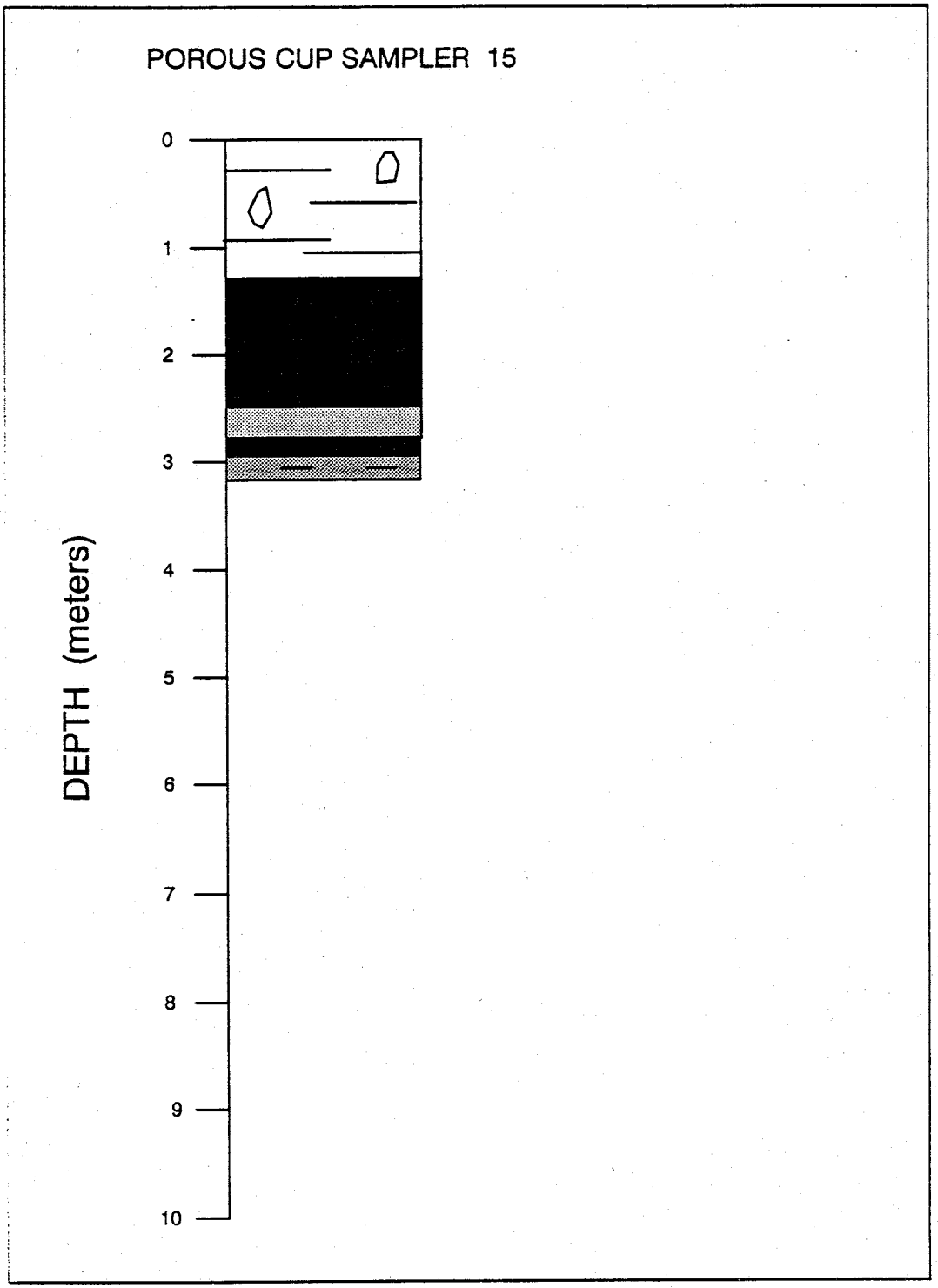
POROUS CUP SAMPLER 15
DEPTH (meters)
0
1
2
3
4
5
6
7
8
9
10

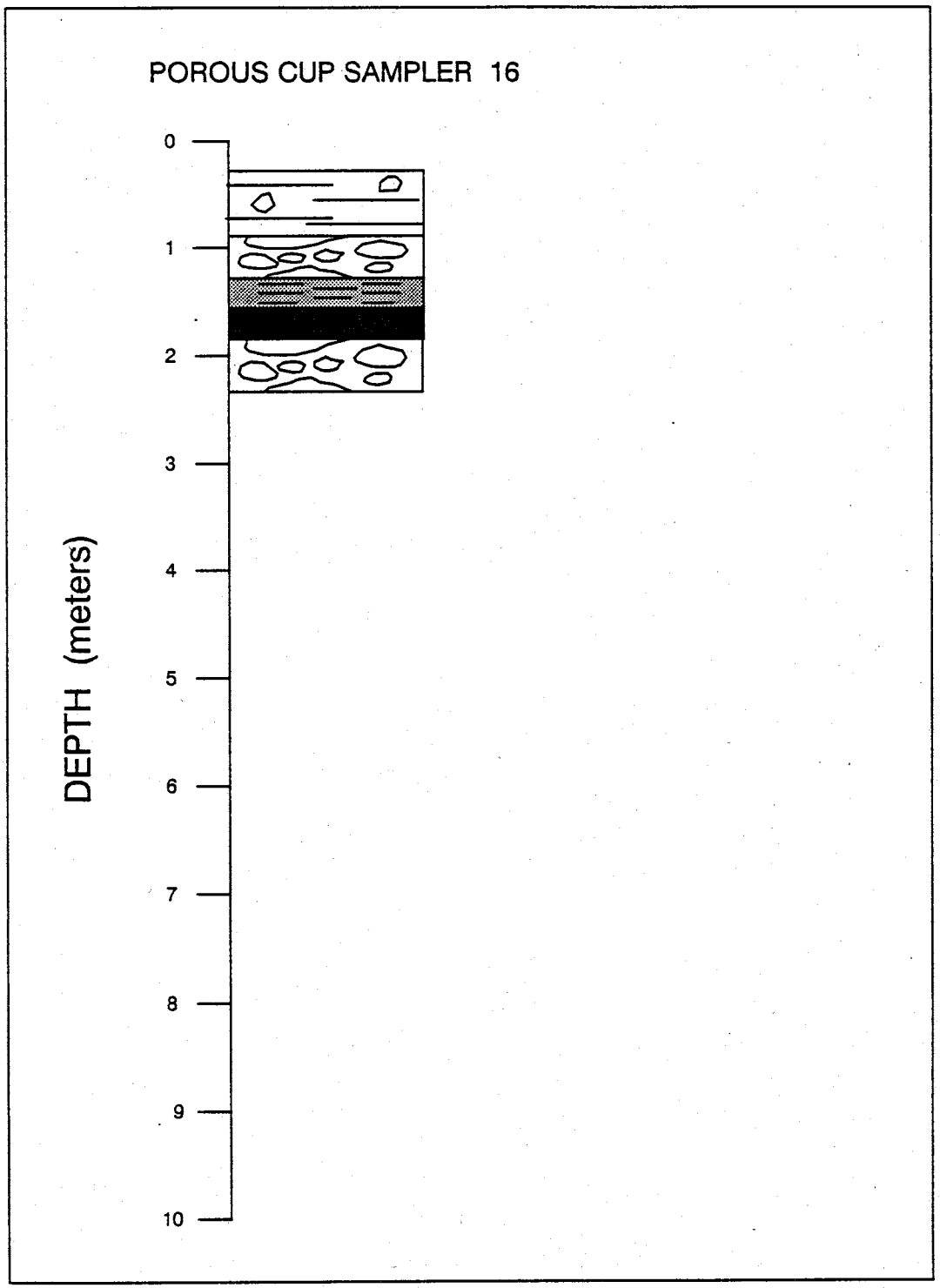
POROUS CUP SAMPLER 16
DEPTH (meters)
0
1
2
3
4
5
6
7
8
9
10

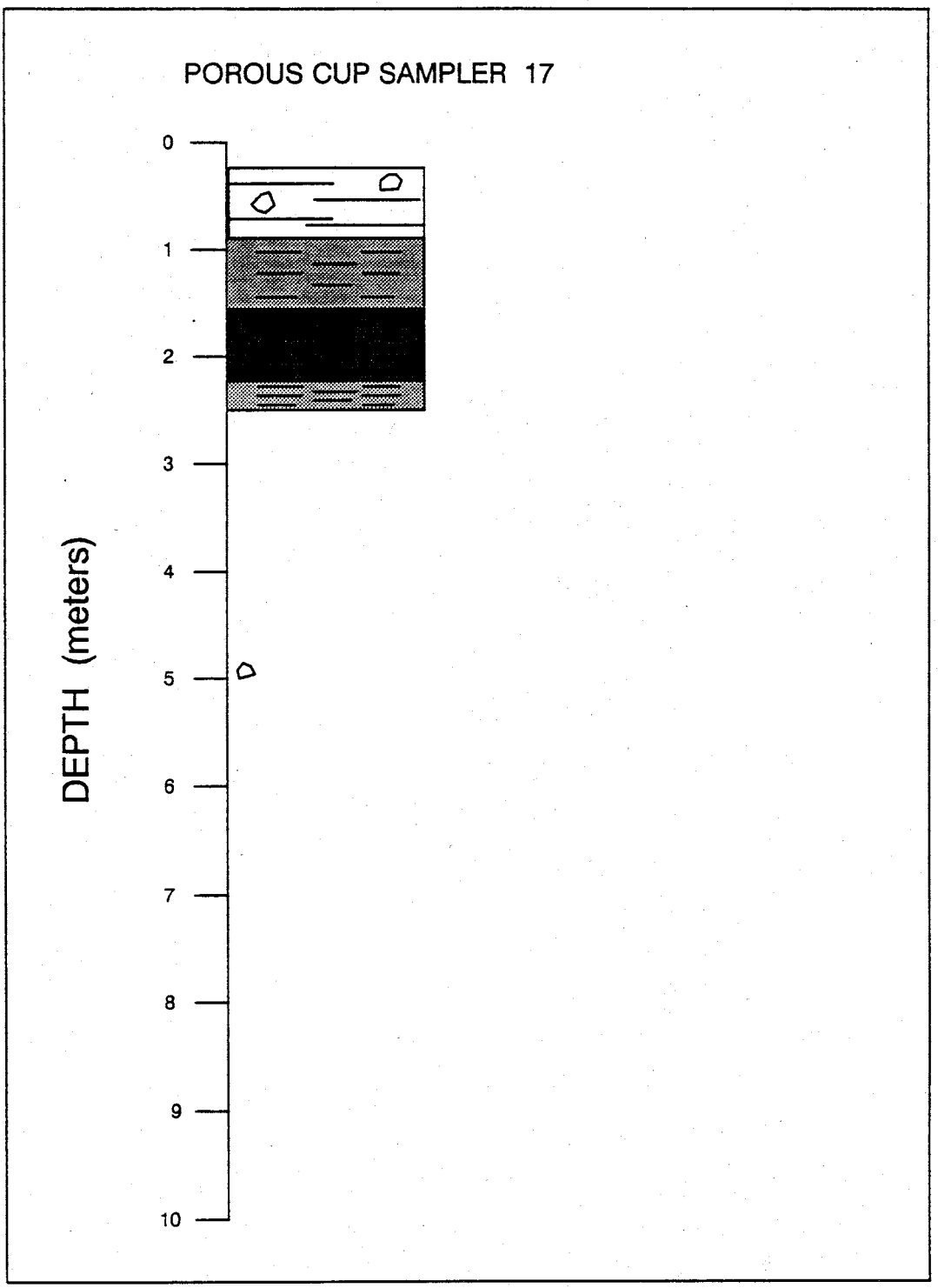
POROUS CUP SAMPLER 17
DEPTH (meters)
0
1
2
3
4
5
6
7
8
9
10

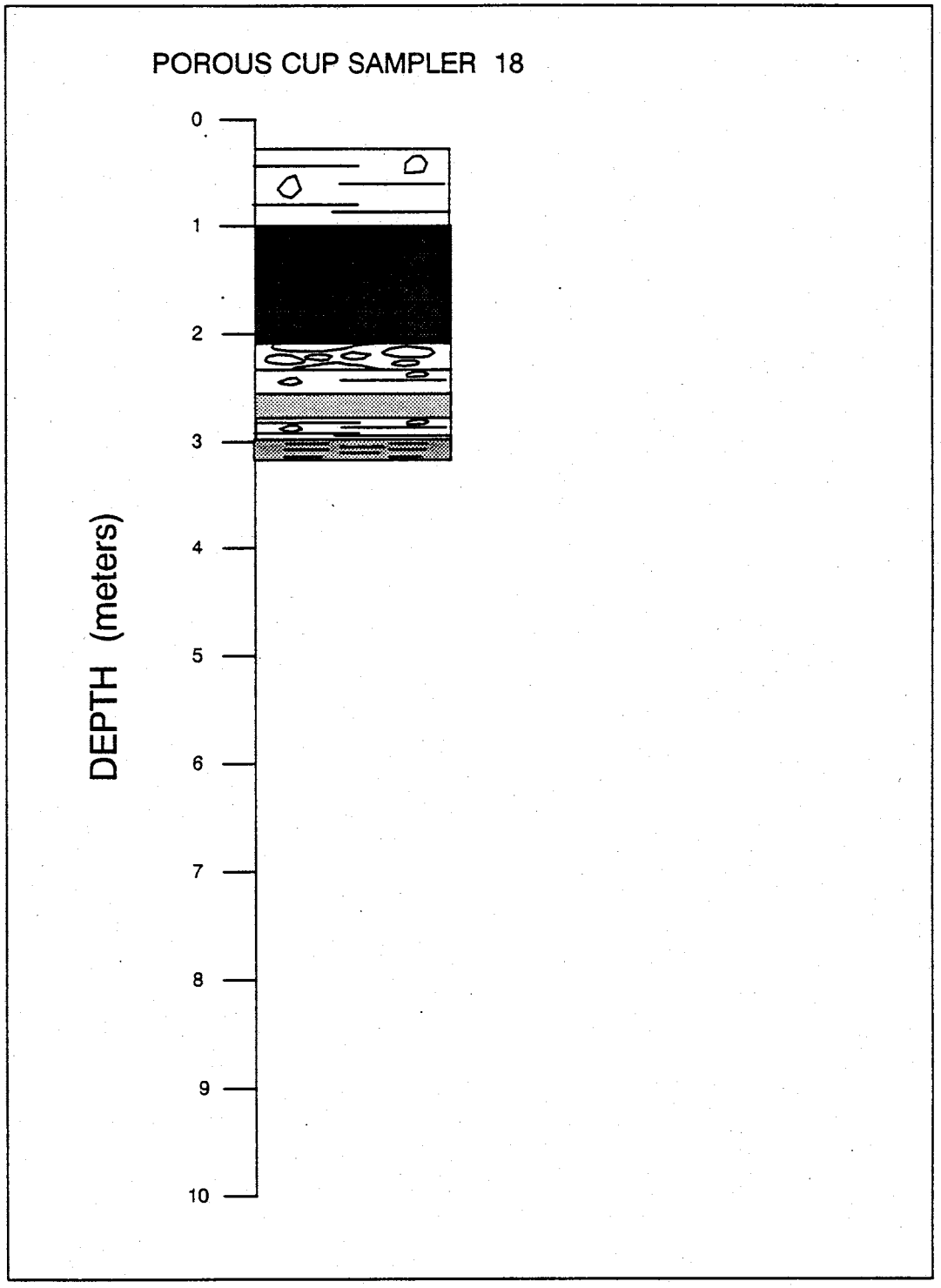
POROUS CUP SAMPLER 18
DEPTH (meters)
0
1
2
3
4
5
6
7
8
9
10

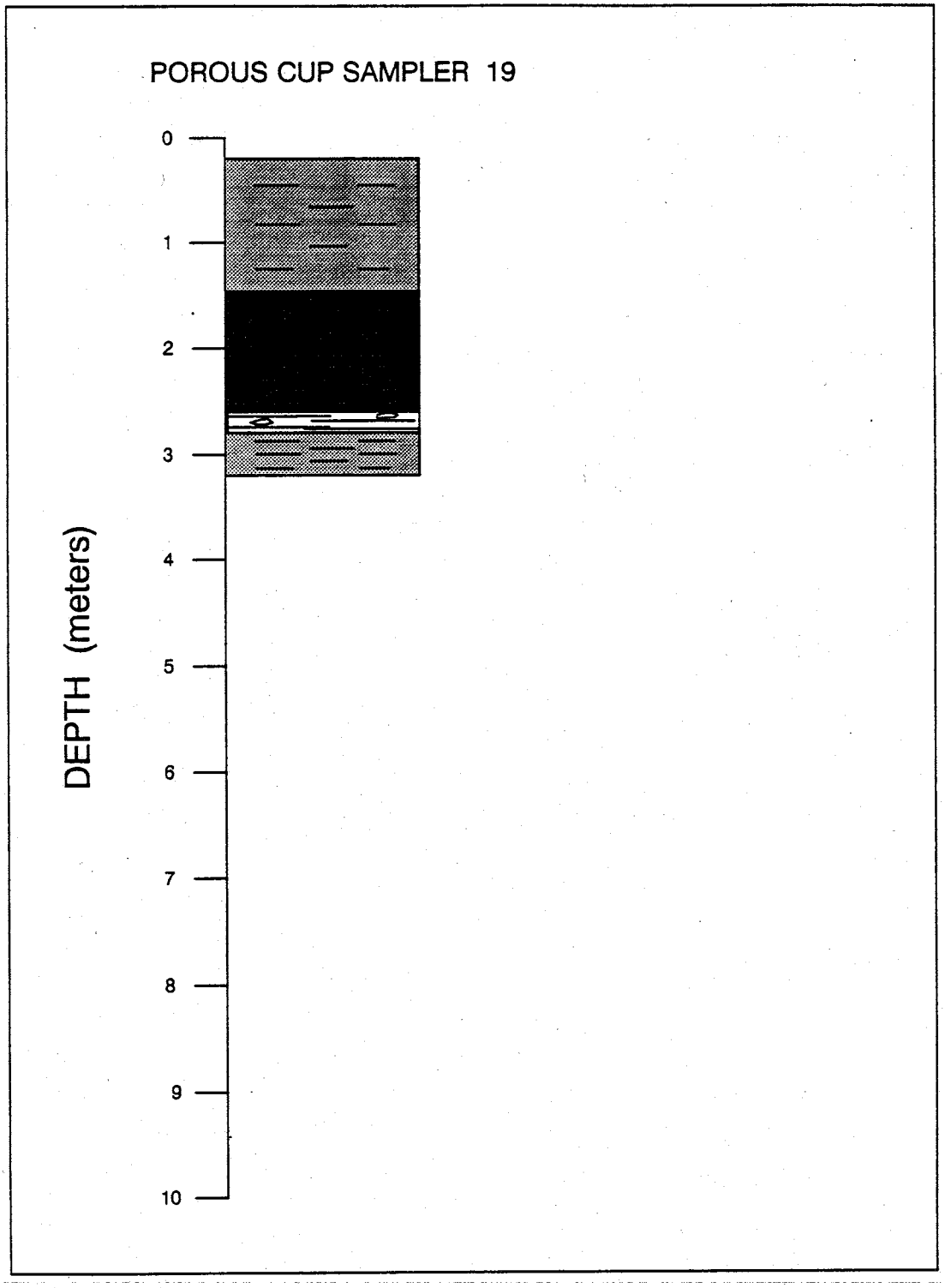
POROUS CUP SAMPLER 19
DEPTH (meters)
0
1
2
3
4
5
6
7
8
9
10

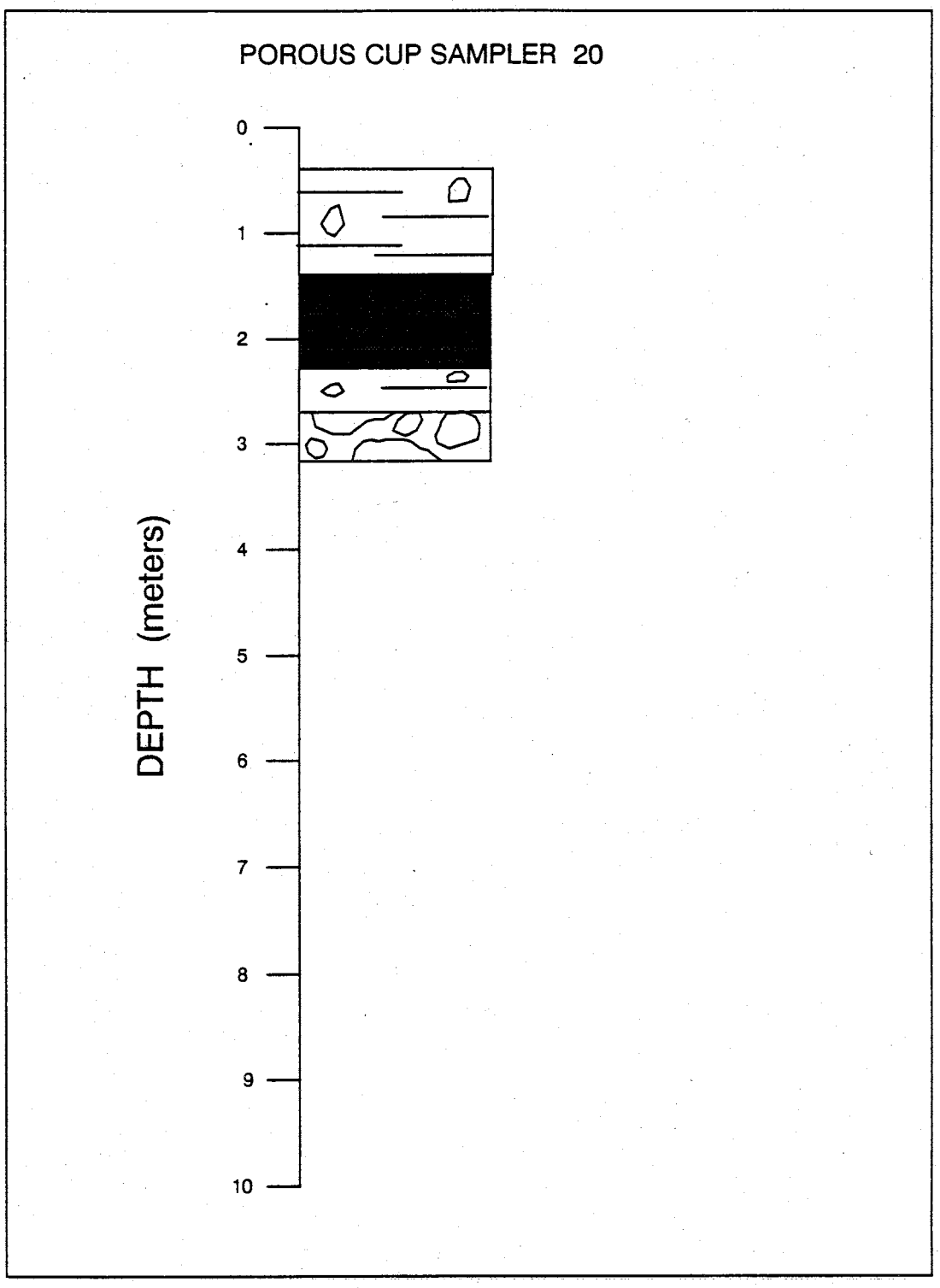
POROUS CUP SAMPLER 20
DEPTH (meters)
0
1
2
3
4
5
6
7
8
9
10

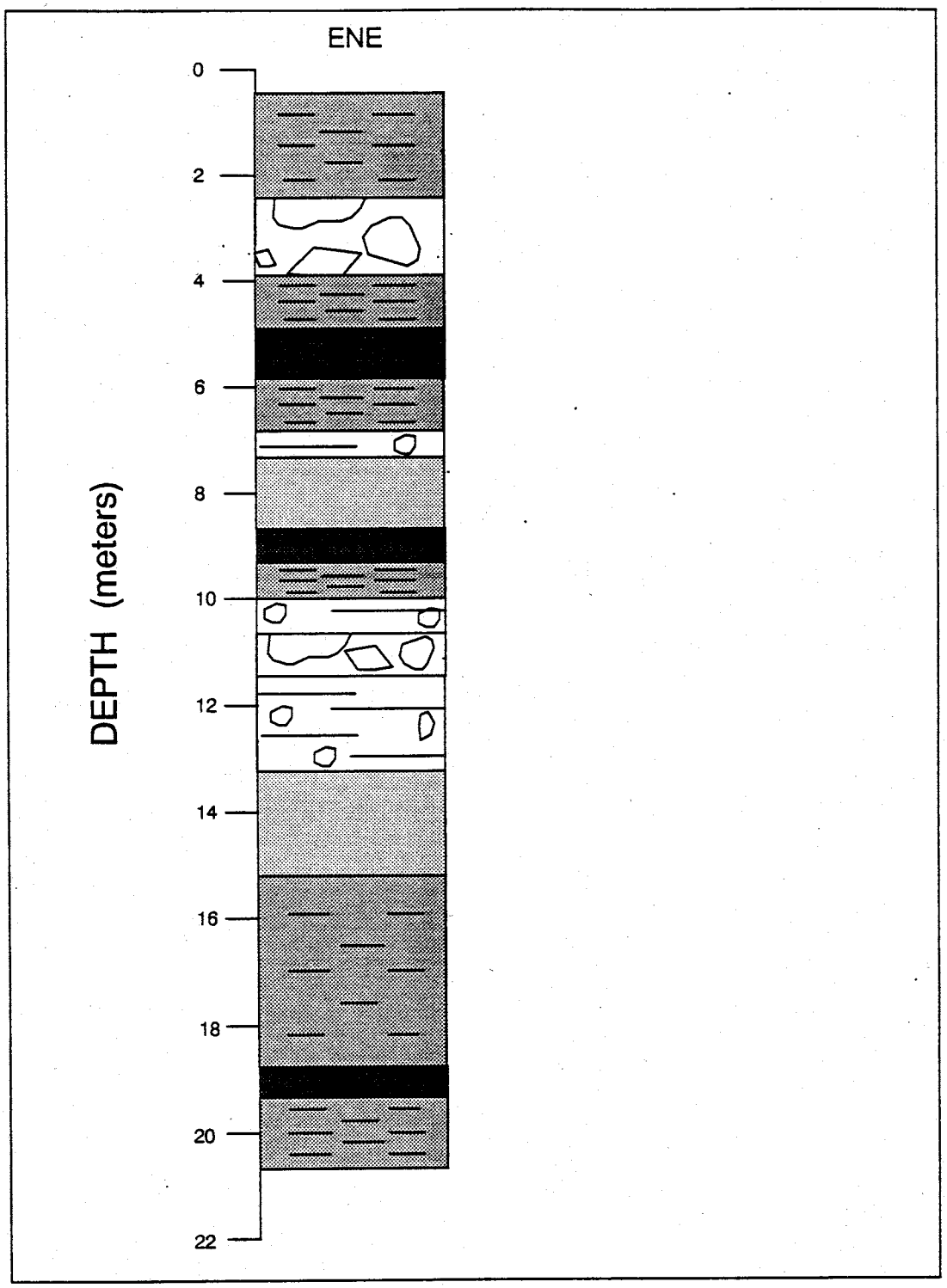
ENE
DEPTH (meters)
0
2
4
6
8
10
12
14
16
18
20
22

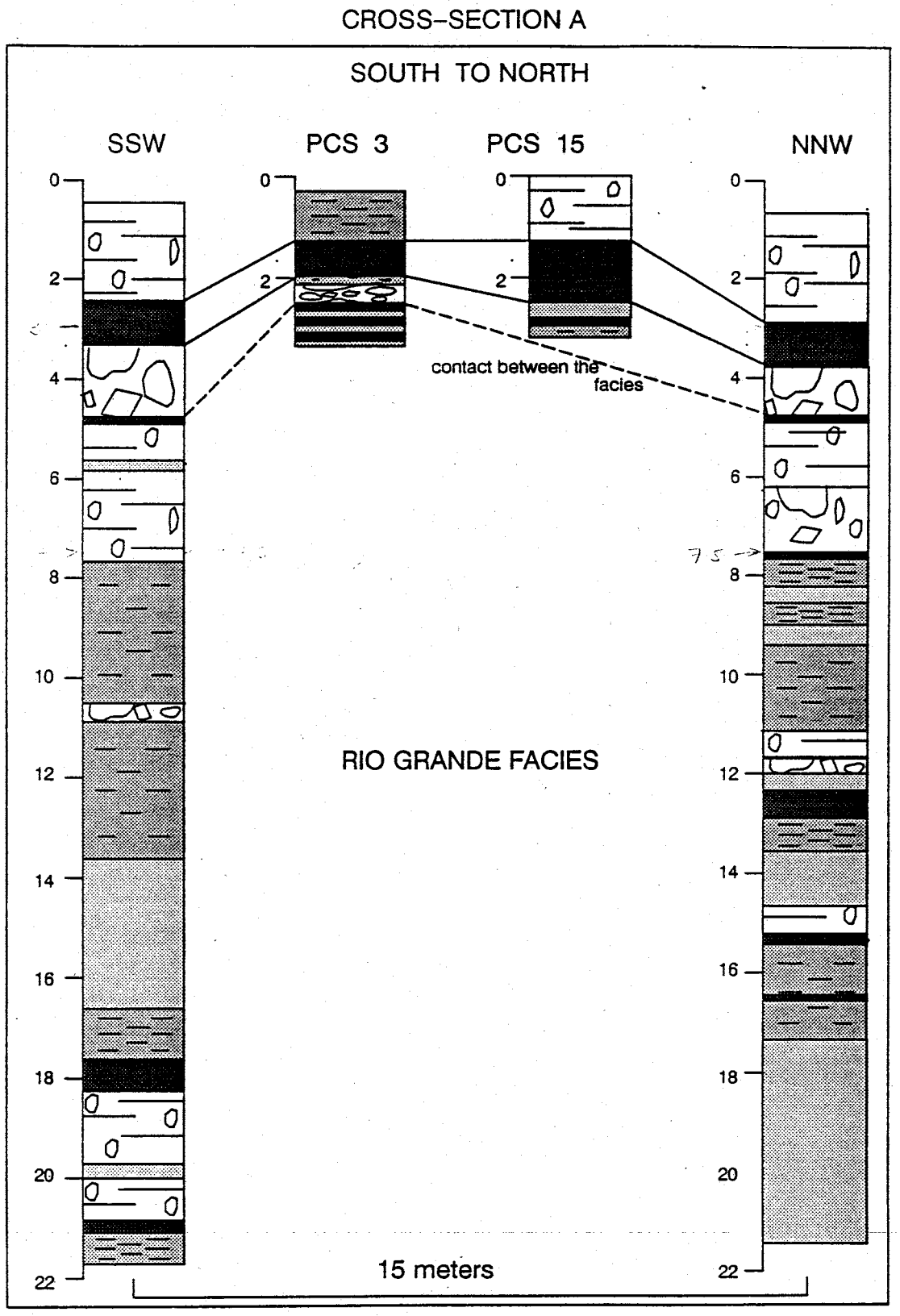
CROSS-SECTION A
SOUTH TO NORTH
SSW
PCS 3
PCS 15
NNW
0
2
4
6
8
10
12
14
16
18
20
22
contact between the facies
RIO GRANDE FACIES
15 meters

CROSS-SECTION B

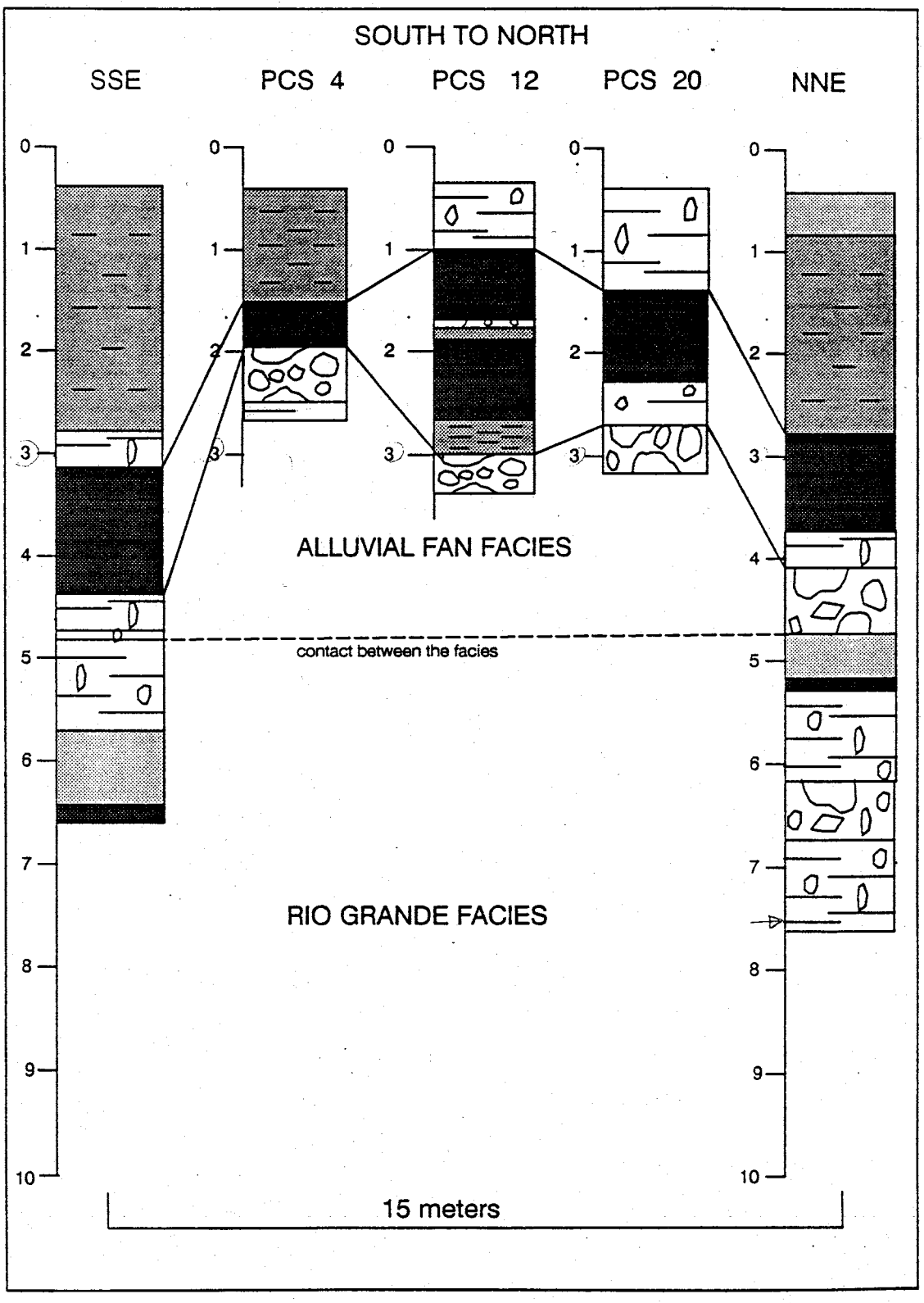

CROSS-SECTION C

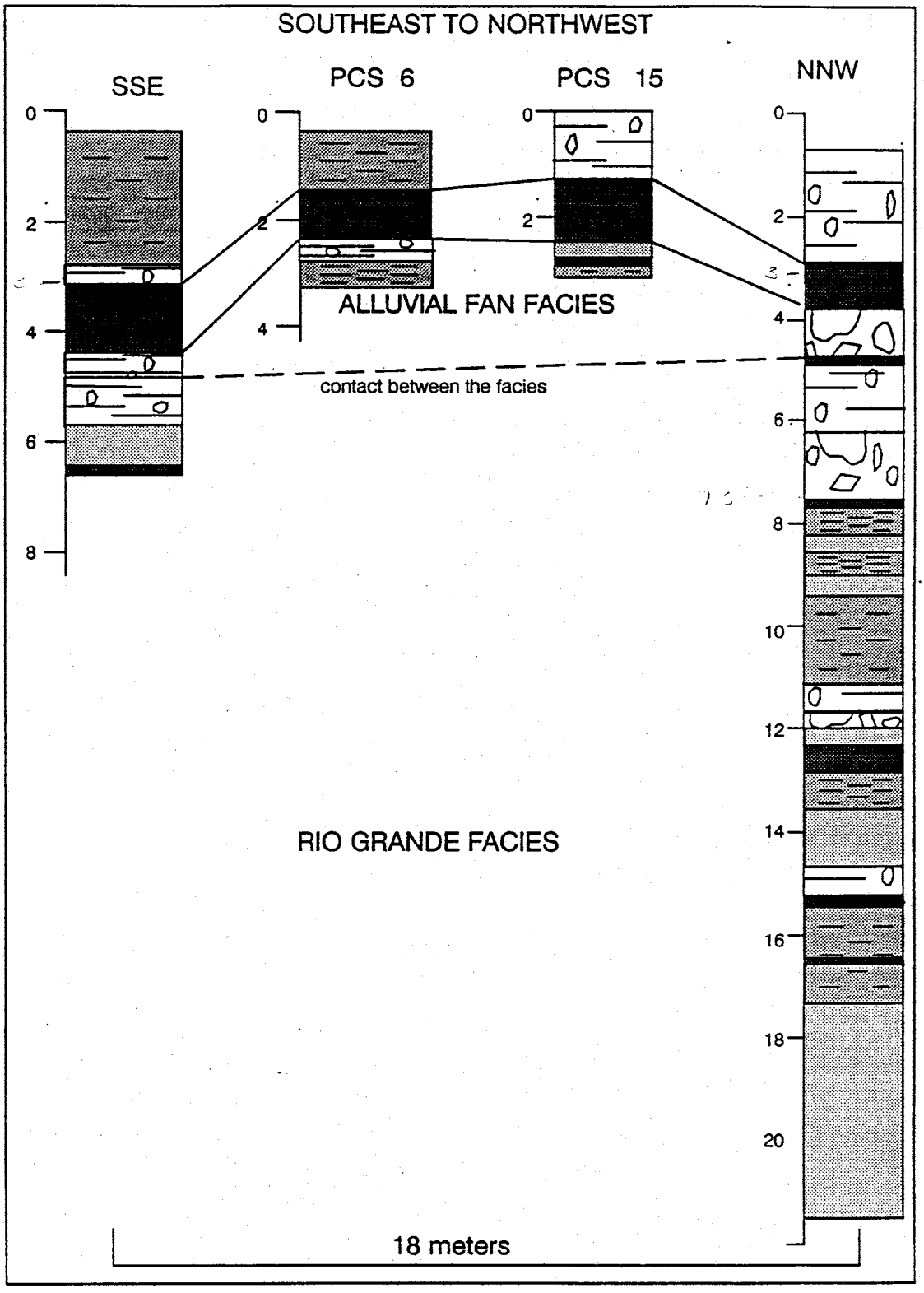

CROSS-SECTION D

SOUTHEAST TO NORTHWEST

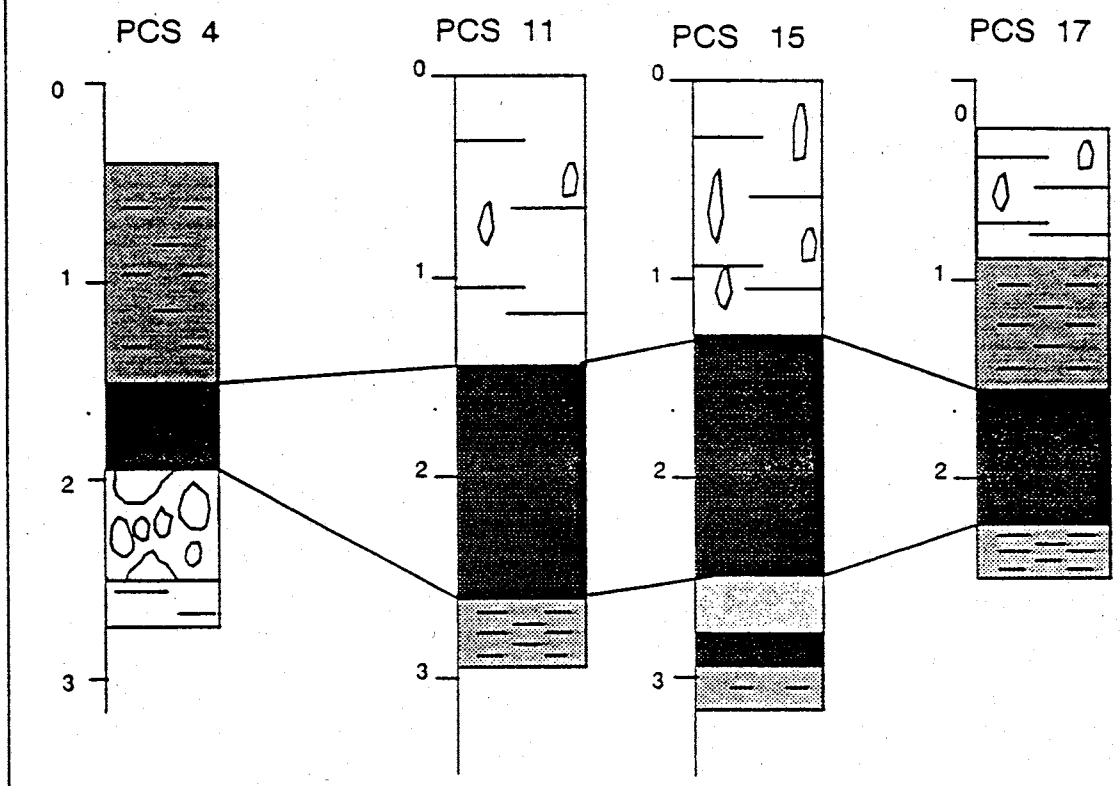

ALLUVIAL FAN FACIES

10 meters

CROSS–SECTION E

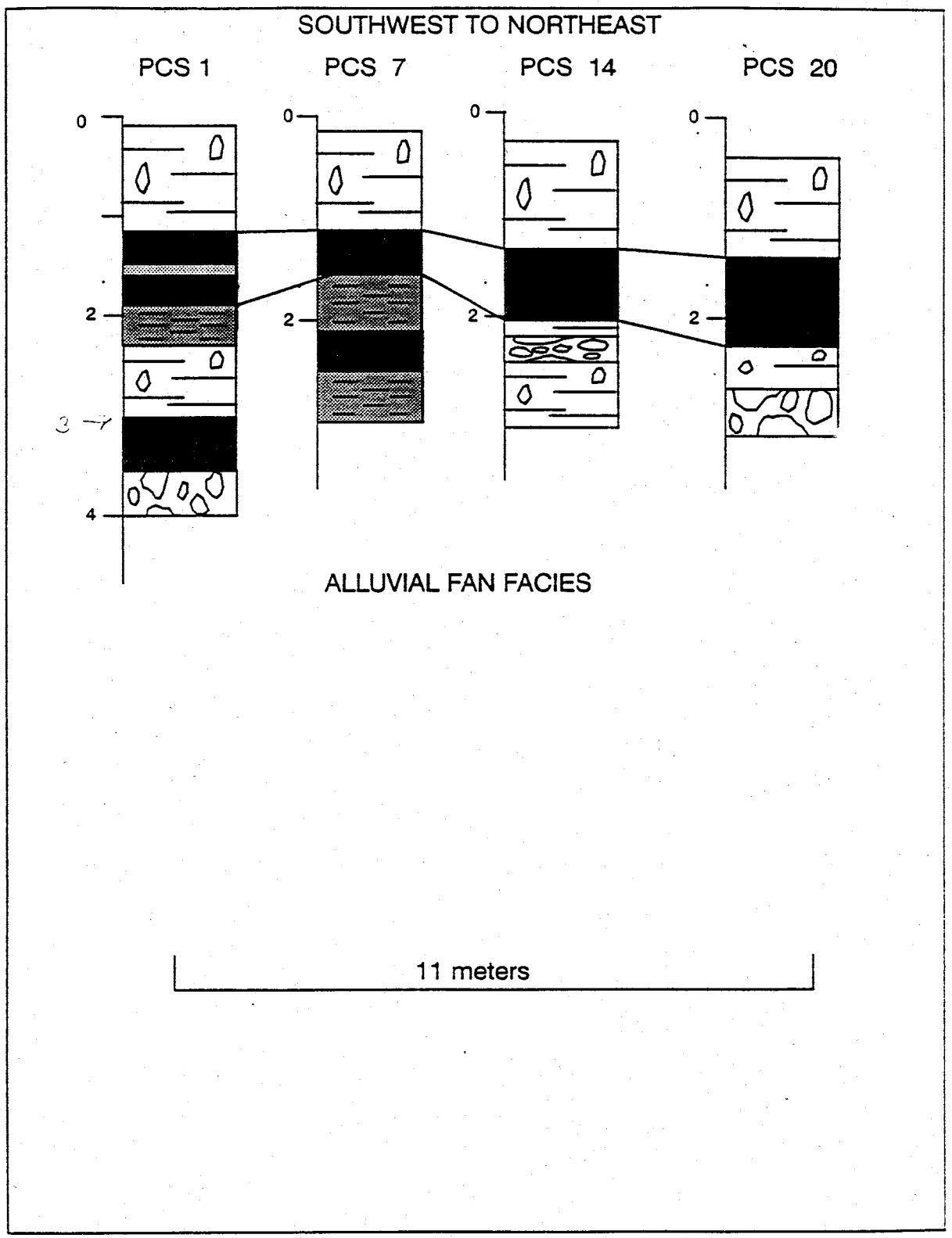

CROSS-SECTION F

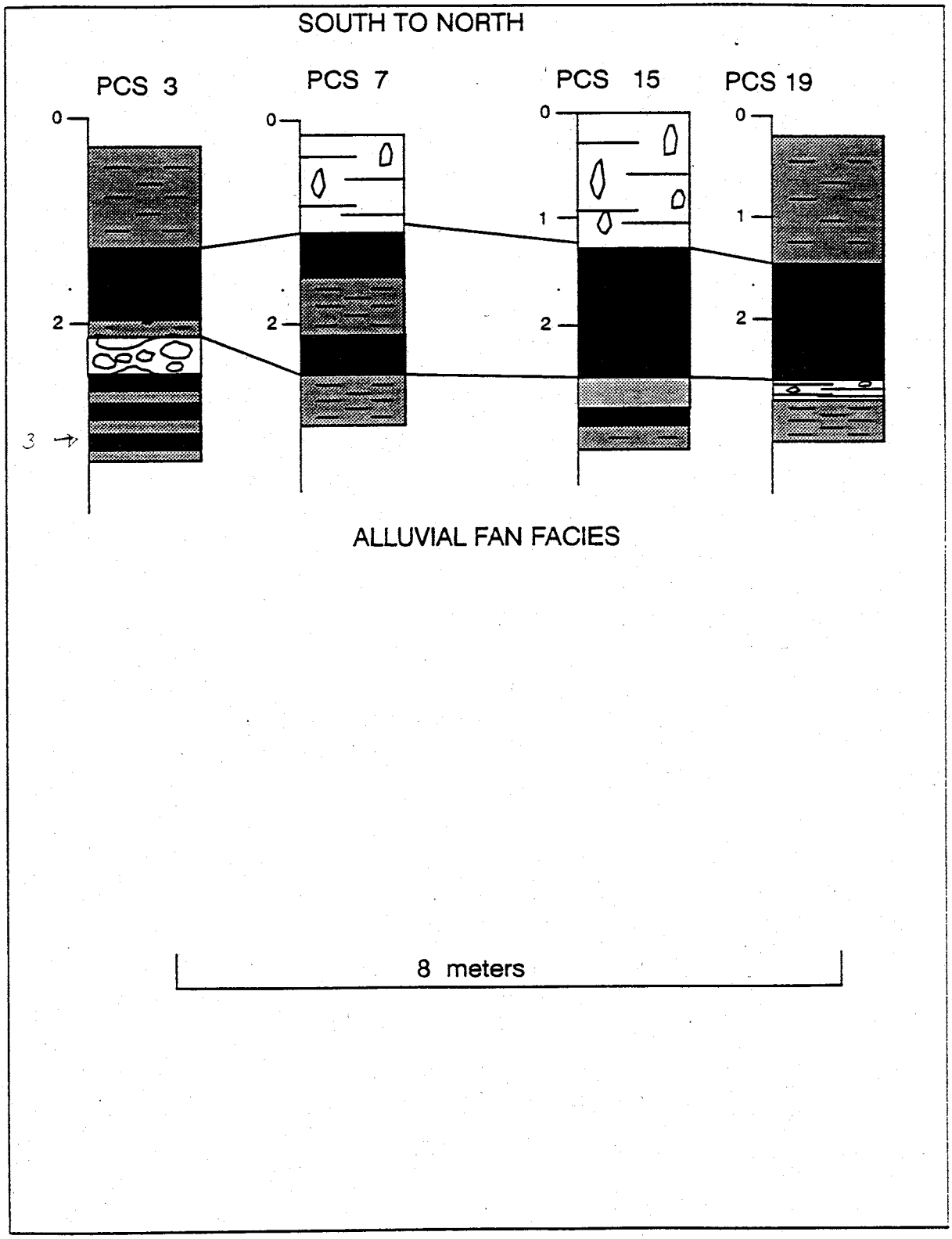

APPENDIX B. Borehole Geologic Logs (access tube stations)

BOREHOLE GEOLOGIC LOG

LOCATION: 15-15
DATUM EL: 1417.45
GND SURFACE EL: 1416.59

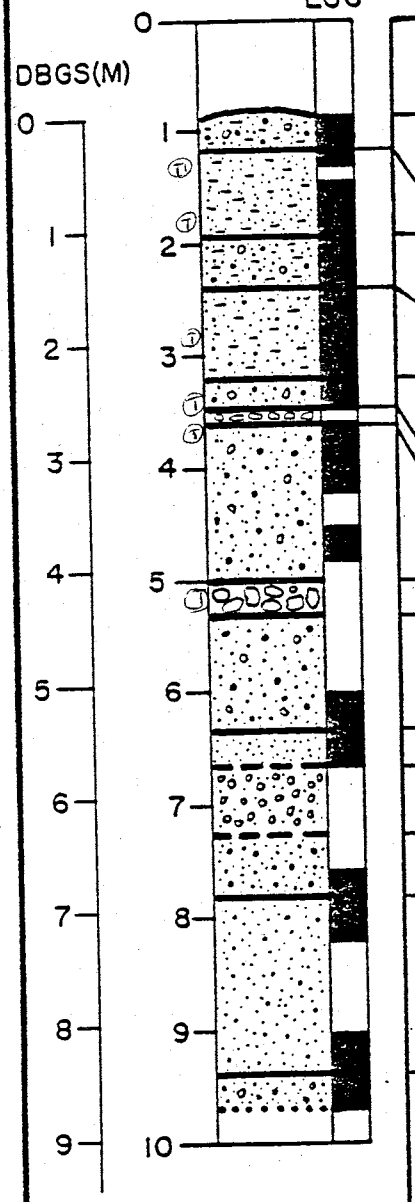

DESCRIPTION

Red brown fine-coarse angular sand, silt, 10% angular fine-medium pebbles

Red brown fine sand, silt

Red brown fine-coarse sand, silt, 5% rounded and angular medium pebbles

Red brown fine-medium sand, silt

Poorly sorted red brown fine-coarse sand, 20% rounded fine-coarse pebbles

Cobbles

Poorly sorted tan fine-coarse sand, 10-20% rounded fine-coarse pebbles

Cobbles

Poorly sorted tan fine-coarse sand, 10-20% rounded fine-coarse pebbles

Well sorted tan fine sand

Pebbles

Poorly sorted orange fine-coarse sand

Clean tan fine-medium subangular sand

Poorly sorted tan fine-coarse sand, 10% fine-coarse angular pebbles

BOREHOLE GEOLOGIC LOG

LOCATION: 12-12
DATUM EL: 1417.45
GND SURFACE EL: 1416.59

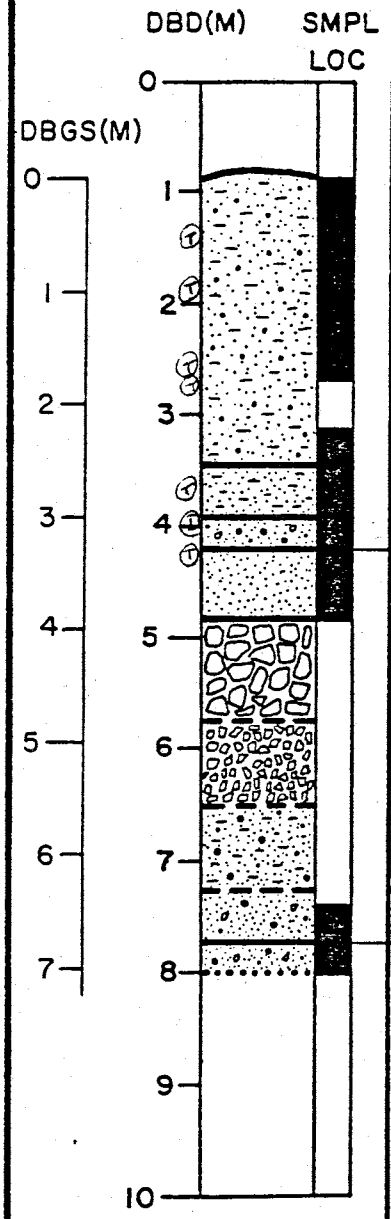

DESCRIPTION

Red brown fine-medium sand, silt

Brown-tan fine sand, silt

Poorly sorted red brown subangular fine-coarse sand, 10% subangular fine pebbles

Well sorted tan fine sand

Cobbles

Pebbles

Fine-coarse sand, silt, pebbles

Tan fine-coarse sand, 2% rounded medium pebbles (mostly fine sand)

Poorly sorted red brown subangular fine-coarse sand, 5% subangular medium pebbles

BOREHOLE GEOLOGIC LOG

LOCATION: 12-18
DATUM EL: 1417.45
GND SURFACE EL: 1416.59

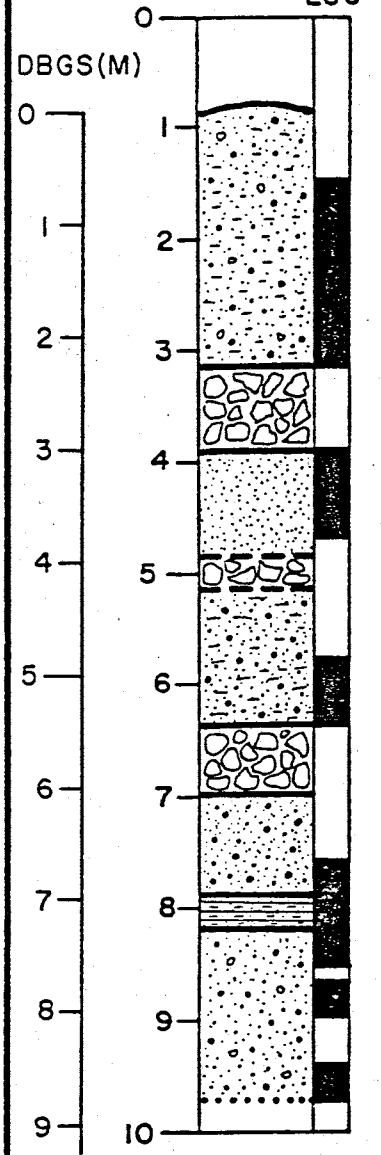

DESCRIPTION

Red brown angular fine-coarse sand, silt, 5% subangular fine pebbles

Cobbles

Well sorted tan fine sand

Cobbles

Poorly sorted red brown fine-coarse sand, silt, 40% subrounded fine pebbles

Cobbles

Clean yellow-tan fine-coarse subangular sand

Green clay, orange fine sand, silt

Clean tan subangular fine-coarse sand, 5% rounded fine pebbles

BOREHOLE GEOLOGIC LOG

LOCATION: 18-18
DATUM EL: 1417.45
GND SURFACE EL: 1416.59

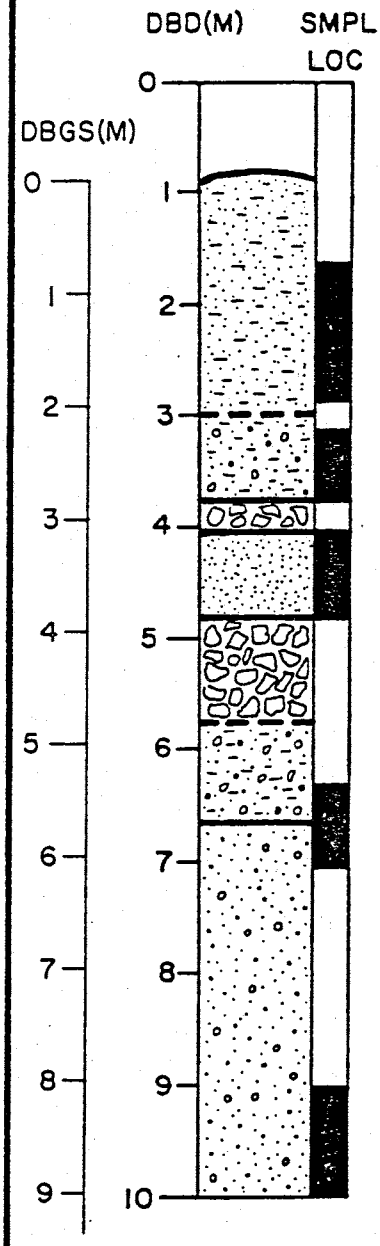

DESCRIPTION

Red brown fine sand, silt

Poorly sorted red brown fine-coarse sand, silt, 30% subangular fine-medium pebbles

Cobbles

Orange-tan fine sand

Cobbles

Poorly sorted red brown fine-coarse sand, silt, 40% subrounded fine-coarse pebbles

Clean tan fine-medium sand, 3-5% rounded fine pebbles

BOREHOLE GEOLOGIC LOG

LOCATION: 18-12
DATUM EL: 1417.45
GND SURFACE EL: 1416.59

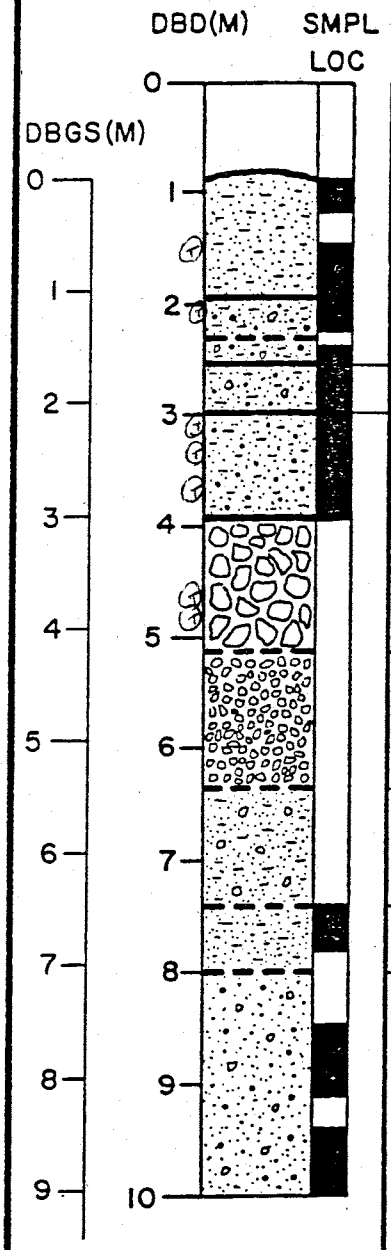

DESCRIPTION

Red brown fine sand, silt

Red brown fine-coarse sand, silt, 2% angular fine pebbles

Red brown poorly sorted fine-coarse sand, silt, 30% subangular fine-medium pebbles

Red brown fine-medium sand, silt, 10% rounded coarse pebbles

Red brown fine-medium sand, silt

Cobbles

Pebbles

Fine sand, silt, pebbles

Orange-tan fine sand, silt

Clean tan fine-coarse sand, 5% subangular medium pebbles

BOREHOLE GEOLOGIC LOG

LOCATION: 15-8
DATUM EL: 1417.45
GND SURFACE EL: 1417.18

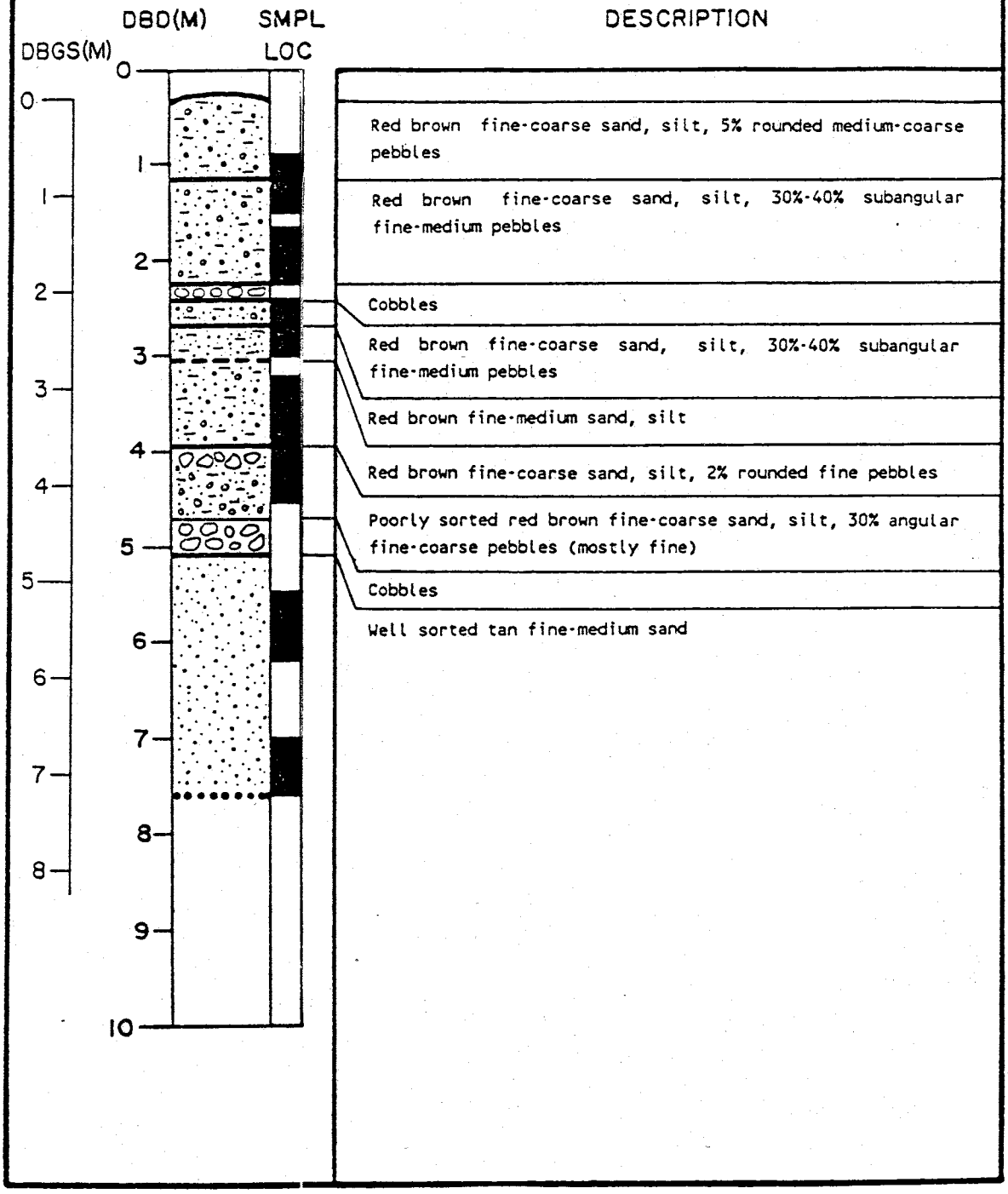

BOREHOLE GEOLOGIC LOG

LOCATION: 15-6
DATUM EL: 1417.45
GND SURFACE EL: 1417.16

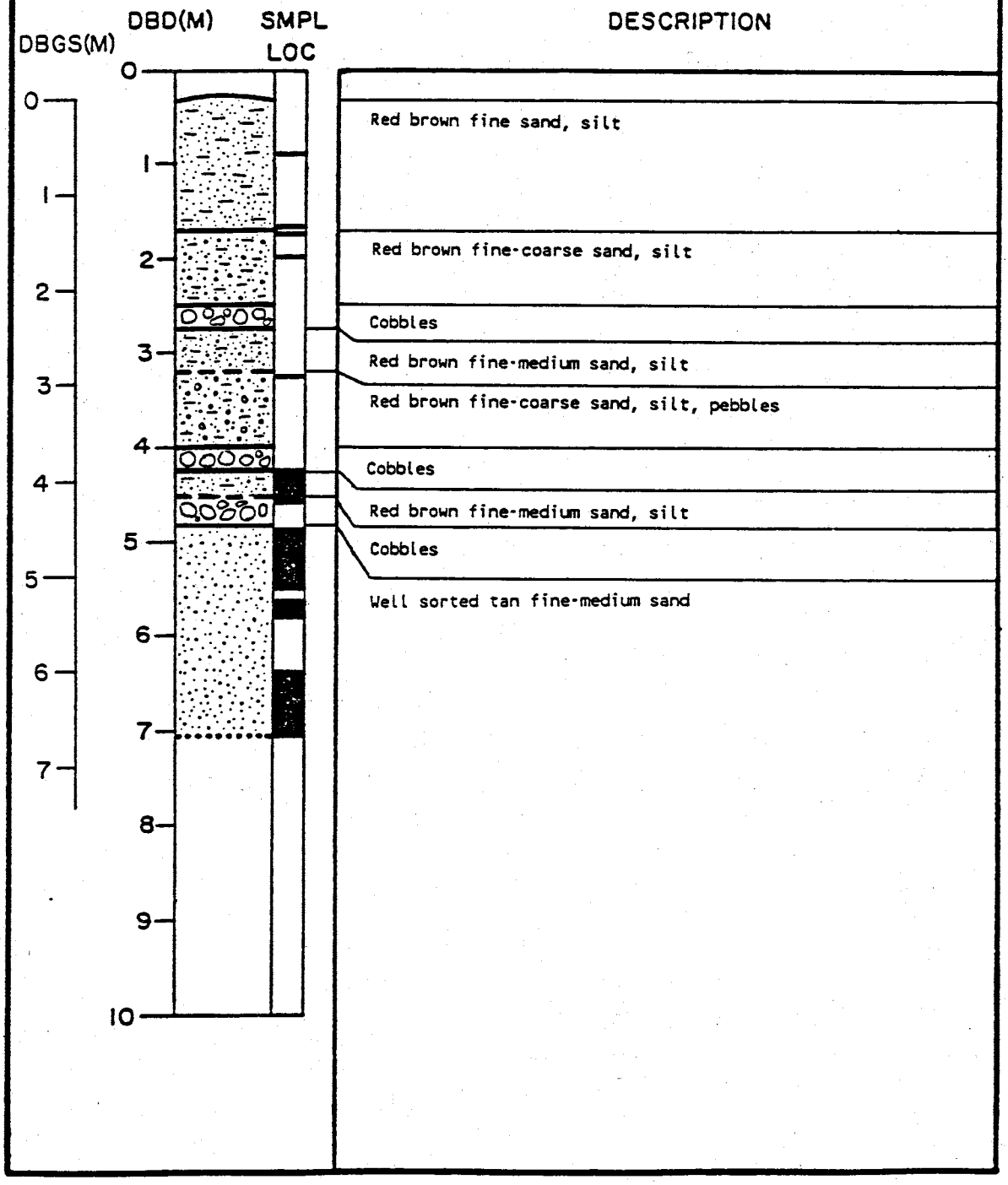

BOREHOLE GEOLOGIC LOG

LOCATION: 6-15
DATUM EL: 1417.45
GND SURFACE EL: 1417.16

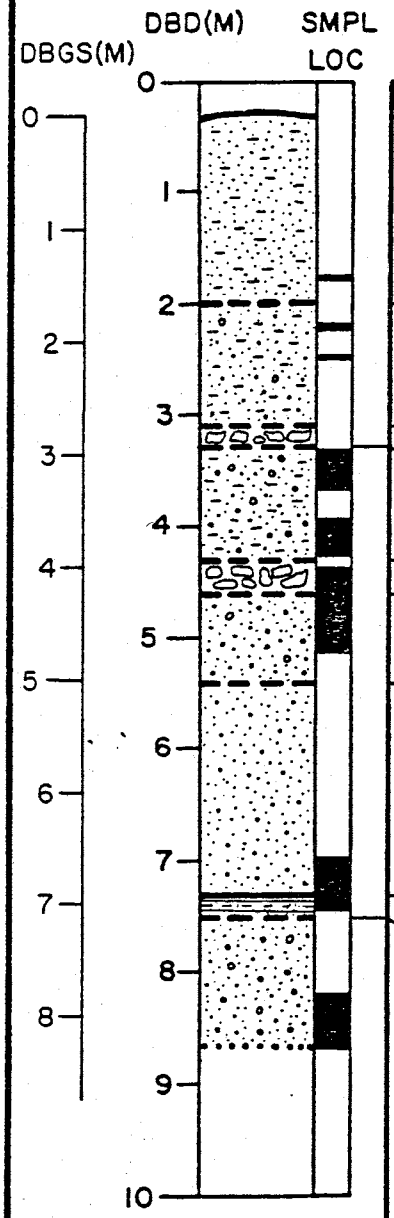

DESCRIPTION

Red brown fine sand, silt

Red brown fine-medium sand, silt, 3% angular fine-medium pebbles

Cobbles

Poorly sorted red brown subangular fine-coarse sand, silt 20% rounded fine-coarse pebbles

Cobbles

Poorly sorted tan subangular fine-coarse sand, 2% rounded medium pebbles

Well sorted tan fine-medium sand

Green clay, silt, fine sand

Poorly sorted tan fine-coarse sand, 15% rounded medium-coarse pebbles

BOREHOLE GEOLOGIC LOG

LOCATION: 8-15
DATUM EL: 1417.45
GND SURFACE EL: 1417.24

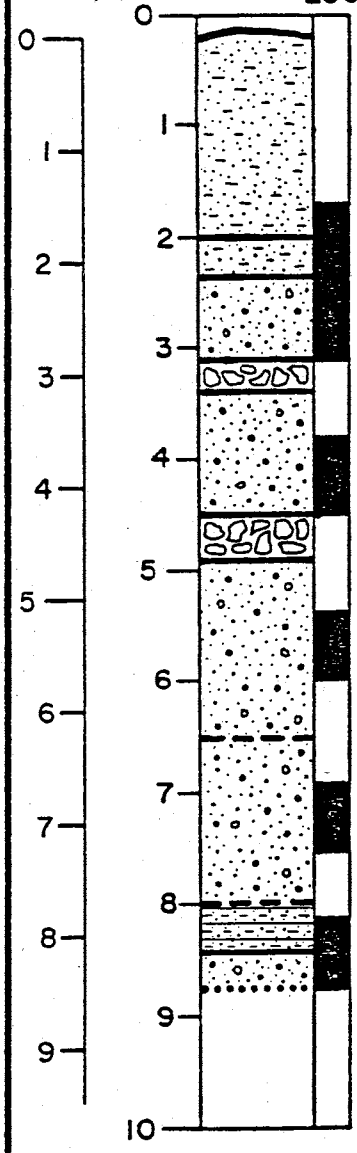

DESCRIPTION
Red brown fine sand, silt
Tan-brown fine-medium sand, silt
Red brown fine-coarse sand, 10% angular medium pebbles
Cobbles
Poorly sorted red brown subangular fine-coarse sand, 5% angular medium pebbles
Cobbles
Dark subangular - coarse sand, fine-medium sand, 10% rounded very coarse pebbles
Poorly sorted tan fine-coarse sand, 5% pebbles
Green clay, silt, fine-medium sand
Poorly sorted tan fine-coarse sand, 3% rounded fine pebbles

BOREHOLE GEOLOGIC LOG

LOCATION: 15-22
DATUM EL: 1417.45
GND SURFACE EL: 1417.06

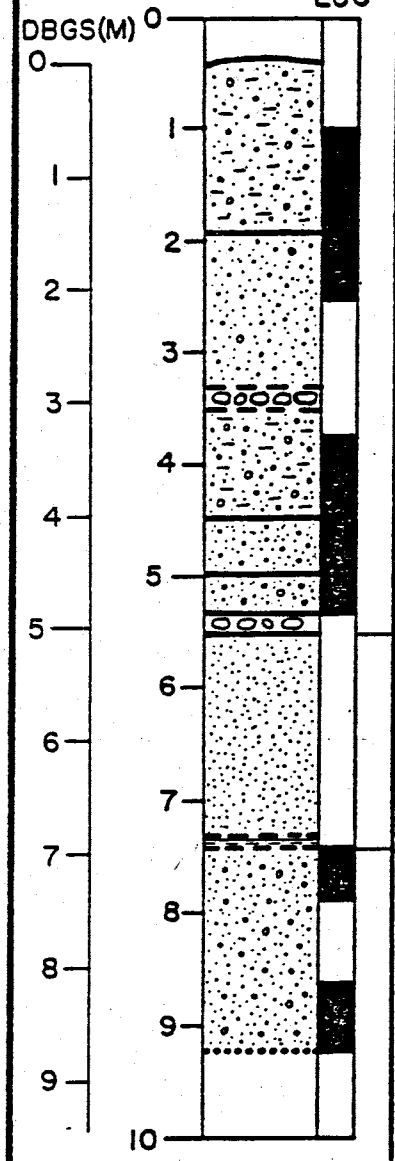

DESCRIPTION

Red brown fine-coarse sand, silt, 5% subrounded fine pebbles

Red brown fine-medium sand, 1% coarse pebbles

Cobbles

Poorly sorted red brown angular fine-coarse sand, silt, 20% rounded fine-coarse pebbles

Well sorted tan fine-medium sand

Tan fine-coarse sand, 2% subangular fine pebbles

Cobbles

Tan fine sand

Green clay

Poorly sorted tan fine-coarse subangular sand, 5% angular fine pebbles

BOREHOLE GEOLOGIC LOG

LOCATION: 15-23
DATUM EL: 1417.45
GND SURFACE EL: 1417.06

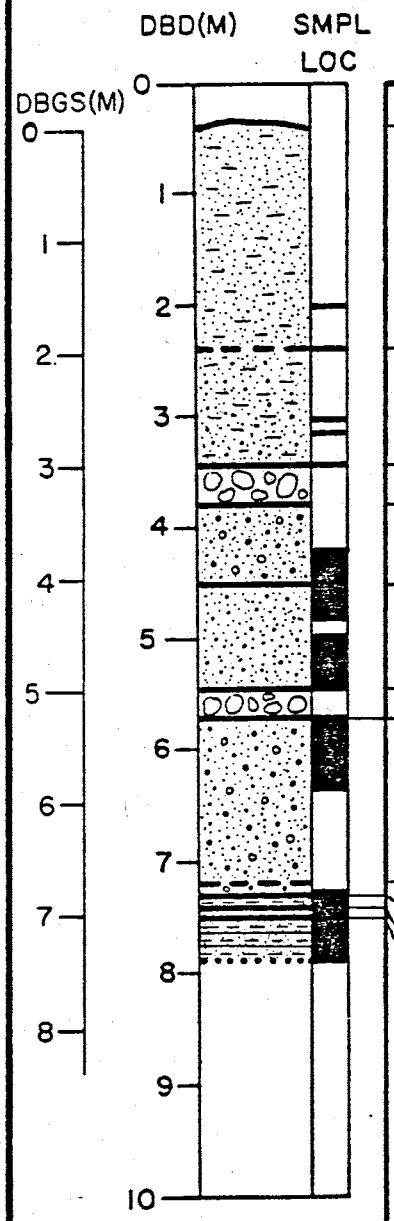

DESCRIPTION

Red brown fine sand, silt

Red brown fine-medium sand, silt

Cobbles

Clean brown subangular fine-coarse sand, 20% rounded fine-medium pebbles

Well sorted tan fine-medium sand

Cobbles

Poorly sorted tan subangular fine-coarse sand, 20% rounded fine-medium pebbles

Orange fine-coarse sand, 5% rounded fine pebbles

Green clay, orange fine sand, silt

Orange fine-coarse sand, silt, green clay, 5% fine pebbles

Green clay, fine-medium orange sand

BOREHOLE GEOLOGIC LOG

LOCATION: 25-25
DATUM EL: 1417.45
GND SURFACE EL: 1416.93

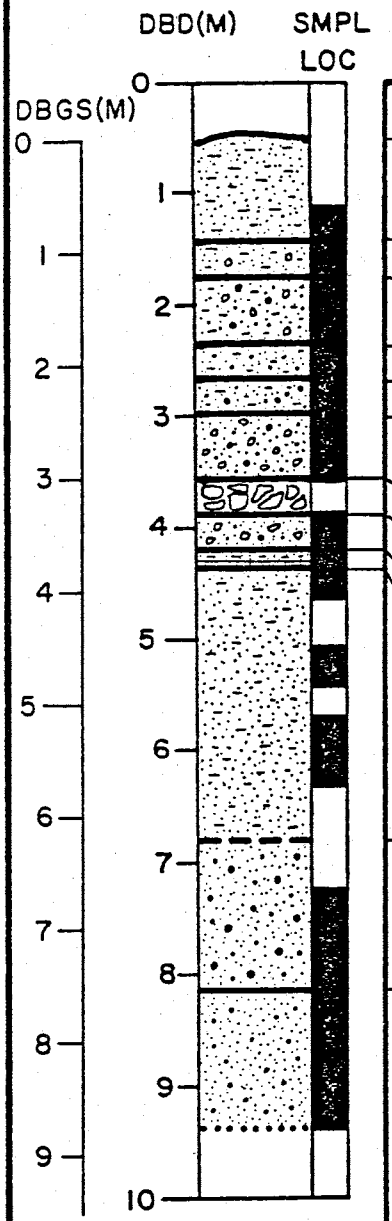

DESCRIPTION

Red brown fine sand, silt

Red brown fine sand, silt, 5% medium pebbles

Red brown fine-coarse sand, silt, 10% subangular fine-medium pebbles

Red brown fine-medium sand, silt

Red brown fine-coarse sand, silt

Poorly sorted red brown subangular fine-coarse sand, 60% subangular fine-coarse pebbles

Cobbles

Poorly sorted red brown subangular fine-coarse sand, 60% subangular fine-coarse pebbles

Red brown fine sand, silt, clay

Well sorted red brown fine sand, silt

Clean tan fine-coarse sand

Well sorted tan fine-medium sand

BOREHOLE GEOLOGIC LOG

LOCATION: 22-15
DATUM EL: 1417.45
GND SURFACE EL: 1416.92

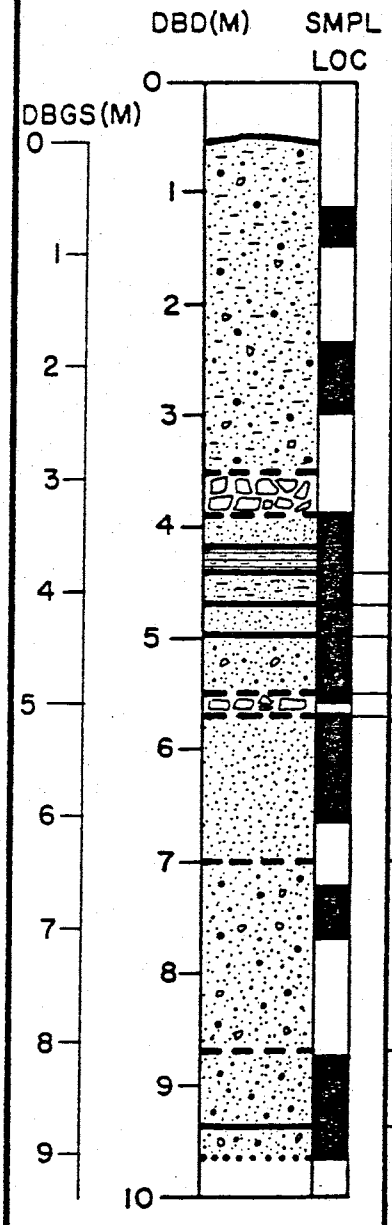

DESCRIPTION

Red brown fine-coarse sand, silt, 10% subangular pebbles

Cobbles

Well sorted tan fine sand

Green clay, tan fine sand, silt

Orange fine sand, silt

Well sorted tan fine sand

Poorly sorted tan fine-medium sand, 2% fine rounded pebbles

Cobbles

Well sorted tan fine sand

Poorly sorted fine-coarse tan sand, 20% rounded medium pebbles

Tan fine-coarse sand

Poorly sorted tan subangular fine-coarse sand, 15% subangular medium-coarse pebbles

BOREHOLE GEOLOGIC LOG

LOCATION: 24-15
DATUM EL: 1417.45
GND SURFACE EL: 1416.85

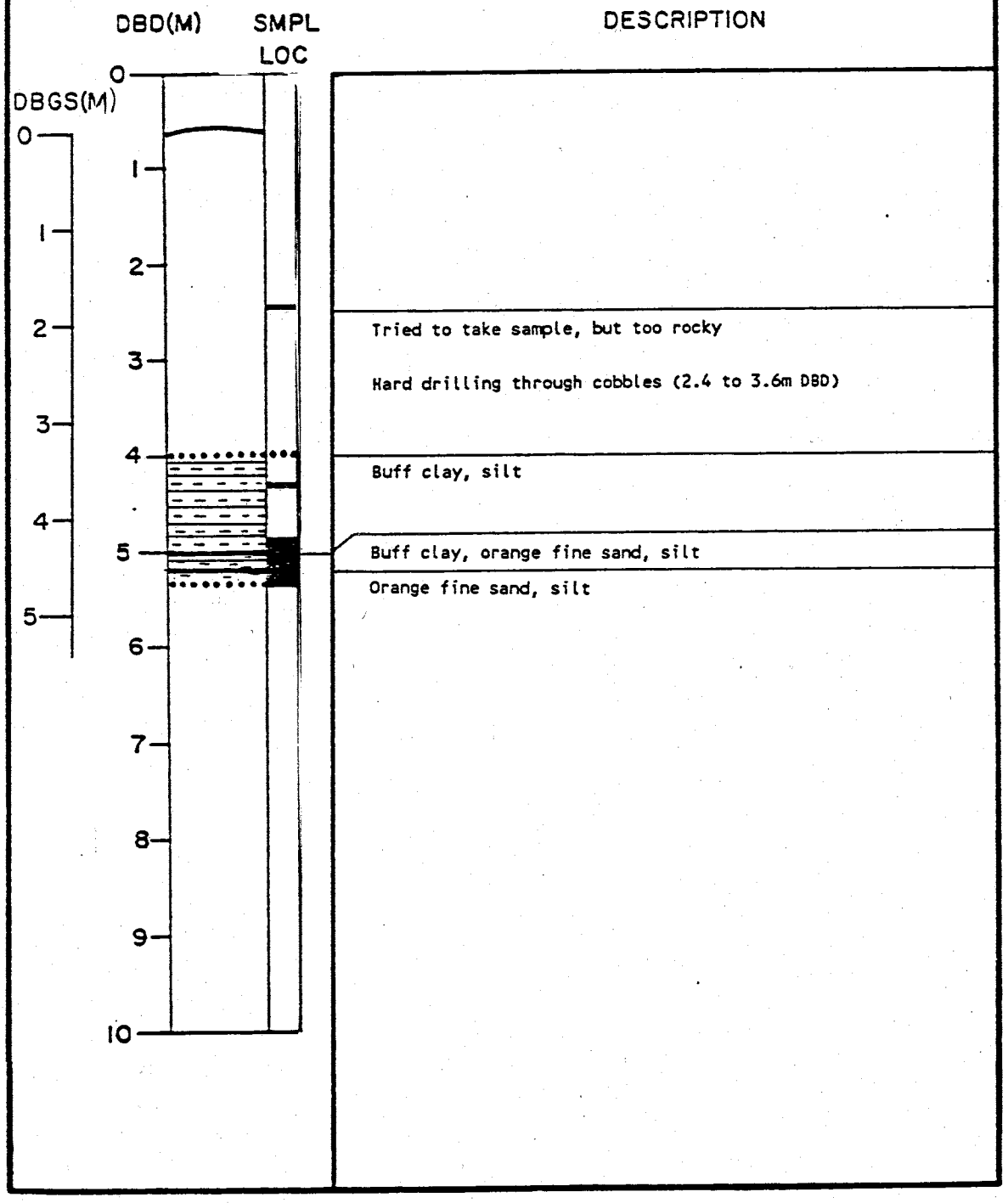

BOREHOLE GEOLOGIC LOG

LOCATION: 28-15
DATUM EL: 1417.45
GND SURFACE EL: 1416.80

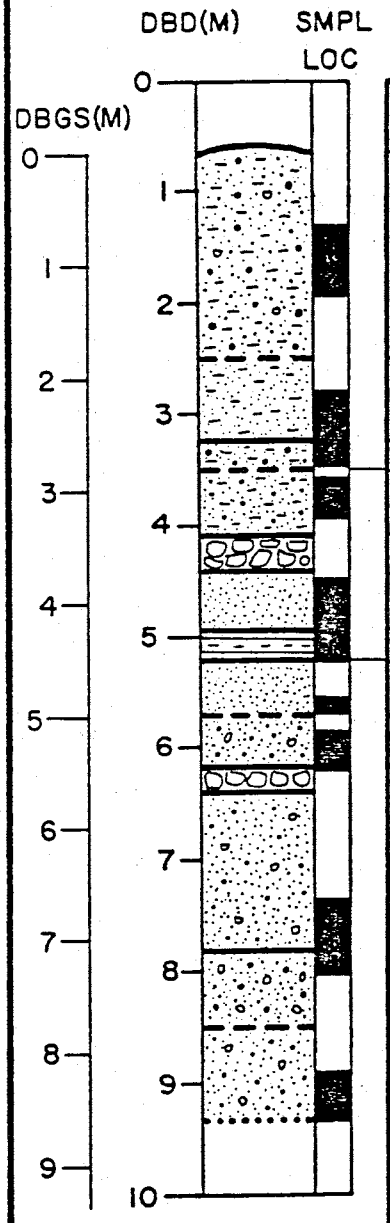

DESCRIPTION

Red brown fine-coarse sand, silt, 10% rounded fine-coarse pebbles

Red brown fine sand, silt

Red brown fine-coarse sand, silt

Red brown fine-medium sand, silt

Cobbles

Well sorted tan fine sand

Buff clay, silt

Well sorted tan fine sand

Tan subangular fine-medium sand, 5% rounded fine pebbles

Cobbles

Tan subangular fine-medium sand, 5% rounded fine pebbles

Tan angular fine-coarse sand, 25% angular and rounded medium pebbles

Tan subangular fine-medium sand, 5% rounded fine pebbles

APPENDIX C. Moisture Content Profiles

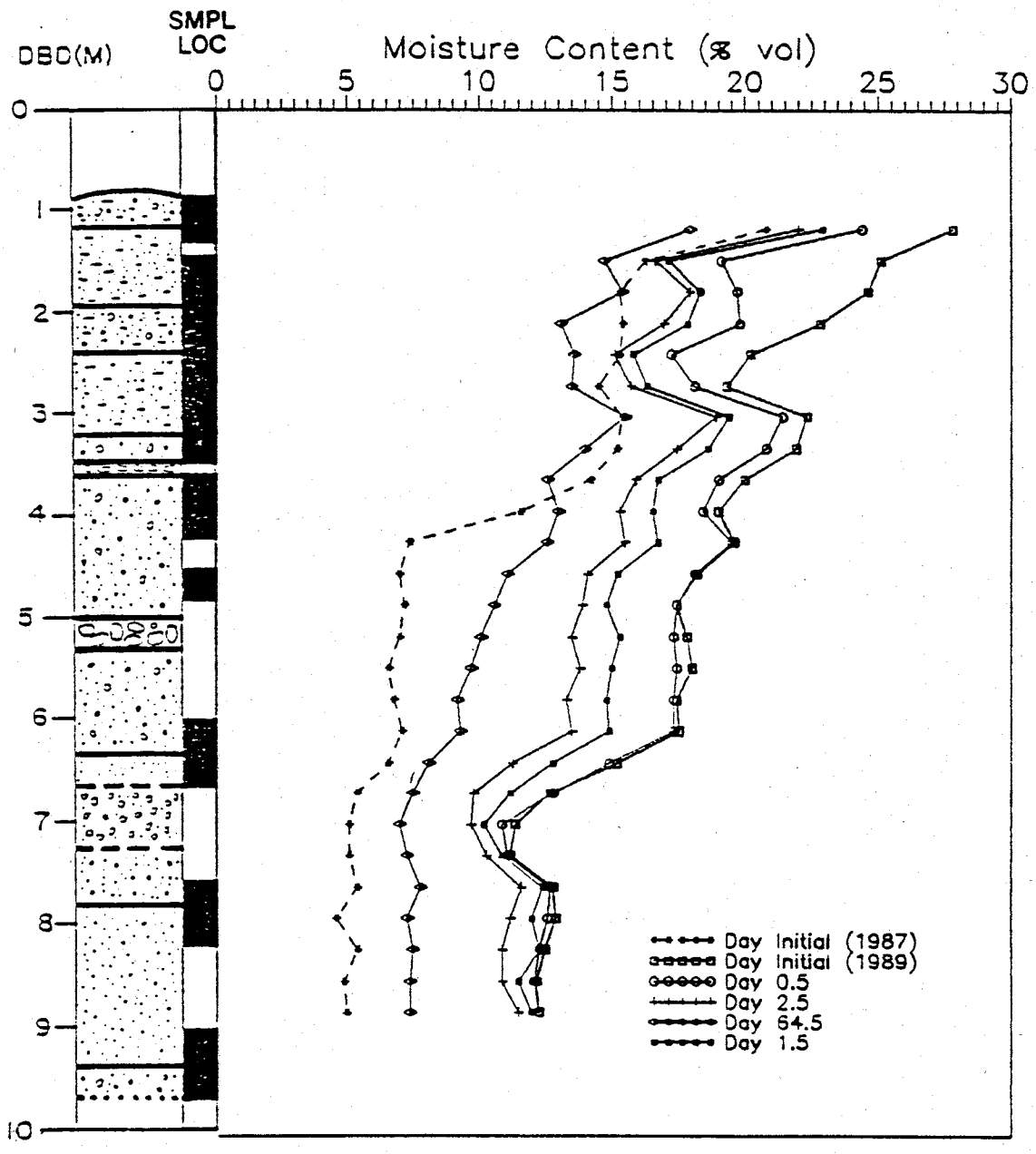

Moisture Content Distribution--Initial and Drainage Station 15-15.

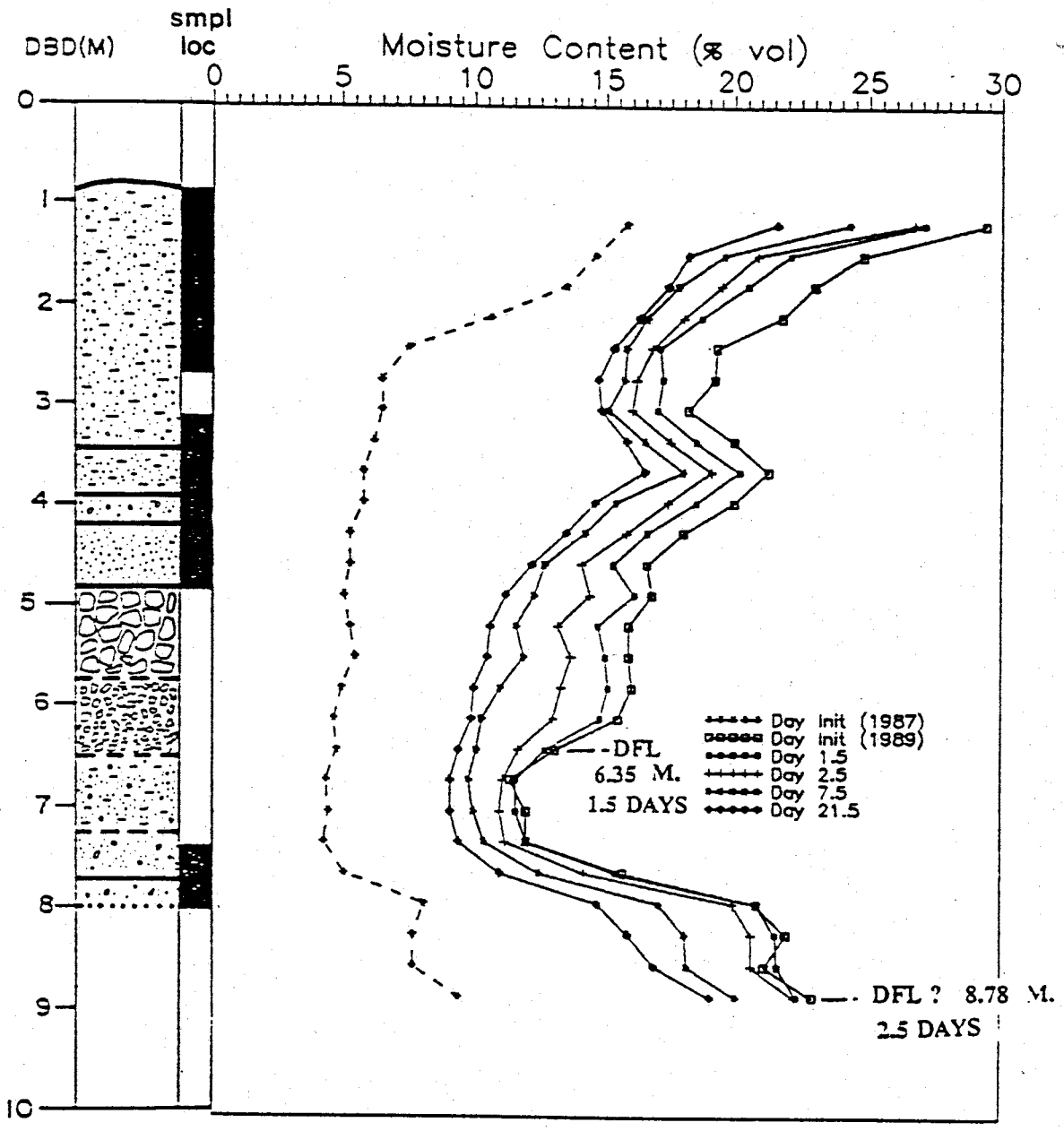

Moisture Content Distribution--Initial and Drainage Station 12-12.

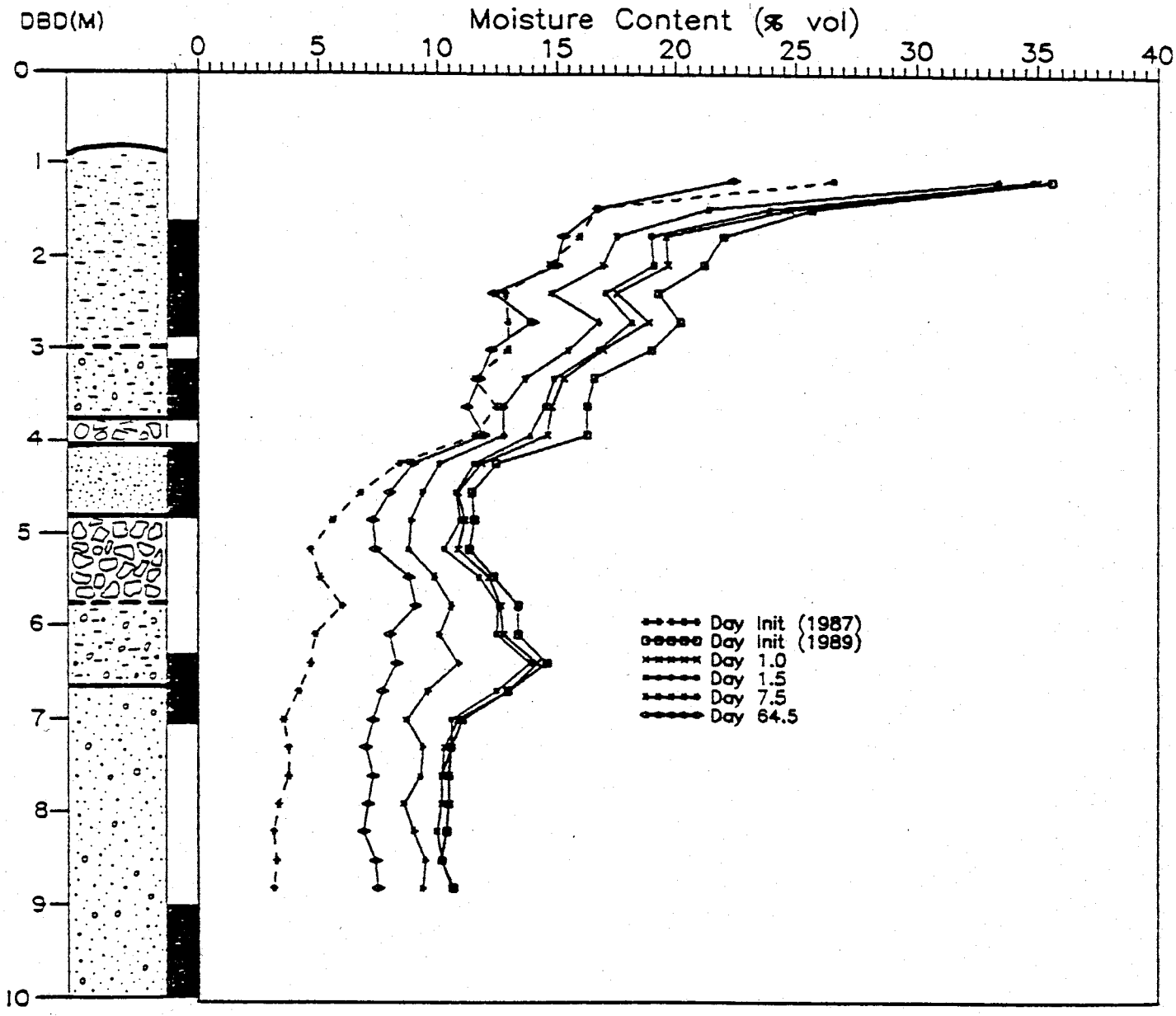

Moisture Content Distribution--Initial and Drainage Station 18-18.

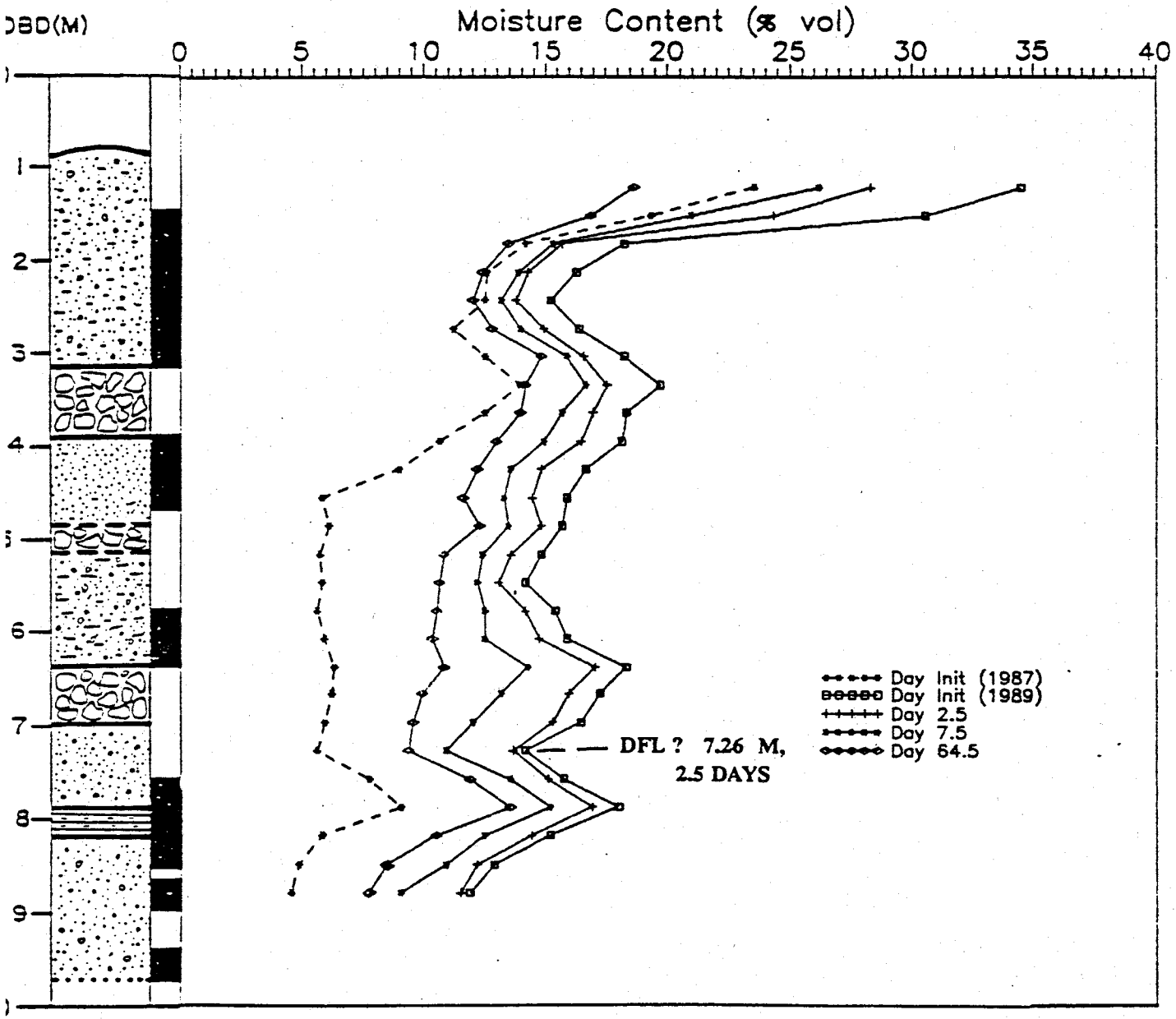

Moisture Content Distribution--Initial and Drainage
Station 12-18.

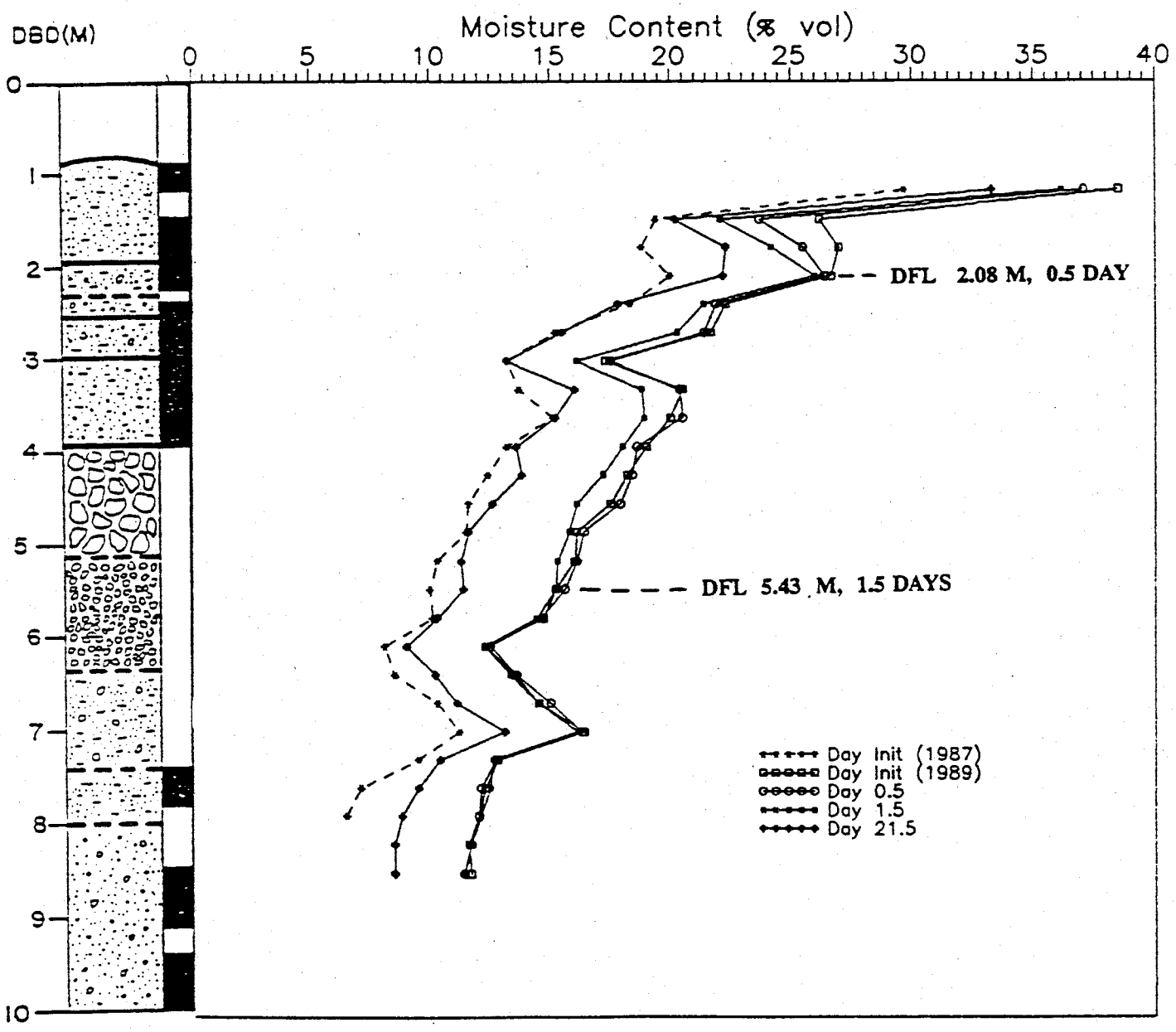

Moisture Content Distribution--Initial and Drainage Station 18-12.

APPENDIX D. ADDITIONAL TABLES

Station/ tensiometer number		Depth below datum (m)	Station/ tensiometer number		Depth below datum (m)
2–15 Nest A	1	0.75	**6–15 Nest A**	1	1.33
	2	1.31		2	1.82
	3	2.51		4	2.61
	4	3.61		5	2.96
	5	4.47		6	3.59
	6	5.25		7	4.16
Nest B	1	0.79	**5–25 Nest A**	1	0.88
	2	1.32		2	1.32
	3	2.21		3	2.42
	4	3.61		4	2.83
	5	4.30		5	3.30
	6	5.33		6	4.34
5–5 Nest A	1	0.71		7	5.31
	2	1.23	**Nest B**	1	0.84
	3	2.05		2	1.23
	4	2.69		3	1.81
	5	3.15		4	2.58
	6	4.10		5	3.29
	7	5.16		6	4.39
Nest B	1	0.68		7	5.28
	2	1.14	**15–23 Nest A**	1	1.58
	3	2.35		3	2.10
	4	2.85		4	2.82
	5	3.14		5	3.16
	6	4.15		6	3.81
	7	5.24		7	4.33

Station / tensiometer number		Depth below datum (m)	Station / tensiometer number		Depth below datum (m)
15–2 Nest A	1	0.95	**8–15 Nest A**	1	0.82
	2	1.44		2	1.28
	3	1.93		3	2.19
	4	2.94		4	2.78
	5	3.71		5	3.26
	6	4.54		6	3.80
Nest B	1	0.94		7	4.12
	2	1.37		8	5.29
	3	2.24	**Nest B**	1	0.86
	4	3.03		2	1.35
	5	3.55		3	2.29
	6	4.00		4	3.31
	7	5.12		5	3.27
15–8 Nest A	1	0.84		6	3.77
	2	1.29		7	4.15
	3	2.31		8	5.24
	4	3.45	**15–22 Nest A**	1	1.01
	5	4.21		2	1.52
	7	5.24		3	2.50
Nest B	1	0.94		4	3.23
	2	1.26		5	3.92
	3	1.71		6	3.95
	4	3.35		7	4.90
	5	3.97	**Nest B**	1	0.92
	6	4.70		2	1.34
	7	5.26		3	2.44
				4	3.47
				5	3.77

Station/ tensiometer number		Depth below datum (m)	Station/ tensiometer number		Depth below datum (m)
15–28 Nest A	1	0.94	**12–18 Nest A**	1	1.42
	2	1.44		2	1.86
	3	1.90		3	2.81
	4	2.46		4	3.25
	6	3.14		5	3.88
	7	3.27		6	4.67
	8	5.39	**Nest B**	1	1.47
Nest B	1	0.91		2	1.87
	2	1.40		3	3.43
	3	1.86		4	2.92
	4	2.22		5	3.26
	5	2.64		6	4.55
	7	3.97	**18–12 Nest A**	1	1.60
	8	5.28		2	3.06
12–12 Nest A	1	1.41		3	3.18
	2	4.90		4	3.71
	3	1.83		5	4.31
	4	2.37		6	4.64
	5	3.61	**Nest B**	1	1.56
	6	4.20		2	2.01
Nest B	1	1.36		3	3.01
	2	1.85		4	3.63
	3	2.43		5	4.09
	4	2.61		6	4.32
	5	4.00		7	4.58

Station/ tensiometer number		Depth below datum (m)	Station/ tensiometer number		Depth below datum (m)
15–15 Nest A	1	1.41	**15–6 Nest A**	1	1.27
	2	1.88		2	1.36
	3	2.82		3	1.72
	4	3.53		4	2.47
	5	3.88		5	3.01
	6	5.12		7	4.27
Nest B	1	1.48	**28–15 Nest A**	1	1.17
	2	1.88		2	1.64
	3	2.62		3	2.66
	4	3.41		4	3.14
	5	3.70		5	3.62
	6	4.99		6	4.07
18–18 Nest A	1	1.37		7	4.61
	2	1.85		8	5.60
	3	2.89	**Nest B**	1	1.28
	4	4.10		2	1.72
	5	4.62		3	2.66
Nest B	1	1.43		4	3.15
	2	1.90		5	3.71
	3	2.55		6	4.20
	4	4.12		7	5.16
	5	4.78		8	5.35
	6	5.14			

Station/ tensiometer number		Depth below datum (m)	Station/ tensiometer number		Depth below datum (m)
22–15 Nest A	1	1.08	**25–5 Nest A**	1	0.96
	2	1.56		2	1.42
	3	2.04		3	1.94
	4	2.50		4	2.41
	5	3.76		5	2.98
	6	4.12		7	4.33
	7	4.59		8	5.41
	8	5.61	**Nest B**	1	0.97
Nest B	1	1.03		2	1.49
	2	1.54		3	2.14
	3	1.98		4	2.45
	4	2.60		5	3.28
	5	3.57		6	4.10
	6	3.77		7	4.55
	7	4.44	**24–15 Nest A**	1	1.66
	8	5.56		2	2.36
25–25 Nest A	1	1.18		3	2.87
	2	1.64		4	3.41
	3	2.47		5	3.84
	4	3.39		6	4.41
	5	3.77		7	4.73
	6	4.44			
	7	5.50			
Nest B	1	1.12			
	2	1.56			
	4	3.53			
	5	3.68			
	6	4.14			

Station	Depth (M)	September (1989)		After 16 Days	
	B. Datum	P. Head(-M)	H.Head(-M)	P. Head (-M)	H.Head(-M)
15-15	1.41	0.53	1.94	0.80	2.21
	1.88	0.51	2.39	0.76	2.64
	2.82	0.81	3.63	0.88	3.70
	3.41	0.57	3.98	0.85	4.26
	3.70	0.25	3.95	0.74	4.44
	5.12	0.38	5.50	0.62	5.74
12-18	1.47	0.18	1.65	1.14	2.61
	1.87	0.52	2.39	1.04	2.91
	2.81	0.41	3.22	0.83	3.64
	2.92	0.60	3.52	0.86	3.78
	3.26	0.19	3.45	0.92	4.18
	3.88	-	-	0.53	4.41
	4.55	0.51	5.06	0.56	5.11
18-12	1.56	0.07	1.63	0.81	2.37
	2.01	0.52	2.53	0.84	2.85
	3.01	0.47	3.48	0.70	3.71
	3.18	0.53	3.71	0.77	3.95
	3.63	0.38	4.01	0.66	4.29
	4.58	0.44	5.02	1.08	5.66
	4.64	0.42	5.06	0.60	5.24
18-18	1.37	0.39	1.76	1.09	2.46
	1.85	0.66	2.51	0.86	2.71
	2.55	0.29	2.84	-	-
	2.89	0.42	3.31	0.72	3.61
	4.10	-	-	1.01	5.11
	4.62	0.36	4.98	-	-
	4.78	0.53	5.31	0.57	5.35
	5.14	-	-	0.69	5.83

*interpolated values

Station	Depth (M)	September	1989	After 16	Days
	B. Datum	P. Head(-M)	H.Head(-M)	P. Head(-M)	H.Head(-M)
12-12	1.41	0.01	1.42	1.15	2.56
	1.85	0.50	2.35	1.18	3.03
	2.43	0.76	3.19	-	-
	2.61	1.50	4.11	1.90	4.51
	3.61	0.41	4.02	0.63	4.24
	4.00	0.24	4.24	0.48	4.48
	4.20	0.20	4.40	0.45	4.65
5-25	0.84	4.35	5.19	-	-
	1.32	5.34	6.66	-	-
	2.42	4.65	7.07	-	-
	2.83	3.31	6.14	-	-
25-5	0.97	4.46	5.43	4.71	5.68
	1.49	4.75	6.24	5.04	6.53
	1.94	4.39	6.33	-	-
	2.14	5.02	7.16	-	-
	2.98	-	-	3.78	6.76
5-5	0.71	4.43	5.14	-	-
	1.23	4.76	5.99	-	-
	2.85	3.73	6.58	-	-
	3.14	2.57	5.71	-	-
	4.15	1.50	5.65	-	-
25-25	1.18	4.94	6.12	5.85	7.03
	3.53	1.55	5.08	2.71	6.24
	4.14	1.21	5.35	1.43	5.57
	4.44	0.63	5.07	0.86	5.30
	5.50	0.62	6.12	0.85	6.35
2-15	1.32	5.64	6.96	-	-
	2.21	2.05	4.26	-	-
	3.61	1.96	5.57	-	-

*interpolated values

Stations	Depth (M)	September	(1989)	After 16	Days
	B. Datum	P. Head(-M)	H.Head(-M)	P. Head(-M)	H.Head(-M)
6-15	1.33	0.64	1.97	1.55	2.88
	1.82	0.86	2.68	-	-
	2.61	0.47	3.08	0.60	3.21
	3.59	0.37	3.96	-	-
	4.16	-	-	0.70	4.86
8-15	0.86	1.13	1.99	-	-
	1.35	0.71	2.06	0.74	2.09
	2.29	0.66	2.95	1.04	3.33
	3.26	0.55	3.81	0.82	4.08
	4.15	0.15	4.30	0.34	4.49
	5.29	0.31	5.60	0.75	6.04
22-15	1.08	5.43	6.51	-	-
	1.54	1.52	3.06	-	-
	2.04	0.72	2.76	-	-
	2.50	1.24	3.74	-	-
	3.57	0.04	3.61	-	-
	3.76	-	-	0.90	4.66
	4.12	-	-	0.98	5.10
	4.44	0.09	4.53	1.04	5.48
	5.61	0.32	5.93	0.72	6.33
24-15	1.66	2.45	4.11	-	-
	2.36	0.87	3.23	1.52	3.88
	2.87	0.81	3.68	-	-
	3.41	0.84	4.25	1.52	4.93
	4.41	0.57	4.98	0.79	5.20
15-6	1.27	2.94	4.21	3.43	4.70
	2.47	1.01	3.48	1.23	3.70
	3.01	-	-	1.35	4.36

*interpolated values

Station	D. B. D. (M)	P. Head(-M)	H.Head(-M)	P. Head(-M)	H.Head(-M)
28–15	1.17	4.68	5.85	4.69	5.87
	1.72	4.27	5.99	4.90	6.62
	2.66	2.50	5.16	3.01	5.67
	3.71	1.58	5.29	1.81	5.52
	4.20	0.57	4.77	0.80	5.00
	5.60	0.51	6.11	–	–
15–28	0.91	2.60	3.51	3.49	4.40
	1.86	1.55	3.41	3.79	5.65
	2.22	0.68	2.90	4.34	6.56
	3.27	1.19	4.46	3.13	6.40
	3.97	0.41	4.38	1.89	5.86
	5.39	0.36	5.75	0.88	6.27
15–23	2.10	1.84	3.94	1.93	4.03
	2.82	0.77	3.59	1.00	3.82
	3.81	0.60	4.41	0.78	4.59
15–22	1.01	2.38	3.39	–	–
	1.35	1.92	3.27	–	–
	2.44	1.25	3.69	–	–
	3.47	0.46	3.93	0.72	4.19
	3.77	0.42	4.19	0.77	4.54
15–8	0.84	1.72	2.56	3.38	4.22
	1.26	1.01	2.27	2.67	3.93
	2.31	0.70	3.01	1.38	3.69
	3.35	0.76	4.11	1.17	4.52
	4.70	0.15	4.85	0.47	5.17
	5.26	0.32	5.58	–	–
15–2	0.95	4.52	5.47	–	–
	1.37	4.60	5.97	–	–
	3.55	0.76	4.31	1.03	4.58
	4.54	0.85	5.39	1.03	5.57
	5.12	1.29	6.41	1.41	6.53

Observed Data for Stations 15–15 and 18–18—characteristic curves.

Station	15–15		Station	18–18	
Depth	P. Head (cm)	M.C. (cc/cc)	Depth	P. Head (cm)	M.C. (cc/cc)
1.47 Meters	73.2	0.248	1.45 Meters	28.5	0.245
	80.4	0.236		33.6	0.244
	88.0	0.164		47.0	0.238
	121.2	0.155		48.0	0.235
	128.2	0.148		57.3	0.231
	136.4	0.143		77.9	0.226
	152.9	0.141		92.3	0.211
5.13 Meters	0.0	0.305		96.5	0.208
	27.2	0.172		116.5	0.200
	28.6	0.172		121.2	0.189
	29.8	0.167		180.9	0.156
	33.0	0.154		192.1	0.131
	33.3	0.149		399.9	0.107
	42.2	0.133	4.57 Meters	28.8	0.113
	64.2	0.121		31.9	0.113
	64.7	0.109		35.0	0.109
				41.6	0.107
				49.3	0.100
				69.9	0.094
				76.6	0.094
				80.2	0.092
				88.4	0.085

Values of conductivity (cm/day) for various values of moisture content (vol/vol) (M.C.).

M.C.	Layer 1	Layer 2	Layer 3	Layer 4	Layer 5	Layer 6
0.00	-	-	-	-	-	-
0.05	-	-	-	-	-	-
0.10	1.22×10^{-7}	-	-	3.63×10^{-9}	0.000327	0.00344
0.11	2.89×10^{-6}	-	-	8.87×10^{-6}	0.00225	0.101
0.12	3.01×10^{-5}	-	-	0.000185	0.0106	0.640
0.13	0.000194	-	1.18×10^{-17}	0.00126	0.0392	2.285
0.14	0.000909	4.90×10^{-13}	5.20×10^{-9}	0.00515	0.120	6.054
0.15	0.00340	1.67×10^{-9}	1.11×10^{-6}	0.0157	0.322	13.327
0.16	0.0108	9.32×10^{-8}	2.83×10^{-5}	0.0393	0.773	25.870
0.17	0.0299	1.38×10^{-6}	0.000288	0.0860	1.705	45.843
0.18	0.0750	1.06×10^{-5}	0.00176	0.170	3.503	75.811
0.19	0.173	5.39×10^{-5}	0.00778	0.312	6.785	118.755
0.20	0.371	0.000211	0.0274	0.537	12.498	178.080
0.21	0.751	0.000678	0.0819	0.879	22.053	257.624
0.22	1.445	0.00189	0.215	1.380	37.483	361.663
0.23	2.659	0.00470	0.511	2.092	61.657	494.920
0.24	4.711	0.0107	1.119	3.076	98.526	662.568
0.25	8.069	0.0226	2.290	4.407	153.438	870.240
0.26	13.410	0.0448	4.427	6.172	233.500	1124.0320
0.27	21.694	0.0844	8.152	8.473	348.024	1430.508

Values of conductivity (cm/day) for various values of moisture content (vol/vol) (M.C.).

M. C.	Layer 1	Layer 2	Layer 3	Layer 4	Layer 5	Layer 6
0.28	34.258	0.152	14.397	11.425	509.042	1796.706
0.29	52.928	0.263	24.514	15.163	731.908	2230.143
0.30	80.164	0.441	40.423	19.837	1036.000	2738.817
0.31	119.234	0.715	64.787	25.620		
0.32	174.422	1.131	101.236	32.703		
0.33	251.284	1.746	154.626	41.299		
0.34		2.638	231.367	51.645		
0.35		3.908	339.791	64.004		
0.36		5.687	490.609	78.663		
0.37		8.142		95.938		
0.38		11.486		116.174		
0.39		15.981		139.747		
0.40		21.957		167.063		
0.41		29.816		198.565		
0.42		40.048		234.728		
0.43		53.250		276.064		
0.44		70.136				
0.45						